Synthesis, Characterization and Modification of Sulfonated Poly(arylene ether sulfone)s for Membrane Separations

Ozma Norma Redd Pierce Lane

Dissertation submitted to the faculty of the Virginia Polytechnic Institute and State University in partial fulfillment of the requirements for the degree of

Doctor of Philosophy

in

Macromolecular Science and Engineering

Judy Riffle, Chair

S. Richard Turner

Richey Davis

Sue Mecham

Bruce Orler

(Blacksburg, VA)

Keywords: reverse osmosis, desalination, membrane electrolysis, fuel cells, morphology, membrane fabrication, poly(arylene ether sulfone)

Synthesis, Characterization and Modification of Sulfonated Poly(arylene ether sulfone)s for Membrane Separations

Ozma Norma Redd Pierce Lane

ABSTRACT

Sulfonated poly(arylene ether sulfone)s are a class of engineering thermoplastics well-known for their mechanical properties and chemical/oxidative stability. The research in this dissertation focuses on modifying the structure of sulfonated poly(arylene ether sulfone)s to improve membrane performance. Blends of a 20% disulfonated poly(arylene ether sulfone) (BPS20) with poly(ethylene glycol) (PEG) were investigated with the objective of promoting water flux across a reverse osmosis membrane.

It was considered desirable to investigate poly(arylene ether sulfone)s with a hydroquinone unit that could be controllably post-sulfonated without degradation, providing a polymer with controlled sulfonation through controlling hydroquinone content. It also avoided the disadvantages noted previously in polymers with post-sulfonated biphenol units. Initial experiments focused on determining sulfonation conditions to confirm quantitative sulfonation of the hydroquinone without side reactions or degradation. A polymer with 29 mole % hydroquinone-containing units was used to study the rate of sulfonation. Successful post-sulfonation was confirmed and reaction conditions were applied to a series of polymers with varying hydroquinone comonomer contents. These polymers were sulfonated, characterized and evaluated for transport properties. Of interest was the high sodium rejection in the presence of

calcium, which in the directly copolymerized disulfonated materials is compromised. The post-sulfonated poly(arylene ether sulfone)s showed no compromise in sodium rejection in a mixed-feed of sodium chloride and calcium chloride.

In the membrane electrolysis of water, Nafion's high permeability to hydrogen, particularly above about 80°C, results in back-diffusion of hydrogen across the membrane. This reduces efficiency, product purity, and long-term electrode stability. Hydrophilic-hydrophobic multiblock copolymers based on disulfonated and non-sulfonated poly(arylene ether sulfone) oligomers feature a lower gas permeability. Various multiblock compositions and casting conditions were investigated and transport properties were characterized. A multiblock poly(arylene ether sulfone) showed a significant improvement in performance over Nafion at 95°C.

Multiblock hydrophilic-hydrophobic poly(arylene ether sulfone)s have been extensively investigated as alternatives for proton exchange membrane fuel cells. One concern with these materials is the complicated multi-step synthesis and processing of oligomers, followed by coupling to produce a multiblock copolymer. An streamlined synthetic process was successful for synthesizing membranes with comparable morphologies and performance to a multiblock synthesized via the traditional method.

In memory of James E. McGrath

Acknowledgements

A PhD is an individual achievement made possible only by the contributions of the many people surrounding that individual. I am very grateful for the support of friends, family, colleagues, professors, and countless others who have helped me along my journey.

First and foremost, none of my work would have been possible without the support, guidance, encouragement, and direction of Dr. James E. McGrath. His tireless dedication to his research and his students is inspirational, and I will always be appreciative of the opportunity I have had in studying with him. I also appreciate the herculean effort made by Dr. Judy Riffle in taking on myself and my fellow graduate students from the McGrath group after his tragic illness and passing. It was an extremely generous offer to make, and she has given us her own support, encouragement, and direction. I am very fortunate to have had two truly exceptional advisers in the course of my research, and I will never forget it.

I would also like to thank my committee members, Dr. Bruce Orler, Dr. Richard Turner, Dr. Richey Davis, and Dr. Sue Jewel Mecham. In particular I would like to thank Sue for her tireless support and direction during her time at Virginia Tech. I benefited from her insights into my research and writing, and she deserves special recognition as well for her support and direction of the McGrath group during its difficult times.

I would like to thank Steve McCartney and Chris Winkler at the Nanoscale Characterization and Fabrication Laboratory of the Institute for Critical Technologies and Applied Sciences (NCFL-ICTAS) for their training and assistance with the instrumentation there. You made microscopy into the best part of my research, and you were excellent company while I

investigated the many fascinating materials from the McGrath-Riffle groups. You will both be missed.

I would not have been able to do any of my research without the support of the administrative staff, who work tirelessly behind the scenes so that graduate students are supported and materials can be ordered, and microscopes maintained. Laurie Good, Tammy Jo Hiner, Cyndy Graham, and Angie Flynn are just a few of the many dedicated people who have made my life easier at Virginia Tech. Thank you all.

Within the lab, I have had countless hours of helpful discussions and entertaining conversations with my collaborators. In particular, I would like to thank the synthetic chemists Hae-seung Lee, Ben Sundell, Jarrett Rowlett, Yu Chen, Natalie Arnett, Rachael VanHouten, Amin Daryaei, Mou Paul, Ali Nebipasagil and Xiang Yu for the endless variety of new copolymers which I had the pleasure of investigating both from morphological and performance perspectives. When the time came for me to learn synthetic chemistry, Ben Sundell, Jarrett Rowlett, and Amin Daryaei were generous with advice and feedback. For discussions on microscopy, morphology, and structure-property-processing relationships, I would like to thank Chang Hyun Lee, Myoungbae Lee, Hae-seung Lee, Anand Badami, and Abhishek Roy.

I have also been extremely fortunate in having an extended family to provide support and many listening ears when I called, exasperated at some roadblock in my research, needing to be heard and probably not making a lot of sense. To my Aunts Mary Jo, Stacy, Becky, Shelly, Miriam, and Mary, thank you for the reminder that even Darwin had very bad days. Thank you for being there, and for listening, and for the care packages. To my uncles David, Andy, Paul, Larry, and Joe, you have been there for advice (solicited or not), for support, and for incredible

patience. Thank you to my countless cousins, who not only ask about my research but listen politely when I start talking about it. I am grateful to my siblings Seana and Lex, and my niblings Lane and Eleanor. You are the best and I love you all. And last but certainly not least, I would like to thank my mom, Caroline Lane.

ATTRIBUTION

Chapter 2.

Chang Hyun Lee, Ph.D. (Department of Macromolecular Science and Engineering) was a post-doctoral research at Virginia Tech. Dr. Lee was a co-author on this paper and prepared the blends investigated in the research.

James E. McGrath, Ph.D. (Department of Macromolecular Science and Engineering) was a professor at Virginia Tech. Dr. McGrath was a co-author on this paper, co-principal investigator for the grant supporting this research and contributed revisions to the final document.

Jianbo Hou, Ph.D (Deparment of Chemistry) was a post-doctoral researcher at Virginia Tech. Dr. Hou contributed NMR analysis and revisions to the final document.

Louis A. Madsen, Ph.D (Department of Chemistry) is a professor at Virginia Tech. Dr. Madsen is a co-author on this paper, co-principal investigator for the grant supporting this research and contributed analysis and revisions to the final document.

Justin Spano, Ph.D (Department of Chemistry) was a graduate researcher at Virginia Tech. He performed thermal analysis and contributed revisions to the final document.

Sungsool Wi, Ph.D (Department of Chemistry) was a post-doctoral researcher at Virginia Tech. He perfomed NMR analysis and contributed revisions to the final document.

Joseph R. Cook, Ph.D. (Department of Chemical Engineering) was a graduate researcher at the University of Texas at Austin. Dr. Cook was a co-author on this paper and contributed to the transport property testing of the prepared blends.

Wei Xie, Ph.D (Department of Chemical Engineering) was a graduate researcher at the University of Texas at Austin. Dr. Xie was a co-author on this paper and contributed to the transport property testing of the prepared blends.

Geoffrey Geise, Ph.D (Department of Chemical Engineering) was a graduate researcher at the University of Texas at Austin. Dr. Geise was a co-author on this paper and contributed to the modeling and analysis of blend processing conditions and their impact on transport properties.

Benny D. Freeman, Ph.D. (Department of Chemical Engineering) is currently a professor at the University of Texas at Austin. Dr. Freeman was a co-author on this paper and contributed revisions to the final document.

Chapter 3. Kinetics of Post-Sulfonation of a Poly(arylene ether sulfone) that Contains Hydroquinone (Radel-A) for Application in Reverse Osmosis Membranes

Sue J. Mecham, Ph.D. (Department of Macromolecular Science and Engineering) is currently a research scientist at the University of North Carolina at Chapel Hill. Dr. Mecham was a co- author on this paper and contributed to the SEC analysis of the polymers.

Eui-Soung Jang, B.S. (Department of Chemical Engineering) is currently a graduate student at the University of Texas at Austin. Mr. Jang was a co-author on this paper and contributed to the water purification property testing of the prepared films.

Benny D. Freeman, Ph.D. (Department of Chemical Engineering) is currently a professor at the University of Texas at Austin. Dr. Freeman was a co-author on this paper and contributed revisions to the final document.

Judy S. Riffle, Ph.D. (Department of Macromolecular Science and Engineering) is a professor at Virginia Tech. Dr. Riffle was a co-author on this paper and contributed revisions to the final document.

James E. McGrath, Ph.D. (Department of Macromolecular Science and Engineering) was a professor at Virginia Tech. Dr. McGrath was a co-author on this paper, co-principal investigator for the grant supporting this research.

Chapter 4. Synthesis, Characterization and Post-sulfonation of a Polysulfone Series Incorporating Hydroquinone for Reverse Osmosis Membranes.

Eui-Soung Jang, B.S. (Department of Chemical Engineering) is currently a graduate student at the University of Texas at Austin. Mr. Jang is a co-author on this paper and contributed to the water purification property testing of the prepared films.

Shreya Roy Choudhury, B.S. (Department of Chemistry) is currently a graduate student at Virginia Tech. Ms. Choudhury is a co-author on this paper and performed the molecular weight characterization of the polymers.

Sue J. Mecham, Ph.D. (Department of Macromolecular Science and Engineering) is currently a research scientist at the University of North Carolina at Chapel Hill. Dr. Mecham was a co- author on this paper and contributed to the SEC analysis of the polymers.

Benny D. Freeman, Ph.D. (Department of Chemical Engineering) is currently a professor at the University of Texas at Austin. Dr. Freeman was a co-author on this paper and contributed

revisions to the final document.

Judy S. Riffle, Ph.D. (Department of Macromolecular Science and Engineering) is a professor at Virginia Tech. Dr. Riffle was a co-author on this paper and contributed revisions to the final document.

James E. McGrath, Ph.D. (Department of Macromolecular Science and Engineering) was a professor at Virginia Tech. Dr. McGrath was a co-author on this paper and co-principal investigator for the grant supporting this research.

Chapter 5. Synthesis and Characterization of a Hydrophilic-Hydrophobic Multiblock Copolymer for Membrane Electrolysis Applications

Jarrett Rowlett, Ph.D (Department of Macromolecular Science and Engineering) was a graduate researcher at Virginia Tech. Dr. Rowlett was a co-author on this paper and synthesized the multiblock copolymers studied in this research.

Cortney Mittlesteadt, Ph.D. is a researcher at Giner. Dr. Mittlesteadt is a co-author on this paper and performed the electrolysis characterization of the membranes.

Jason Willey, Ph.D. is a researcher at Giner. Dr. Willey is a co-author on this paper and performed the electrolysis characterization of the membranes

Amin Daryaei, B.S. (Department of Macromolecular Science and Engineering) is a graduate researcher at Virginia Tech. Mr. Daryaei assisted with the multiblock polymer synthesis and is a co-author on this paper.

James E. McGrath, Ph.D. (Department of Macromolecular Science and Engineering) was a professor at Virginia Tech. Dr. McGrath was a co-author on this paper, co-principal investigator for the grant supporting this research and contributed revisions to the final document.

Judy S. Riffle, Ph.D. (Department of Macromolecular Science and Engineering) is a professor at Virginia Tech. Dr. Riffle was a co-author on this paper and contributed revisions to the final document.

Sue J. Mecham, Ph.D. (Department of Macromolecular Science and Engineering) is currently a research scientist at the University of North Carolina at Chapel Hill. Dr. Mecham was a co-author on this paper and contributed to the SEC analysis of the polymers.

Chapter 6. Synthesis and Characterization of Hydrophobic-Hydrophilic Block Copolymers for Proton Exchange Membranes

Rachael A. VanHouten, Ph.D was a graduate researcher at Virginia Tech. Dr. Vanhouten is a co-author on this paper and performed the synthesis of the materials studied therein.

Desmond J. VanHouten, Ph.D is currently a research scientist at Corning. Dr. Vanhouten is a co-author on this paper and performed thermomechanical analysis on the materials studied in this paper.

James E. McGrath, Ph.D. (Department of Macromolecular Science and Engineering) was a professor at Virginia Tech. Dr. McGrath was a co-author on this paper, co-principal investigator for the grant supporting this research and contributed revisions to the final document.

Judy S. Riffle, Ph.D. (Department of Macromolecular Science and Engineering) is a professor at Virginia Tech. Dr. Riffle was a co-author on this paper and contributed revisions to the final

document.

Table of Contents

1.0 Literature Review

Drinkable clean water has been widely available in the United States for most of recent history. However, increasingly parts of the United States as well as large regions in the rest of the world have either become stressed for sufficient supplies of drinkable water, or are dealing with absolute shortages of even non-potable water. Over 1 billion people have no access to safe, clean drinking water and over 2 billion people experience regular water shortages. Regions which may be only slightly stressed for water at present are projected to suffer increasingly severe water stress and shortages in the future as a result of increasing population, shifting patterns of water distribution due to climate change, and decreasing supplies of drinkable fresh water.[1, 2] As fresh water supplies become more stressed and contamination of remaining supplies more severe, desalination of ocean water and brackish water is the most obvious solution.

In anticipation of the need to produce greater amounts of clean water in the future, there is a need both for more water production facilities, and for an improvement in efficiency of the systems currently in use.[3] A number of different water treatment methods exist which produce water, either with thermal phase changes (primarily distillation) or using a membrane separation process. While multistage flash (MSF) distillation was originally the most economical and most reliable method of desalination, the rapid development of membrane separation technology in the 1970s and 1980s has resulted in more competitive technology that surpassed MSF in production.[4] The most affordable and efficient commercial method for producing clean drinking water from seawater and brackish water is reverse osmosis.[3, 5]

1.1 The Need for Development of Clean Water Production

The United States Geological Survey estimates that less than one percent of the available water on the planet is viable, available freshwater, with the remainder ranging from slightly brackish to saltwater, with some additionally tied up in the polar ice caps.[4] Given the present scarcity of clean drinking water and the increasing need for the future due to the pressures of population growth, agriculture, industry, and a decreasing supply due to pollution, there is an urgent need to develop economically advantageous solutions for producing larger volumes of clean, affordable drinking water.[3, 6] As water treatment and water management have been recognized as increasingly critical issues in recent decades, projections of future water demands continually stress the need for development of newer, more efficient means of providing potable water.[7-9] Further complicating the issue is the requirement of available, affordable energy for clean water production, regardless of whether it is desalination or water recycling. Areas experiencing or projected to experience water stress frequently also lack the infrastructure for supplying reliable and affordable energy which can be dedicated to drinking water production.[3, 10, 11] Combined, these factors point to a future where water supply concerns meet or exceed those of fossil fuel availability, and research to help supply those needs before they become critical is essential.[4, 12-14]

In addition to a lag in planning and preparation for meeting future water demands, shifts in water supply or reliability of water supply are also projected due to changes in precipitation patterns as a result of potential climate change. While areas of the world outside the United States have been experiencing water stress or water shortages for some time and have responded with an exponential increase in desalination capacity, the rate of increase in desalination capacity in the United States has been less dramatic.[7] However, there are now desalination plants or membrane-based water treatment plants in almost every state, with over 75% of production directed towards municipal or industrial supplies. [7] Across the country, desalination plants are most commonly

found in California, and reverse osmosis plants have increased sharply both in total number and in relative share of the water treatment methods since 1995.[13, 15, 16]

While there are different water filtration mechanisms to remove contaminants of varying size, reverse osmosis is the most viable process for the removal of small ions such as those found in seawater. Salts and suspended materials are removed from brackish water (2,000 to 5,000 ppm salinity) and saltwater (35,000-45,000 ppm salinity) by desalination, and there are a variety of desalination methods which will be reviewed.[6] Acceptable total dissolved solids (TDS) limits for potable water vary widely for different applications. The TDS limit for water classified as fresh water is 1,000 ppm.[4] Above this point the taste, color, odor, and corrosiveness can be affected. There are also further limits on tolerable levels of individual molecular species for the consumption of potable water.

There are frequently additional standards for water used for irrigation, which may vary by country or state, such as the total allowed limit of chlorine, boron, or other components in addition to the total dissolved solids (TDS) content.[4] Of the desalination processes available, municipal consumption uses a far greater percentage of treated water than industrial, military, agricultural, power production, or other uses.[3] There is also a growing need for the production of ultrapure water used in the manufacturing of electronics and pharmaceuticals, both of which require a much higher standard of purity than the production of drinking water.[16-18] Furthermore, softened water is required for use in boilers, and while this niche was previously served by ion exchange resins, reverse osmosis is replacing or complementing this method by improving performance and avoiding the maintenance costs of regenerating the ion exchange resin.[16] The reverse osmosis system is an ideal candidate to meet the needs of all of these markets, and will likely become more

effective with future improvements in performance and with greater demand for potable water.[14, 16, 19, 20]

While reverse osmosis (RO) is primarily used to treat seawater and brackish water, there is an obvious economic advantage in also using RO to recover drinking water from domestic or industrial wastewater. This water is generally more dilute than brackish water, and therefore it is energetically cheaper than brackish water or seawater to separate, but it is too contaminated with different components to be applicable for direct consumption. The membrane treatment of this water therefore requires several steps for the separation of components of varying sizes, to be discussed in further detail later in this chapter. The ionic exclusion component of the separation process may still be able to tolerate lower levels of rejection from a cheaper, less efficient method such as nanofiltration, as the overall requirements for TDS reduction are less severe than in the case of seawater or brackish water. This is a newer focus of research and development as awareness of water stress increases around the world, and is a potentially novel application for materials which may be selective for a wider range of solutes or resistant to other pollutants.[3-5] The steady increase in demand for the production of drinkable water requires additional improvements in efficiency and selection.[4, 13, 21] There is also growing interest in membrane processes to remove contaminants to produce or recycle water for agricultural use, and this requires less stringent standards than for potable water production.[22]

1.2 Osmotic Pressure and Reverse Osmosis

When a selectively permeable membrane (one highly permeable to one component but resistant to another) is used to separate solutions of different concentrations, the result of random movement will be for the more permeable component to migrate across to the region of less concentrated solution. This phenomenon is called osmosis, and the amount of pressure that must

be exerted on a given solution to prevent the influx of water from pure water is known as the osmotic pressure. When the applied pressure to a given solution exceeds the osmotic pressure, the direction of water flow reverses and pure water can be extracted from a pressurized solution.

The process of osmosis was first observed in 1748 by Abbe Nollet, but the relationship between osmotic pressure and solute concentration was not mathematically described until the 19th century by Jacobus Henrius Van't Hoff. The relationship was improved shortly afterwards by Harmon Northrup Morse to achieve the osmotic pressure equation used today.[16] The osmotic pressure, π, may be determined from the following Van't Hoff equation:

$$\pi = iMRT$$

Above, *i* is the unitless Van't Hoff factor equal to the number of ions created by each atom of dissolved solute, M is the solution molarity (mole/L), R is the gas constant (8.314 J/K*mole), and T is the absolute temperature in degrees Kelvin. The Van't Hoff equation calculates the pressure created by a concentrated solution against a neat solvent, but the overall π between a concentrated and dilute solution can be calculated from the difference of the individual osmotic pressures. The osmotic pressure of a concentrated solution is defined as the pressure required to resist the influx of pure water (as will be discussed later in the case of forward osmosis). In reverse osmosis a higher pressure is applied in order to drive the migration of water in the opposite direction, from the more concentrated to the less concentrated solution.[4, 14, 15]

While reverse osmosis is one of the primary mechanisms used for desalination, there are other methods for separating relatively pure water from brackish or salt water, or for separating dissolved or suspended components which are larger than monovalent salts. These methods may

be separated into two primary categories based on the mechanism of action: thermal separation (phase change) processes and membrane (single phase) processes. [4, 14, 15]

1.3 Thermal Processes of Desalination

Distillation is the oldest method of desalination, having been used for hundreds of years before the advent of more refined processes, and it is still used today on an industrial scale. Thermal processes (frequently using some application of distillation) are therefore better established and are used more widely than the more recent membrane separation technologies. However, they are losing market share due to their greater energetic and economic costs. As of 2008, thermal processes covered 43% of the global desalination market.[7, 14, 22] Thermal processes consist primarily of vapor compression and multi-effect flash distillation, although the majority of the world's thermal distillation plants now use multi-stage distillation. Thermal processes are defined by the requirement of a phase change, although membrane distillation also incorporates a semi-permeable membrane. Due to the phase change, thermal processes generally have the advantage of simplicity over membrane separation processes, as high purity can be reached without lengthy pre-treatment processes or extensive monitoring of feedwater components. However, recovery levels range from 15-45%, which is generally lower than the ranges offered by membrane processes such as reverse osmosis or nanofiltration.[23-25]

One of the primary concerns in a distillation system is conservation of the thermal energy used to produce the phase changes. Energy conservation designs are typically centered on re-using the heat from condensation to warm feedwater for the evaporation phase.[7, 26] A new focus in developing potable water production facilities is hybridization between reverse osmosis and thermal distillation systems to optimize process design.[15, 27]

1.3.1 Vapor Compression

Vapor compression, also referred to as the mechanical vapor compression process is a simple but low-output method of producing fresh drinking water from a saline feed source. It operates by drawing vapor from the air above the feedwater/brine source and feeding it into a vapor compressor. The compressed vapor, which is warmer than the feedwater due to compression, is then introduced on the outside of the tubes through which the relatively cooler feedwater or brine is transported, thus condensing the vapor while heating the feedwater. It may be the more favorable of thermal desalination methods in an area with relatively cheap energy, but not in locations where low-cost steam and cooling water are difficult to supply.[7] This method is used primarily for maintaining small amounts of drinkable water, generally less than 100 m^3/day, at resorts and for industrial purposes.[7, 13, 28]

1.3.2 Multi-stage Flash Distillation and Multi-effect Distillation

Multi-stage flash distillation (MSF) is the simplest distillation procedure used industrially, and has been in common use since the 1950s. It is more frequently found in the Middle East, where water supplies are stressed and the cost of energy is comparatively low. Its relative simplicity and reliability is an advantage over membrane separation processes.[23, 25] Significant advantages are that the feedwater has a much lower pretreatment requirement, and the product water features a higher output than RO, and also a much lower level of total dissolved solids.[7, 23, 29]

The MSF process entails passing seawater through a series of chambers where it is boiled and the water vapor is collected as the pressure becomes progressively lower. By reaching the end of the series of chambers, the remaining seawater has been concentrated into heated brine. This is then pumped back through the tanks in order to re-use the heat for evaporating feedwater downstream as well as to conserve costly water-conditioning chemicals.[29] The brine is corrosive

and in addition to the expense of thermal energy, MSF requires labor to inspect and frequently replace fittings used in the chambers. The process also requires a large amount of space for the distillation chambers.[23, 29] A major disadvantage is the steep energetic cost of producing water at 18 kWh/m^3 which is much higher than the 5 kWh/m^3 of reverse osmosis.[13, 23, 30]

Multi-effect distillation (MED) is a variation on the MSF process in two aspects. First, the pipes used for vaporization and condensation tend to be horizontal rather than vertical. Secondly and more importantly, MED features a more efficient use of heat than MSF at 15 kWh/m^3. Although it has the advantage of greater energetic efficiency and was developed prior to MSF, it features a lower output and has not been as widely utilized.[23, 29] MED was commercially implemented prior to MSF, and the first commercial MED plant was established in 1928 in the Netherlands.[13, 23]

1.3.3 Membrane Distillation

Membrane distillation is a process which is thermally driven. It incorporates a microporous hydrophobic membrane that is impermeable to liquid water but will allow water vapor to pass through the pores.[31] A typical membrane distillation unit contains a high-temperature flow of feedwater on one side of a condensation chamber containing a microporous membrane, producing high levels of water vapor. The water vapor diffuses across the membrane into the condensation chamber, where it cools and condenses on a plate maintained at a lower temperature. The coolant used in the condensation plate is then cycled back to use the newly absorbed heat to raise the temperature of the feed water.[7] As with other thermal processes, membrane distillation is energetically expensive and could be more viable in a system where some or all of the energetic expense can be provided by alternative energy.[31, 32] Compared to other distillation systems, it is not yet competitive and is primarily in the stage of

research and development.[3, 30, 33-36]

1.4 Overview of Membrane Processes of Desalination and Other Separations

Membrane separation processes, referred to as single-phase processes, entail different degrees of separation and can most easily be categorized by the size of the particles or molecules which are being excluded and the type of force driving the separation. Typically, this force is primarily applied pressure but may also include species concentration, temperature and voltage.[29] The discussion here is confined to processes used in the production of potable water and focuses on the removal of ions and particles from water. Similar principles, however, may also apply to separations of gases and vapors. The five common processes used in the treatment of water for human consumption are reverse osmosis (RO), nanofiltration (NF), ultrafiltration (UF), microfiltration (MF), and electrodialysis/electrodialysis reversal (ED/EDR).[14] The separation characteristics of the first four methods are illustrated in Figure 1-1. The exclusion process takes place either via contaminants being physically too large to enter the pores of a membrane, in the case of size exclusion, or by the components being unable to diffuse into the membrane and across through the free volume as the permeate, in the case of solution-diffusion.

These processes are frequently used in combination, as they may be used to remove contaminants of differing sizes and functionalities. Microfiltration and ultrafiltration in particular are very similar with respect to operating conditions and materials, varying primarily in the size of excluded particles. Of these five processes, only nanofiltration, reverse osmosis and electrodialysis/electrodialysis reversal can be used in desalinating water, and reverse osmosis is the most efficient method.[4] However, the other methods are described as they are frequently used

in conjunction with reverse osmosis or nanofiltration as pre-treatment processes. While these processes are primarily used to desalinate or decontaminate water, they may also be used to concentrate dissolved or suspended solids of interest in the feedwater. This process is termed dewatering and is used in certain industrial and agricultural applications.[16] Of those three processes, reverse osmosis is the only practical process for desalination of seawater. The other two methods are more suited for brackish conditions, remediation of contaminated freshwater, or removal of particulates for agricultural or industrial applications which do not require complete purification of feed water.[4, 37] Additionally, membrane processes not used for the production of drinkable water such as forward osmosis, pressure retarded osmosis, and pervaporation will be discussed as they feature very similar concepts and use similar or identical materials to those used in reverse osmosis.[15, 16]

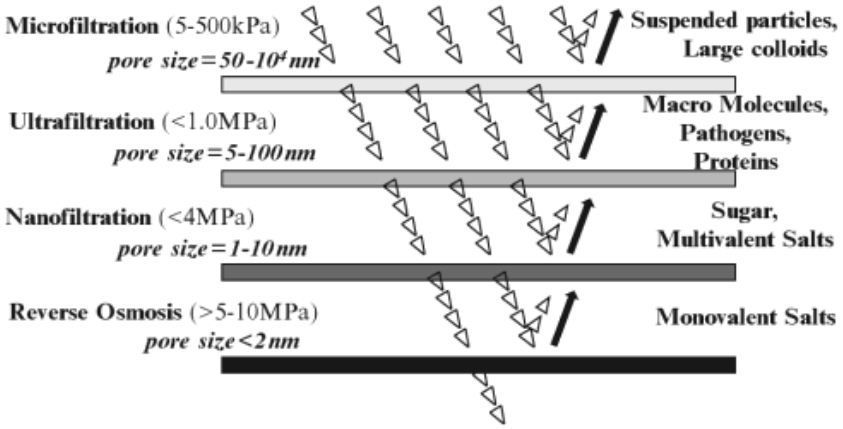

Figure 1-1. Comparison of pore size and exclusion capacity of membrane separation systems.[19, 26]

1.4.1 Microfiltration and Ultrafiltration

Microfiltration and ultrafiltration are pressure-driven processes that use a sieving mechanism through pores in a membrane to screen out particles above a given size. Due to the

exclusion mechanism, the primary disadvantage to both of these systems is the need to manage membrane fouling. Both MF and UF have applications in food, agriculture, and industry for concentrating products and removing water or unwanted components. They also are used in the pretreatment phase of reverse osmosis for removing particles or microbes which might cause fouling of the RO membrane.[38, 39] The first large-scale MF/UF plant in the USA began operations in 1994, and so this is still a relatively new field with opportunities for research and development. As costs have dropped rapidly due to economies of scale and technological innovation, the number of MF or UF installations has increased significantly.[5, 40]

The primary advantages of MF and UF over conventional water treatment processes which do not require a membrane are 1) the filtration mechanism allows for selective removal of particulates larger than the given pore size without the expense of physicochemical removal, and 2) the highly uniform pore sizes afforded by MF and UF membrane fabrication techniques allow for nearly quantitative elimination of the target solids or microbes. Levels of a given particulate or microorganism can be reduced by several orders of magnitude and so reductions are described in 'logs' of reduction, rather than the percent rejection used in other membrane treatment processes.[40]

Ultrafiltration is a pressure-driven process that can remove bacteria and protozoa from the water. It is typically intended to screen out viruses and large organic macromolecules on the order of 5,000-100,000 g/mole. Ultrafiltration cannot reliably screen out smaller macromolecules or dissolved species, and both internal and external fouling are significant challenges. The membrane is typically comprised of cellulose acetate, polypropylene, or other synthetic polymers, which are frequently formed into hollow fibers but may include membrane sheets in either spiral-wrapped, tubular, or plate-and-frame configurations.[5] Hollow fibers predominate due to unparalleled packing density, high surface area and low energy consumption. Regardless of module geometry,

ultrafiltration membranes tend to be anisotropic structures formed by phase inversion.[5, 14] Ultrafiltration can also be useful for separation and/or concentration of agricultural and dairy products.[37, 40]

Microfiltration (MF) is a pressure-driven process wherein microporous membrane sieves are used to remove particulates, precipitates, and very small microorganisms (such as *Giardia lamblia* and *Cryptosporidium parvum,* both pathogens of concern for immunocompromised individuals) from feedwater.[14] It cannot remove dissolved species, or particles smaller than about 100 nm or under about 100,000 g/mole. It is frequently utilized as a pre-treatment step for removing compounds which are likely to cause fouling from the feedwater during a reverse osmosis process. Microfiltration is also a valuable component in separations in the food and agricultural industry. Like ultrafiltration, operations must contend with internal and external fouling, which require constant surveillance and treatment.[37, 40]

Microfiltration frequently uses hollow fibers or membranes made from cellulose acetate, polypropylene, polysulfone, poly(vinylidene fluoride), poly(ether sulfone), or other materials.[14] An important feature of MF membranes, as with ultrafiltration membranes, is the uniformity of the pore size, assuring 'absolute' or near-complete removal of a given particle or microbe which is more difficult to accomplish when using coagulation-based water treatment membranes.[40] The sieving mechanism of microfiltration has a principal disadvantage in the necessity for managing fouling, which is the focus of a significant portion of MF research.[40-42]

Hollow fibers have rapidly become a standard geometry for microfiltration due to efficient production via a superior surface area to volume ratio per unit of module space, as well as bi-

directional strength which allows for designs incorporating either inside-out or outside-in flow and backwashing with air and/or water.[5, 40]

1.4.2 Nanofiltration

Nanofiltration (NF) is a pressure-driven process which can be used to treat 'hard' water by removing divalent ions, and may partially remove certain monovalent ions as well as dissolved organic molecules over approximately 300 g/mole. It can filter out larger particles and single-celled organisms as well, but this carries a higher risk of fouling. Sometimes nanofiltration is used to refer to reverse osmosis, but the processes differ, as NF uses both solution-diffusion and size/charge exclusions in the membrane separation process.[7, 14] While nanofiltration membranes may feature a dense layer, they also frequently feature pores ranging from 1-10 nm in diameter, which will permit passage of most monovalent salts. The required pressure in feedwater to produce permeate in nanofiltration is approximately 70-120 psi, an order of magnitude lower than pressures required in reverse osmosis. The primary advantage of nanofiltration over reverse osmosis is that of cost due to the lower energy and pressure requirements, but the limitations of NF constrain it to niche applications of water purification.[14, 16]

Nanofiltration was developed in the 70s and refined in the 80s as a variation of reverse osmosis membranes that required lower operating pressures and had lower rejection mandates.[4] As in reverse osmosis, nanofiltration membranes are typically either cellulose acetate or crosslinked polyamides, and the majority of modules use the spiral-wound configuration (explained in detail in Section 1.5.4).[14] While nanofiltration is unable to adequately desalinate feedwater with a high salt concentration, such as sea water or the highly saline waters found in the Middle East, it can desalinate brackish water and performs well in applications such as water softening. It may have an additional niche in boron removal.[4, 14, 43-45] It can also be used as a lower-

cost alternative to reverse osmosis for concentrating agriculture and dairy products.[37] There is a growing interest in using nanofiltration to remediate produced or processed water which has become contaminated in the process of fossil fuel extraction.[46, 47] Like reverse osmosis, nanofiltration uses a multistep process of pre-treatment, membrane treatment, and post-treatment of water prior to distribution for consumption.[2, 5, 14]

1.4.3 Reverse Osmosis

Reverse osmosis (RO) is a pressure-driven process in which ions are removed from solution via selectively permeable membranes such as cellulose acetate, polyamides, or sulfonated poly(arylene ether sulfone)s. These materials are different from those seen in microfiltration and ultrafiltration membranes because they require water to be absorbed into and diffused across the membrane, necessitating a degree of hydrophilicity. Although RO is capable of separating larger molecules and particles, in practical applications these must be reduced or eliminated in an earlier treatment step (using microfiltration, ultrafiltration, or a coagulating/flocculating technique and possibly nanofiltration) in order to minimize fouling, and additional fouling prevention methods are sometimes necessary.[39, 48]

Reverse osmosis requires 3-10 kWh per cubic meter of freshwater produced, which makes it one of the most energetically affordable desalination technologies.[1, 31] The specific energy requirements for any given RO system are determined by the salinity of the water to be treated, and the properties of the selected RO membrane. An ideal RO membrane has excellent water transport with near-complete salt rejection, a very thin, pinhole-free selective skin layer for promoting rapid water transport, and must have sufficient mechanical properties to withstand the driving pressure of the process.[3, 15] In order to improve flux, a free-standing dense membrane is unsuitable and either a thin film composite (a submicron layer of selective material supported by

a layer of polysulfone foam and a nonwoven fabric to provide mechanical integrity) or an asymmetric membrane (a thin film and support foam cast simultaneously from the same material) are used to optimize membrane performance.[14] These structures and their fabrication will be discussed at a later section in much greater detail.

The first experimental membranes developed for desalination were dense cellulose acetate membranes made by Reid and Breton in 1959, after evaluating a series of different partially hydrophilic materials for permeability of water and for salt rejection.[49] While they established satisfactory rejection values, the water flux was too low. Loeb and Sourirajan developed asymmetric membranes from cellulose acetate in the 1960's to improve water flux while maintaining satisfactory salt rejection values. This resulted in the commercial viability of RO membranes and the birth of the RO industry.[14, 49] Improvements in the fabrication and design of membranes led to a rapid growth in the performance of commercial RO units in the late 1960's and early 1970's, the most significant being the development of spiral-wound and then tubular or hollow fiber membranes to replace flat-sheet membranes. The introduction of linear aromatic polyamides provided a much higher water flux at a slightly lower, and therefore more affordable, pressure.[16] Another breakthrough with an interfacially-produced crosslinked polyamide was made by John Cadotte, in the form of a thin film composite. This offered advantages in both water flux and salt rejection, and has since been established by Dow Chemical Company as the predominant industry standard under the name "FT30".[15, 16, 29]

Since the rapid development in the 1970s, there have only been small improvements in salt rejection and fouling resistance in commercial processes, as well as developments for niche applications such as boron removal and co-contaminants. The primary hurdles of a chlorine tolerant membrane and a significantly fouling-resistant membrane remain elusive.[15, 16] However,

even without resolution of these membrane limitations, the use of RO systems and the number of applications for which RO is ideal have rapidly increased. Although the primary application is desalination of seawater, there are also RO plants constructed for the more economically feasible desalination of brackish water, as well as for treatment of contaminated groundwater and reclamation of wastewater.[29]

Reverse osmosis plants have been desalinating brackish water in the Middle East since the late 1960s, and began desalinating seawater in the late 1970s.[15, 30] Due to improvements in RO technology, it is the fastest growing process for desalination, and in the United States it is the predominant process. Across Europe, large-scale RO desalination plants have been constructed rapidly in the last two decades.[29] In the Middle East, where the relatively low cost of energy and high demand for large outputs of drinkable water favored multi-stage flash distillation, MSF still predominates but RO plant construction is increasing. Reverse osmosis is clearly the desalination method that will dominate the desalination industry in future years, particularly as more regions become water stressed and as RO technology becomes more economical and efficient. The use of reverse osmosis to desalinate seawater for human consumption was one of the first applications of membrane science, and the development of this application is a growing field of interest today.[4, 14] A comparison of RO and other membrane treatment processes is shown in Table 1-1.

A typical reverse osmosis system features feedwater, which can be brackish or seawater, transferred across a semipermeable membrane at an elevated pressure. As pressure forces the water permeate across the membrane, the feedwater becomes more concentrated until it is removed from the system. While operations desalinating seawater generally require a feedwater pressure of 800 to 1200 psi, brackish water desalination requires a much lower and more affordable (energetically speaking) feedwater pressure of 100-600 psi, and offers obvious advantages where available.[5, 14]

Table 1-1. Comparison of membrane separation processes.[5]

Process Type	Membrane type	Mechanism	Energy requirement	Application	Exclusion size/MW
Reverse Osmosis	Asymmetric or thin film composite	Solution-Diffusion	Pressure (5-8MPa for seawater desalination)	Removal of all dissolved components	Monovalent ions
Nanofiltration	Asymmetric or thin film composite	Solution-Diffusion, size exclusion	Pressure (0.5-1.5MPa)	Removal of divalent components and larger molecules	Divalent ions, organic carbon, Color, limited monovalent ions
Ultrafiltration	Microporous Sieves	Filtration	Pressure (50-500 KPa)	Removal of small microscopic contaminants	Bacteria and viruses
Microfiltration	Microporous sieves	Filtration	Pressure (50-500 KPa)	Removal of microscopic contaminants	Bacteria and protozoa, coagulated organic particles, precipitated matter >100 nm
ED/EDR	Dense membrane	Ion exchange	Electricity	Removal of dissolved ions	Dissolved ions

1.4.4 Electrodialysis/Electrodialysis Reversal

Electrodialysis/Electrodialysis Reversal (ED/EDR), which has been in use since the early 1960's, includes the same size range of excluded ions as reverse osmosis, but does not remove pathogens, suspended solids or any noncharged or nonionic components.[5, 14] As opposed to the typical transport mechanism in the filtration- or solution-diffusion-based processes where contaminated water is treated by migration through the body of a membrane, ED consists of contaminated water passing along or across the surface of parallel ion-exchange membranes. These membranes selectively remove cations and anions using electrical energy rather than a pressure gradient, and require both good selectivity for the respective ions as well as a low resistance to ion

transfer. [5, 14] The primary disadvantages of ED include a high propensity towards fouling and a slightly higher operations cost compared to reverse osmosis, but the process also offers the flexibility of high pH range tolerance (ED is viable from pH 1.0-13.0), high temperature tolerance at 43 °C, and conversion rates (the percentage of feedwater which is actually converted to product water) ranging from 50-90%, depending on operating conditions.[29]

Electrodialysis reversal utilizes the same physical setup as ED, but the polarity of the electrodes is periodically reversed, along with the wastewater and product water outlets, in order to reduce the accumulation of scale, biofoulants, and other contaminants. This reduces the need for cleaning procedures and increases the water recovery potential over a system using ED, but EDR also requires more skilled labor due to the more complex requirements for maintenance and operation of the system. [5, 14]

Although technically capable of treating seawater, ED/EDR is more typically used for brackish water, wastewater treatment, and reclamation of components in the food and pharmaceutical industries. Electrodialysis is only applicable for feedwaters where the total dissolved solids level is less than 5 g/L as the level of electrical current needed to remove higher levels of contamination is impractical. Electrodialysis can be used to separate and concentrate acids, bases, or salts from a dilute aqueous solution. [5, 14]

1.4.5 Cost effectiveness and comparative advantages of different desalination processes

Overall, membrane separations processes are much more energy-efficient than phase-changing processes due to the significant heats of vaporization and fusion of water. The relative costs vary according to geography, as some regions such as the Middle East feature both an intense

need for drinkable water, with only seawater as a viable feed source, and a very low cost of energy. The increasingly volatile cost of energy should be factored in when making predictions about the viability and competitiveness of phase change versus membrane separation-based desalination plants.[11, 12, 50] Furthermore, while thermal distillation methods offer a simple process, reverse osmosis operates at ambient temperature and relies on non-corroding polymers, which simplifies the heating and cooling steps as well as reduces the cost of systems monitoring and maintenance. Additional advantages are the use of elements which can be easily replaced without extensive training and small industrial footprint. These are not as immediately obvious as the energy use advantage of reverse osmosis, but nonetheless are significant in the daily operations of a plant.[15]

Cost concerns include both the capital costs of starting up a plant and the daily operations cost of producing a given amount of water at a given level of quality, according to levels of individual contaminants and total dissolved solids.[29, 51] Another cost concern which may be more difficult to quantify precisely is the environmental impact, such as the impact of discharged treatment chemicals or in the case of RO, brine disposal. A cost comparison of desalination methods is listed below in Table 1-2.

Table 1-2. Comparison of costs for varying desalination systems, in 2003-2006 US Dollars.[7, 13, 23, 25, 51, 52]

	Pretreatment Requirements	Energy Required	Cost of Water	Environmental Impact	Notes
Reverse Osmosis	High	2.5-5kWh/ m^3	\$0.50-0.70/m^3, seawater \$0.26-0.54/ m^3, brackish water	No temperature disturbance, high-TDS brackish water disposal problematic	Values are for large volume plants, over 50,000 m^3/day
Multistage Flash	Low	3-5kWh/ m^3	\$1.10/m^3	Brine concentrate features higher temperatures	Low product water TDS
Multieffect Distillation	Low	1.5-2.5kWh/ m^3	\$0.80/m^3	Similar to MSF	Low product water TDS
ED/EDR	Medium	\$0.5kWh/ m^3	m^3	Low	Not suitable for large volumes of highly saline water, cost is TDS-based

Reverse osmosis is by far the most versatile and economical desalination technology in use, and a clear trend towards improved performance and decreased cost in recent years has been demonstrated, as shown in Figure 1-2. There is a marked economy of scale, as small plants of less than 5,000 m^3/day may cost as much as \$1.20-3.90/m^3 depending on operating conditions, while larger plants of over 60,000 m^3/day see the cost of water production drop to \$0.50-0.70.[51]

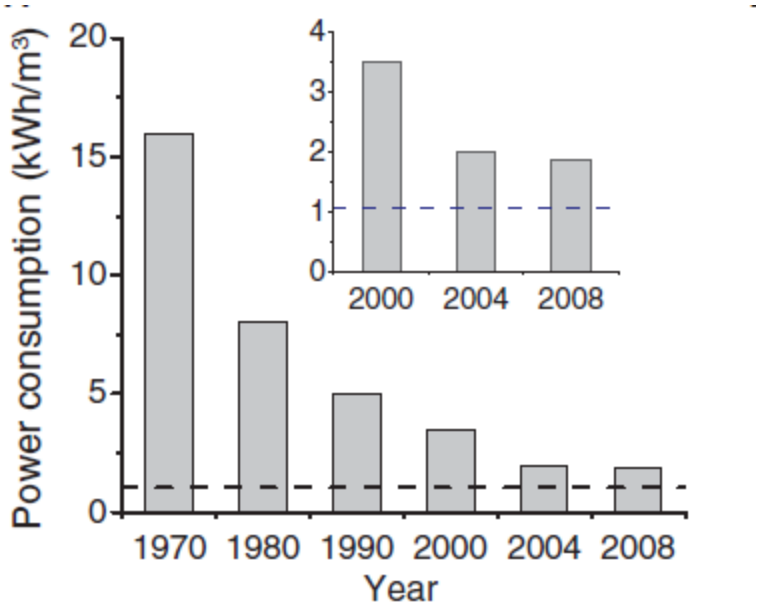

Figure 1-2. Power consumption of seawater reverse osmosis has rapidly decreased since its development in the 60s and 70s, and is now approaching the theoretical minimum.[1]

1.4.6 Pressure Retarded Osmosis and Forward Osmosis

Both pressure retarded osmosis (PRO) and forward osmosis (FO) are processes in which energy is produced from the osmotic pressure generated by separating fresh water (or more dilute contaminated water, sometimes wastewater) from seawater or other concentrated solution by means of a semipermeable membrane. They are sometimes referred to jointly as osmotically driven membrane processes. In both processes, the concentrated solution is also referred to as the draw solution. This is typically seawater although research is ongoing to identify a more competitive draw solution.

The difference between PRO and FO is illustrated in Figure 1-3. Forward osmosis harnesses energy directly from the dilution of seawater, while PRO uses a small applied pressure on the permeate side to reduce the operating pressure to provide more efficient energy conversion. The reason for the pressure retardation is illustrated in Figure 1-4. PRO is more often used for

power generation, and while FO is also a possible power generation process, it is more frequently used for osmotic dilution or concentration of solutions with minimal energy consumption.[53]

Pressure retarded osmosis (PRO) is the process by which energy is generated using an applied force on the brine side of the membrane in order to optimize the efficiency of the work done by osmotic pressure. PRO, which may also be referred to as engineered osmosis, is unique among power generation methodologies in that it harnesses energy produced by the entropic energy of mixing two solutions, and offers a source of renewable energy which features a negligible impact on the environment. Forward osmosis is a closely related process where no pressure is applied on the brine side, as illustrated in Figure 1-3.

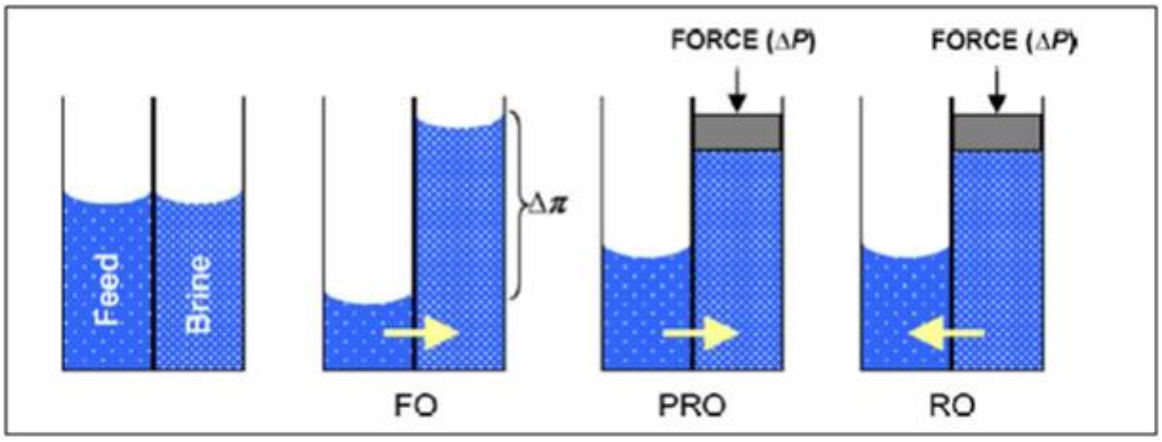

Figure 1-3. Comparison of forward osmosis, pressure retarded osmosis, and reverse osmosis.

As the energy is generated from a pressure differential, it may seem counterintuitive to apply a pressure on the permeate side of the process, as is done in PRO. However, when considering the equations for power density and water flux (the significance of these equations for reverse osmosis applications will be discussed in Section 1.5), the need for applied pressure becomes apparent. The following equation describes the water flux:

$$J_w = A(\Delta P - \Delta\pi)$$

Above, J_w represents water flux, A represents the permeability constant for the given membrane material, ΔP represents the applied pressure and $\Delta\pi$ represents the osmotic pressure generated between the draw solution and the feed solution. The below equation for determining power density is given as follows, where W is power density and the remaining terms are as previously described.[54]

$$W = J_w \Delta P = \Delta P \cdot A(\Delta P - \Delta\pi)$$

Differentiating the power density equation below gives a peak in the power density when the applied pressure equals half the osmotic power, disregarding A as a material-specific variable.[54]

$$\frac{dW}{dP} = 0, \quad \Delta P = \frac{\Delta\pi}{2}$$

When $\frac{\Delta\pi}{2}$ is substituted for ΔP in the equation for power density, we arrive at a maximum power density as a function of the permeability constant and the osmotic pressure, thus providing only two variables to modify for increased power production.[54] As the osmotic pressure can only be modified by the composition and concentration of the draw solute (which is generally seawater due to its availability and high concentration), this leaves high-flux materials and composites the primary focus of research in the field of pressure retarded osmosis. It also provides impetus to develop PRO in areas where highly saline bodies of water offer even higher concentrations than seawater.[55, 56]

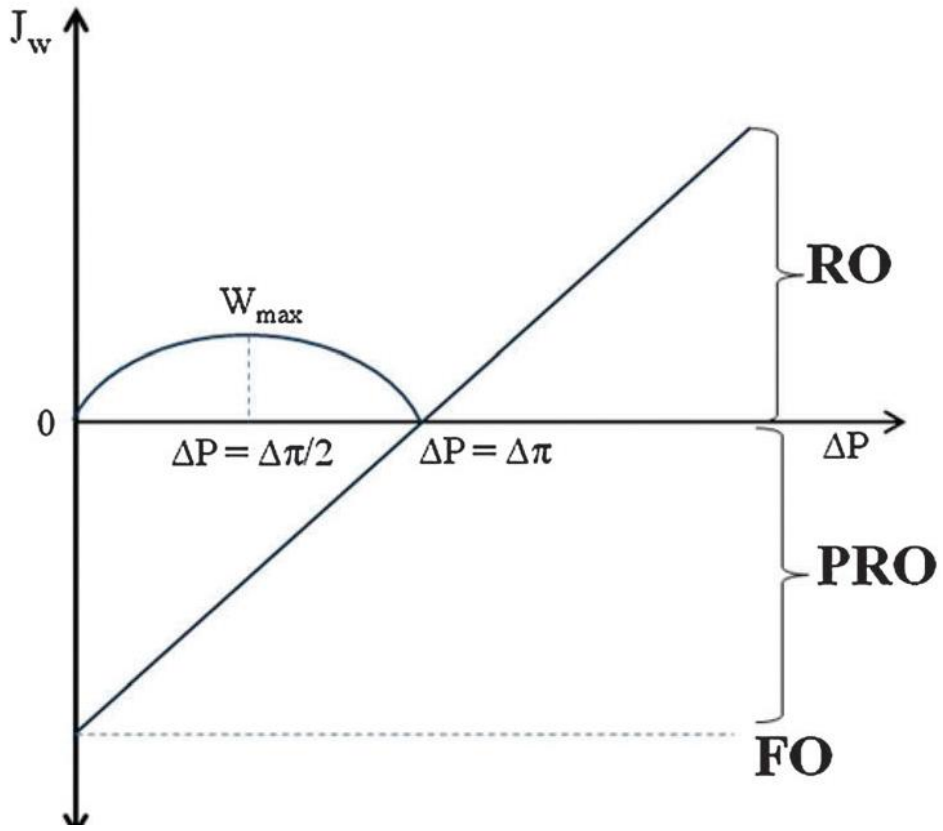

Figure 1-4. Comparison of osmotic and applied pressures for PRO, FO and RO.[57]

While PRO is not used for production of clean drinking water, the principles and materials used are very similar to RO and research done on behalf of improving one application is frequently used in the other. Although FO is also not used directly for the production of clean drinking water, it has been used in hybrid RO/FO systems, in which FO is used both in the pretreatment of feed seawater to reduce boron levels and to dilute the product brine generated by the RO step.[58]

As the primary goal of FO/PRO is sufficient water flux, these processes feature lower requirements for salt rejection and generated pressure tolerance (0 for FO, 10-15 bar for PRO). Fouling is also a much smaller concern in FO as the pressure is generated on the 'pure' feed water side of the membrane, with few opportunities for microbes, inorganic components, or organic material and silt to accumulate on the film surface. The complex maintenance required in RO may

be reduced to a simpler occasional physical cleaning or even by careful control of the feed stream alone (in contrast to a combination of chemical and physical steps required for RO).[59]

Forward osmosis and pressure retarded osmosis are technologies under development, with details of efficiency and cost still being evaluated. The primary areas of investigation for FO/PRO technology are the development of new selective layers,[60, 61] surface treatment options,[62, 63] and hydrophilic support layers,[64-66] the economics of energy generation,[57, 67-72] the efficacy of FO as a pretreatment or hybrid step in conjunction with RO or nanofiltration,[57, 73] and evaluation of various draw solutes.[74-79]

Pressure retarded osmosis and forward osmosis processes have an additional challenge of suffering from concentration polarization on both sides of the membrane, as opposed to the problem caused only on the feed side in reverse osmosis, which will be discussed in greater detail in Section 1.6. In PRO and FO, there is the challenge of external concentration polarization, where water transported from the freshwater feed stream dilutes the draw solution, reducing the osmotic pressure and therefore causing a sharp decrease in flux. This can be mitigated by thorough mixing and module design, so the diluted solution moves rapidly across the membrane and leaves the module before the osmotic pressure is significantly affected. There is also internal concentration polarization (ICP), where small amounts of solute diffuse across the membrane into the support layer, reducing osmotic pressure from the freshwater side as well.[54, 57, 80, 81] Of the two, the internal concentration polarization is considered to be the more challenging, as laminar flow of the feed stream cannot penetrate the porous foam.[53, 82-85]

While initially the materials used in PRO and FO were identical to those used in RO, some changes were made to improve water flux, while some decrease in salt rejection was considered

tolerable. For example, the nonwoven backing used in thin film composites in RO was removed, as the lower operating pressures would tolerate lower levels of mechanical support. After removing the nonwoven backing, the structural resistance to flow was reduced significantly and the flux increased by a factor of 5-10.[53] There are at least three current commercial membranes for osmotically driven membrane processes available, two of which are thin film composites based on cellulose triacetate and a third which is undisclosed.[53]

Modifying the chemical and physical structure of the support foam is also a major thrust of research, since the direction of water flow is from the foam side towards the dense layer. A hydrophilic support foam offers potential advantages in minimizing fouling and facilitating improved water flux.[86-88] There is not yet a consensus on what foam structure will be most advantageous for PRO/FO, be it with or without macrovoids or with an open scaffold or more closed structure. Macrovoids reduce mechanical strength, but they also reduce internal concentration polarization and so they may be tolerated within limits. There are also membranes which feature a very thin dense layer on both sides of the foam structure to minimize irreversible internal fouling.[86-88]

There is some controversy in the membrane separations field over whether the benefits and costs of PRO have been exaggerated.[89, 90] However, several analyses have found that at least 2.5W/m^2 is a reasonable estimate for power generation,[71, 72] and other researchers have suggested more optimistic projections of 5W/m^2 if sufficient improvements in membrane design can be achieved or if higher concentrations of draw solution become available.[54, 80] The latter option may be viable for plants located at high-salinity bodies of water such as the Dead Sea or the Great Salt Lake. PRO does offer the advantage of continuously available renewable power, as opposed to the periodic or entirely unpredictable nature of solar, wind, and other renewable energy sources.[71]

Meeting cost requirements for competitive power generation is more challenging, but may be possible with improvements in material development.[80, 90]

Forward osmosis also may be hybridized with reverse osmosis, in which the concentrated brine produced by RO is then diluted once more using seawater, generating energy to help drive the RO process. This hybrid system offers the additional advantage of providing a pretreatment step for the RO feedwater, which may help avoid the necessity of a two-pass system by removing part of the boron content during the FO step.[57] A hybrid system is illustrated in Figure 1-5.[83, 91]

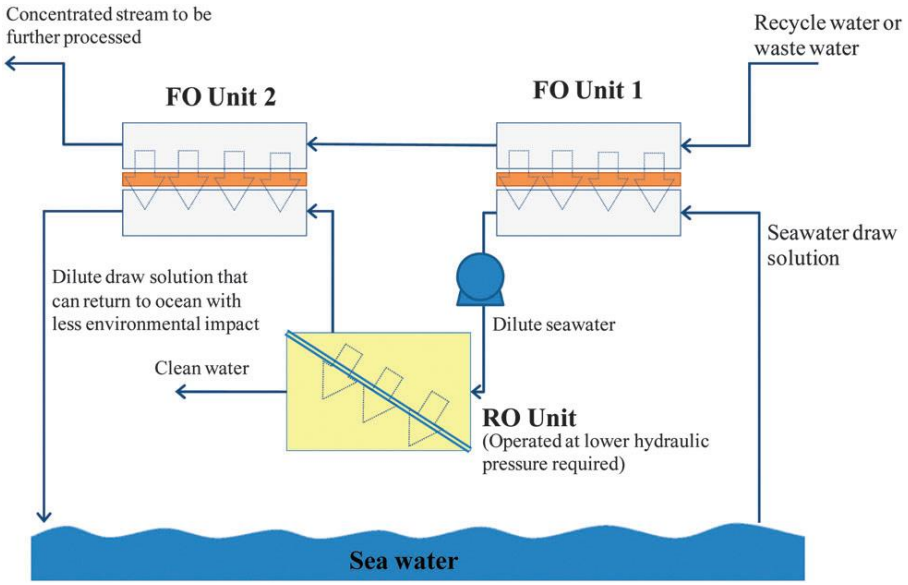

Figure 1-5. Illustration of hybrid RO-FO system.[53]

The pressure gradient between two solutions of different concentrations may also be harnessed in the process of reverse electrodialysis (RED) in order to generate electricity. Reverse electrodialysis is considered one of the most efficient means for extracting electrical energy from the thermodynamic energy of mixing solutions.[92]

While PRO systems predominantly use seawater as a draw solution due to its negligible cost, there are investigations into four main classes of alternative draw solutes to improve

performance: inorganic salts; thermolytic/volatile compounds; organic molecules such as alcohol, sugar, protein, and organic salts; and polymer-based solutes such as polyethylene glycol, dendrimers, hydrogels, and magnetic nanoparticles.[53] The primary inorganic salt in use is NaCl in the form of seawater, but overall this class of solutes offers an inexpensive and easily accessible means of generating a high osmotic pressure in PRO or FO, albeit with a difficult means of separation or recovery. In the case of seawater this is not a challenge as the dilute water can be returned to the ocean in an area of brackish water, but for other inorganic salts it remains a challenge. Thermolytic/volatile solutes are a particularly interesting class, since they may be evaporated and recovered by using relatively low temperatures generated from waste heat (particularly power plants). [76, 79, 93, 94]

The most studied and promising of these alternative solutes is a solution of NH_3/CO_2, which can easily generate much higher osmotic pressures than seawater and can be recovered at 58^{o}C. However, meeting satisfactory recovery levels of NH_3 remains a significant technical challenge. This process is being pursued commercially by Oasys Water. Organic molecules are not as competitive in terms of generating high water flux, but offer the advantage of easier recovery than inorganic salts due to a higher molecular weight, as well as being frequently biodegradable after use or in the event of accidental leaks. Finally, polymer-based solutes offer the advantage of low-cost and simple solute recovery, most often with UF, as well as easily tailored structures for the desired osmotic pressure and performance, but are not always easy to obtain or maintain. [53]

Pressure retarded osmosis and forward osmosis are both developing technologies and as such have a number of features which are currently under investigation for improvement. However, with sufficient improvement PRO/FO may become a commercially competitive entity. The most critical is improvement in membrane material and structure to get sufficient water flux

and structure parameter values,[85] followed by controlling internal and external concentration polarization, and the evaluation of more effective draw solutes. However, currently the use of seawater, brine concentrate produced from desalination, and the ammonia-carbon dioxide system utilized by Oasys water are the most viable options.[57, 80, 82, 85, 95]

1.4.7 Pervaporation

Pervaporation is technically a membrane separation process, but is sometimes also classified as a thermal process as it involves a phase change. It was first identified as a possible separations process in 1906, but did not see commercial implementation until the early 1980s with the application of asymmetric membranes and composites. It is now seen as competitive with, if not more efficient than, traditional distillation. Pervaporation features a liquid feed stream and a membrane which allows permeation only to water vapor. The permeate vapor is collected on the permeate side and then fed to a condenser where it is removed as a liquid, as shown below in Figure 1-6.[96, 97]

Although pervaporation is predominantly used to separate ethanol from water in industrial, agricultural, and beverage production applications, it is also a possibility in the removal of small amounts of volatile organic compounds (VOCs) from contaminated groundwater or industrial processes.[96, 98] Pervaporation typically relies on a solution-diffusion mechanism through a dense or asymmetric membrane, but the pressure differential needed is small compared to reverse osmosis.[29, 99]

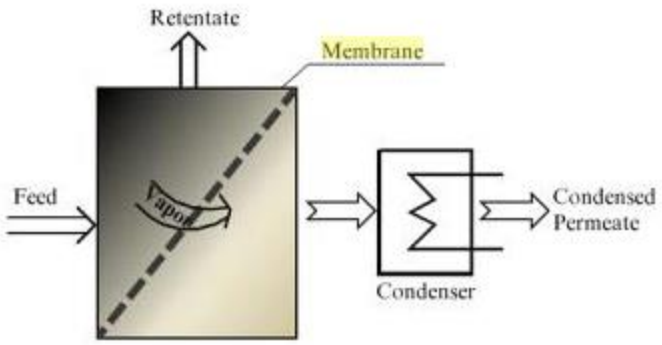

Figure 1-6. Schematic of a pervaporation system, in which feed and retentate streams are liquid but permeate stream consists of vapor.[29]

1.5 Design of the Reverse Osmosis Process

The reverse osmosis process can be broken down into three primary stages. The first is that of pretreatment, where the source water is rendered more suitable for treatment in order to minimize fouling and have a more efficient process. This is followed by the actual membrane treatment process in RO modules, and then post-treatment, where the produced water is degasified, and any needed disinfectants or chemicals are added prior to distribution. The process by which RO produces desalinated water using a solid polymer membrane is termed solution-diffusion separation. There are a number of terms which will be discussed in greater detail in a later section used to describe the efficiency of both potable water production, salt rejection, and other parameters of the RO process.[14]

1.5.1 Solution-Diffusion Mechanism

In the membrane selection processes, there are two primary mechanisms of separation depending on the membrane structure. In the pore flow mechanism, a porous membrane excludes components which exceed the pore size. Porous membranes as a result have very stringent requirements of maximum pore size and pore size distribution, and the rejection of suspended

components such as microbes can be measured on a log scale due to highly successful selection.[40] They also produce a higher volume of permeate at a lower pressure than solution-diffusion membranes, but due to the open structure of the membrane experience a much higher incidence of fouling.[14] In porous membranes, fouling may be external (reversible caking, scaling, or growth on the membrane surface) or internal (particulates lodged in pores in the thickness of the membrane, which is largely irreversible).[19] In pore flow separation as in solution-diffusion, the driving force is pressure, but in the case of the former it is specifically the solution properties and the differential between the entry and exit pores or cylinders and the radii of the solutes or particles of interest used to model the structure of the membrane.[10, 19, 29]

In the solution diffusion mechanism, a dense, perfectly pinhole-free membrane separates one component of a mixture based on the relative solubility and diffusivity of the different components. Since the permeate component is separated by physical diffusion through a solid, rather than by passing through a porous sieve, the throughput for a solution diffusion membrane is much lower than processes relying on pore flow mechanisms. Due to the reliance of reverse osmosis on solution diffusion mechanisms, this work will focus more heavily on this mechanism rather than pore flow. [19, 29]

Physically speaking, the distinction between the pore-flow sieving model and the solution-diffusion model consists of the size of the membrane pores. Although the membranes that separate by means of solution diffusion are dense, they do possess very small pores. While the pore size in the pore-flow model is an obvious factor, the presence of pores in dense membranes using solution-diffusion-based selection may seem counterintuitive. However, membranes used to separate by means of the solution-diffusion mechanism do have very small pores on the scale of 0.5-1.0 nm, which are created and removed by the thermal motion of polymer chains within the membranes.

According to Baker, these pores appear and disappear on a brief timescale, similar to that of the permeants crossing the membrane. The larger these temporary pores are, the more time they are present before moving away, providing more of an influence on membrane transport properties and approaching the behavior of pore-flow membranes. [19, 29]

While the equations for the description of a given membrane's efficacy as an RO membrane will be discussed in the following section, the basic equation that describes the transport of a given component across a membrane barrier as a result of a concentration gradient is shown below. In this equation, J_i represents flux, D_i the coefficient of diffusion, and $\frac{dc_i}{dx}$ the concentration gradient across a distance x. The negative sign adjusts for the direction of water flow. This is termed Fickian diffusion and can be used to describe transport of water within the hydrated membrane, excluding considerations of applied pressure. [19, 29, 100]

$$J_i = -D_i \frac{dc_i}{dx}$$

There is a three-step process to the transport of a solute using the solution-diffusion process. The first is the initial contact between the solute and the solution/polymer interface, in which the solute dissolves into the membrane. The second step is the actual transport driven by the applied pressure across the thickness of the polymer membrane is the primary focus of RO material research. The final step is the dissociation of the solute from the permeate side of the membrane. The solution-diffusion model assumes that the first and last steps are much more rapid than the diffusion-controlled transport, and therefore do not need to be described mathematically. It is also assumed that the membrane has a uniform gradient across its thickness and that each side of the membrane is at equilibrium with the liquid or gas at its interface. The solution-diffusion

model further assumes that the membrane, when pressurized, evenly distributes pressure within the system. These assumptions are illustrated in Figure 1-7. [19, 29]

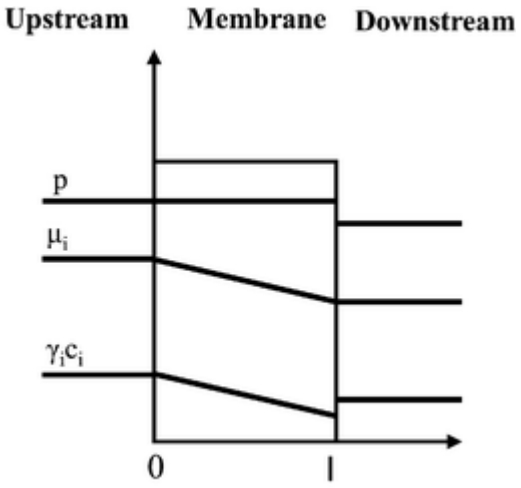

Figure 1-7. Illustration of solution-diffusion model, in which p represents applied pressure, μ_i indicates the chemical potential of dissolved species i, and $\gamma_i c_i$ represents the solvent activity of i.[29]

The critical portion of Figure 1-7 is that of chemical potential, which is influenced by concentration and pressure (as well as other forces such as temperature, but for reverse osmosis pressure is the primary factor). As with concentration, a given dissolved species *i* will move from higher values to lower values of μ_i.[29, 37]

$$A = \frac{D_w K_w^L c_{w0} v_w}{lRT}$$

$$J_w = A(\Delta P - \Delta\pi)$$

Above, the second equation describes the calculation of A (which is typically empirically determined, but a reproducible A value can be used to back-calculate the diffusivity coefficient), in which, D_w is the diffusivity of water, K_w^L is the sorption coefficient, c_{w0} is the concentration of water on the feed or upstream side of the membrane, v_w is the molar volume, l is the thickness of

the membrane, R is the gas constant and T the temperature in Kelvins. The following equation models the flux of water, J_w, against a gradient as a result of pressure applied (ΔP) in excess of osmotic pressure ($\Delta\pi$), with a water permeability constant A.[29, 37]

The solution diffusion mechanism was not discovered until after the advent of reverse osmosis membranes. It was heavily disputed during its initial decade of development as initially pore flow theory was thought to be a better model, as it applied to other membrane separations applications such as microfiltration and ultrafiltration. Donald R. Paul was instrumental in the development of the solution-diffusion theory (SDT), which accurately models solute transport across a dense, pore-free and pinhole-free membrane. Further research has indicated that while highly effective for describing transport in separations of aqueous solutions, this model does not apply well to separations of organic liquids. More detailed modeling and calculations have been performed for those applications.[100-102]

1.5.2. Terms and Equations in Membrane Transport Theory

The two most important parameters in membrane separation measure the capacity of the membrane to exclude a given solute, most frequently sodium chloride, and to allow water to diffuse across the membrane. These parameters can be expressed in several different terms. All equations given here assume a solution-diffusion model of transport rather than a sieving or filtration mechanism.[19, 37]

The calculation of water flux J_w and water transport coefficient was described in the previous section. Salt rejection may be expressed in terms of salt transport, J_s, as determined by the following equation, were B is the salt permeability coefficient, C_{BL} is the concentration of salt at the boundary layer (or in the bulk feedwater, if boundary layer data is unavailable or if fluid

velocity is sufficient to disregard concentration polarization), and C_P is the concentration of salt in the permeate. The second equation below describes the calculation of the B term, which also may be observed empirically. In this equation, D_s is the diffusivity of salt in a given material, K_s is the sorption constant, and l is the thickness of the membrane. It should be noted here that while the water transport may be increased by applying additional pressure, the salt transport (and conversely, rejection) is not influenced by pressure.[29, 37]

$$J_s = B(C_F - C_P)$$

$$B = \frac{D_s K_s}{l}$$

In the production of clean permeate water, the recovery term Y is used to describe the level of conversion from the feed to the permeate, as much of the water remains in the retentate. This is described by taking the percentage of the ratio between the permeate flux Q_p and the feed flux, Q_f, both of which can be measured empirically rather than by calculation. Typical Y values may range from 40-60%, since excessively concentrating retentate becomes economically unviable in the separations process when seawater or even brackish water is the feed source. Highly concentrated retentate also contributes to fouling and scaling as minerals precipitate onto the membrane surface.[15, 37]

$$Y = \frac{Q_P}{Q_f} * 100$$

The structure parameter S is a factor only considered important in membrane systems such as osmotic power and pressure retarded osmosis, where the critical factor is more the facilitation of a high water flux rather than a highly selective salt rejection. Since these processes frequently feature fluid flow from the support foam side of the membrane towards the selective layer, the

ability of water to move quickly through the foam and skin is important for good flux data. The structure parameter measures the structural resistance of the entirety of the membrane towards water flow, and this parameter also dictates the required performance of the membrane in terms of both salt rejection and water flux. It is calculated as shown below, in which t represents the thickness of the membrane, τ indicates tortuosity, D represents diffusivity and ε the porosity of the foam.[37]

$$S = \frac{\tau * t}{D * \varepsilon}$$

Given that C_f represents the concentration of a component in the feed, and Cp the concentration of that same component in the permeate stream, the percent rejection is calculated below, along with the percent salt flux or passage.

$$Salt\ Rejection = \left[\frac{C_f - C_p}{C_f}\right] * 100$$

$$Percent\ Salt\ Flux = 100 - Percent\ Rejection = \left(\frac{C_p}{C_f}\right) * 100$$

Concentration polarization in a given system is sometimes measured quantitatively in terms of Beta, a unitless number representing the ratio of a given ion concentration at the membrane surface to its concentration in the bulk feedwater. A higher Beta number indicates a greater probability of fouling or scaling on the membrane surface.[16]

1.5.3 Pre-treatment

Pre-treatment of feedwater is widely regarded as the most critical component of seawater RO plant design, due to the importance of minimizing fouling in order to optimize membrane performance and lifetime.[31, 38, 103-105] In particular, biofouling requires careful monitoring as the

short generation time of microbes results in rapid contamination of membranes. In monitoring the RO modules, care must also be taken not to add any unneeded chemicals or treatments as they may damage the membrane or simply cause extra expense both in their application and in their removal from the feed water. As the concentrations of individual feed water components can vary widely from one treatment facility to the next as well as through the months of the years, continuous monitoring of water quality and components is necessary for effective pre-treatment. The primary concern addressed with pre-treatment procedures is preventing fouling, and the main approaches consist of identifying and treating the most common types of scaling, particulates, organic material and microbial organisms which might propagate in the nutrient-rich environment provided by the first three components.[16, 106-109]

The proper pre-treatment procedures are usually determined through a combination of consistent feed water testing and monitoring of the level and types of fouling on the membranes observed before cleaning, as well as any components that may still be present in the permeate water. Pre-treatment testing involves identifying both cations and anions which may produce scaling, as well as variables such as dissolved oxygen which may contribute to microbial growth in the form of biofouling.[4, 16]

The pretreatment stage entails the addition of scale inhibitor and acid (typically sulfuric acid), which increase the solubility of partially insoluble salts (primarily calcium carbonate and magnesium hydroxide) that might precipitate and foul the membranes. The source water also is passed through a 5 to 20 μm cartridge to remove particulates that may also foul or damage the membrane. The removal of particulates is more critical for reverse osmosis than for membrane processes which remove larger contaminants. This is because RO uses a dense membrane rather than a porous filter, and therefore backwashing to flush any accumulated particulates will not be

effective for removing the fouling layer. Fouling is a significant concern in the development and design for RO systems for this reason, as significant particulate accumulation can quickly damage the system. Pre-treatment may also entail air flotation or sedimentation, or any number of filtration processes not including those described above.[14, 15, 31, 37]

In reverse osmosis as well as multistage flash and some other desalination processes, chlorine is frequently added at a dosage level of 1-2 ppm in order to deter biofouling. Due to the potential for rapid deterioration of the RO membrane, the chlorine is removed immediately prior to the actual treatment process by adding 2-8 ppm of sodium bisulfite or by means of UV treatment.[3, 29]

1.5.4 Membrane treatment

In the membrane process, the source water is passed through a series of modules containing the selective membranes for sodium and chlorine removal. A module design should feature safe operation under high operating pressures, ease of flushing and maintenance cleaning, minimal pressure drops, resistance to corrosion, and viability for long-term operation.[15] In membrane testing procedures and limited commercial applications, membranes are operated in dead-end filtration mode, in which feed water flow is normal to the membrane surface, requiring 100% conversion of feed water to permeate and rapidly producing a fouling cake layer. This mode is not viable for high-volume commercial applications, but does offer the advantage of a simple design and operation for evaluating new membranes. Commercial membrane separation almost always features cross-flow filtration, in which the feed water flows over the membrane surface rather than being pressurized directly against it. This design reduces opportunities for fouling as the pressure parallel to the membrane surface inhibits deposition and adhesion of particulates and microbes.[15, 16, 37]

While original membranes were developed in the flat sheet or so-called plate and frame configuration, this was an expensive and inefficient method of membrane separation. Modern modules typically use spiral-wound flat sheet membranes or hollow fibers. See Table 1-3 for a comparison of flat sheet, spiral-wound and hollow fiber element properties, and Figures 1-8 and 1-9 for an illustration of each type of module.

Table 1-3. Comparison of module types used in reverse osmosis.[15, 16]

Module Type	Advantages	Disadvantages	Fouling Potential	Cost	Notes
Flat sheet (plate and frame)	Limited fouling	Low surface area to volume ratio	Moderate	High	No longer used commercially
Spiral Wound	Easy to handle and clean, fouling resistant, widely available	Some concentration polarization, low recovery value Y	Moderate to high	Moderate	Mostly crosslinked polyamide composite
Hollow Fiber	High surface area to volume ratio	Fouling problematic, limited variety in supply	Extremely high	Moderate	Mostly cellulose Acetate or asymmetric aramids

Spiral-wound elements are produced from flat sheets of membrane, folded over a permeate stream space to produce a long envelope which is glued along both ends of its length such that it is only open on the feedwater end, and wound around a pipe to collect the product water. Feed water is introduced to the outside of this envelope and flows along its length, thus reducing fouling by maintaining pressure parallel rather than normal to the surface, and the concentrated brine is collected at the end of the envelope from the feedwater spacer.[5] Spiral wound elements have the advantage of being resistant to fouling due to the open feed channels, and are easy to clean when

fouling does impair performance. They are widely available, easy to handle and may be replaced without significant interruption to the overall system.[15]

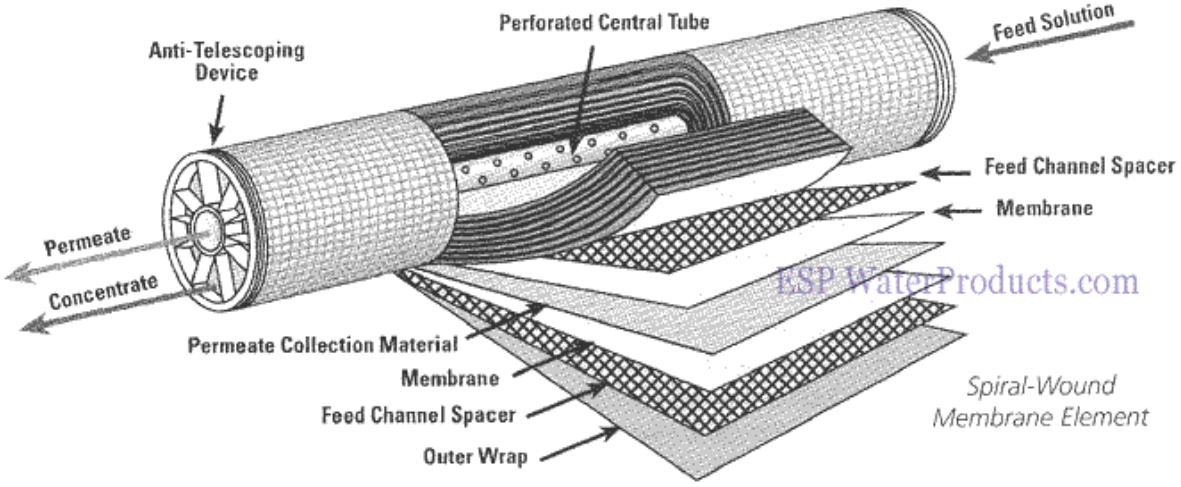

Figure 1-8. Illustration of a spiral-wound RO module.

Hollow fibers, also referred to as hollow fine-fiber elements (HFF) in order to distinguish them from the hollow fibers with a larger diameter used in microfiltration and ultrafiltration, are a module type where a bundle of hollow fibers are contained within the module element. Pressurized feed water is typically introduced via a pipe in the center of the element, and water passes radially from the outside of the hollow fibers toward the inside, where it flows outside of the module to be collected. In Figure 1-6, a schematic of the hollow fiber unit illustrates that the fibers feature both ends of the fibers fixed in the permeate-collecting side of the module, while at the opposite side, the folded bend of each fiber is held in place. Hollow fibers offer a much higher active surface area per module in comparison to spiral-wound elements, but are much more susceptible to fouling and feature a lower flux than spiral wound elements. During the treatment process, the membranes may require cleaning, either through chemical cleaning (to combat fouling) or backflushing the system (to remove scale and biofilms with or without the additional application of chemicals).[5]

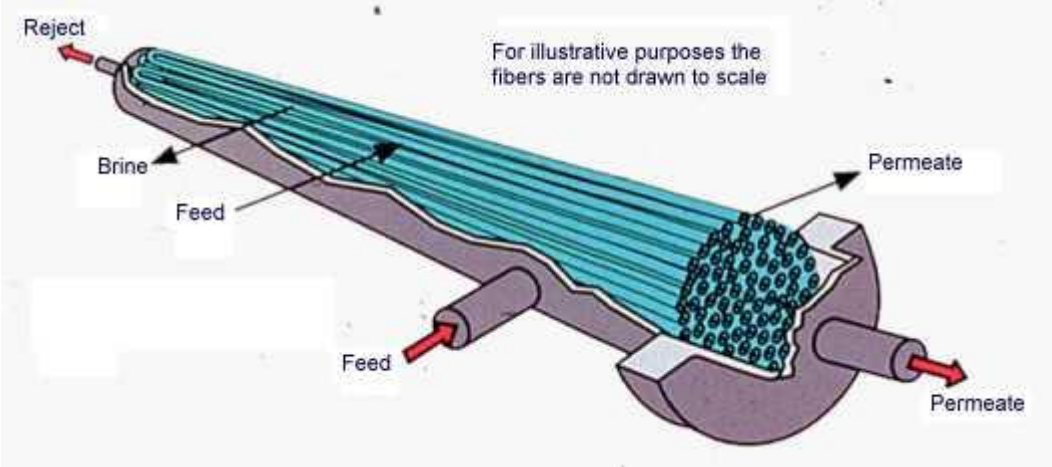

Figure 1-9. Schematic of a hollow fiber RO element.

1.5.5 Post-treatment

The post-treatment phase consists of chemical remediation and disinfection of the product water. This entails pH remediation, most commonly by elevating an overly acidic permeate with lime or sodium bicarbonate, as well as decarbonation or degasification of the treated water to remove carbon dioxide produced during the acidification process. This is necessary as membranes do not generally reject carbon dioxide and when allowed to remain in the product water it can contribute to excess acidity and/or deplete the anionic resin used in ion exchange treatment at the end of the post-treatment process.[15, 29] This is followed by the addition of disinfectants and stabilizing chemicals in order to ensure the water remains drinkable by the time it arrives at its intended location.[15] The most common additive is chlorine or a chlorine-containing compound, in order to deter microbial contamination. Another step frequently used is ion exchange, sometimes referred to as ion exchange polishing, for the removal of any residual ionic groups, boron or organic molecules that may still exist in the system.[15, 110-113]

1.6 Challenges in reverse osmosis

While the objective of reverse osmosis is relatively simple, the modeling and prediction of RO performance in a given membrane can be greatly hindered by the problem of fouling. While fouling is largely controlled by means of pre-treatment of the feed water, it remains an issue with even the most thorough pre-treatment procedure. Concentration polarization is an inherent problem in reverse osmosis and any membrane separation procedure, and can be a significant contributor to several categories of foulants. In addition, there are concerns of being able to remove dissolved contaminants other than monovalent and divalent salts, specifically boron, and these can offer distinct challenges to RO systems which are largely developed with the intent to exclude sodium, chloride, magnesium, and other major components of seawater. Another area of research is solutions to the problem of brine disposal, which is the primary issue prohibiting RO from being considered a more environmentally friendly option.

1.6.1 Fouling

Fouling is the decline in water flux due to the accumulation of solids on the membrane, particularly in the pores of a porous membrane or on a rough surface produced by a crosslinking process.[21] Internal fouling of the pores is effectively not a problem in RO membranes, and so for the purpose of this application only surface fouling will be discussed. These solids may consist of biological cultures of algae or other microbes, requiring treatment with chemicals which will not only kill but detach the cell walls or adhesive gels from the membrane surface without damaging it physically, or they may be scales of inorganic salts which have precipitated on the surface. The two primary complications caused by fouling are: an excessive operating pressure to maintain sufficient flux in spite of accumulated fouling layers, and an increased pressure drop between feed and permeate streams due to the barrier layer formed by fouling. These are both due to the decreased water flux since the fouling layer physically impedes the contact of feed water with the

membrane. Fouling can also decrease membrane performance by physically damaging the thin selective layer via abrasion or other mechanical degradation. Fouling is the primary problem in operating a sea water reverse osmosis (SWRO) facility, as it reduces module lifetimes and reduces flux while increasing maintenance costs.

While most fouling is partially reversible, there is generally a small amount of performance lost to irreversible fouling even with regular backflushing and chemical cleaning. Likewise, membrane modules will need to be replaced either due to irreversible fouling or membrane failure due to accumulated fouling. Fouling may also be minimized by the selection of membrane materials which are smoother or offer lower surface adhesion to fouling components. The development of surface treatments or novel materials which provide a greater resistance to fouling is a significant area of research today.[106, 114-121]

Concentration polarization is a frequent precursor to fouling cake formation, and occurs when both water flux and salt rejection decrease due to the higher concentration of rejected solutes near the membrane-permeate interface. Fouling can also reduce the rejection of trace contaminants other than the target salts.[122] There are four primary categories of fouling: suspended particulates, inorganic scale which precipitates from dissolved salts, organic material, and microbes which form colonies that grow rapidly in the presence of inorganic and organic components collected on the membrane surface.[37] The first three are largely preventable by proper pretreatment procedures and careful monitoring of feedwater composition, while biofouling requires both pretreatment and cleaning procedures in order to be properly controlled.

1.6.1.1 Suspended Particulates and Colloids

Suspended particulates such as silt and other largely inorganic solids present some physical hazard to RO membranes, and can effectively be removed by a pretreatment step of MF/UF, in which case they do not require remediation or cleaning during the RO treatment process. These particulates cover a wide range of sizes, from 10 nm to 10 μm, and may sometimes require filtration at several different scales to sufficiently reduce accumulation.[29]

The level of pretreatment to be included for a given system is determined by calculating the silt density index (SDI) for the feed water. The SDI test consists of filtering feedwater through a 0.45 mm microfiltration membrane at 30 psi, where an initial sample and a final sample are separated by a test time. The SDI is determined by the following equation, in which T_i represents the time to collect the initial sample of 500 mL, T_f represents the time to collect the second sample of the same size, and T_t represents the total time required for the experiment.[19]

$$SDI = \frac{100(1 - {T_i}/{T_f})}{T_t}$$

A very low SDI of less than 1 indicates that no pretreatment step is necessary and that the system may run for several years without cleaning, and SDI values of up to 3 indicate that more frequent cleaning is necessary but still cost effective. In the range of 3-5 indicates that either frequent cleaning or moderate pretreatment is necessary, and above 5 there must be sufficient pretreatment steps to reduce to the SDI of the feedwater before it encounters the RO module.[19]

1.6.1.2 Inorganic Scale

Poorly soluble inorganic salts are prone to precipitating and forming scale during the reverse osmosis process. This is particularly pronounced in systems with a high level of recovery and therefore a high degree of feedwater concentration, as well as systems with significant

concentration polarization problems. Scale is normally well-controlled in the RO system if there is sufficient monitoring of feedwater quality and proper pre-treatment procedures and chemicals.[15, 123, 124]

Calcium carbonate and to a lesser degree, calcium sulfate, phosphate, and silica species are the primary culprits in fouling from the precipitation of inorganic scale. This is less of a problem in seawater RO than it is in brackish water RO, due to the lower recovery available in SWRO which prevents precipitation during concentration polarization.[4]

Scale accumulation occurs in three stages, the first two of which are reversible. First, the organization of cations and anions into loose associations, followed by the nucleation and alignment of ionic groups as ions move closer to each other; and finally the precipitation and growth of salt crystals around the nuclei.[4] Scale is prevented by the addition of antiscalant compounds during pre-treatment. The use of antiscalant requires some caution, however, as they are both expensive and when used excessively can contribute to fouling themselves, particularly in the presence of other non-target contaminants. When pretreatment has not been sufficient to prevent scale accumulation on membranes, a combination of acidic and basic cleaning chemicals may be used to remove the accumulation.[29, 125-130]

1.6.1.3 Organic Material

Organic material is primarily an issue in RO treatment of wastewater, due to the high levels of organic particulate contaminants. Organic foulants, which consists mostly of humic acids, decomposed organisms and waste products, are sometimes referred to categorically as natural organic matter (NOM). Pretreatment with flocculation and microfiltration or ultrafiltration is usually sufficient to prevent significant performance loss, and in the event of caked accumulation

it can be reversed by backwashing. NOM contributes to fouling both directly by forming cakes of material on the membrane surface and by providing a source of nutrients for the more significant problem of biofouling by microorganisms. Hydrophobic membrane surfaces are more favorable for NOM adsorption, and so investigation of more hydrophilic surfaces as a means of avoiding both NOM fouling and biofouling is an area of investigation for combating the problem of fouling.[131-134]

1.6.1.4 Biofouling

Biofouling is the most challenging type of fouling to prevent and remove, as given an environment with sufficient nutrients; a single microorganism can rapidly form a large colony. Biofouling microorganisms tend to be oligotrophs, or organisms which are specifically adapted to thriving in an environment where few nutrients are available. While sufficient monitoring and pretreatment of the first three types of fouling will help limit biofouling, the cleaning steps required during occasional maintenance service are largely focused on maximum removal of microbial colonies on the membrane surface. Biofouling is controlled or minimized by water pretreatment, through microfiltration and ultrafiltration, by the addition of antimicrobial chemicals to the feedstream, and by the development of fouling-resistant membranes.[135] It is much more difficult to remove a microbe or young colony which has already adhered to the membrane surface than it is to deter adhesion prior to any form of attachment, particularly as even a small colony forms a gel-like area to which other foulants may easily adhere and serve as nutrients for further growth. A colony may become irreversibly adhered after several days.[15, 16, 106-108]

Biofouling consists of microbes which have accumulated on and attached to the surface, and a gel-like biopolymer slime produced by the bacteria. This slime may be referred to as the glycocalyx, slime layer, capsule, or extracellular polymeric substance (EPS). It has been argued

that the bulk of flux decline due to biofouling is caused by the EPS rather than the accumulated bacteria.[5, 14] The primary method of preventing biofouling is adding chlorine as a biocide, but in the two primary commercial membranes, cellulose acetate and crosslinked polyamide, chlorine causes chemical degradation of the polymer and loss of performance. Therefore, chlorine must be removed from the feed water prior to exposure to the membrane. Chlorine removes the EPS before actually damaging the microbial colonies, and microbes secrete additional EPS in response to ambient chlorine.[15]

In the presence of biocide, microbial colonies may be dead or greatly reduced in living numbers, yet still present a physical barrier to water flux and an adhesive mass where other nonliving foulants may become lodged. Ozone is another biocide which is more versatile than chlorine and almost as effective, yet still may pose an indirect risk to chlorine-sensitive materials as it may oxidize bromide present in the seawater feed, which may undergo a similar but slower reaction with polyamides.[15]

Surface treatments predominate over the evaluation of new materials in the literature, as biofouling is more easily avoided by the inclusion of more hydrophilic components in or on the membrane surface. Finding a new material that is competitive with commercial membranes is more difficult. Developing biofouling resistance has been studied primarily by surface treatments which modify the very upper portion of the selective layer, or by polymerizing a thin layer of low hydraulic-resistance hydrophilic material such as poly(ethylene glycol) on top of the selective layer.[62, 136-141]

Another objective is the formation of a smoother membrane surface. A rougher topology is created during the crosslinking of the aromatic polyamides most frequently used in commercial

modules, which can provide a larger surface area for foulants to lodge. On rough surfaces, the initial microbes may adhere themselves and be relatively sheltered from the shear force of the pressurized feedstream.[142] In forward osmosis and pressure retarded osmosis membranes, fouling is a less significant concern but new materials in the support layer or across the asymmetric layer are still of interest.[60, 62, 143]

1.6.2 Concentration Polarization

Concentration polarization is an obstacle in reverse osmosis caused by the disparity between the rate of convective flow in the feedwater, and the much lower rate of diffusive flow of water molecules across the thickness of the membrane. As feed water moves along the length of a module bordered by two active membrane surfaces, there is a boundary layer at either surface where the flow is slower and less mixed. This is shown for one surface in Figure 1-10, in which C_s, bulk represents the concentration of the solute in the bulk phase of the feed, $C_{s,0}$ represents the elevated concentration near the membrane surface, and $C_{s,l}$ represents the concentration of the permeate. Due to the high level of ion rejection and low level of fluid movement, the boundary layer next to the membrane surface features a much higher concentration of the dissolved solute(s) than that of the bulk feedwater. Concentration polarization impedes performance of the reverse osmosis membrane by not only providing physical obstruction to feedwater flow, but also by increasing the osmotic pressure π. This reduces the driving force for producing water flux, and sometimes increases the flux of ions across the membrane.[16, 29]

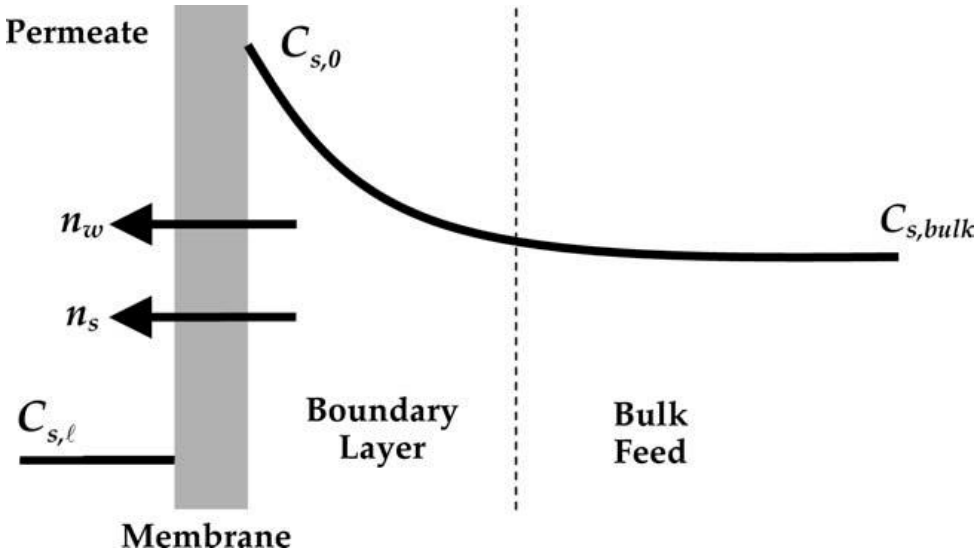

Figure 1-10. Illustration of concentration polarization.[10]

Concentration polarization can result in either a decreased water flux due to a disrupted water gradient near the membrane surface, decreased salt rejection due to an increased ion gradient, or both. Concentration polarization can with time also produce gels or cakes from precipitated or agglomerated species of foulants as discussed previously.[144] Aside from careful pre-treatment of the feed water and regular testing and inspection of RO modules, concentration polarization can be minimized by good mixing of the feed solution and a high velocity parallel to the surface to disrupt accumulated solute.[3]

1.6.3 Removal of heavy metals

In some regions, water which is technically fresh (less than 1000 ppm TDS) may still not be drinkable due to heavy lead, arsenate, or other heavy metal content.[145-149] In this case, materials with a high selectivity towards heavy metals are of interest for producing potable water or for remediation of industrial wastewater prior to discharge.[150, 151] While research in this area has not

received the same level of attention as the desalination of freshwater and brackish water, as more areas become water stressed, there may be increased reliance on underground sources that may be contaminated, and as more industrial pollution occurs, it is likely to be an important area of development for future research. Arsenic III and V in particular are contaminants of concern that have been investigated with conventional RO membranes, with the more promising rejection values at higher pH levels.[147]

1.6.4 Removal of boron

Boron, which generally is found in seawater in the form of boric acid, presents a unique challenge for membrane separations research. While boron at very low levels is beneficial and possibly essential for humans, it frequently occurs in higher levels in both seawater and brackish water that exceed WHO standards and is considered detrimental to human health. Boron is difficult to remove via membrane separations due to the resistance of boron compounds to forming ions unless they are in an alkaline environment. While raising the pH does allow for practical boron removal, additional problems are created by causing increased fouling via precipitated magnesium and calcium salts, and the pH must be lowered again to be fit for human consumption.[144, 152]

Boron removal, particularly in older RO facilities, generally entail repeated passes through RO modules which decreases productivity and increases operations cost. After many years of poor results, there are some initial reports of single-pass boron rejection exceeding 90%. Research is ongoing to find a practical solution to removing boron, although some efforts suggest that the most cost-effective solution at present may entail passing product water through an ion exchange unit tailored specifically for boron removal.[49, 110, 153]

1.6.5 Sustainable power use

Historically RO plants have been driven using power derived from the surrounding energy grid. However, due to increasing concerns over the cost and availability of conventional energy sources there are growing interests in research to provide clean water using alternative energies with low or no environmental impact and a limitless, if interrupted energy supply. This frequently involves design plans which integrate solar, hydroelectric, biomass, geothermal and/or wind supplies with or in place of conventional fossil fuel energy sources. In order to maximize the production capacity of these sources, there is also research into further improving the efficiency of elements in the reverse osmosis process (i.e. pumping and energy recovery from heated output water), although the membrane treatment process itself is already closely approaching its theoretical minimum efficiency.[1, 57] Investigative studies into the possibility of combined alternative energy and desalination technologies emphasize the long-term nature of these investments, but the inevitable increase in the cost of fossil fuel-based energy requires a thorough investigation into future alternatives.[31, 50, 154]

Solar energy has been a strong historical energy source for the desalination of water, either by harnessing it directly for purification via distillation or for the conversion from thermal to electrical energy in order to drive a membrane process. In regions which receive high levels of sunlight, passive solar energy is already used in part of the waste disposal procedure to evaporate residual water from the produced brine in order to produce sea salt, as well as integrating solar energy panels to supplement plant energy costs.[69, 155-157]

Wind energy is another favorable renewable energy source for supporting RO plants, as there is a great potential for the coincident development of offshore wind farms, which could power in part or entirety a seawater desalination plant. Some initial studies have indicated that the most

feasible option under current circumstances is using a wind farm as back power support for a plant which draws most of its energy from conventional sources.[31]

Wave energy is also a convenient energy source for an RO plant, as both would be conveniently located for immediate energy use. Wave energy also offers the advantage of being consistent and predictable in timing, due to its dependency on the tides. Hydrostatic pressure is not an energy source, but it is possible to reduce the energy costs of submarine RO units by using the pressure of surrounding seawater. This saves energy both by eliminating the energetic demand of pumping in feedwater and by using the hydrostatic pressure to drive the production of freshwater at atmospheric pressure.[31, 158]

1.6.6 Brine Disposal

One of the ongoing challenging in the establishment of SWRO as a viable water production technology is addressing the environmental impact of brine disposal, which has been a challenge since the first desalination plants were constructed. Brine is not only an environmental hazard due to its high salinity, but also due to the introduction of pretreatment chemicals, cleaning chemicals, and other contaminants which may be incurred during the desalination process. While the environmental impact is considered to be detrimental, the precise impact on seawater quality and local ecology is not well studied and requires further investigation. A number of ideas for brine disposal have been proposed, including dilution with treated wastewater, transport and dilution far offshore, injection into empty mines, and potential commercial applications from evaporated brine. The primary solutions currently used for desalination plants include dilution with industrial wastewater, conversion to sea salt in on-land evaporation ponds, and offshore dilution into ocean waters.[159-161]

One promising candidate for resolving the brine disposal issue is the construction of a hybrid FO/SWRO plant as discussed previously in Section 1.4.7. This not only provides a means of diluting and recycling brine, but also provides a preliminary pass for removing boron and other solutes which are challenging to separate at high levels. However, it is a limited solution as practically speaking, since only part of the brine can be added to the feedwater, and so some must still be disposed of safely.[57]

1.7 Membranes and composites used in reverse osmosis and osmotic power

1.7.1 Materials used in reverse osmosis

The high pressures, threat of biological and chemical degradation, and high performance standards for reverse osmosis membranes provide a very demanding environment for the materials used in these membranes. An ideal membrane features high water flux, high salt rejection, resistance to chlorine and other oxidizing chemicals, resistance to biological attack and fouling, resistance to fouling by colloids and suspended materials, resistance to compaction during use, a low cost of synthesis and fabrication, ease of fabrication into thin films, asymmetric membranes or hollow fibers, good mechanical properties, chemical and hydrolytic stability, and tolerance of high temperatures. While no membrane yet features all of these qualities, several exist with specific advantages for different applications. While no novel membranes have entered the commercial market in several decades, investigations are ongoing in the development of new materials that may overcome the advantages of the current commercial membranes, primarily in the areas of improved transport behavior and increased fouling resistance.[5, 14, 15]

Most modern reverse osmosis RO systems utilize either an asymmetric membrane or a thin film composite, or TFC. The thin film composite consists of a polysulfone foam supported by a

tough nonwoven fabric, generally polyester, for mechanical strength. On the foam support, a a thin film of cellulose acetate (CA) or interfacially polymerized crosslinked aromatic polyamide (CPA) serves as the selective layer. The TFC was first developed in the early 1980s by FilmTec Corporation, which is presently a part of Dow Chemical Company, and Fluid Systems, which is now a part of Koch Membrane Systems.[14]

1.7.1.1 Cellulose Acetate

Cellulose acetate films were initially invented in 1960 by Loeb and Sourirajan.[162] CA films are typically asymmetric membranes produced from cellulose diacetate, cellulose triacetate, or a blend of the two membranes. They have a dense layer thickness of 0.2-0.3 μm and an overall membrane thickness of about 100 μm, and are supported by a highly porous substrate. Their primary advantage are a low materials cost and easy availability, and a greater tolerance to minor chlorine exposure than their crosslinked polyamide competitors. Their comparatively smooth surface offers some resistance to the adhesion of fouling. However, they are vulnerable to compaction, which results in the flux that is lower than polyamide membranes, in part due to the thicker selective layer. More critically, chemical and biological degradation can occur over their performance lifetime, which may be shortened at high or low pH levels or high temperatures.[16]

Cellulose acetate asymmetric membranes can operate continuously at pH levels ranging from 4.0 to 6.5 and up to 30°C, which is slightly cooler than what crosslinked polyamides can tolerate. This is important due to the increase in membrane flux and overall capacity with elevated temperature. They were primarily used during the early development of reverse osmosis systems, but have become less common with the invention of crosslinked polyamide. Currently CA hollow fibers occupy less than 10% of the RO/NF market, largely by virtue of their chlorine tolerance and lower cost. They are also more frequently found in brackish water desalination systems.[14, 20, 49]

1.7.1.2 Crosslinked polyamide

Crosslinked polyamide (CPA) films are the predominant commercial RO material in use at present, occupying over 90% of the RO/NF market.[49] Primarily used in TFC membranes in the late 1980s, CPA shows improved salt rejection over the CA films, with a steady improvement in flux over the following decade of development.[20] Although they have a greater stability over a wider pH range and are resistant to biological degradation, they are very sensitive to degradation by chlorine, and are ideally not used at temperatures higher than 45 ^{o}C.[5, 14, 163, 164] The increased surface roughness due to the crosslinking reaction provides greater surface area for adsorption of water, but also create dead zones where foulants may easily accumulate without being disturbed by the feedwater flow.[16] Due to a much thinner selective layer (40-100 nm) than CA membranes, CPA-based films require a lower operating pressure in order to achieve a satisfactory water flux. Research into polyamide materials which may be more tolerant of small amounts of chlorine exposure has yielded some results, but nothing which has been adopted to replace the CPA standard.[165]

1.7.1.3 Alternative membranes and materials for SWRO

Although the CA and CPA films comprise most of the commercial market, there are investigations underway to develop alternative materials. One approach is to interfacially polymerize a copolymer with polyamide, such as polyurea or polyurethane in a thin film composite (TFC) with the intent of obtaining a higher salt rejection and higher fouling resistance.[166, 167] Other approaches have included the incorporation of lyotropic liquid crystals (LLCs), carbon nanotubes, or nanoparticles in a polymer membrane in order to offer improved fouling, flux and rejection characteristics, but these membranes have not yet shown commercial viability.[16, 4930]

Alternative polymers investigated for RO applications include aromatic systems such as sulfonated polysulfones and sulfonated poly(ether ether ketones) and related materials, which offer advantages in chemical resistance and mechanical properties.[168, 169] Other materials such as polyureas and sulfonated polyethers are under commercial development by Nitto Denko.[15] Surface modification techniques for both conventional and novel membrane materials are also under investigation in order to augment chlorine resistance, water permeability, and fouling resistance.[65, 142, 170-172]

1.7.2 Materials used in pressure retarded osmosis/forward osmosis

Due to the lower pressures used in osmotic power, a greater tolerance is available for the construction of osmotic power membranes in terms of accepting a lower salt rejection so long as the membrane provides a higher flux. The membrane can also be less resistant to compaction and less tolerant of fouling, given some offset advantage in another property, as the direction of flow from low to high concentration provides less opportunity for fouling. As forward osmosis is a developing technology, the same CA and CPA membrane materials which are used in reverse osmosis are used in FO, although other materials are being explored. Unlike RO membranes, potential FO candidates do not need to show the same resistance to oxidizing agents and will be exposed to lower pressures, allowing for greater flexibility in both membrane composition and thickness.[57, 70, 173] This has resulted in the exploration of polybenzimidazoles and polyamide-imides with specific PRO-FO applications.[64, 174, 175]

An additional topic of research which is more of interest in osmotic power applications due to the hazard of internal concentration polarization is the development of a hydrophilic support with a thinner layer, resulting in a lower S or Structure parameter. As a lower S parameter results

in reduced internal concentration polarization, sulfonated materials are of interest in forming these support layers, either for a thin film composite or asymmetric composite.[64, 87, 176-178]

1.7.3 Asymmetric membranes and Thin Film Composites

Due to ongoing competition to increase production of drinkable water, even dense membranes with excellent water permeability are generally insufficient for commercial use. They are studied in the early stages of research to determine a given material's transport and rejection properties, but at the commercial level these materials may be fabricated into thin film composites (TFCs) or asymmetric membranes (ASMs). This hybrid structure allows for an increased flux due to a thinner selective layer while maintaining ideal salt rejection values. The structures of dense membranes, thin film composites, asymmetrical membranes, as well as the microporous isotropic membrane used in microfiltration, ultrafiltration, and in support foams are illustrated in Figure 1-11. While currently TFCs are the primary option for SWRO modules, ASMs are still used in some niche applications. Both types of membranes are used in other related membranes separations processes, such as pervaporation, forward osmosis, and gas separations.[29]

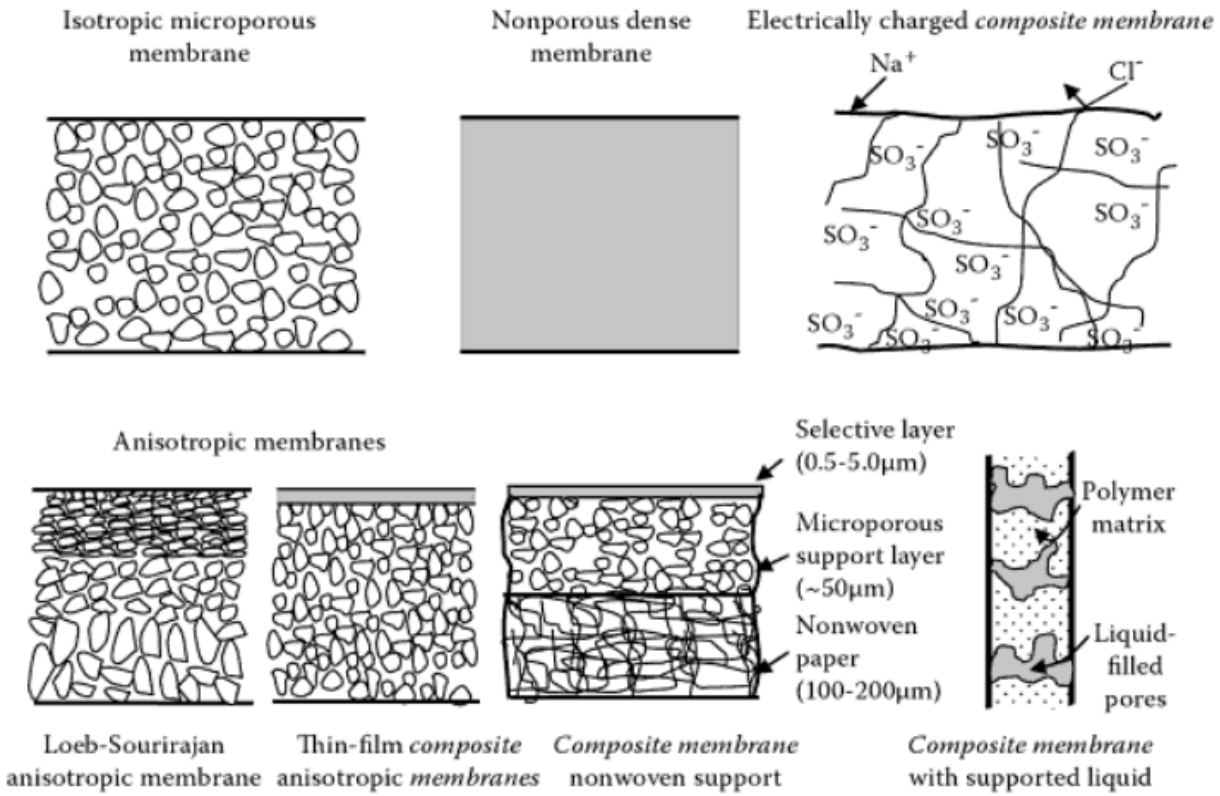

Figure 1-11. Comparison of membrane structures used in different separations processes.[19]

Thin film composites (TFCs) are comprised of three layers, generally made from three different polymers: a highly porous hydrophobic nonwoven paper (120-150 μm thick) for mechanical support (generally polyester), a porous, isotropic or anisotropic foam (40-60 μm thick) for direct mechanical support of the selective layer (polysulfone), and the selective layer itself (cellulose acetate or a crosslinked polyamide), which is typically 200 nm thick.[49] The selective layer is most often applied by interfacial polymerization on top of the support foam, but also by solution casting or plasma polymerization.[29] This composite system offers several advantages, most notably that it is able to withstand significant pressures during RO operations. It also allows

for selection of different materials to optimize performance in the support foam as well as the selective layer. Unfortunately, the complex multilayered structure and specifically its hydrophobic components result in a lowered permeability and diminished structure factor.[3]

A simpler version of the TFC, and the first of the two to be developed, is the asymmetric membrane which consists of two layers: the selective layer, generally less than one micrometer in thickness, and the substantially thicker supportive foam layer of 50-100 microns, which provides mechanical strength. The foam layer may occasionally feature an isotropic foam structure, where pore size is largely uniform from the top to the bottom of the foam layer, but more frequently it features a gradient where pores become larger and more open (sometimes referred to as a scaffold structure) moving away from the skin layer. These two components are made from the same copolymer source and are fabricated simultaneously using phase inversion.[14, 15]

The primary limitations of asymmetrical membranes are due to their source material. For example, cellulose acetate and related materials commonly used in commercial asymmetric membranes today face short lifetimes due to hydrolysis, which is more rapid at elevated temperatures and pH levels outside of 4.5-6.5. However, all asymmetric membranes tend to suffer from a loss of flux due to compaction in the support foam layer, as well as the concern of screening out pinholes and other flaws during fabrication. However, due to the simpler production and uniformly hydrophilic composition of the membrane material, an asymmetric membrane offers the advantage of a competitive structure factor and a potentially increased flux over a thin film composite of comparable dimensions.[14, 20, 37]

1.7.4 Phase inversion

Asymmetric membranes are produced by the phase inversion of a polymer solution. Phase inversion can be performed using a variety of techniques, including thermal inversion and vapor phase inversion, but the primary method used in RO membranes and to be discussed here is that of nonsolvent immersion, also called immersion precipitation, which entails the submersion of a thin film of polymer solution into a bath of nonsolvent liquid.[19, 162, 179]

The immersion causes very rapid precipitation of the polymer from the top (skin) layer downwards, and the single-phase polymer solution becomes a two-phase solid, the polymer-rich dense skin layer and the polymer-poor support foam. Because the formation of the ASM depends on the kinetics of solvent and nonsolvent transport as well as the thermodynamics of the solution itself, being able to produce and reproduce ASMs of a desired structure is difficult. While there are models and trends for the overall process, working with a given material and solvent/nonsolvent system requires extensive empirical work rather than mathematical predictions. The following discussion will address the phase separation process both from the stages of precipitation, and from the impact of the precipitation kinetics on the final membrane structure.[19, 29]

Phase inversion via precipitation immersion, also referred to as the Loeb-Sourirajan process, first takes place by means of spreading out a thin layer of polymer solution on a casting surface. This solution is allowed to stand undisturbed for a period of time ranging from several seconds to several minutes, during which solvent evaporation from the top of the solution creates a higher polymer concentration region in what will shortly become the polymer-rich phase of the ASM. After this wait time, the solution is immersed in nonsolvent (typically water), and the precipitation commences. Skin thickness and coherence are strongly influenced by polymer

concentration, evaporation time, solution and air temperatures as well as the volatility of the selected solvent.[16, 180]

While the process of developing a phase inversion protocol is largely empirical and requires a lengthy period of trial and error, there are several guidelines provided by Baker in *Membrane Technology and Applications* that may be of use. The first guideline is that the polymer being used is amorphous and tough, and has a high molecular weight, preferably at least 40,000 g/mol. Polymers which are semi-crystalline or rigid glasses will be too brittle after casting and susceptible to failure during processing. The solvent used is ideally an aprotic solvent with a high solubility in water (the most common nonsolvent used in phase inversion), such as dimethyl formamide, dimethyl acetamide, and *N*-methyl pyrrolidone. These solvents will dissolve a wide range of polymers and when immersed, tend to provide an anisotropic membrane with a good porosity and pore gradient. The ideal nonsolvent is water, not only for affordability and convenience but because membranes of comparable material cast in organic nonsolvents such as acetone or isopropanol have a tendency to show lower fluxes and greater membrane density. In the situation of a material where water is not a good nonsolvent, some adjustments can be made. The temperature of the nonsolvent also strongly affects ASM structure and performance, which in the case of water a reduced temperature produces lower flux and improved salt rejection.[19, 181]

According to Baker and Wang *et al.,* during the phase inversion process there are four distinct regions of polymer phases, as indicated by their region number in Figure 12: Region I is the single-phase polymer solution prior to any precipitation. The time spent going from the single-solution phase to the liquid-liquid two-phase solution in Region II is called the delay time, and it is the precursor to the precipitation of the solid polymer. Region II consists of two liquid solutions, one which is polymer-rich and will form the polymer skin, and the other which features a more

dilute polymer concentration. Region IV consists of a glassy polymer with small components of solvent, and is not typically part of a successful phase-inversion process.[19, 29]

The boundary between the two regions is termed the binodal boundary, and C is the C-point, or the "critical coagulation point", which is the ceiling concentration of solvent in a nonsolvent bath that will still precipitate a solid polymer. For the fabrication of asymmetrical membranes with good mechanical strength, the nonsolvent concentration must exceed C in the nonsolvent bath, as it is the boundary between having two liquid solution phases and merely having a highly swollen polymer gel. That point sets one end of the gelation boundary between the C-point and point B, which refers to the so-called Berghmans' point. The Berghmans' point is located at the intersection of the swelling boundary and the gelation boundary, and indicates the point of vitrification of the polymer-rich phase.[19, 29]

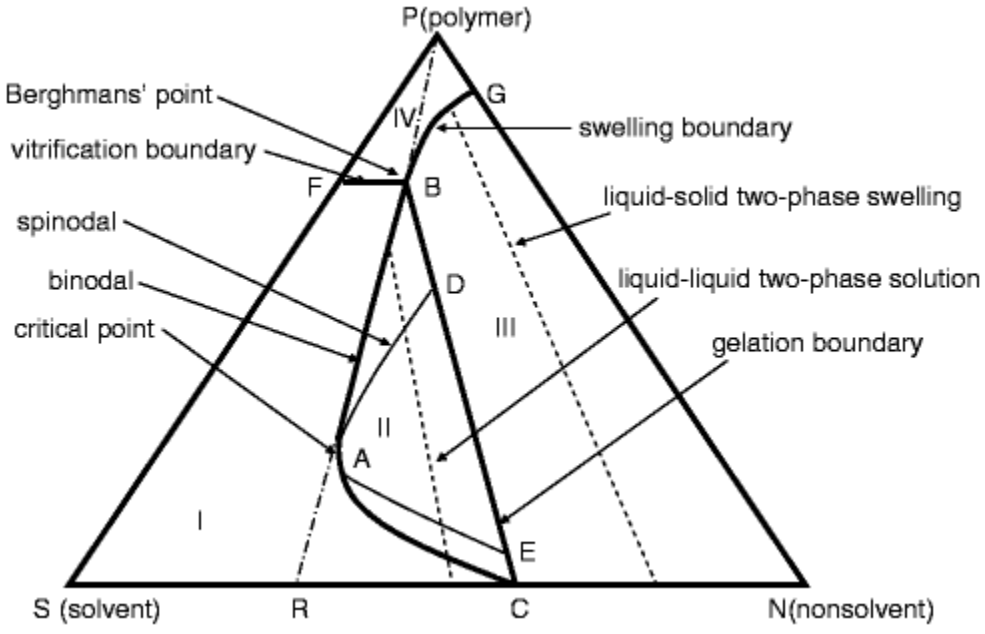

Figure 1-12. Three-phase system describing precipitation inversion for producing asymmetric membranes.[19, 29]

Within Region II, there are lines indicating binodal and spinodal curves, and it should be noted that compositions between the spinodal line and the gelation boundary will be unstable, and that the final porous membrane formed from those compositions will lack mechanical integrity. Those compositions which fall between the binodal and spinodal curves are considered metastable and therefore able to withstand small stresses while in transition to the final, more stable structure. This may be visualized in practice by precipitating a low-concentration solution and a high-concentration solution. If the former is sufficiently dilute, it will precipitate in the unstable region below the critical point and upon drying, producing a brittle polymer that fragments upon handling. Region III indicates the onset of physical precipitation of the polymer-rich phase into a swollen solid polymer, and the polymer-poor phase becomes a mixed-liquid system of both solvent and nonsolvent. Region IV represents the final and fixed phase of entirely solid polymer, with a vitrified skin layer and swollen foam support.[19, 29]

While the boundaries illustrated in Figure 1-12 are useful for a qualitative understanding of phase relationships and the immersion precipitation process, they can be quantified and described mathematically. An important part of initial evaluations of polymer/solvent/nonsolvent systems is the determination of cloud point correlations. Cloud points are determined by adding small amounts of nonsolvent to a polymer solution and recording the point at which the solution remains cloudy after stirring, indicating the approach of precipitation as the polymer is no longer entirely soluble. These cloud points can be used to qualitatively approximate the phase boundaries for a given polymer-solvent-nonsolvent mixture and phase inversion process.[19, 29]

When considering the impact of kinetics on phase separation as depicted in Figure 1-13, the interplay both between the rates of diffusion of the nonsolvent and the solvent are important for the final membrane structure. The precipitation of the polymer-poor phase below the initially

precipitated skin, or polymer-rich phase, will inevitably be a slower process as both solvent and nonsolvent must be transported by diffusion across an increasingly solidified polymer skin. The lag behind the skin precipitation is dependent on the speed at which the polymer-rich phase precipitates, which may range from near-instantaneous to a full minute. For good physical integrity of the asymmetric membrane, it is critical that both phases of the solution remain above the critical point of the phase diagram.[19, 29]

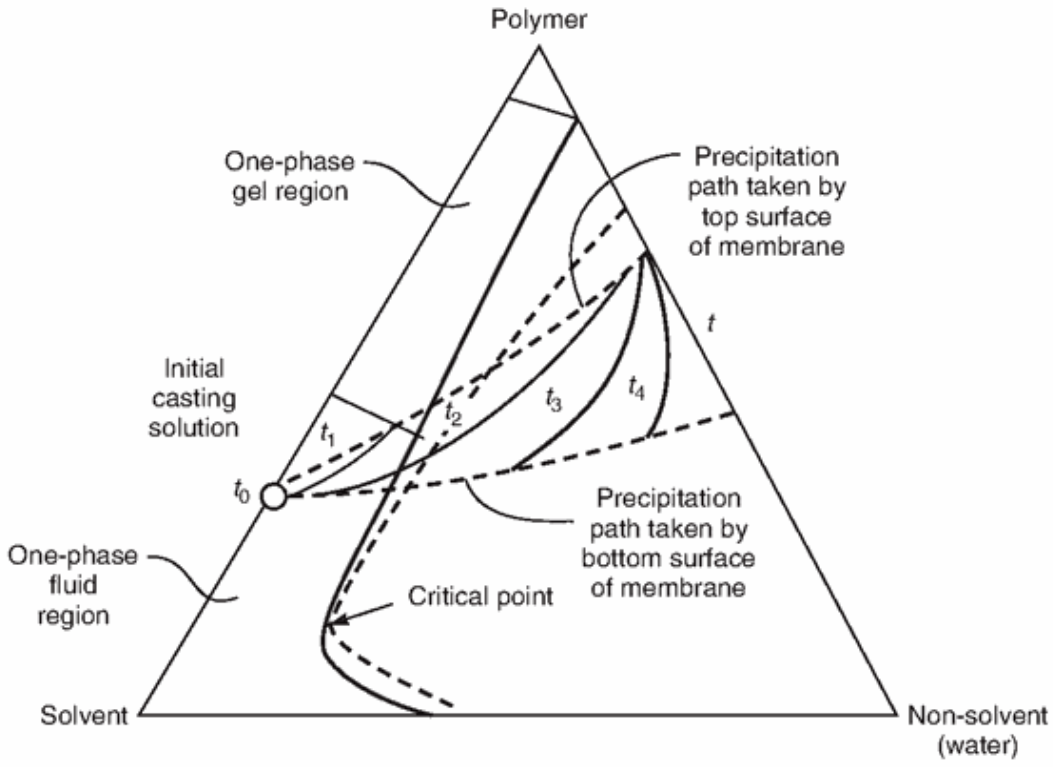

Figure 1-13. Depiction of the development of the polymer-rich and polymer-poor phases of the asymmetric membrane during fabrication. [19, 29]

While there are many variables impacting the structure of the resulting foam and the ASM thickness, as well as the presence and abundance of voids in the foam, the overall procedure is qualitatively well-represented by the above figures. With thorough empirical data quantitative

phase diagrams may also be constructed and used efficiently to optimize a phase inversion process. Tie lines are established in the three-phase balance between polymer, solvent and nonsolvent. The inclusion of additives in the nonsolvent bath is a frequent tactic to shift the point of precipitation, which requires the construction of a second diagram or simple empirical study in order to determine the optimum concentration for the desired impact on the phase separation process. [19, 29]

1.7.5 ASM finishing techniques

The phase separation process is an effective way to produce a selective membrane structure from a single material in a simple and efficient manner, although producing a defect-free membrane is a challenge. To resolve any pinholes that may have formed, the membrane goes through an annealing step post-production, by submerging into a high temperature bath, with the exact conditions depending on the chemical structure of the membrane. This step causes small pores and pinholes to collapse as the membrane approaches its hydrated glass transition temperature, however it also causes thickening of the selective layer through the collapse of the narrower end of the pore gradient, which is next to the skin layer.[182, 183] This reduces the flux of the membrane and so is applied carefully. [19, 29]

In asymmetric membranes cast for gas separation, pinholes are sometimes resolved by the introduction of what is termed a ‘gutter layer’ which is the application of a very thin layer of highly permeable material over the selective layer of the ASM. While the gutter layer still permits the easy and rapid passage of both the desired permeate and the components which are ideally excluded, it does provide a barrier to the fluid flow behavior of the undesired components. Likewise, it greatly improves rejection behavior in the event of one or several pinholes in the membrane.

1.8 Sulfonated poly(arylene ether sulfone)s and membrane separations

1.8.1 Sulfonated poly(arylene ether sulfone)s

The poly(arylene ether) (PAES) family, typically with sulfonic acid derivatization, have been explored in the literature as promising reverse osmosis membrane candidates, due to their excellent mechanical properties and good chlorine resistance. Poly(arylene ether) copolymers are encompass a range of related materials that have been investigated for possible use in reverse osmosis and other membrane separations processes, including poly(arylene ether sulfones)s, poly(arylene ether ketone)s, poly(arylene ether ether ketone)s, poly(ether ketone)s and other copolymers. Nonsulfonated and sulfonated bisphenol-A and 4,4'-biphenol based poly(arylene ether sulfone)s and related materials have been investigated in a variety of other membrane applications, such as proton exchange membrane fuel cells (PEMFCs),[184, 185] ultrafiltration,[186-188] nanofiltration,[189-191] and gas separation.[192]

Of the materials available in the poly(arylene ether) material family, PAES materials show superior thermal stability due to the resonance structure afforded by the sulfone group and the high oxidation state of the sulfur atom, which may allow for melt processability at up to 400°C in non-ion-containing copolymers.[193] The flexible ether linkages allow for reduced material rigidity, and the mechanical properties and ion selectivity may be tailored by incorporating different functional groups into the polymer backbone. In applications where partially sulfonated PAES copolymers may offer advantages from both hydrophilic and hydrophobic phases, a synthetic approach employing the synthesis of a multiblock copolymer or crosslinked copolymer may offer optimal tailoring of membrane properties, i.e. improved salt rejection.[194-196] While the adaptation of multiblock partially sulfonated PAES copolymers to reverse osmosis applications is in the

relatively early stages, some generalizations may be made from the extensive research which has been performed in the field of proton exchange membranes for fuel cells.

1.8.2 Post-sulfonated poly(arylene ether sulfone)s and reverse osmosis

The nonsulfonated poly(arylene ether sulfone)s (PAESs)have been used for some time as the foam support in thin film composite membranes, as well as compaction-resistant porous membranes for use in ultrafiltration and microfiltration. Research was performed in the 1980s on post-sulfonated Udel ®, which was sulfonated after polymerization using fuming sulfuric acid or chlorosulfonic acid, and its applicability as a selective membrane for reverse osmosis.[169] The post-sulfonated polysulfone was studied both as a dense membrane and as an asymmetric membrane, although producing void-free and defect-free films was problematic.[196]

While the sulfonated polysulfones showed good potential, particularly for their tolerance to chlorine exposure necessary for disinfection as well as for expected resistance to fouling, the difficulty in tailoring the molecular weight and degree of sulfonation discouraged further research for several decades. Asymmetric membranes cast from post-sulfonated polysulfones and polyethersulfones have also been evaluated for use in nanofiltration and pervaporation, with some promising performances but voids may form in the foam structure that detract from ASM mechanical stability.[197, 198]

A possible alternative to the post-sulfonated PAES materials lies in polymers containing small amounts of hydroquinone units. John Rose demonstrated that in poly(phenylene ether sulfone)s, poly(phenylene ether ether sulfone)s and related polymers, monosulfonation of a hydroquinone co-monomer could be obtained exclusively without modification of the rest of the

polymer chain by dissolving in and reacting with sulfuric acid. This modification may provide a novel alternative material for reverse osmosis applications.[199-202]

1.8.3 Directly copolymerized sulfonated poly(arylene ether sulfone)s and reverse osmosis

With the development in the early 2000s of sulfonated poly(arylene ether sulfone)s from the direct copolymerization of the sulfonated monomer, 3,3'-disulfonated, 4,4'dichlorodiphenyl sulfone (SDCDPS), 4,4'dichlorodiphenyl sulfone (DCDPS), and biphenol, a greater degree of chemical stability as well as control and reproducibility of both sulfonation and molecular weight prompted renewed interest in this material, particularly with the introduction of crosslinking.[194] The synthesis of SDCDPS monomer used in the production of the directly copolymerized poly(arylene ether sulfone)s is shown in Figure 1-14, and has not only been well documented in the literature but also has well established procedures to confirm monomer purity which allows for precise tailoring of the polymer structure.[185, 203]

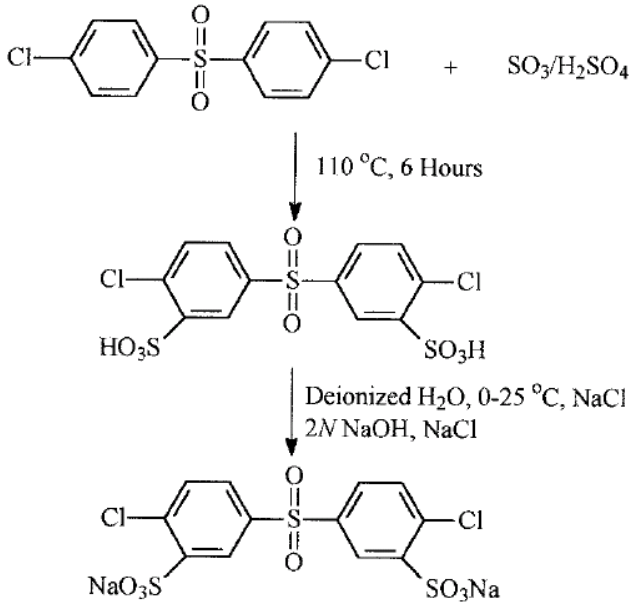

Figure 1-14. Synthesis of SDCDPS used in the production of directly polymerized sulfonated PAESs.

The structures of post-sulfonated and directly copolymerized PAES are compared in Figure 1-15, where the greater stability of the sulfonate groups on the deactivated sulfone group should be noted. Although the directly polymerized sulfonated PAES materials were initially developed for use in proton exchange membrane fuel cells as proton conductors, the studies on water uptake and transport properties provided a helpful foundation for reopening studies on applications for reverse osmosis. A new synthetic approach has been developed to overcome the previous disadvantages of an RO membrane, a series of biphenol- and bisphenol A-based copolymers were synthesized and evaluated.[10, 204-209]

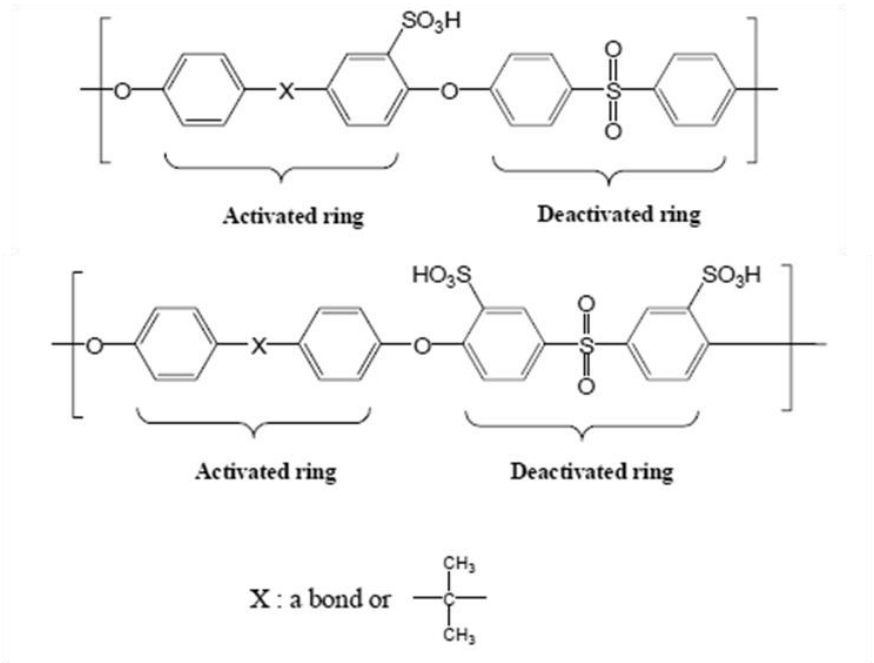

Figure 1-15. Comparison of post-sulfonated and directly copolymerized PAES structures.

Initial studies into the application of SPAES copolymers for reverse osmosis focused on the structure-property relationships of these materials as a function of sulfonation level. Increases in the hydrophilic group produced a marked increase in the water flux, but produced a sharp

decrease in salt rejection and a decrease in the mechanical properties of the hydrated membrane. SPAES copolymers with a higher free volume tend to show higher water flux and slightly lower salt rejection values due to the increased volume fraction and self-diffusion coefficient of water, according to studies performed at Virginia Tech and the University of Texas.[10, 204, 209, 210]

Since the development of directly copolymerized SPAESs, investigations inside and outside of the McGrath group have focused on improved salt rejection and water flux characteristics. One approach is to crosslink a dense membrane in order to limit water uptake in the membrane and fix hydrophilic groups into a more dense arrangement, thus improving salt rejection.[194, 211, 212] Another approach is to investigate the use of a multiblock copolymer membrane, where the mechanical properties of a hydrophobic block and the transport properties of a hydrophilic block might be optimized with nanophase-separated morphology.[213]

1.9 Characterization of RO Membranes

In the development of RO membranes, many factors beyond the raw material's ability to select for the transport of water while rejecting sodium chloride must be evaluated in the tuning of a new system. Membranes must be hydrolytically stable over a range of pH levels for long durations of time, and preferably should be resistant to degradation by common disinfectants and other additives, such as chlorine. Resistance to fouling is also ideal, and selectivity for ions and contaminants other than sodium and chloride, i.e. boron, arsenic, and pharmaceuticals would be ideal. A membrane which is capable of withstanding the hydrocarbon contaminants in oily water without degrading or experiencing a significant drop in rejection is also greatly desired and under investigation.[214] When producing an asymmetrical membrane or thin film composite, confirmation of both the film and support foam layer structures is important both to observe continuous film thickness, the absence of pore plugging in the foam, and the absence of pinholes in the skin layer.

While the final testing must be performed inside of a RO testing unit in order to understand the salt rejection and water flux behavior, prior to RO evaluation a number of other evaluations are performed in order to determine that a given material or membrane is a suitable RO candidate. Mechanical property testing can help indicate whether a membrane can withstand the stress of the applied pressure inside a module. Dynamic mechanical analysis (DMA) can help to identify low-temperature transitions that may help a material to be more stress resilient, or in the case of a cross-linked or multiblock copolymer, to identify the increase in glass transition temperature or the degree of phase separation between blocks. AFM is useful to characterize a multi-component surface such a nanophase-separated multiblock membrane, or to quantify the amount of surface roughness in the case of a cross-linked polymer, which frequently has surface inconsistencies. Imaging via scanning electron microscopy may help quantify skin thickness of an ASM or TFC, as well as pore size and pore size gradients in the case of the former.

1.9.1 Mechanical properties

Tensile testing is frequently used to complement DMA evaluation. Instron testing is ideal for the determination of mechanical properties such as modulus, yield stress, yield strain, and stress/strain at break. This test is performed by punching out samples with a uniform die to insure minimal variation in sample variations, typically using a dogbone shape. The dogbone shape is preferred because stresses focus on the narrow portion of the film, away from the thicker ends used for attaching clamps. During testing, the clamps are secured at each end and the sample is elongated at a constant rate, while the force needed to maintain this elongation is measured.[215]

The stress is measured by the following equation, where σ represents stress, typically in units of Pa, F is the applied load in units of N, and A is the initial cross-sectional area of the narrow portion of the dogbone (m^2).

$$\sigma = \frac{F}{A}$$

The strain, ε, is determined by the change in length over the original length, and is unitless but typically reported in percent (%).

$$\varepsilon = \frac{\Delta L}{L}$$

$$E = \frac{\sigma}{\varepsilon}$$

The ratio of the stress to the strain is the Young's Modulus, E, and their relationship described in the above equation is known as Hooke's Law. It is commonly used to gauge the stiffness or rigidity of a material. The Young's modulus is measured from the initial portion of a stress-strain curve as shown in Figure 1-16, prior to the material's yielding or fracture, where the deformation is elastic or reversible. After the amount of elastic deformation possible in the sample has been exhausted, the stress peaks with additional strain and then begins to decrease as irreversible deformation occurs, known as the yield point. The sample then undergoes a phase of elongation at a constant, lower stress called necking, where the thin portion of the dogbone becomes much narrower until the sample reaches the point of failure.[215]

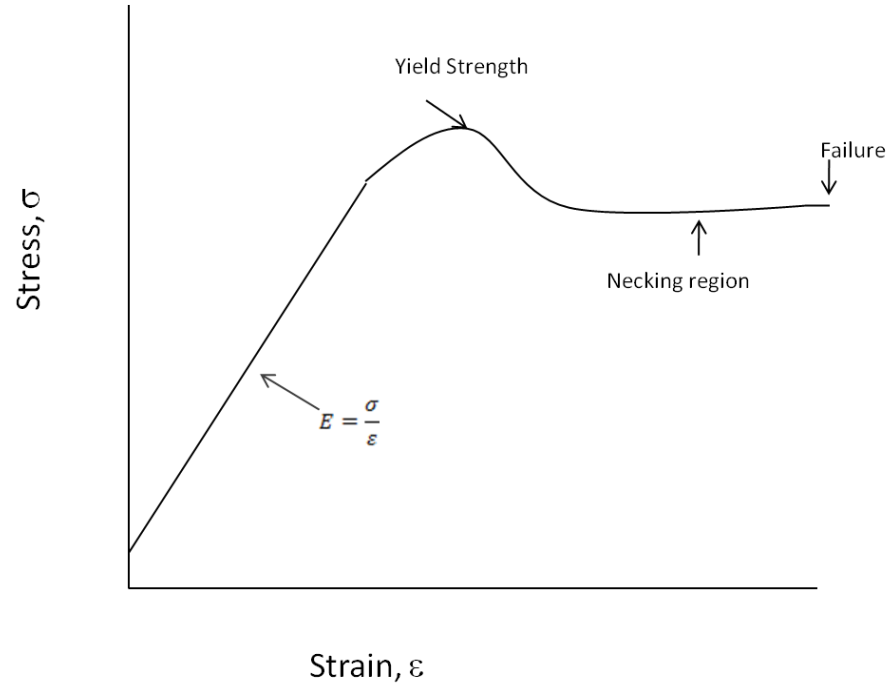

Figure 1-16. Model stress-strain curve of a polymer with elastic and nonelastic deformation.

1.9.2 Thermomechanical behavior via dynamic mechanical analysis

In dynamic mechanical analysis, a material's transition temperature(s) are measured in terms of the change of storage and loss moduli (E' and E'' respectively) as a function of temperature and/or frequency. While DMA may be performed on thin films, fibers, or on bars in single or double cantilever testing, all samples entail a material being fixed into a given frame and a deforming oscillating force being applied at one end, and the response to that force is measured. When a force is applied to a sample, there is a small lag before the material responds by deforming. The difference between this initial applied stress, σ_o, and the material response, ε_o, is called the phase lag, represented by δ. The storage modulus E' and the loss modulus E" are determined by the following equations:

$$E' = \frac{\sigma_o}{\varepsilon_o}\cos\delta$$

$$E'' = \frac{\sigma_o}{\varepsilon_o} \sin \delta$$

The most important information available in a DMA test is that of thermal transitions. While other instrumentation can detect glass transition shifts, DMA is much more sensitive to the onset of the glass transition. It can frequently also pick up beta and gamma transitions, which are attributed to smaller molecular motions of side groups and bending and stretching within the chain. These transitions are frequently missed in analysis using the less sensitive differential scanning calorimetry (DSC). If a plasticizing agent has been added in small quantity, the greater sensitivity of the DMA may be useful for confirming the T_g depression observed in DSC. In the case of a blend, the T_g of the minority polymer can be detected as low as 2% content.

While the storage and loss moduli are also useful information, they are typically not the objective of DMA testing. Young's modulus is better measured from Instron testing, but an approximation can be found for an estimate by determining the complex modulus from DMA, calculated by the following equation:

$$E^* = E' + iE''$$

1.9.3 Scanning Electron Microscopy

Scanning Electron Microscopy, or SEM, is an imaging technique in which an electron beam is used to bombard a sample. If the sample is electronically conductive and stable under ultra high vacuum (UHV), it can be imaged without further processing. A sample which is not electronically conductive must be sputter-coated with a conductive material such as gold or silver prior to imaging, or painted with carbon. Samples which must be partially humidified, such as biological samples, may be imaged in an environmental SEM (E-SEM), where a lower vacuum is held at low temperature, albeit at reduced resolution. For reverse osmosis applications, SEM

imaging is critical for imaging not only pore size and pore gradients in the cross-section of a thin film composite or asymmetric membrane, but also the selective skin thickness. It can also be used for a qualitative analysis of the membrane surface roughness before proceeding with the more time-consuming quantitative characterization possible with atomic force microscopy (AFM).[29]

1.9.4 Atomic Force Microscopy

Atomic Force Microscopy (AFM) is the primary application of scanning probe microscopy (SPM), in which information about the height and surface hardness of a given material is obtained by scanning a nanomachined probe tip with a defined rigidity across a small defined surface area. This information is compiled, line by line, to create a composite 'image' which illustrates the material morphology and topography. AFM is one of the few characterization techniques which features atomic resolution, although most imaging is performed on a much coarser level. The quality of imaging resolution and reproducibility is most dependent on the tip quality and compatibility with the sample surface in terms of spring constant, applied force, and tip composition, as well as a sample surface and working environment free of contamination.[216]

While scanning, the probe tip is maintained at a constant height above the material surface by feedback to the piezoelectric actuator upon which it is mounted. This feedback is acquired from a laser beam which bounces off of the probe tip as it scans across the sample surface, and then lands upon a photodiode. The position of the beam on the photodiode is used to both calculate the surface topography and to determine the amount of correction necessary to return the probe tip to a constant height.[216]

During each scan of the probe tip, there are several different types of energetic interactions between the tip and surface. At very low tip-surface distances favored by contact mode AFM,

repulsive forces dominate. As the tip moves further away from the surface, the repulsive forces quickly drop off and are replaced by attractive forces such as Van der Waals, which is the region typically favored by non-contact mode.[216]

There are three primary modes for collecting AFM images, non-contact mode, contact mode (in which the scanning probe or tip comes into actual contact with the material surface) and tapping mode (in which the probe or tip is repelled from the surface). There are also a number of specialized applications of AFM, such as electrostatic force microscopy, chemical force microscopy, AFM coupled with thermomechanical analysis, and magnetic force microscopy.[216]

Non-contact mode is distinguished by the distance at which the tip oscillates, typically 5-15 nm from the surface, without physical contact with the surface at any point. At this distance, while long range Van der Waals forces are detected by the tip, the repulsive and much of the attractive forces which predominate tapping and contact mode are not influential. However, non-contact mode does leave the tip susceptible to errors caused by any solid or liquid components suspended in the air which have adsorbed onto the sample area.[216]

Contact mode is distinguished by the tip maintained in near-actual physical contact with or effectively in contact with the sample surface, where repulsive atomic forces push the tip away. Constant deflection maintains the distance between the surface and the tip static. Tapping mode is a hybrid of both contact and non-contact mode in which the tip is lowered while osciallating at resonance frequency until it comes into physical contact with the tip surface. The oscillations prevent destruction of the fragile tip as the tip is lifted from the surface before any features on the surface may damage it. This mode is ideal for the high-resolution topographical mapping of complex surfaces.[216]

In the tapping mode, images are constructed depicting both the scale of surface rigidity (phase image) and the physical topography of the imaged surface (height image). The information from the latter can be understood qualitatively, from viewing the image, or quantitatively by analyzing the height information collected during imaging to calculate the root mean square of the heights, or RMS. This is a useful descriptor of the average surface roughness, so long as the image captured is reflective of the rest of the membrane surface. This is particularly useful when characterizing membranes for RO applications as surface roughness in a RO module creates dead zones where low fluid turbulence enables foulants, particularly microbes, to settle and adhere to the membrane surface. A lower RMS membrane fabricated from the same material as a high RMS membrane could be expected to feature lower levels of fouling.[216]

References

1. Elimelech, M.; Phillip, W. A., The Future of Seawater Desalination: Energy, Technology, and the Environment. *Science* **2011,** *333* (6043), 712-717.
2. Wilf, M. A. L., *The guidebook to membrane desalination technology : reverse osmosis, nanofiltration and hybrid systems : process, design, applications and economics*. Balaban Desalination Publications: L'Aquila, Italy, 2007.
3. Escobar, I. C. S. A. I., *Sustainable water for the future : water recycling versus desalination*. Elsevier Science: Amsterdam; Boston, 2010.
4. Greenlee, L. F.; Lawler, D. F.; Freeman, B. D.; Marrot, B.; Moulin, P., Reverse osmosis desalination: Water sources, technology, and today's challenges. *Water Res.* **2009,** *43* (9), 2317-2348.
5. Hager, L. S. W. E. F., *Membrane systems for wastewater treatment*. WEF Press : McGraw-Hill: New York, 2006.
6. Dawoud, M. A., The role of desalination in augmentation of water supply in GCC countries. *Desalination* **2005,** *186* (1-3), 187-198.
7. National Research Council, C. o. A. D. T. N. A. P., *Desalination : a national perspective*. National Academies Press: Washington, D.C., 2008.
8. McDonald, R. I.; Green, P.; Balk, D.; Fekete, B. M.; Revenga, C.; Todd, M.; Montgomery, M., Urban growth, climate change, and freshwater availability. *Proc. Natl. Acad. Sci. U. S. A.* **2011,** *108* (15), 6312-6317, S6312/1-S6312/2.
9. Thorne, O. M.; Fenner, R. A., Risk-based climate-change impact assessment for the water industry. *Water Sci Technol* **2009,** *59* (3), 443-51.

10. Geise, G. M.; Lee, H.-S.; Miller, D. J.; Freeman, B. D.; McGrath, J. E.; Paul, D. R., Water purification by membranes: the role of polymer science. *J. Polym. Sci., Part B: Polym. Phys.* **2010,** *48* (15), 1685-1718.
11. Tsiourtis, N. X., Desalination and the environment. *Desalination* **2001,** *141* (3), 223-236.
12. Service, R. F., Desalination Freshens Up. *Science* **2006,** *313* (5790), 1088-1090.
13. Khawaji, A. D.; Kutubkhanah, I. K.; Wie, J.-M., Advances in seawater desalination technologies. *Desalination* **2008,** *221* (1–3), 47-69.
14. Bergman, R., *Reverse osmosis and nanofiltration.* American Water Works Association: Denver, CO, 2007.
15. Amjad, Z., *Reverse osmosis : membrane technology, water chemistry & industrial applications*. Van Nostrand Reinhold: New York, 1993.
16. Kucera, J., *Reverse osmosis : design, processes, and applications for engineers*. Scrivener Pub. ; Wiley: Salem, Mass.; Hoboken, N.J., 2010.
17. Focazio, M. J.; Kolpin, D. W.; Barnes, K. K.; Furlong, E. T.; Meyer, M. T.; Zaugg, S. D.; Barber, L. B.; Thurman, M. E., A national reconnaissance for pharmaceuticals and other organic wastewater contaminants in the United States - (II) Untreated drinking water sources. *Sci. Total Environ.* **2008,** *402* (2-3), 201-216.
18. Focazio, M. J.; Kolpin, D. W.; Furlong, E. T. In *Occurrence of human pharmaceuticals in water resources of the United States: a review*, Springer GmbH: 2004; pp 91-105.
19. Baker, R. W., *Membrane Technology and Applications*. 2004.
20. Li, N. N., *Advanced membrane technology and applications*. Wiley: Hoboken, N.J., 2008.
21. Malaeb, L.; Ayoub, G. M., Reverse osmosis technology for water treatment: State of the art review. *Desalination* **2011,** *267* (1), 1-8.
22. Penate, B.; Garcia-Rodriguez, L., Reverse osmosis hybrid membrane inter-stage design. A comparative performance assessment. *Desalination* **2011,** *281*, 354-363.
23. Al-Sahali, M.; Ettouney, H., Developments in thermal desalination processes: Design, energy, and costing aspects. *Desalination* **2007,** *214* (1–3), 227-240.
24. Scenna, N. J., Synthesis of thermal desalination processes. Part I. Multistage flash distillation system (MSF). *Desalination* **1987,** *64* (0), 111-122.
25. Reddy, K. V.; Ghaffour, N., Overview of the cost of desalinated water and costing methodologies. *Desalination* **2007,** *205* (1-3), 340-353.
26. Summers, E. K.; Arafat, H. A.; Lienhard, J. H. V., Energy efficiency comparison of single-stage membrane distillation (MD) desalination cycles in different configurations. *Desalination* **2012,** *290*, 54-66.
27. Almulla, A.; Hamad, A.; Gadalla, M., Integrating hybrid systems with existing thermal desalination plants. *Desalination* **2005,** *174* (2), 171-192.
28. Prakash, S.; Bellman, K.; Shannon, M. A. In *Recent advances in water desalination through biotechnology and nanotechnology*, CRC Press: 2012; pp 365-382.
29. Wang, L. K., *Membrane and Desalination Technologies*. Springer: 2008.
30. Van, d. B. B.; Vandecasteele, C., Distillation vs. membrane filtration: overview of process evolutions in seawater desalination. *Desalination* **2002,** *143* (3), 207-218.
31. Charcosset, C., A review of membrane processes and renewable energies for desalination. *Desalination* **2009,** *245* (1-3), 214-231.
32. Garcia-Rodriguez, L., Renewable energy applications in desalination: state of the art. *Sol. Energy* **2003,** *75* (5), 381-393.
33. Alklaibi, A. M.; Lior, N., Membrane-distillation desalination: Status and potential. *Desalination* **2005,** *171* (2), 111-131.
34. Al-Obaidani, S.; Curcio, E.; Macedonio, F.; Di Profio, G.; Al-Hinai, H.; Drioli, E., Potential of membrane distillation in seawater desalination: Thermal efficiency, sensitivity study and cost estimation. *Journal of Membrane Science* **2008,** *323* (1), 85-98.

35. Qtaishat, M. R.; Banat, F., Desalination by solar powered membrane distillation systems. *Desalination* **2013,** *308* (0), 186-197.
36. Susanto, H., Towards practical implementations of membrane distillation. *Chemical Engineering and Processing: Process Intensification* **2011,** *50* (2), 139-150.
37. Nielsen, W., *Membrane Filtration and Related Molecular Separation Technologies*. APV Systems: 2000.
38. Bonnelye, V.; Sanz, M. A.; Durand, J.-P.; Plasse, L.; Gueguen, F.; Mazounie, P., Reverse osmosis on open intake seawater: Pre-treatment strategy. *Desalination* **2004,** *167* (1-3), 191-200.
39. Brehant, A.; Bonnelye, V.; Perez, M., Assessment of ultrafiltration as a pretreatment of reverse osmosis membranes for surface seawater desalination. *Water Sci. Technol.: Water Supply* **2003,** *3* (5-6), 437-445.
40. American Water Works, A., *Microfiltration and ultrafiltration membranes for drinking water*. American Water Works Association: Denver, CO, 2005.
41. Kang, S.-T.; Subramani, A.; Hoek, E. M. V.; Deshusses, M. A.; Matsumoto, M. R., Direct observation of biofouling in cross-flow microfiltration: mechanisms of deposition and release. *J. Membr. Sci.* **2004,** *244* (1-2), 151-165.
42. Lebleu, N.; Roques, C.; Aimar, P.; Causserand, C., Role of the cell-wall structure in the retention of bacteria by microfiltration membranes. *J. Membr. Sci.* **2009,** *326* (1), 178-185.
43. Afonso, M. D.; Jaber, J. O.; Mohsen, M. S., Brackish groundwater treatment by reverse osmosis in Jordan. *Desalination* **2004,** *164* (2), 157-171.
44. Tu, K. L.; Nghiem, L. D.; Chivas, A. R., Boron removal by reverse osmosis membranes in seawater desalination applications. *Sep. Purif. Technol.* **2010,** *75* (2), 87-101.
45. Tu, K.-L.; Chivas, A. R.; Nghiem, L. D., Effects of membrane fouling and scaling on boron rejection by nanofiltration and reverse osmosis membranes. *Desalination* **2011,** *279* (1-3), 269-277.
46. Mondal, S.; Hsiao, C.-I.; Wickramasinghe, S. R., Nanofiltration/reverse osmosis for treatment of coproduced waters. *Environ. Prog.* **2008,** *27* (2), 173-179.
47. Mondal, S.; Wickramasinghe, S. R., Produced water treatment by nanofiltration and reverse osmosis membranes. *Journal of Membrane Science* **2008,** *322* (1), 162-170.
48. Amiri, M. C.; Samiei, M., Enhancing permeate flux in a RO plant by controlling membrane fouling. *Desalination* **2007,** *207* (1-3), 361-369.
49. Lee, K. P.; Arnot, T. C.; Mattia, D., A review of reverse osmosis membrane materials for desalination. Development to date and future potential. *J. Membr. Sci.* **2011,** *370* (1-2), 1-22.
50. Mathioulakis, E.; Belessiotis, V.; Delyannis, E., Desalination by using alternative energy: Review and state-of-the-art. *Desalination* **2007,** *203* (1-3), 346-365.
51. Mezher, T.; Fath, H.; Abbas, Z.; Khaled, A., Techno-economic assessment and environmental impacts of desalination technologies. *Desalination* **2011,** *266* (1-3), 263-273.
52. Karagiannis, I. C.; Soldatos, P. G., Water desalination cost literature: review and assessment. *Desalination* **2008,** *223* (1-3), 448-456.
53. Klaysom, C.; Cath, T. Y.; Depuydt, T.; Vankelecom, I. F. J., Forward and pressure retarded osmosis: potential solutions for global challenges in energy and water supply. *Chem. Soc. Rev.* **2013,** *42* (16), 6959-6989.
54. Achilli, A.; Childress, A. E., Pressure retarded osmosis: From the vision of Sidney Loeb to the first prototype installation - Review. *Desalination* **2010,** *261* (3), 205-211.
55. Loeb, S., Large-scale power production by pressure-retarded osmosis, using river water and sea water passing through spiral modules. *Desalination* **2002,** *150* (2), 205.
56. Loeb, S., One hundred and thirty benign and renewable megawatts from Great Salt Lake? The possibilities of hydroelectric power by pressure-retarded osmosis with spiral module membranes: Desalination, 141 (2001) 85–91. *Desalination* **2002,** *142* (2), 207.
57. Cath, T. Y.; Childress, A. E.; Elimelech, M., Forward osmosis: Principles, applications, and recent developments. *Journal of Membrane Science* **2006,** *281* (1–2), 70-87.

58. Jin, X.; She, Q.; Ang, X.; Tang, C. Y., Removal of boron and arsenic by forward osmosis membrane: Influence of membrane orientation and organic fouling. *J. Membr. Sci.* **2012,** *389*, 182-187.
59. Xie, M.; Nghiem, L. D.; Price, W. E.; Elimelech, M., Comparison of the removal of hydrophobic trace organic contaminants by forward osmosis and reverse osmosis. *Water Res.* **2012,** *46* (8), 2683-2692.
60. Duong, P. H. H.; Zuo, J.; Chung, T.-S., Highly crosslinked layer-by-layer polyelectrolyte FO membranes: Understanding effects of salt concentration and deposition time on FO performance. *J. Membr. Sci.* **2013,** *427*, 411-421.
61. Huang, L.; Bui, N.-N.; Meyering, M. T.; Hamlin, T. J.; McCutcheon, J. R., Novel hydrophilic nylon 6,6 microfiltration membrane supported thin film composite membranes for engineered osmosis. *Journal of Membrane Science* **2013,** *437* (0), 141-149.
62. Arena, J. T.; McCloskey, B.; Freeman, B. D.; McCutcheon, J. R., Surface modification of thin film composite membrane support layers with polydopamine: Enabling use of reverse osmosis membranes in pressure retarded osmosis. *Journal of Membrane Science* **2011,** *375* (1–2), 55-62.
63. Zhang, S.; Fu, F.; Chung, T.-S., Substrate modifications and alcohol treatment on thin film composite membranes for osmotic power. *Chemical Engineering Science* **2013,** *87* (0), 40-50.
64. Alsvik, I. L.; Hagg, M.-B., Preparation of thin film composite membranes with polyamide film on hydrophilic supports. *J. Membr. Sci.* **2013,** *428*, 225-231.
65. Han, G.; Zhang, S.; Li, X.; Widjojo, N.; Chung, T.-S., Thin film composite forward osmosis membranes based on polydopamine modified polysulfone substrates with enhancements in both water flux and salt rejection. *Chem. Eng. Sci.* **2012,** *80*, 219-231.
66. Hoover, L. A.; Schiffman, J. D.; Elimelech, M., Nanofibers in thin-film composite membrane support layers: Enabling expanded application of forward and pressure retarded osmosis. *Desalination* **2013,** *308*, 73-81.
67. Jeong, B.-R.; Kim, J.-H.; Kim, B.-S.; Park, Y.-I.; Song, D.-H.; Kim, I.-C., Effect of support membrane property on performance of forward osmosis membrane. *Membr. J.* **2010,** *20* (3), 235-240.
68. Lee, S. H.; Yoo, Y. B.; Seo, S. G. Method for manufacturing forward osmosis membrane for water treatment. KR990168B1, 2010.
69. Subramani, A.; Badruzzaman, M.; Oppenheimer, J.; Jacangelo, J. G., Energy minimization strategies and renewable energy utilization for desalination: A review. *Water Res.* **2011,** *45* (5), 1907-1920.
70. Wang, R.; Shi, L.; Tang, C. Y.; Chou, S.; Qiu, C.; Fane, A. G., Characterization of novel forward osmosis hollow fiber membranes. *J. Membr. Sci.* **2010,** *355* (1-2), 158-167.
71. Thorsen, T.; Holt, T., The potential for power production from salinity gradients by pressure retarded osmosis. *J. Membr. Sci.* **2009,** *335* (1+2), 103-110.
72. Thorsen, T.; Holt, T., Finding hidden energy in membrane processes. *Filtr. Sep.* **2005,** *42* (3), 28-30.
73. Cath, T. Y., Osmotically and thermally driven membrane processes for enhancement of water recovery in desalination processes. *Desalin. Water Treat.* **2010,** *15* (1-3), 279-286.
74. Achilli, A.; Cath, T. Y.; Childress, A. E. In *Inorganic draw solutions for forward osmosis processes*, American Chemical Society: 2010; pp ENVR-69.
75. Ge, Q.; Ling, M.; Chung, T.-S., Draw solutions for forward osmosis processes: Developments, challenges, and prospects for the future. *J. Membr. Sci.* **2013,** *442*, 225-237.
76. Ge, Q.; Su, J.; Amy, G. L.; Chung, T.-S., Exploration of polyelectrolytes as draw solutes in forward osmosis processes. *Water Res.* **2012,** *46* (4), 1318-1326.
77. Stewart, F. F.; Benson, M. T.; Stone, M. L. Draw solutes, methods of forming draw solutes, and methods of using draw solutes to treat an aqueous liquid. US20130048564A1, 2013.
78. Stone, M. L.; Rae, C.; Stewart, F. F.; Wilson, A. D., Switchable polarity solvents as draw solutes for forward osmosis. *Desalination* **2013,** *312*, 124-129.
79. Stone, M. L.; Wilson, A. D.; Harrup, M. K.; Stewart, F. F., An initial study of hexavalent phosphazene salts as draw solutes in forward osmosis. *Desalination* **2013,** *312*, 130-136.

80. Achilli, A.; Cath, T. Y.; Childress, A. E., Power generation with pressure retarded osmosis: An experimental and theoretical investigation. *J. Membr. Sci.* **2009,** *343* (1-2), 42-52.
81. McCutcheon, J. R.; Elimelech, M., Influence of concentrative and dilutive internal concentration polarization on flux behavior in forward osmosis. *J. Membr. Sci.* **2006,** *284* (1+2), 237-247.
82. Chung, T.-S.; Zhang, S.; Wang, K. Y.; Su, J.; Ling, M. M., Forward osmosis processes: Yesterday, today and tomorrow. *Desalination* **2012,** *287*, 78-81.
83. Li, G.; Li, X.; Wang, D.; He, T.; Gao, C., Forward osmosis membranes and applications. *Huagong Jinzhan* **2010,** *29* (8), 1388-1398.
84. McCutcheon, J.; Bui, N.-N. In *Forward osmosis*, Scrivener Publishing LLC: 2014; pp 255-285.
85. Zhao, S.; Zou, L.; Tang, C. Y.; Mulcahy, D., Recent developments in forward osmosis: Opportunities and challenges. *J. Membr. Sci.* **2012,** *396*, 1-21.
86. Wang, K. Y.; Ong, R. C.; Chung, T.-S., Double-Skinned Forward Osmosis Membranes for Reducing Internal Concentration Polarization within the Porous Sublayer. *Ind. Eng. Chem. Res.* **2010,** *49* (10), 4824-4831.
87. Widjojo, N.; Chung, T.-S.; Weber, M.; Maletzko, C.; Warzelhan, V., A sulfonated polyphenylenesulfone (sPPSU) as the supporting substrate in thin film composite (TFC) membranes with enhanced performance for forward osmosis (FO). *Chemical Engineering Journal* **2013,** *220* (0), 15-23.
88. Yang, Q.; Wang, K. Y.; Chung, T.-S. Dual-layer hollow fibers with enhanced flux as forward osmosis membranes for water reuses and protein enrichment. WO2010045430A2, 2010.
89. Field, R. W.; Wu, J. J., Mass transfer limitations in forward osmosis: Are some potential applications overhyped? *Desalination* **2013,** *318*, 118-124.
90. Field, R. W.; Wu, J. J., Analysis of Forward Osmosis: Is it Overhyped? *Procedia Eng.* **2012,** *44*, 264-266.
91. Boo, C.; Elimelech, M.; Hong, S., Fouling control in a forward osmosis process integrating seawater desalination and wastewater reclamation. *J. Membr. Sci.* **2013,** *444*, 148-156.
92. Post, J. W.; Veerman, J.; Hamelers, H. V. M.; Euverink, G. J. W.; Metz, S. J.; Nymeijer, K.; Buisman, C. J. N., Salinity-gradient power: Evaluation of pressure-retarded osmosis and reverse electrodialysis. *J. Membr. Sci.* **2007,** *288* (1+2), 218-230.
93. Bowden, K. S.; Achilli, A.; Childress, A. E., Organic ionic salt draw solutions for osmotic membrane bioreactors. *Bioresour. Technol.* **2012,** *122*, 207-216.
94. Wang, W.; Sun, J.; Wang, B., Effect of process parameters on osmosis performance during forward osmosis. *Gaofenzi Cailiao Kexue Yu Gongcheng* **2012,** *28* (1), 86-88,92.
95. Chung, T.-S.; Li, X.; Ong, R. C.; Ge, Q.; Wang, H.; Han, G., Emerging forward osmosis (FO) technologies and challenges ahead for clean water and clean energy applications. *Curr. Opin. Chem. Eng.* **2012,** *1* (3), 246-257.
96. Baker, R. W., Separation of volatile organic compounds from water by pervaporation. *MRS Bull.* **1999,** *24* (3), 50-53.
97. Neel, J. In *The pervaporation process*, Oxford & IBH: 1992; pp 313-29.
98. Wijmans, J. G.; Baker, R. W.; Mairal, A. P. Membrane separation of organic mixtures using gas separation or pervaporation and dephlegmation. US20030233934A1, 2003.
99. Zhu, C.; Xu, W.; Feng, J. In *Description of pervaporation (PVAP) mechanism with separation-characteristics graphs*, Bakish Mater. Corp.: 1988; pp 44-53.
100. Paul, D. R., Reformulation of the solution-diffusion theory of reverse osmosis. *J. Membr. Sci.* **2004,** *241* (2), 371-386.
101. Paul, D. R., The solution-diffusion model for swollen membranes. *Sep. Purif. Methods* **1976,** *5* (1), 33-50.
102. Wijmans, J. G.; Baker, R. W. In *The solution-diffusion model: a unified approach to membrane permeation*, John Wiley & Sons Ltd.: 2006; pp 159-189.
103. Edzwald, J. K.; Haarhoff, J., Seawater pretreatment for reverse osmosis: Chemistry, contaminants, and coagulation. *Water Res.* **2011,** *45* (17), 5428-5440.

104. Elguera, A. M.; Perez, B. S. O., Development of the most adequate pre-treatment for high capacity seawater desalination plants with open intake. *Desalination* **2005,** *184* (1-3), 173-183.
105. Kim, S.-H.; Min, C.-S.; Cho, J., Comparison of different pretreatments for seawater desalination. *Desalin. Water Treat.* **2011,** *32* (1-3), 339-344.
106. Al-Juboori, R. A.; Yusaf, T., Biofouling in RO system: Mechanisms, monitoring and controlling. *Desalination* **2012,** *302* (0), 1-23.
107. Flemming, H.-C., Reverse osmosis membrane biofouling. *Experimental Thermal and Fluid Science* **1997,** *14* (4), 382-391.
108. Herzberg, M.; Elimelech, M. In *The role of EPS in biofouling of reverse osmosis membranes*, American Chemical Society: 2007; pp SUST-088.
109. Herzberg, M.; Elimelech, M., Biofouling of reverse osmosis membranes: Mechanisms and performance. *Prepr. Ext. Abstr. ACS Natl. Meet., Am. Chem. Soc., Div. Environ. Chem.* **2006,** *46* (2), 1272-1275.
110. Bernstein, R.; Belfer, S.; Freger, V., Toward Improved Boron Removal in RO by Membrane Modification: Feasibility and Challenges. *Environ. Sci. Technol.* **2011,** *45* (8), 3613-3620.
111. Glueckstern, P.; Priel, M., Boron removal in brackish water desalination systems. *Desalination* **2007,** *205* (1-3), 178-184.
112. Glueckstern, P.; Priel, M., Optimization of boron removal in old and new SWRO systems. *Desalination* **2003,** *156* (1-3), 219-228.
113. Jacob, C., Seawater desalination: boron removal by ion exchange technology. *Desalination* **2007,** *205* (1-3), 47-52.
114. Boo, C.; Lee, S.; Elimelech, M.; Meng, Z.; Hong, S., Colloidal fouling in forward osmosis: Role of reverse salt diffusion. *J. Membr. Sci.* **2012,** *390-391*, 277-284.
115. Hyun, J.; Jang, H.; Kim, K.; Na, K.; Tak, T., Restriction of biofouling in membrane filtration using a brush-like polymer containing oligoethylene glycol side chains. *J. Membr. Sci.* **2006,** *282* (1+2), 52-59.
116. Louie, J. S.; Pinnau, I.; Ciobanu, I.; Ishida, K. P.; Ng, A.; Reinhard, M., Effects of polyether-polyamide block copolymer coating on performance and fouling of reverse osmosis membranes. *J. Membr. Sci.* **2006,** *280* (1+2), 762-770.
117. Matin, A.; Khan, Z.; Zaidi, S. M. J.; Boyce, M. C., Biofouling in reverse osmosis membranes for seawater desalination: Phenomena and prevention. *Desalination* **2011,** *281*, 1-16.
118. Mohammadi, T.; Esmaeelifar, A., Wastewater treatment of a vegetable oil factory by a hybrid ultrafiltration-activated carbon process. *J. Membr. Sci.* **2005,** *254* (1-2), 129-137.
119. Pandey, S. R.; Jegatheesan, V.; Baskaran, K.; Shu, L., Fouling in reverse osmosis (RO) membrane in water recovery from secondary effluent: a review. *Rev. Environ. Sci. Bio/Technol.* **2012,** *11* (2), 125-145.
120. Yang, H. L.; Huang, C.; Pan, J. R., Characteristics of RO foulants in a brackish water desalination plant. *Desalination* **2008,** *220* (1-3), 353-358.
121. Yiantsios, S. G.; Sioutopoulos, D.; Karabelas, A. J., Colloidal fouling of RO membranes: an overview of key issues and efforts to develop improved prediction techniques. *Desalination* **2005,** *183* (1-3), 257-272.
122. Ng, H. Y.; Elimelech, M., Influence of colloidal fouling on rejection of trace organic contaminants by reverse osmosis. *J. Membr. Sci.* **2004,** *244* (1-2), 215-226.
123. Amjad, Z.; Pugh, J.; Harn, J., Membranes. Antiscalants and dispersants in reverse osmosis systems. *Ultrapure Water* **1996,** *13* (8), 48-52.
124. Malekar, S., Role of antiscalants in reverse osmosis. *Chem. Ind. Dig.* **2005,** *18* (3), 47-48,51-52.
125. Abejon, R.; Garea, A.; Irabien, A., Analysis, modelling and simulation of hydrogen peroxide ultrapurification by multistage reverse osmosis. *Chem. Eng. Res. Des.* **2012,** *90* (3), 442-452.
126. Antony, A.; Low, J. H.; Gray, S.; Childress, A. E.; Le-Clech, P.; Leslie, G., Scale formation and control in high pressure membrane water treatment systems: A review. *Journal of Membrane Science* **2011,** *383* (1–2), 1-16.

127. Badruzzaman, M.; Subramani, A.; DeCarolis, J.; Pearce, W.; Jacangelo, J. G., Impacts of silica on the sustainable productivity of reverse osmosis membranes treating low-salinity brackish groundwater. *Desalination* **2011,** *279* (1-3), 210-218.
128. Boffardi, B. P. In *Scale and deposit control for reverse osmosis systems*, American Water Works Association: 1997; pp 681-693.
129. Bonne, P. A. C.; Hofman, J. A. M. H.; Van, d. H. J. P., Scaling control of RO membranes and direct treatment of surface water. *Desalination* **2000,** *132* (1-3), 109-119.
130. Lee, S.; Cho, J.; Elimelech, M., Influence of colloidal fouling and feed water recovery on salt rejection of RO and NF membranes. *Desalination* **2004,** *160* (1), 1-12.
131. Al-Amoudi, A. S., Factors affecting natural organic matter (NOM) and scaling fouling in NF membranes: A review. *Desalination* **2010,** *259* (1–3), 1-10.
132. Kim, S.; Park, N.; Lee, S.; Cho, J., Membrane characterizations for mitigation of organic fouling during desalination and wastewater reclamation. *Desalination* **2009,** *238* (1-3), 70-77.
133. Lee, S.; Ang, W. S.; Elimelech, M. In *Role of divalent cations in organic fouling of reverse osmosis membranes*, American Chemical Society: 2004; pp ENVR-264.
134. Lee, S.; Elimelech, M., Relating Organic Fouling of Reverse Osmosis Membranes to Intermolecular Adhesion Forces. *Environ. Sci. Technol.* **2006,** *40* (3), 980-987.
135. Misdan, N.; Lau, W. J.; Ismail, A. F., Seawater reverse osmosis (SWRO) desalination by thin-film composite membrane: Current development, challenges, and future prospects. *Desalination* **2012,** *287*, 228-237.
136. Bereschenko, L. A.; Prummel, H.; Euverink, G. J. W.; Stams, A. J. M.; van, L. M. C. M., Effect of conventional chemical treatment on the microbial population in a biofouling layer of reverse osmosis systems. *Water Res.* **2011,** *45* (2), 405-416.
137. Mansouri, J.; Harrisson, S.; Chen, V., Strategies for controlling biofouling in membrane filtration systems: challenges and opportunities. *J. Mater. Chem.* **2010,** *20* (22), 4567-4586.
138. Matsuura, T.; Ismail, A. F.; Rana, D. In *Applications of surface modifying macromolecules for various membrane separation processes*, American Chemical Society: 2011; pp I+EC-112.
139. Xu, J.; Wang, Z.; Yu, L.; Wang, J.; Wang, S., Reverse osmosis membrane with regenerable anti-biofouling and chlorine resistant properties. *J. Membr. Sci.* **2013,** *435*, 80-91.
140. Sagle, A. C.; Van Wagner, E. M.; Ju, H.; McCloskey, B. D.; Freeman, B. D.; Sharma, M. M., PEG-coated reverse osmosis membranes: Desalination properties and fouling resistance. *J. Membr. Sci.* **2009,** *340* (1-2), 92-108.
141. McCloskey, B. D.; Park, H. B.; Ju, H.; Rowe, B. W.; Miller, D. J.; Chun, B. J.; Kin, K.; Freeman, B. D., Influence of polydopamine deposition conditions on pure water flux and foulant adhesion resistance of reverse osmosis, ultrafiltration, and microfiltration membranes. *Polymer* **2010,** *51* (15), 3472-3485.
142. Kang, G.-d.; Cao, Y.-m., Development of antifouling reverse osmosis membranes for water treatment: A review. *Water Res.* **2012,** *46* (3), 584-600.
143. Yip, N. Y.; Phillip, W. A.; Schiffman, J. D.; Elimelech, M. High flux thin-film composite forward osmosis and pressure-retarded osmosis membranes. WO2011069050A1, 2011.
144. Hilal, N.; Kim, G. J.; Somerfield, C., Boron removal from saline water. A comprehensive review. *Desalination* **2011,** *273* (1), 23-35.
145. Mondal, P.; Majumder, C. B.; Mohanty, B., Laboratory based approaches for arsenic remediation from contaminated water: Recent developments. *J. Hazard. Mater.* **2006,** *137* (1), 464-479.
146. Galvin, R. M., Occurrence of metals in waters: An overview. *Water SA* **1996,** *22* (1), 7-18.
147. Akin, I.; Arslan, G.; Tor, A.; Cengeloglu, Y.; Ersoz, M., Removal of arsenate [As(V)] and arsenite [As(III)] from water by SWHR and BW-30 reverse osmosis. *Desalination* **2011,** *281*, 88-92.
148. Coronell, O.; Mi, B.; Marinas, B. J.; Cahill, D. G., Modeling the Effect of Charge Density in the Active Layers of Reverse Osmosis and Nanofiltration Membranes on the Rejection of Arsenic(III) and Potassium Iodide. *Environ. Sci. Technol.* **2013,** *47* (1), 420-428.

149. Xu, P.; Capito, M.; Cath, T. Y., Selective removal of arsenic and monovalent ions from brackish water reverse osmosis concentrate. *J. Hazard. Mater.* **2013,** *260*, 885-891.
150. Yoon, J.; Amy, G.; Chung, J.; Sohn, J.; Yoon, Y., Removal of toxic ions (chromate, arsenate, and perchlorate) using reverse osmosis, nanofiltration, and ultrafiltration membranes. *Chemosphere* **2009,** *77* (2), 228-235.
151. Yoon, J.; Amy, G.; Yoon, Y., Transport of target anions, chromate (Cr (VI)), arsenate (As (V)), and perchlorate (ClO-4), through RO, NF, and UF membranes. *Water Sci. Technol.* **2005,** *51* (6-7, Water Environment--Membrane Technology), 327-334.
152. Xu, J.; Gao, X.; Chen, G.; Zou, L.; Gao, C., High performance boron removal from seawater by two-pass SWRO system with different membranes. *Water Sci. Technol.: Water Supply* **2010,** *10* (3), 327-336.
153. Dydo, P.; Nems, I.; Turek, M., Boron removal and its concentration by reverse osmosis in the presence of polyol compounds. *Sep. Purif. Technol.* **2012,** *89*, 171-180.
154. Blank, J. E.; Tusel, G. F.; Nisanc, S., The real cost of desalted water and how to reduce it further. *Desalination* **2007,** *205* (1-3), 298-311.
155. Bouguecha, S.; Hamrouni, B.; Dhahbi, M., Small scale desalination pilots powered by renewable energy sources: case studies. *Desalination* **2005,** *183* (1-3), 151-165.
156. Ghaffour, N.; Reddy, V. K.; Abu-Arabi, M., Technology development and application of solar energy in desalination: MEDRC contribution. *Renewable Sustainable Energy Rev.* **2011,** *15* (9), 4410-4415.
157. Qiu, T. Y.; Davies, P. A., The scope to improve the efficiency of solar-powered reverse osmosis. *Desalin. Water Treat.* **2011,** *35* (1-3), 14-32.
158. Charcosset, C.; Falconet, C.; Combe, M., Hydrostatic pressure plants for desalination via reverse osmosis. *Renewable Energy* **2009,** *34* (12), 2878-2882.
159. Afrasiabi, N.; Shahbazali, E., RO brine treatment and disposal methods. *Desalin. Water Treat.* **2011,** *35* (1-3), 39-53.
160. Melian-Martel, N.; Sadhwani, J. J.; Baez, S. O. P., Saline waste disposal reuse for desalination plants for the chlor-alkali industry. The particular case of Poso Izquierdo SWRO desalination plant. *Desalination* **2011,** *281*, 35-41.
161. Voutchkov, N., Overview of seawater concentrate disposal alternatives. *Desalination* **2011,** *273* (1), 205-219.
162. Loeb, S., The Loeb-Sourirajan membrane: how it came about. *ACS Symp. Ser.* **1981,** *153* (Synth. Membr., Vol. 1), 1-9.
163. Kang, G.-D.; Gao, C.-J.; Chen, W.-D.; Jie, X.-M.; Cao, Y.-M.; Yuan, Q., Study on hypochlorite degradation of aromatic polyamide reverse osmosis membrane. *J. Membr. Sci.* **2007,** *300* (1+2), 165-171.
164. Avlonitis, S.; Hanbury, W. T.; Hodgkiess, T., Chlorine degradation of aromatic polyamides. *Desalination* **1992,** *85* (3), 321-34.
165. Shintani, T.; Matsuyama, H.; Kurata, N., Development of a chlorine-resistant polyamide reverse osmosis membrane. *Desalination* **2007,** *207* (1-3), 340-348.
166. Liu, L.-F.; Yu, S.-C.; Wu, L.-G.; Gao, C.-J., Study on a novel antifouling polyamide-urea reverse osmosis composite membrane (ICIC-MPD). III. Analysis of membrane electrical properties. *J. Membr. Sci.* **2008,** *310* (1+2), 119-128.
167. Liu, L.-F.; Xu, D.-Z.; Mao, P.-Q.; Zhang, L.; Gao, C.-J., Preparation and characterization of a novel polyimide-urethane reverse osmosis composite membrane material. *Gaodeng Xuexiao Huaxue Xuebao* **2012,** *33* (7), 1605-1612.
168. McGrath, J. E.; Park, H. B.; Freeman, B. D. Chlorine resistant desalination membranes based on directly sulfonated poly(arylene ether sulfone) copolymers. US20070163951A1, 2007.
169. McGrath, J. E.; Wightman, J. P.; Lloyd, D. R. *Novel poly(aryl ether) membranes for desalination by reverse osmosis*; Virginia Polytech. Inst. and State Univ.: 1984; p 139 pp.
170. **!!! INVALID CITATION !!! {}**.

171. Kang, G.-d.; Liu, Z.-n.; Yu, H.-j.; Cao, Y.-m., Enhancing antifouling property of commercial polyamide reverse osmosis membrane by surface coating using a brush-like polymer containing poly (ethylene glycol) chains. *Desalin. Water Treat.* **2012,** *37* (1-3), 139-145.
172. Yu, S.; Lue, Z.; Chen, Z.; Liu, X.; Liu, M.; Gao, C., Surface modification of thin-film composite polyamide reverse osmosis membranes by coating N-isopropylacrylamide-co-acrylic acid copolymers for improved membrane properties. *J. Membr. Sci.* **2011,** *371* (1-2), 293-306.
173. Yip, N. Y.; Tiraferri, A.; Phillip, W. A.; Schiffman, J. D.; Elimelech, M., High Performance Thin-Film Composite Forward Osmosis Membrane. *Environ. Sci. Technol.* **2010,** *44* (10), 3812-3818.
174. Alsvik, I. L.; Hagg, M.-B., Pressure retarded osmosis and forward osmosis membranes: materials and methods. *Polymers (Basel, Switz.)* **2013,** *5* (1), 303-327, 25 pp.
175. Wang, K. Y.; Yang, Q.; Chung, T.-S.; Rajagopalan, R., Enhanced forward osmosis from chemically modified polybenzimidazole (PBI) nanofiltration hollow fiber membranes with a thin wall. *Chem. Eng. Sci.* **2009,** *64* (7), 1577-1584.
176. Bui, N.-N.; McCutcheon, J. R., Hydrophilic Nanofibers as New Supports for Thin Film Composite Membranes for Engineered Osmosis. *Environ. Sci. Technol.* **2013,** *47* (3), 1761-1769.
177. Jeong, B.-H.; Hoek, E. M. V.; Yan, Y.; Subramani, A.; Huang, X.; Hurwitz, G.; Ghosh, A. K.; Jawor, A., Interfacial polymerization of thin film nanocomposites: A new concept for reverse osmosis membranes. *J. Membr. Sci.* **2007,** *294* (1+2), 1-7.
178. Widjojo, N.; Chung, T.-S.; Weber, M.; Maletzko, C.; Warzelhan, V., The role of sulphonated polymer and macrovoid-free structure in the support layer for thin-film composite (TFC) forward osmosis (FO) membranes [Erratum to document cited in CA155:616441]. *J. Membr. Sci.* **2012,** *389*, 544.
179. Sourirajan, S. M. T. A. C. S. D. o. I.; Engineering Chemistry, A. C. S. M. In *Reverse osmosis and ultrafiltration*, Washington, D.C., 1985; American Chemical Society: Washington, D.C.
180. Pinnau, I.; Koros, W. J., A qualitative skin-layer formation mechanism for membranes made by dry/wet phase inversion. *J. Polym. Sci., Part B: Polym. Phys.* **1993,** *31* (4), 419-27.
181. So, M. T.; Eirich, F. R.; Strathmann, H.; Baker, R. W., Preparation of asymmetric Loeb-Sourirajan membranes. *J. Polym. Sci., Polym. Lett. Ed.* **1973,** *11* (3), 201-5.
182. Duarte, A. P.; Bordado, J. C.; Cidade, M. T., Cellulose acetate reverse osmosis membranes: optimization of preparation parameters. *J. Appl. Polym. Sci.* **2007,** *103* (1), 134-139.
183. Su, J.; Zhang, S.; Chen, H.; Chen, H.; Jean, Y. C.; Chung, T.-S., Effects of annealing on the microstructure and performance of cellulose acetate membranes for pressure-retarded osmosis processes. *J. Membr. Sci.* **2010,** *364* (1-2), 344-353.
184. Bae, B.; Miyatake, K.; Watanabe, M., Sulfonated Poly(arylene ether sulfone ketone) Multiblock Copolymers with Highly Sulfonated Block. Synthesis and Properties. *Macromolecules (Washington, DC, U. S.)* **2010,** *43* (6), 2684-2691.
185. Hickner, M. A.; Ghassemi, H.; Kim, Y. S.; Einsla, B. R.; McGrath, J. E., Alternative Polymer Systems for Proton Exchange Membranes (PEMs). *Chem. Rev. (Washington, DC, U. S.)* **2004,** *104* (10), 4587-4611.
186. Bosak, V. Z.; Vakulyuk, P. V.; Burban, A. F.; Isaev, S. D.; Vortman, M. Y.; Klimenko, N. S.; Shevchenko, V. V., Charged ultrafiltration polysulfone membranes formed in the presence of ionogenic surface-active oligomers. *Dopov. Nats. Akad. Nauk Ukr.* **2007,** (11), 130-134.
187. Bosak, V. Z.; Vakulyuk, P. V.; Burban, A. F.; Antonyuk, N. G.; Isaev, S. D.; Lavrik, V. I., Production of charged polysulfone ultrafiltration membranes and the study of their properties. *Dopov. Nats. Akad. Nauk Ukr.* **2007,** (8), 127-132.
188. Bosak, V. Z.; Vakulyuk, P. V.; Burban, A. F., Surface modification of polysulfone membranes by UV-initiated graft polymerization of N-vinyl-2-pyrrolidone. *Ukr. Khim. Zh. (Russ. Ed.)* **2007,** *73* (7-8), 116-120.
189. Ismail, A. F.; Lau, W. J., Theoretical studies on structural and electrical properties of PES/SPEEK blend nanofiltration membrane. *AIChE J.* **2009,** *55* (8), 2081-2093.

190. Lau, W. J.; Ismail, A. F., Theoretical studies on the morphological and electrical properties of blended PES/SPEEK nanofiltration membranes using different sulfonation degree of SPEEK. *J. Membr. Sci.* **2009,** *334* (1+2), 30-42.
191. Lau, W.-J.; Ismail, A. F., Effect of SPEEK content on the morphological and electrical properties of PES/SPEEK blend nanofiltration membranes. *Desalination* **2009,** *249* (3), 996-1005.
192. Yamada, S.; Kawabe, N. Aromatic polysulfone gas separation membranes. JP01242123A, 1989.
193. Rao, V.; Friedrich, K. A.; Stimming, U. In *Proton-conducting membranes for fuel cells*, CRC Press: 2009; pp 759-820.
194. Paul, M.; Park, H. B.; Freeman, B. D.; Roy, A.; McGrath, J. E.; Riffle, J. S., Synthesis and crosslinking of partially disulfonated poly(arylene ether sulfone) random copolymers as candidates for chlorine resistant reverse osmosis membranes. *Polymer* **2008,** *49* (9), 2243-2252.
195. Kim, Y.-J.; Lee, K.-S.; Jeong, M.-H.; Lee, J.-S., Highly chlorine-resistant end-group crosslinked sulfonated-fluorinated poly(arylene ether) for reverse osmosis membrane. *J. Membr. Sci.* **2011,** *378* (1-2), 512-519.
196. Kinzer, K. E.; Lloyd, D. R.; Gay, M. S.; Wightman, J. P.; Johnson, B. C.; McGrath, J. E., Phase-inversion sulfonated polysulfone membranes. *J. Membr. Sci.* **1985,** *22* (1), 1-29.
197. Blanco, J. F.; Nguyen, Q. T.; Schaetzel, P., Novel hydrophilic membrane materials: sulfonated polyethersulfone Cardo. *Journal of Membrane Science* **2001,** *186* (2), 267-279.
198. Blanco, J.-F.; Sublet, J.; Nguyen, Q. T.; Schaetzel, P., Formation and morphology studies of different polysulfone-based membranes made by wet phase inversion process. *J. Membr. Sci.* **2006,** *283* (1+2), 27-37.
199. Rose, J. B. Sulfonated polyarylethersulphone copolymers. EP8894A1, 1980.
200. Rose, J. B. Sulfonated polyaryletherketones. EP8895A1, 1980.
201. Rose, J. B. Sulfonated poly(aryl ether ketones). EP41780A1, 1981.
202. Al-Omran, A.; Rose, J. B., Synthesis and sulfonation of poly(phenylene ether ether sulfone)s containing methylated hydroquinone residues. *Polymer* **1996,** *37* (9), 1735-1743.
203. Li, Y.; VanHouten, R. A.; Brink, A. E.; McGrath, J. E., Purity characterization of 3,3'-disulfonated-4,4'-dichlorodiphenyl sulfone (SDCDPS) monomer by UV-vis spectroscopy. *Polymer* **2008,** *49* (13-14), 3014-3019.
204. Geise, G. M.; Park, H. B.; Sagle, A. C.; Freeman, B. D.; McGrath, J. E., Water permeability and water/salt selectivity tradeoff in polymers for desalination. *J. Membr. Sci.* **2011,** *369* (1-2), 130-138.
205. Geise, G. M.; Paul, D. R.; Freeman, B. D., Fundamental water and salt transport properties of polymeric materials. *Prog. Polym. Sci.* **2014,** *39* (1), 1-42.
206. Xie, W.; Ju, H.; Geise, G. M.; Freeman, B. D.; Mardel, J. I.; Hill, A. J.; McGrath, J. E., Effect of Free Volume on Water and Salt Transport Properties in Directly Copolymerized Disulfonated Poly(arylene ether sulfone) Random Copolymers. *Macromolecules (Washington, DC, U. S.)* **2011,** *44* (11), 4428-4438.
207. Lee, C. H.; McCloskey, B. D.; Cook, J.; Lane, O.; Xie, W.; Freeman, B. D.; Lee, Y. M.; McGrath, J. E., Disulfonated poly(arylene ether sulfone) random copolymer thin film composite membrane fabricated using a benign solvent for reverse osmosis applications. *Journal of Membrane Science* **2012,** *389* (0), 363-371.
208. Lee, C. H.; Spano, J.; McGrath, J. E.; Cook, J.; Freeman, B. D.; Wi, S., Solid-state NMR molecular dynamics characterization of a highly chlorine-resistant disulfonated poly(arylene ether sulfone) random copolymer blended with poly(ethylene glycol) oligomers for reverse osmosis applications. *J. Phys. Chem. B* **2011,** *115* (21), 6876-6884.
209. Xie, W.; Park, H.-B.; Cook, J.; Lee, C. H.; Byun, G.; Freeman, B. D.; McGrath, J. E., Advances in membrane materials: desalination membranes based on directly copolymerized disulfonated poly(arylene ether sulfone) random copolymers. *Water Sci. Technol.* **2010,** *61* (3), 619-624.
210. Xie, R. J.; Gomez, M. J.; Xing, Y. J., Understanding permeability decay of pilot-scale microfiltration in secondary effluent reclamation. *Desalination* **2008,** *219* (1–3), 26-39.

211. McGrath, J. E. In *Chlorine resistant membranes for reverse osmosis and nanofiltration*, American Chemical Society: 2009; pp POLY-224.
212. Sundell, B. J.; Lee, K.-s.; Cook, J. R.; Shaver, A.; Jang, E. S.; Freeman, B. D.; McGrath, J. E. In *Effect of backbone structure, degree of sulfonation and crosslinking on water transport properties for sulfonated poly(arylene ether sulfone) copolymers*, American Chemical Society: 2014; pp POLY-487.
213. Hou, J.; Li, J.; Madsen, L. A., Anisotropy and Transport in Poly(arylene ether sulfone) Hydrophilic-Hydrophobic Block Copolymers. *Macromolecules* **2010,** *43* (1), 347-353.
214. Zhang, H.; Fang, S.; Ye, C.; Wang, M.; Cheng, H.; Wen, H.; Meng, X., Treatment of waste filature oil/water emulsion by combined demulsification and reverse osmosis. *Separation and Purification Technology* **2008,** *63* (2), 264-268.
215. Ebewele, R. O., *Polymer science and technology*. CRC Press: 2000.
216. Sawyer, L. C.; Grubb, D. T., *Polymer microscopy*. Chapman and Hall: London; New York, 1996.

2.0 Disulfonated Poly(arylene ether sulfone) Random Copolymer Blends Tuned for Rapid Water Permeation via Cation Complexation with Poly(ethylene glycol) Oligomers

Chang Hyun Lee[a], Ozma Lane[a], James E. McGrath[a], Jianbo Hou[a], Louis A. Madsen[a], Justin Spano[a], Sungsool Wi[a], Joseph Cook[b], Wei Xie[b], Geoffrey Geise[b], and Benny Freeman[b*]

[a] Macromolecules and Interfaces Institute, Virginia Polytechnic Institute And State University, Blacksburg, VA 24061

[b]Department of Chemical Engineering, Center for Energy and Environmental Resources, University of Texas at Austin, Austin, TX 78758

Reproduced with permission from Chemistry of Materials[1]

Here we present fundamental studies of a new blending strategy for enhancing water permeability in ionomeric reverse osmosis membrane materials. A random disulfonated poly(arylene ether sulfone) copolymer containing 20 mol percent hydrophilic units (BPS-20) in the potassium salt form was blended with hydroxyl-terminated poly(ethylene glycol) oligomers (PEG, M_n= 600-2000 g/mol) to increase the water permeability of BPS-20. Blending PEG with the copolymer resulted in pseudoimmobilization of the BPS-20 polymers chains because PEG complexes with cations in the sulfonated polymer matrix. Strong ion-dipole interactions between the potassium ions of the BPS-20 sulfonate groups ($-SO_3K$) and the PEG oxyethylene ($-CH_2CH_2O-$) were observed via NMR spectroscopy. These interactions are similar to those reported between crown ethers and free alkali metal systems. The PEG oligomers were compatible with the copolymer at 30 ^oC in an aqueous environment. Transparent and ductile BPS-20/PEG blend films exhibited a Fox-Flory-like

glass transition temperature depression as the PEG volume fraction increased. This depression depended on both PEG chain length and concentration within the BPS-20 matrix. Both ion-dipole interactions and high coordination of $–CH_2CH_2$- with $–SO_3K$ yielded a defined and interconnected hydrophilic channel structure. The water permeability and free volume of BPS-20/PEG lend films containing 5 or 10 wt% PEG increased relative to BPS-20. The blend films, however, exhibited reduced sodium choride (NaCl) rejection compared to BPS-20. Addition of PEG did not significantly alter the material's mechanical properties in the dry or hydrated states. Unlike commercial state-of-the-art polyamide RO membranes, the blend materials do not degrade when exposed to aqueous chlorine (hypochlorite) at pH 4. This comprehensive suite of measurements provides an understanding of the molecular and morphological features needed for rational design of next-generation, chlorine-tolerant water purification materials.

2.1 Introduction

The ability to efficiently and economically produce fresh water from brackish and seawater is critical to addressing the growing global water shortage.[2] Reverse osmosis (RO) processes can be used to effective remove salts and large solutes, including bacteria, from natural water using membranes with high flux and high salt rejection characteristics.[3, 4] Currently, interfacially polymerized aromatic polyamide (PA) thin film composite membranes are the state-of-the-art RO technology because they offer high water flux and salt rejection (>99%) over a wide pH range.[5] PA membranes, however, exhibit poor resistance to degradation by chlorine-based chemicals such as sodium hypochlorite, which is used to disinfect water.[6, 7] As a result, RO membrane performance degrades when PA membranes are exposed to even low concentrations of available chlorine.[6, 8, 9]

Disulfonated poly(arylene ether sulfone) copolymers, now being developed for desalination membrane applications, are more stable in chlorinated solution than commercial PA membranes.[10, 11] This result may be due to the absence of amide bonds in the sulfonated polysulfone; amide bonds, such as those found in commercial PA RO membranes, are vulnerable to attack by chlorine-based chemicals.[12, 13] Figure 2-1 presents the chemical structure of 20 mol % disulfonated poly(arylene ether sulfone) random copolymer (BPS-20). This copolymer, when studied as a cast film, exhibits stable RO performance, i.e., no substantial decrease in salt rejection or increase in water flux, after continuous exposure to chlorinated water at both high and low pH (>40 h at 500 ppm chlorine).[10] In contrast, a commercial PA membrane (SW30HR, Dow Film-Tec) experienced a 20% decrease in salt rejection within 20 h of exposure to the same chlorinated conditions.[10] The water flux and salt rejection of BPS random copolymers exhibit a trade-off relationship; highly water-permeable BPS materials tend to exhibit relatively low NaCl rejection and vice versa. BPS-20 has been identified as an alternative candidate for desalination membrane applications because its NaCl rejection is >99%.[10] However, the BPS-20 water permeability (0.033L μm $m^{-2}h^{-1}bar^{-1}$) is low. To put this value in perspective, consider a scenario where the BPS-20 material has a 100 nm active layer in a composite membrane structure, similar to that of commercially available state-of-the-art PA RO membranes. In this case, the water permeance would be expected to be 0.33 L m^{-2} h^{-1} bar^{-1} (2000 ppm NaCl feed at 27.6 bar and pH 8). This value can be compared to a DOW SW30HR RO membrane, whose performance is 1.1 L m^{-2} h^{-1} bar^{-1}.[14]

This paper describes a new approach to increase the water permeability of BPS-20 and thus improve the material's desalination performance, via the addition of poly(ethylene glycol) (PEG, Figure 2-1), a hydrophilic cation complexing agent. PEG oligomers were blended with BPS-20 to

tailor the resulting blend's water permeability without changing the degree of sulfonation of the BPS material. PEG systems have been widely used in gas separations,[15, 16] water purification,[17-21] and biomedical applications.[22]

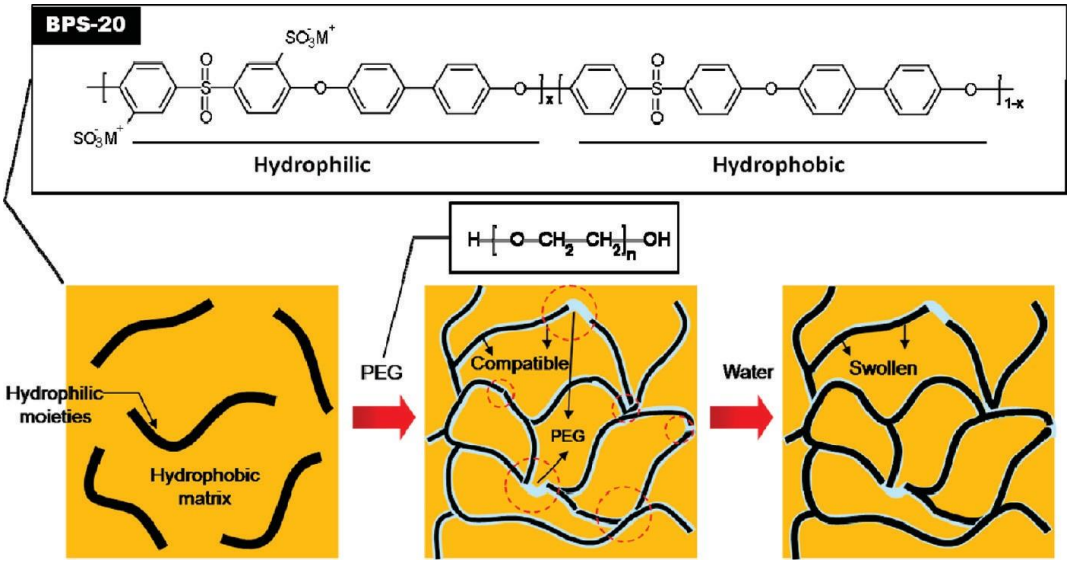

Figure 2- 1. Pseudoimmobilization of PEG molecules with BPS-XX (M^{+} = Na^{+} or K^{+}, XX = degree of sulfonation in mol %). In BPS-20, *x* is 0.2.

The water-soluble nature of PEG may limit its application in aqueous systems. PEG is often immiscible with many polymers because it does not interact favorably with many polymer matrices. As a result, water often extracts PEG from blends with many polymers. To prevent such leaching, PEG chains can be immobilized via chemical modification or hydrogen bonding with acidic polymers.[18, 23] There are, however, applications for PEG where blending has been successfully employed.[15, 24]

PEG ether oxygen atoms form complexes with a variety of metal cations (Li^+, Na^+, K^+, Cs^+, and Rb^+) via ion-dipole interactions similar to the behavior of cyclic ethers.[25-27] Such interactions in aqueous environments have been suggested to explain the miscibility of PEG and salt form sulfonated polymers, which are composed of sulfonate anions and metal cations (-SO_3M,

where M is a cation of an alkali metal element such as Na or K).[28] If PEG does complex with metal cations in sulfonated polymers, physical enthalpic interactions might effectively immobilize PEG in the sulfonated polymer matrix. If PEG does complex with metal cations of sulfated polymers, physical enthalpic interactions might effectively immobilize PEG in the sulfonated polymer matrix without the use of covalent bonds (pseudoimmobilization, Figure 2-1). This interactions could prevent PEG from leaching out of the polymer matrix upon exposure to water provided that the interactions are strong and sustained. Additionally, PEG may increase the water permeability of the sulfonated polymer matrix. This study seeks to understand the nature of the interaction between PEG and the disulfonated copolymer, BPS-20. The main objective is to systematically investigate the influence of PEG complexing agents, with different molecular weights and concentrations, on the physicochemical characteristics of the salt form of sulfonated polymers membranes. To probe these polymer blends, we employed pulsed-field gradient stimulated echo (PGSTE) NMR spectroscopy, which can track diffusion of water molecules in mixed matrices over time using magnetic field gradients to label nuclear spins with NMR frequencies based on their locations.[29] Another major objective is to verify the efficacy of our pseudoimmobilization approach for forming fast water transport pathways for desalination membranes. Finally, the chlorine resistance of the blend films was compared to a PA membrane.

2.2 Experimental

2.2.1 Materials

BPS-20 in the potassium salt form was synthesized by Akron Polymer Systems (Akron, OH) following published procedures.[30-35] The material used in this study, BPS-20 (the exact degree of sulfonation was 20.1 mol %, measured using ^{1}H NMR) has an intrinsic viscosity of 0.82 dL g^{-1} in NMP with 0.05 M LiBr at 25^{o}C. PEG oligomers (molecular weight M_n= 600 (0.6k), 1000

(1k), and 2000 (2k) with hydroxyl terminal endgroups (Figure 2-1) were purchased from Aldrich Chemical Co. and were used as received. Dimethylacetamide (DMAc) (Aldrich Chemical Co.) was used as a casting solvent without additional purification.

2.2.2 BPS-20/PEG Blends

After 2 g of BPS-20 was completely dissolved in DMAc at 30 ^{o}C, a PEG oligomer of the desired molecular weight was added to the BPS-20 solutions in two different concentrations, 5 wt % and 10 wt %, where wt % was defined relative to the mass of BPS-20 in the solution. The resulting solutions were mixed for 1 day. Each solution (total solids concentration, 10 wt% in DMAc) was degassed under vacuum at 25 ^{o}C for at least 1 day and cast on a clean glass plate. Then the cast solution was dried for 4 h at 90 ^{o}C and heated to 150 ^{o}C for 1 day under vacuum. The resulting films were easily peeled off of the glass plate and stored in deionized water at 30 ^{o}C for 2 days to further remove residual solvent. The nominal thickness of all films was approximately 30-40 μm, except those used for FT-IR measurement (20μm). Transparent, ductile, and light yellow BPS-20/PEG blend films were obtained. The yellow color increased with increasing PEG molecular weight and concentration. The BPS-20/PEG films are denoted as BPS-20_PEG molecular weight_PEG concentration (wt%). For example, BPS-20_PEG0.6k-5 denotes a BPS-20 film containing 5 wt % of 0.6 kDa PEG.

2.2.3 Characterization

The thermal decomposition of BPS-20_PEG films was investigated using a thermogravimetric analyzer (TGA) (TA Instruments Q500 TGA) operated at a heating rate of 10 ^{o}C min^{-1} from 50 to 600 ^{o}C in a 60 mL min^{-1} nitrogen sweep gas. Prior to the thermal decomposition measurements, all films were preheated in the TGA furnace at 110 ^{o}C for 15 min.

Transmission Fourier Transform Infrared (FT-IR) spectroscopy was used to study the interactions between BPS-20 and PEG. FT-IR spectra in the range of 4000-900 cm^{-1} were obtained using a Tensor 27 spectrometer (Bruker Optics).

Cross-polarization magic-angle spinning (CPMAS) ^{13}C NMR spectra were taken with a Bruker Avance II 300 MHz wide-bore spectrometer operating at Larmor frequencies of 75.47 MHz for ^{13}C and 300.13 MHz for ^{1}H nuclei. Thin films samples (50-60 mg) were cut into small pieces and packed into 4 mm magic angle spinning (MAS) rotors. Cross-polarization for 1 ms mixing time was achieved at 50 kHz rf-field at the ^{13}C channel with the ^{1}H rf field ramped linearly over a 25% range centered at 38 kHz. A pulse technique known as total suppression of spinning side bands (TOSS) was combined with a CP sequence to obtain sideband-free ^{13}C MAS spectra at a 6 kHz spinning speed.[36] The NMR signal averaging was achieved by coadding 2048 transients with a 4 s acquisition delay time. ^{1}H and ^{13}C $\pi/2$ pulse lengths were 4 and 5 μs, respectively. Small phase incremental alternation with 64 steps (SPINAL-64) decoupling sequence at 63 kHz power was used for proton decoupling during ^{13}C signal detection.[37]

To determine the glass transition temperature (T_g) of BPS-20 and BPS-20/PEG blend films, dynamic mechanical analysis (DMA) was conducted using a TA DMA 2980 (TA Instruments) in thin film tension mode; the temperature range was 0 to 300 ^{o}C with a ramp of 5 ^{o}C min^{-1} in a nitrogen atmosphere. The films samples were 4 mm in width, and each was subjected to a preload force of 0.025 N with an amplitude of 25 μm at a frequency of 1 Hz.

Water uptake (%) was calculated using the following equation, where W_D and W_W are the measured masses of dry and fully hydrated film samples, respectively. Each sample, approximately

5 cm x 5 cm, was dried in a vacuum oven at 110 °C for 1 day before measuring W_D and immersed in deionized water at 25 °C for 1 day before measuring W_W.

$$Water\ Uptake = \frac{W_w - W_D}{W_D} * 100$$

Surface morphologies were examined via tapping mode atomic force microscopy (AFM), using a Digital Instruments MultiMode scanning probe microscope with a NanoScope Iva controller. A silicon probe (Veeo, end radius < 10 n, with a force constant k= 5 N m^{-1}) was used to image the samples, and the set point ratio was 0.82. Prior to measurement, all samples were equilibrated to 30 °C and 40% relative humidity (RH) for at least 12 h.

For pulsed field gradient NMR spectroscopy, each film was cut into 5 x 5 mm peacies and stacked together to a total mass of about 40 mg in a custom-built Teflon cell that was sealed to maintain water content during diffusion measurements. The test cell was loaded into a Bruker Avance III WB 400 MHz NMR spectrometer equipped with both a Micro5 triple-axis-gradient (maximum 300 G cm^{-1}) microimaging probe and an 8 mm double resonance ($^1H/^2H$) rf coil. The pulsed-gradient stimulated echo pulse sequence (PGSTE) was applied with a $\pi/2$ pulse time of 32 μs, a gradient pulse duration (δ) ranging from 1 to 3 ms, and diffusion time (Δ) ranging from 20 to 800 ms.[29] Each measurement was repeated with 32 gradient steps, and the maximum gradient strength was chosen to achieve 70-90% NMR signal attenuation.

The water permeability (P_w, L μm m^{-2} h^{-1} bar^{-1}) of BPS-20 and BPS-20_PEG films was evaluated at 25 °C using a dead-end cell apparatus with a feed of 2000 ppm in deionized water. P_w was defined as the volume of water (V) permeated per unit time (t) through a membrane sample of area (A) and thickness (l) at a pressure difference (ΔP = 400 psig):

$$P_w = \frac{Vl}{At\Delta P}$$

Salt rejection (R, %) was measured using a dead-end cell filtration apparatus with an aqueous feed solution containing 2000 ppm NaCl at pH 6.5-7.5 and a pressure of 400 psig. Salt rejection (R) was calculated as follows, wherein C_f and C_p are the NaCl concentrations in the feed and permeate, respectively. Salt concentration was measured with a NIST-traceable expanded digital conductivity meter (Oakton Con 110 conductivity and TDS meter).

$$R = \frac{C_f - C_p}{C_f} * 100$$

Tensile properties of the films were determined using an Instron 5500R universal testing machine equipped with a 200 lb load cell at 30 ^oC and 44-54% RH. Crosshead displacement speed and gauge length were set to 5 mm min^{-1} and 25 mm, respectively. Dogbone specimens (50 mm long and at least 4 mm wide) were cut from a single film. Prior to the measurement, each specimen was dried under vacuum at 110 ^oC for at least 12 h, and then equilibrated at 30 ^oC and 4% RH.

2.3 Results and Discussion

Because PEG is water-soluble and these materials are being evaluated for desalination applications, the stability of the hydrated films was explored. To determine whether PEG leached from the blend films, samples were stored in 30 ^oC deionized water for 150 days. After the 150 day soaking period, PEG content in the blend films was investigated using TGA, FT-IR, and NMR spectroscopy. Figure 2-2 presents dynamic TGA thermograms of BPS-20 and BPS0-20/PEG blend films. All of the materials exhibit three distinct thermal decomposition steps: (I) thermal

evaporation of water molecules [<215 °C], (III) thermal desulfonation of BPS-20 [375-420 °C], and (IV) thermo-oxidation of BPS-20.[35, 38] The initial weight loss was ascribed to desorption of water from the samples; this weight loss increased with PEG concentration suggesting that water hydrates both the PEG molecules and BPS-20 sulfonate groups.

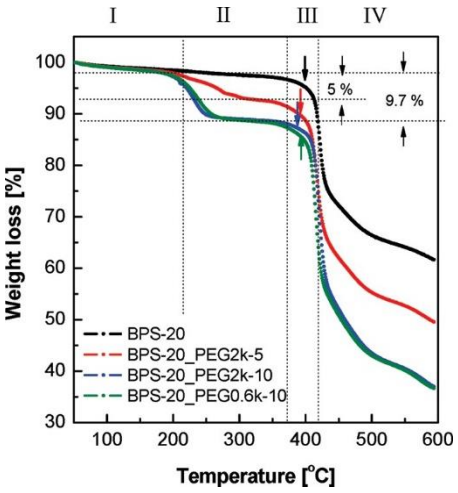

Figure 2-2. TGA Thermograms of BPS-20 and BPS-20/PEG blends after soaking in deionized water for 150 days.

An additional thermal decomposition step (II), which is ascribed to thermo-oxidation of PEG [215-375 °C], was observed for the BPS20-Peg blend samples. Thermal decomposition of PEG began around 215 °C, this temperature is higher than the initial thermal decomposition temperature (T_d) of pure PEG (~175 °C) and similar to the T_d of the ester bridge grafted PEG.[39, 40] This increase in the initial decomposition temperature suggests that PEG interacts with BPS-20. Interactions of this nature may have bond energies similar to a weak covalent bond, such as an ester.[40] PEG decomposition was quantified and compared to the amount of PEG initially added to the BPS-20 polymer matrix. The mass of PEG that remained in the blend matrix after the water soaking step was essentially equal to the mass of PEG that was initially present in the blend. Therefore, PEG did not leach from the blend matrix under our test conditions. We believe that the

physical interaction between PEG and BPS-20 may arise from two sources: bonding interactions between the BPS-20 sulfonate groups and PEG –OH groups and ion-dipole interactions between PEG and the metal cation (K^+) associated with the BPS-20 sulfonate groups. The maximum BPS-20 thermal desulfonation temperature (T_{DS} ~398 ^oC) decreases by 5-12 ^oC upon addition of PEG. The reduction of T_{DS} was more significant for the BPS-20/PEG blends containing higher molecular weight PEG and higher PEG concentration.

Figure 2-3 presents FT-IR spectra of BPS-20 and BPS-20/PEG samples over the relevant range of vibration frequencies to confirm the identity of the interactions between PEG and BPS-20. To ensure that peak intensities were normalized, dry films of equivalent thicknesses (20 μm) were analyzed. The strong band at 2850 cm^{-1} in Figure 2-3 (a) is assigned to the stretching vibration of the aliphatic alkyl PEG groups. The peak intensity of these groups increased with PEG concentration, but the peak position did not shift. The bands at 1075 and 1030 cm^{-1} in Figure 2-3 (b) are attributed to the symmetric stretching vibration of sulfonate ions in BPS-20. The absorption band at 1107 cm^{-1} is associated with the (-SO_3K) asymmetric stretching vibration. Its frequency is higher than the frequency of the corresponding vibration for the –SO_3Na form of the same BPS-20 polymer.[41, 42] After the addition of the PEG, most of the peaks, including a stretching vibration band of diphenyl ether at 1006 cm^{-1}, did not shift. This result indicates that hydrogen bonding between BPS-20 and PEG is not significant when the sample is in the dry state. In this discussion, the relative intensity changes in the SO_3^- bands were excluded because of the presence of a strong characteristic PEG band occurring between 1020 and 1200 cm^{-1}.[43]

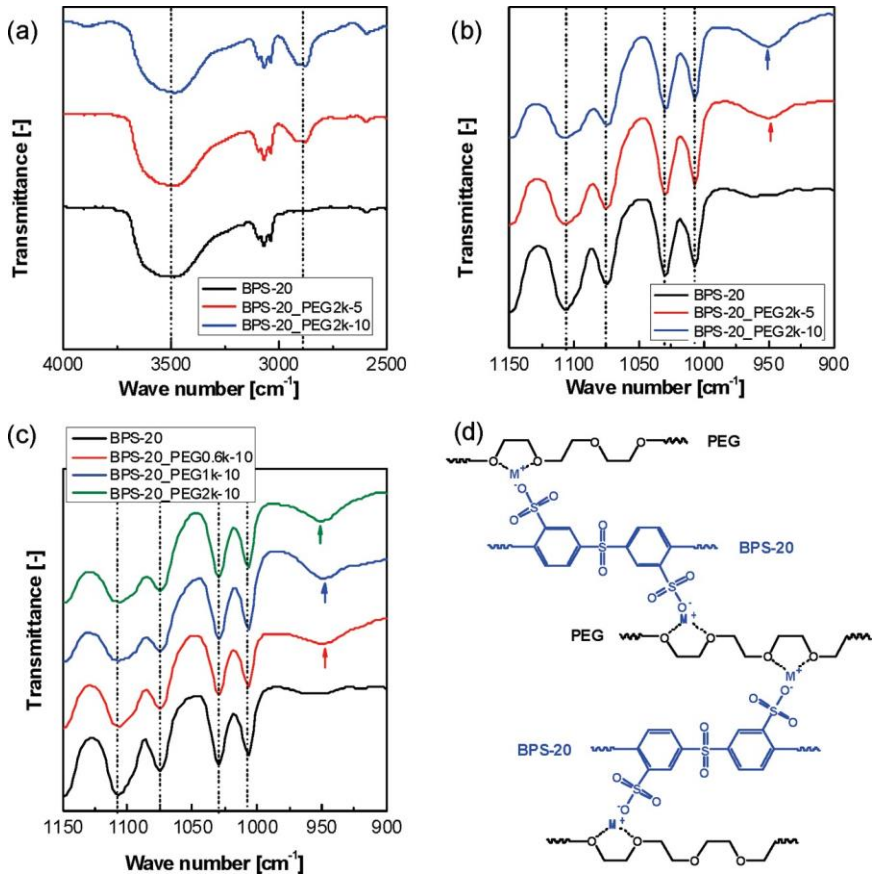

Figure 2-3. FT-IR spectra of BPS-20 and BPS-20_PEG materials with different concentrations (a and b) and molecular weights (c) of PEG. (d) Simulated cation binding with PEG molecules ($M^+ = Na^+$, K+, and other cations).

In contrast, the absorption band (~950 cm^{-1}) in Figure 2-3b, assigned to the PEG aliphatic ether, became more distinct and shifted to higher frequency as PEG concentration increased. An analogous band shift was observed in BPS-20/PEG samples containing high molecular weight PEG (Figure 2-3c). The peak shift suggests that a chemical species exists in the vicinity of the PEG molecules and physically interacts with the PEG aliphatic ether groups.

Free alkali metal cations, such as Na^+ and K^+, form complexes with PEG repeat units in both aqueous and non-aqueous solvents.[26, 44-46] Furthermore, the ion-dipole interaction of PEG with the free metal cations is strengthened when long PEG chains (>9 repeat units) are used.[47] In particular, the selectivity of long PEG chains to potassium ions are promoted to the equivalent

level of crown ethers.[28] PEG chains with more than 14 repeat units used in this study may interact strongly with the potassium ions that are associated with the potassium sulfonate groups on the BPS-20 chains (Figure 2-3d). This is because the ionic bond strength of the potassium sulfonate group is theoretically stronger than the ion-dipole interaction between PEG and the sulfonate group metal cations and the PEG repeat units have higher potassium coordination numbers (6-7) compared to sodium ions (2-4).[48, 49]

Solid state ^{13}C NMR spectroscopy of BPS-20/PEG blends provided information about the interactions of BPS-20 and PEG (Figure 2-4). The solid state ^{13}C NMR used here was sensitive enough to monitor infinitesimal changes in the environment of the fully hydrated polymer system. Characteristic peaks for hydrated BPS-20 were consistently observed at the same chemical shifts regardless of PEG addition. Therefore, hydrogen bonding is not significant in hydrated BPS-20, and the ion-dipole interaction governs the macroscopic properties of both the dry and hydrated BPS-20/PEG system.

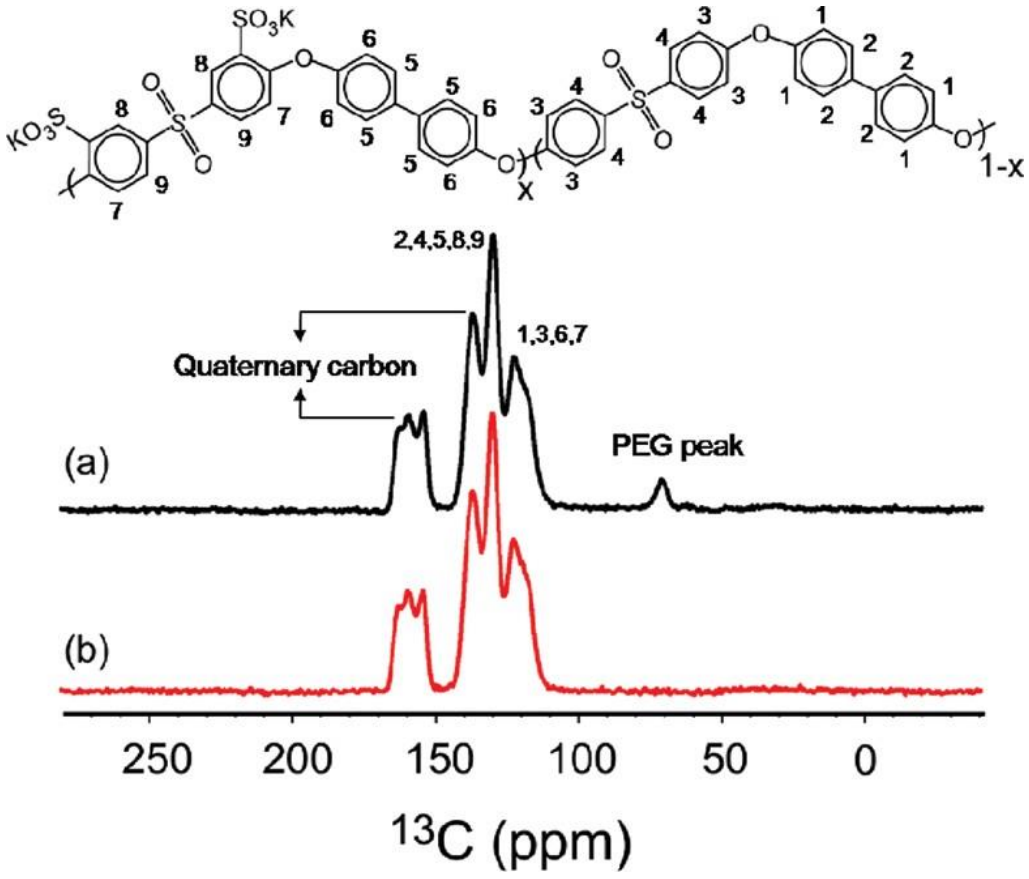

Figure 2-4. Solid state ^{13}C NMR spectra of (a) BPS-20_PEG 0.6k-5 and (b) BPS-20.

We believe that the ability of PEG to complex with metal cations affected the BPS-20/PEG blend glass transition temperature (T_g). Generally, the T_g of sulfonated polymers increases with the degree of sulfonation due to the bulky and ionic nature of the sulfonate groups.[50] For example, the BPS-20 T_g (270 ^oC, Figure 2-5), is higher than that of BPS-00 (Radel, T_g = 220 ^oC). Also, BPS-20 displays a broad T_g range, since the sulfonate groups are randomly distributed and may form ionic domains of different sizes within the hydrophobic matrix. When incorporated into BPS-20, PEG may disrupt the intermolecular and/or intramolecular ionic interactions between the sulfonate groups in the BPS-20 ionic domains (entropic effect); a decrease in T_g could indicated this

disruption. A broad tan δ peak between 150 and 200 °C was observed using DMA. This broad peak can be attributed to sulfonated ionic domain dilution that occurs when PEG is introduced to BPS-20. Glass transition temperature depression behavior was especially significant in BPS-20/PEG blend samples containing long PEG chains and higher PEG concentration. For example, the T_g of BPS-20_PEG2k_10 dropped by 43 °C, comparable to that of nonsulfonated BPS-00. The T_g of BPS-20/PEG blend samples decreased linearly with a slope dependent on PEG molecular weight, which makes it possible to estimate the theoretical T_g change in BPS-20 upon PEG addition.

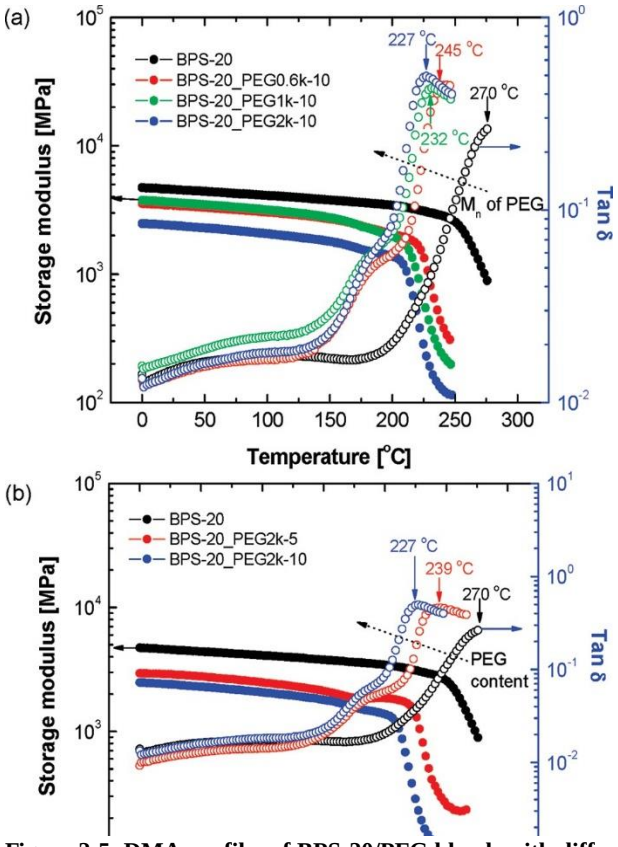

Figure 2-5. DMA profiles of BPS-20/PEG blends with different (a) molecular weights and (b) PEG concentrations.

BPS-20/PEG blend samples are binary systems composed of BPS-20 and PEG, which has a T_g of -60 °C. The PEG homopolymer T_g is effectively contant over the molecular weights chosen

for this study.[51, 52] Unlike immiscible systems that show distinct and constant T_gs for each component, the T_g of the BPS-20/PEG binary system depended on PEG concentration. The measured glass transition temperatures are very similar to theoretical predictions made using the Flory equation.[53] This comparison is commonly used to determine whether binary systems are miscible, compatible, or immiscible. In the following equation, $T_{g,i}$ and W_i represent the T_g and weight fraction of component i, respectively.

$$\frac{1}{T_{g,BPS-20/PEG}} = \frac{W_{BPS-20}}{T_{g,BPS-20}} + \frac{W_{PEG}}{T_{g,PEG}}$$

On the basis of the agreement between the measured BPS-20/PEG glass transition temperature data and predictions made using the Flory-Fox equation, we conclude that BPS-20 and Peg form a compatible system as a result of ion-dipole interactions between PEG and the BPS-20 sulfonate groups.

As the degree of sulfonation increases, the density of the BPS copolymer increases relative to unsulfonated BPS-00 (1.30 g cm^{-3}).[54] When PEG is incorporated into BPS-20, the density of the blended material decreases (Figure 2-6a). This decrease in density occurs because PEG acts as a plasticizer that increases BPS-20 chain spacing and free volume. The BPS-20/PEG blend density, when compared to the blend density calculated by assuming volume additivity, suggests that blending PEG with BPS-20 results in free volume changes that extend beyond what would be expected by simple mixing (Figure 2-6a). Dry BPS-20/PEG samples exhibit higher density than

wet samples. Density measurements also suggest that the free volume of BPS-20/PEG increased as PEG chains became longer and more concentrated.

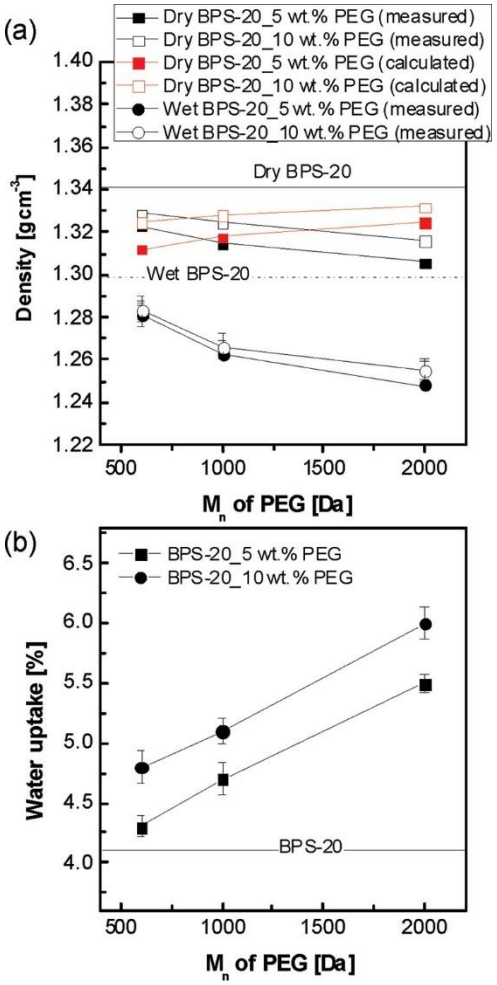

Figure 2-6. (a) Density and (b) water uptake of BPS-20/PEG blends. Calculated densities were obtained from volume additivity.

The water uptake of BPS-20/PEG correlated inversely with density (Figure 2-6b). Water uptake increased as hydrophilic PEG was incorporated into BPS-20. Figure 2-6 indicates that low density BPS-20/PEG samples (high free volume samples) showed greater water uptake than samples of higher density (low free volume samples). Free volume is expected to influence water and salt transport properties in these polymers.[55]

In addition to water uptake, the surface morphology of sulfonated polymers can influence water permeability. AFM images (Figure 2-7) indicate that the strong ion-dipole interaction of PEG with potassium ions in BPS-20 sulfonate groups can induce a hydrophilic-hydrophobic interaction even though BPS-20 is a random copolymer. In BPS-20, hydrophilic rod-like structures indicated in the darker regions are randomly distributed throughout the light-colored hydrophobic copolymer matrix.[35] When PEG was added to BPS-20, the morphology of the matrix changed. In BPS-20_PEG2k-5 (Figure 2-7b), hydrophilic phase connectivity and uniformity both appeared to improve. This result may be related to strong ion-dipole interactions and the high coordination number of PEG repeat units to potassium ions in the BPS-20 sulfonate groups.[49, 56] PEG with more than 9 repeat units typically prefers a meander or helical coil structure when exposed to free alkali metal cations.[47] The observed hydrophilic-hydrophobic phase separation depends on both PEG chain length and concentration. As PEG chain length increased, at a constant concentration (10 wt%, Figure 2-7c-e), the hydrophilic domains became more interconnected but generally decreased in size. Another morphological change was observed as the PEG concentration in BPS-20/PEG2k was varied from 5 to 10 wt % (Figure 2-7b,e). Unlike BPS-20_PEG2k-5, BPS-20_PEG2k-10 appears to have two different kinds of ionic domains: irregularly distributed ionic domains, with sizes similar to BPS-20_PEG2k5, and capillary-shape ionic domains. The ionic domains appear to be connect by long, tortuous hydrophilic pathways. The unevenly developed morphology may cause BPS-20_PEG2k-10 to have a lower water permeability than BPS-20_PEG2k-5.

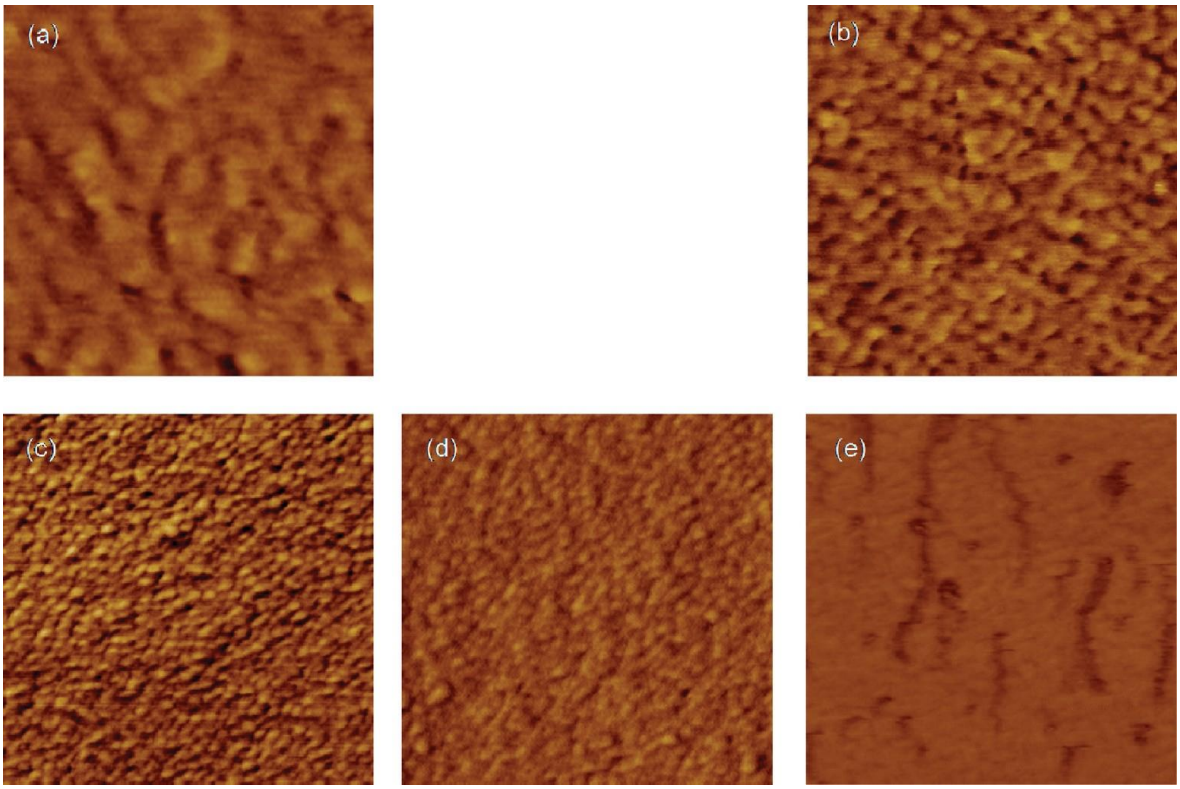

Figure 2-7. AFM images of (a) BPS-20, (b) BPS-20_PEG2k-5, (c) BPS-20_PEG0.6k-10, (d) BPS-20_PEG1k-10, and (e) BPS-20_PEG2k-10 materials in tapping mode. The dimensions of the images are 250 x 250 nm^2. The phase scale is 0-20°. The measurement was conducted at 35% RH.

PGSTE-NMR provides information about the diffusion of molecules in materials, such as the self-diffusion coefficient D of water in a polymer matrix. This technique is sensitive to the identity of the mobile species and changes in the sample environment. D in a polymer matrix depends strongly on water uptake and temperature. Morphological changes also strongly influence the diffusion of water through the material. In fact, all samples exhibited reduced D values at long diffusion times, indicating the existence of tortuous hydrophilic pathways similar to those observed in the AFM images of Figure 2-7. However, interpreting the water permeation behavior in these materials is not trivial since the PEG influences the hydrophilicity and ionic domain structure of the material. In this study, we used the Mitra equation for porous media to assess diffusive

restrictions (related to the surface-to-volume ratio of diffusion pathways, S/V) that result from the material's morphology.[57]

$$D = D_0\left(1 - \frac{4}{9\sqrt{\pi}}\frac{S}{V}\sqrt{D_0\Delta}\right)$$

Here, S/V (m^{-1}) is a factor associated with the internal roughness in the mixed matrix. An increase in S/V is expected to enhance water diffusion. By fitting D vs diffusion time Δ, we extracted values for the effective 'free' water diffusion coefficient D_0 (that expected at very small Δ) and S/V. Here, D_0 is interpreted as the effective intradomain diffusion coefficient of "free" water through the polymer's hydrophilic domain structure. Figure 2-8 shows the change in D_o*S/V as a function of PEG molecular weight. D_o*S/V values appear to correlated with water permeability data in Figure 2-9. This scaled water diffusion behavior in the mixed matrix materials decreased with increasing PEG chain length. However, the D_o*S/V values for the BPS-20/PEG blend samples were greater than that for BPS-20. This finding indicates that S/V plays an important role in the diffusion and permeation of water through these samples.

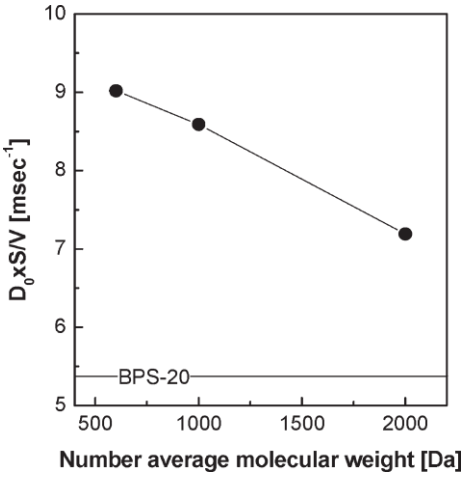

Figure 2-8. Diffusion behavior through tortuous water pathways in BPS-20/PEG 10% materials.

Figure 2-9 presents water permeability and salt rejection data for BPS-20/PEG films. In the samples containing PEG, the water permeability of BPS-20/PEG increased relative to BPS-20. The increase in water permeability depended on both PEG concentration and chain length. Water permeability was greater in samples that contained a higher concentration of PEG; these samples, with 10 wt % PEG, also exhibited higher water uptake. Water permeability of BPS-20/PEG, however, decreased as PEG chain length increased. The water permeability of the BPS-20/PEG blend films is likely affected by the morphological changes that occur upon adding PEG, as indicated by AFM and scaled PGSTE-NMR (Mitra analysis). We believe that the morphological contribution was particularly significant in BPS-20_PEG2k, which contained the highest PEG molecular weight. The long and tortuous channels in BPS20_PEG2k-10 may restrict water diffusion and cause the water permeability to decrease even though the water uptake increased relative to that of BPS-20_PEG2k-5.

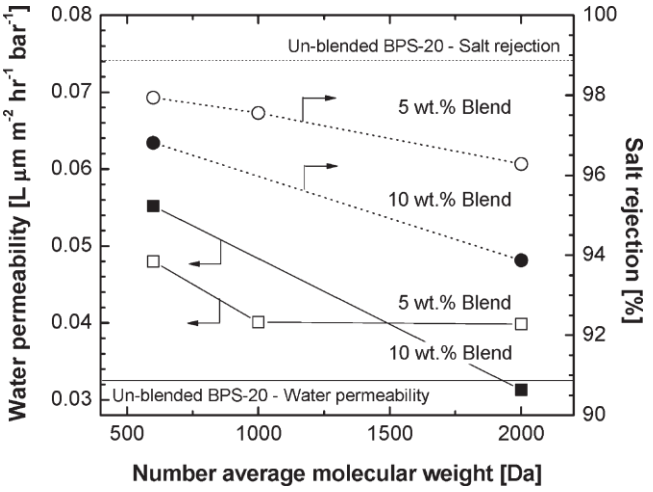

Figure 2-9. RO performance of BPS-20/PEG blend films: water permeability (left) and salt rejection (right).

The water permeability of the blend materials may also be influenced by hydrogen bonding between water molecules and hydrophilic functional groups in the blend materials: BPS-20 sulfonate, PEG hydroxyl terminal endgroups, and PEG ether groups. A constant amount of BPS-

20 was used in BPS-20/PEG blends. Because the number of sulfonate groups was fixed, the difference in hydrogen bonding activity within different BPS-20/PEG blend samples is theoretically derived from the number of nonionic hydroxy and ether groups.[58] Table 2-1 shows the calculated number of the two functional groups per gram of BPS-20. The relative number of hydroxyl groups increased as PEG molecular weight decreased. Furthermore, the relative number hydroxyl groups increased when PEG concentration increased from 5 to 10 wt %. These results are similar to the water permeability results in Figure 2-9, suggesting that the hydroxy groups may contribute more to water permeability that the ether groups.

Table 2-1. Properties of BPS-20 and BPS-20/PEG blends

	PEG functional groups per gram of BPS-20				mechanical properties [MPa]			
sample	−OH groups [equivalents/ gram (BPS-20)]	relative ratio[a]	−O− groups [equivalents/ gram (BPS-20)]	relative ratio[b]	tensile modulus	standard deviation	tensile strength	standard deviation
BPS-20					1580	10	56	3
BPS-20_PEG0.6k-5	1.0×10^{20}	3.3	7.0×10^{20}	1.1	1500	270	48	2
BPS-20_PEG0.6k-10	2.0×10^{20}	6.7	1.4×10^{21}	2.2	1620	240	48	6
BPS-20_PEG1k-5	6.0×10^{19}	2.0	6.3×10^{20}	1.0	1810	240	55	1
BPS-20_PEG1k-10	1.2×10^{20}	4.0	1.3×10^{21}	2.0	1840	250	54	5
BPS-20_PEG2k-5	3.0×10^{19}	1.0	6.7×10^{20}	1.0	1750	210	57	2
BPS-20_PEG2k-10	6.0×10^{19}	2.0	1.3×10^{21}	2.0	1600	290	58	3

[a] Number of $[-OH]_{sample}$/number of $[-OH]_{BPS\text{-}20\_PEG2k\text{-}5}$. [b] Number of $[-O-]_{sample}$/number of $[-O-]_{BPS\text{-}20\_PEG2k\text{-}5}$

On the basis of the results shown in Figure 2-9, salt rejection decreases substantially with increases in PEG concentration and molecular weight. For example, in a BPS-20 sample prepared with 10 wt % of 2 kDa PEG, the rejection was 93.9%. For comparison, the rejection of pure BPS-20 was 98.9%. We speculate that the ion-dipole interaction between K^+ ions in the BPS-20 sulfonate groups and PEG oxyethylene units may weaken the electrostatic interaction of the sulfonate groups that would typically form physically cross-linked, ion-selective domains. Additionally, PEG incorportation into BPS-20 increases the material's water uptake. This increase in swelling reduces the concentration of sulfonate groups in the polymer matrix. This reduction in the sulfonate group concentration may result in decreased ion exclusion and thus decrease salt

rejection.[59] Both the disruption of ion-selective domains and the dilution of sulfonate group concentration could result in reduced salt rejection as PEG concentration increases, which is consistent with the experimental observations. The reduced salt rejection was more significant in BPS-20/PEG samples prepared with high molecular weight PEG. Longer PEG chains are associated with the formation of stronger ion-dipole interactions with K^+ ions in the BPS-20 sulfonate groups and highly water swollen polymer matrices.

Plasticizers increase the free volume of a polymer matrix and weaken the inter- and intramolecular interactions between the polymer chains; these effects often result in reduced mechanical properties. In the samples containing PEG, the tensile modulus and strength were unaffected by the blend composition (Table 2-1).

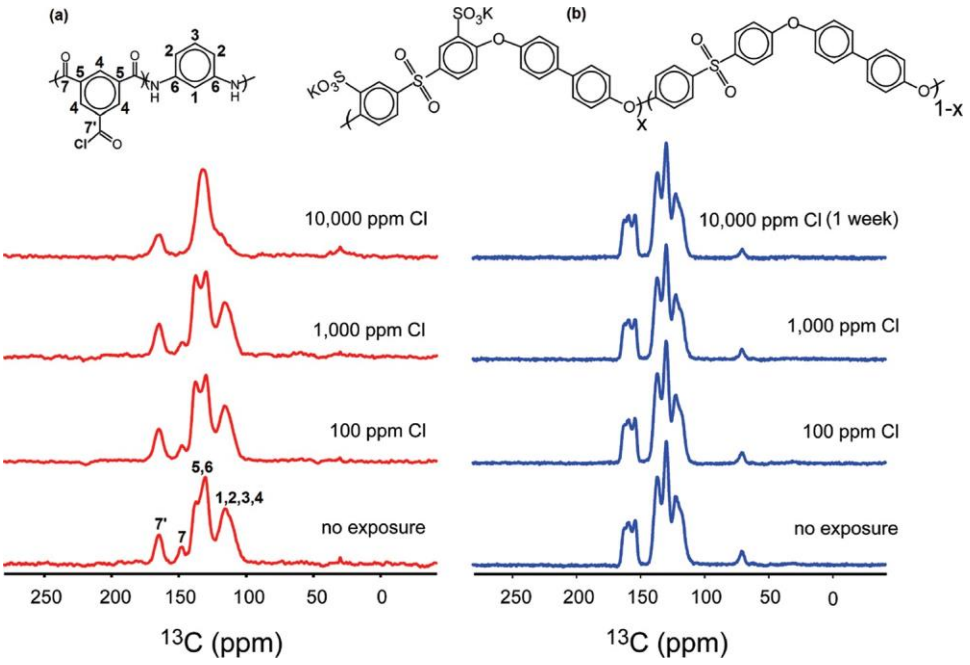

Figure 2-10. Solid state ^{13}C NMR spectra of (a) PA and (b) BPS-20_PEG0.6k-5 after exposure to different chlorine concentrations.

Resistance to degradation by chlorine-based disinfectants is critical for the long-term performance of RO membranes. An accelerated chlorine stability test was conducted by immersing

each sample in a sealed vial containing a pH 4.0 +/- 0.3 buffered aqueous solution of sodium hypochlorite (NaOCl) at concentrations of 100, 1000, and 10000 ppm.[60] Each material was immersed in the chlorinated solution for 2 time periods: 1 day and 1 week. Structural changes were monitored with solid state ^{13}C NMR spectroscopy (Figure 2-10). A reference PA film was obtained from the interfacial polymerization of *m*-phenylenediamine (3 wt% in water) and trimesoyl chloride (5 mM). The aromatic ring in the PA was vulnerable to electrophilic chlorine attack as reported in the literature.[61-63] The phenyl ring C-H peaks of the PA film decreased with exposure to chlorine due to the formation of C-Cl bonds (Figure 2-10a). Also, the intensity of the carbonyl carbon peak for the PA film decreased as PA chains were degraded by chlorine attack at the carbonyl sites. In contrast, none of the BPS-20 peaks showed changes in position or intensity after exposure at 10000 ppm chlorine for 1 week (Figure 2-10b). We note, however, that PEG concentration in the blend materials decreases as chlorine concentration or exposure time increases. For example, in BPS-20_PEG0.6k-5, the PEG content obtained from relative peak integration with respect to the BPS20 peaks fell to about 60% of its initial value after 1 day of immersion in 1000 ppm of chlorine. This may be related to oxidative degradation of PEG.[64] No additional PEG was lost when the films were exposed to highly concentrated solutions of chlorine for a long time. A similar trend was observed for BPS20_PEG0.6k-10. This suggests that the ion-dipole interaction between BPS-20 and PEG is stable under harsh conditions, although exposure to chlorinated water may weaken the interaction.

2.4 Conclusions

Blends of PEG with BPS-20, a potassium salt form sulfonated random copolymer, gave rise to strong ion-dipole interactions between potassium ions in the BPS-20 sulfonate groups and PEG. These interactions are similar to the behavior seen in crown ethers and alkali metal cations. These interactions resulted in high compatibility between BPS-20 and PEG and prevented PEG

from being extracted from the blends by exposure to water for long periods of time (pseudoimmobilization). The strength of the ion-dipole interaction was similar to a weak covalent bond, as shown in the thermal decomposition behavior of PEG in the blend materials. The cation complexing capability of PEG molecules weakened the inter- or intramolecular hydrogen bonding between sulfonate groups, which typically form physically cross-linked ionic domains. Increases in PEG molecular weight and concentration resulted in a reduction of the blend's T_g. This plasticization led to increased free volume and increased water uptake. The ion-dipole interaction and the high coordination number of the PEG repeat units to potassium ions in the BPS-20 sulfonate groups converted the sample surface morphology from a random distribution of hydrophilic domains in the hydrophobic matrix into a more defined hydrophilic-hydrophobic nanophase separated morphology. This trend was more pronounced in BPS-20/PEG blends containing high concentrations of PEG. Increased water uptake and interconnected hydrophilic domains, resulting from the addition of PEG, increased the water permeability of BPS-20/PEG blends compared to BPS-20. Long PEG chains formed tortuous hydrophilic channels that decreased water diffusion and thus water permeation. Furthermore, NaCl rejection decreased upon the addition of PEG like because of weakened electrostatic interactions between potassium ions and sulfonate groups, and reduced ionic exclusion due to dilution of the BPS-20 sulfonate groups caused by increased water uptake. The decrease in NaCl rejection was minimized when short PEG chains (e.g., 0.6k) were used. With the addition of PEG, water permeability increased to about 200% compared to the unblended BPS-20. The influence of PEG addition on sample toughness and ductility was neglible. Unlike PA membranes, which degrade rapidly in the presence of chlorine, BPS20/PEG blends resisted degradation after prolonged exposure to high chlorine concentrations.

Incorporating PEG molecules into low disulfonated random copolymers offers and effective and economical avenue to increase the material's water permeability and fouling resistance. However, the BPS-20 polymer matrix and hydroxyl-terminated PEG blends may not exhibit the necessary water permeability and salt rejections to be an attractive RO membrane material. Therefore, our ongoing studies are focusing on random copolymers with higher degrees of sulfonation and ion-selective PEG. Finally, we will attempt to synthesize multiblock copolymers containing PEG moieties to improve the hydrophilic and hydrophobic phase separation of these chemically stable materials.

Acknowledgment. This work was supported by Dow Water and Process Solutions. This work was also supported in part by the National Science Foundation (NSF)/Partnership for Innovation (PFI) Program (Grant No. IIP-0917971). This material is based in part (L.A. Madsen and J. Hou) upon work supported by the National Science Foundation under Award Number DMR 0844933.

Supporting information available: Glass transition temperature changes depending on PEG molecular weight and concentration and stress-strain curves of BPS-20 and BPS-20/PEG materials (PDF). This information is available free of charge via the internet at http://pubs.acs.org.

Reference:

1. Lee, C. H.; Van, H. D.; Lane, O.; McGrath, J. E.; Hou, J.; Madsen, L. A.; Spano, J.; Wi, S.; Cook, J.; Xie, W.; Oh, H. J.; Geise, G. M.; Freeman, B. D., Disulfonated Poly(arylene ether sulfone) Random Copolymer Blends Tuned for Rapid Water Permeation via Cation Complexation with Poly(ethylene glycol) Oligomers. *Chem. Mater.* **2011,** *23* (4), 1039-1049.
2. Service, R. F., Desalination Freshens Up. *Science* **2006,** *313* (5790), 1088-1090.
3. Baker, R. W., *Membrane Technology and Applications*. 2004.
4. Geise, G. M.; Lee, H.-S.; Miller, D. J.; Freeman, B. D.; McGrath, J. E.; Paul, D. R., Water purification by membranes: the role of polymer science. *J. Polym. Sci., Part B: Polym. Phys.* **2010,** *48* (15), 1685-1718.
5. Amjad, Z., *Reverse osmosis : membrane technology, water chemistry & industrial applications*. Van Nostrand Reinhold: New York, 1993.
6. Knoell, T.; Martin, E.; Ishida, K.; Phipps, D. In *The effects of chlorine exposure on the performance and properties of polyamide reverse osmosis membranes*, American Water Works Association: 2005; pp 504-516.
7. Petersen, R. J.; Codotte, J. E.; Porter, M. C., *Handbook of Industrial Membrane Technology*. 1990; p 307.
8. Kucera, J., *Reverse osmosis : design, processes, and applications for engineers*. Scrivener Pub. ; Wiley: Salem, Mass.; Hoboken, N.J., 2010.
9. Do, V. T.; Tang, C. Y.; Reinhard, M.; Leckie, J. O., Effects of Chlorine Exposure Conditions on Physiochemical Properties and Performance of a Polyamide Membrane - Mechanisms and Implications. *Environ. Sci. Technol.* **2012,** *46* (24), 13184-13192.
10. Park, H. B.; Freeman, B. D.; Zhang, Z.-B.; Sankir, M.; McGrath, J. E., Highly chlorine-tolerant polymers for desalination. *Angew. Chem., Int. Ed.* **2008,** *47* (32), 6019-6024.
11. Paul, M.; Park, H. B.; Freeman, B. D.; Roy, A.; McGrath, J. E.; Riffle, J. S., Synthesis and crosslinking of partially disulfonated poly(arylene ether sulfone) random copolymers as candidates for chlorine resistant reverse osmosis membranes. *Polymer* **2008,** *49* (9), 2243-2252.
12. Brousse, C.; Chapurlat, R.; Quentin, J. P., New membranes for reverse osmosis. I. Characteristics of the base polymer: sulfonated polysulfones. *Desalination* **1976,** *18* (2), 137-53.
13. Drzewinski, M.; Macknight, W. J., Structure and properties of sulfonated polysulfone ionomers. *J. Appl. Polym. Sci.* **1985,** *30* (12), 4753-70.
14. Van Wagner, E. M.; Sagle, A. C.; Sharma, M. M.; Freeman, B. D., Effect of crossflow testing conditions, including feed pH and continuous feed filtration, on commercial reverse osmosis membrane performance. *J. Membr. Sci.* **2009,** *345* (1-2), 97-109.
15. Chakrabarty, B.; Ghoshal, A. K.; Purkait, M. K., SEM analysis and gas permeability test to characterize polysulfone membrane prepared with polyethylene glycol as additive. *J. Colloid Interface Sci.* **2008,** *320* (1), 245-253.
16. Chakrabarty, B.; Ghoshal, A. K.; Purkait, M. K., Effect of molecular weight of PEG on membrane morphology and transport properties. *J. Membr. Sci.* **2008,** *309* (1+2), 209-221.
17. Ju, H.; McCloskey, B. D.; Sagle, A. C.; Kusuma, V. A.; Freeman, B. D., Preparation and characterization of crosslinked poly(ethylene glycol) diacrylate hydrogels as fouling-resistant membrane coating materials. *J. Membr. Sci.* **2009,** *330* (1+2), 180-188.
18. Ju, H.; McCloskey, B. D.; Sagle, A. C.; Wu, Y.-H.; Kusuma, V. A.; Freeman, B. D., Crosslinked poly(ethylene oxide) fouling resistant coating materials for oil/water separation. *J. Membr. Sci.* **2008,** *307* (2), 260-267.
19. La, Y.-H.; McCloskey, B. D.; Sooriyakumaran, R.; Vora, A.; Freeman, B.; Nassar, M.; Hedrick, J.; Nelson, A.; Allen, R., Bifunctional hydrogel coatings for water purification membranes: Improved fouling resistance and antimicrobial activity. *J. Membr. Sci.* **2011,** *372* (1-2), 285-291.

20. McCloskey, B. D.; Ju, H.; Freeman, B. D., Composite Membranes Based on a Selective Chitosan-Poly(ethylene glycol) Hybrid Layer: Synthesis, Characterization, and Performance in Oil-Water Purification. *Ind. Eng. Chem. Res.* **2010,** *49* (1), 366-373.
21. Sagle, A. C.; Van Wagner, E. M.; Ju, H.; McCloskey, B. D.; Freeman, B. D.; Sharma, M. M., PEG-coated reverse osmosis membranes: Desalination properties and fouling resistance. *J. Membr. Sci.* **2009,** *340* (1-2), 92-108.
22. Wang, P.; Tan, K. L.; Kang, E. T.; Neoh, K. G., *J. Mater. Chem.* **2001,** *11*, 783.
23. Revanur, R.; McCloskey, B.; Breitenkamp, K.; Freeman, B. D.; Emrick, T., Reactive amphiphilic graft copolymer coatings applied to polyvinylidene fluoride ultrafiltration membranes. *Macromolecules (Washington, DC, U. S.)* **2007,** *40* (10), 3624-3630.
24. Chou, W. L.; Yu, D. G.; Yang, M. C.; Jou, C. H., *Sep. Purif. Technol.* **2007,** *57*, 209.
25. Gokel, G. W., *Crown Ethers and Cryptands*. 1991.
26. Okada, T., *Macromolecules* **1990,** *23*, 4216.
27. Doan, K. E.; Heyen, B. J.; Ratner, M. A.; Shriver, D. F., *Chem. Mater.* **1990,** *2*, 539.
28. Yanagida, S.; Takahasi, K.; Okahara, M., *Bull. Chem. Soc. Jpn.* **1977,** *50*, 1386.
29. Madsen, L. A.; Li, J.; Hou, J., Probing transport in ionomer membranes via NMR anisotropy and diffusion measurements. *Polym. Prepr. (Am. Chem. Soc., Div. Polym. Chem.)* **2009,** *50* (2), 788-789.
30. Li, Y.; VanHouten, R. A.; Brink, A. E.; McGrath, J. E., Purity characterization of 3,3'-disulfonated-4,4'-dichlorodiphenyl sulfone (SDCDPS) monomer by UV-vis spectroscopy. *Polymer* **2008,** *49* (13-14), 3014-3019.
31. Li, Y.; Wang, F.; Yang, J.; Liu, D.; Roy, A.; Case, S.; Lesko, J.; McGrath, J. E., Synthesis and characterization of controlled molecular weight disulfonated poly(arylene ether sulfone) copolymers and their applications to proton exchange membranes. *Polymer* **2006,** *47* (11), 4210-4217.
32. Sankir, M.; Bhanu, V. A.; Harrison, W. L.; Ghassemi, H.; Wiles, K. B.; Glass, T. E.; Brink, A. E.; Brink, M. H.; McGrath, J. E., Synthesis and characterization of 3,3'-disulfonated-4,4'-dichlorodiphenyl sulfone (SDCDPS) monomer for proton exchange membranes (PEM) in fuel cell applications. *J. Appl. Polym. Sci.* **2006,** *100* (6), 4595-4602.
33. Kim, Y. S.; Dong, L.; Hickner, M. A.; Glass, T. E.; Webb, V.; McGrath, J. E., State of Water in Disulfonated Poly(arylene ether sulfone) Copolymers and a Perfluorosulfonic Acid Copolymer (Nafion) and Its Effect on Physical and Electrochemical Properties. *Macromolecules* **2003,** *36* (17), 6281-6285.
34. Sumner, M. J.; Harrison, W. L.; Weyers, R. M.; Kim, Y. S.; McGrath, J. E.; Riffle, J. S.; Brink, A.; Brink, M. H., Novel proton conducting sulfonated poly(arylene ether) copolymers containing aromatic nitriles. *J. Membr. Sci.* **2004,** *239* (2), 199-211.
35. Wang, F.; Hickner, M.; Kim, Y. S.; Zawodzinski, T. A.; McGrath, J. E., Direct polymerization of sulfonated poly(arylene ether sulfone) random (statistical) copolymers: candidates for new proton exchange membranes. *J. Membr. Sci.* **2002,** *197* (1-2), 231-242.
36. Dixon, W. T.; Schaefer, J.; Sefcik, M. D.; Stejskal, E. O.; McKay, R. A., Total suppression of sidebands in CPMAS carbon-13 NMR. *J. Magn. Reson.* **1982,** *49* (2), 341-5.
37. Fung, B. M.; Khitrin, A. K.; Ermolaev, K., An Improved Broadband Decoupling Sequence for Liquid Crystals and Solids. *J. Magn. Reson.* **2000,** *142* (1), 97-101.
38. Lee, C. H.; Park, H. B.; Chung, Y. S.; Lee, Y. M.; Freeman, B. D., Water Sorption, Proton Conduction, and Methanol Permeation Properties of Sulfonated Polyimide Membranes Cross-Linked with N,N-Bis(2-hydroxyethyl)-2-aminoethanesulfonic Acid (BES). *Macromolecules* **2006,** *39* (2), 755-764.
39. Hechavarria, L.; Mendoza, N.; Altuzar, P.; Hu, H., In situ formation of polyethylene glycol-titanium complexes as solvent-free electrolytes for electrochromic device application. *J. Solid State Electrochem.* **2010,** *14* (2), 323-330.
40. Cappelli, A.; Galeazzi, S.; Giuliani, G.; Anzini, M.; Grassi, M.; Lapasin, R.; Grassi, G.; Farra, R.; Depas, B.; Aggravi, M.; Donati, A.; Zetta, L.; Boccia, A. C.; Bertini, F.; Samperi, F.; Vomero, S., *Macromolecules* **2009,** *42*, 2368.
41. Zundel, G., *Hydration and Intermolecular Interaction*. 1969.

42. Zundel, G., Hydration structure and intermolecular interaction in polyelectrolytes. *Angew. Chem., Int. Ed. Engl.* **1969,** *8* (7), 499-509.
43. Kim, C. H.; Kim, D. W.; Cho, K. Y., *Polym. Bull.* **2009,** *63*, 91.
44. Izatt, R. M.; Bradshaw, J. S.; Nielsen, S. A.; Lamb, J. D.; Christensen, J. J.; Sen, D., Thermodynamic and kinetic data for cation-macrocycle interaction. *Chem. Rev.* **1985,** *85* (4), 271-339.
45. Izatt, R. M.; Bradshaw, J. S.; Pawlak, K.; Bruening, R. L.; Tarbet, B. J., Thermodynamic and kinetic data for macrocycle interaction with neutral molecules. *Chem. Rev.* **1992,** *92* (6), 1261-354.
46. Izatt, R. M.; Pawlak, K.; Bradshaw, J. S.; Bruening, R. L., *Chem. Rev.* **1991,** *91*, 1721.
47. Chan, K. W. S.; Cook, K. D., *Macromolecules* **1983,** *16*, 1736.
48. Kerres, J. A., *Fuel Cells* **2005,** *5*, 230.
49. Besner, S.; Vallee, A.; Bouchard, G.; Prud'homme, J., *Macromolecules* **1992,** *25*, 6480.
50. Xu, K.; Li, K.; Khanchaitit, P.; Wang, Q., *Chem. Mater.* **2007,** *19*, 5937.
51. Back, D. M.; Schmitt, R. L., *Kirk-Othmer Encyclopedia of Chemical Technology*. 2004; Vol. 10, p 673.
52. Read, B. E., *Polymer* **1962,** *3*, 529.
53. Fox, T. G., *Bull. Am. Phys. Soc.* **1956,** *1*, 123.
54. Polyers, S. A.
55. Yasuda, H.; Lamaze, C. E.; Ikenberry, L. D., *Die Makromol. Chem.* **1968,** *118*, 19.
56. Philippova, O. E.; Karibyants, N. S.; Starodubtzev, S. G., *Macromolecules* **1994,** *27*, 2398.
57. Mitra, P. P., *Physica A* **1997,** *241*, 122.
58. Porter, M. R., *Handbook of Surfactants*. 1994.
59. Helfferich, F., *Ion Exchange*. 1995.
60. Jayarani, M. M.; Rajmohanan, P. R.; Kulkarni, S. S.; Kharul, U. K., *Desalination* **2000,** *130*, 1.
61. Carmo, M.; Fritz, D. L.; Mergel, J.; Stolten, D., A comprehensive review on PEM water electrolysis. *Int. J. Hydrogen Energy* **2013,** *38* (12), 4901-4934.
62. March, J., *Advanced Organic Chemistry: Reactions, Mechanisms, and Structure*. 1992.
63. Bieron, J. F.; Dinan, F. J.; Zabicky, J., *The Chemistry of Amides*. 1970; p 263.
64. Chen, S. F.; Zheng, J.; Li, L. Y.; Jiang, S. Y., *J. Am. Chem. Soc.* **2005,** *127*, 14473.

3.0 Kinetics of Post-Sulfonation of a Poly(arylene ether sulfone) that Contains Hydroquione (Radel-A) for Application in Reverse Osmosis Membranes

Ozma Lane, S. J. Mecham, Eui Soung Jang, B. D. Freeman, J. S. Riffle, J. E. McGrath
Macromolecules and Interfaces Institute, Virginia Tech, Blacksburg, VA 24061

Abstract

Partially hydrophilic engineering thermoplastics have been investigated as potential alternative materials for reverse osmosis. Post-sulfonated poly(arylene ether sulfone)s containing hydroquinone are of particular interest as they feature facile synthesis with precise tailoring of composition. This research focuses on optimizing post-sulfonation conditions for achieving controlled sulfonation on the hydroquinone unit, while avoiding significant secondary reactions or chain scission. It was found that the copolymer with 29% of the repeat units containing hydroquinone could be efficiently sulfonated within an hour at 50 ^{o}C without significant chain degradation. Sulfonation of the polymer was determined to be a function of the rate of powder dissolution.

3.1 Introduction

Projections for increasing demand for potable water coupled with greater levels of contamination in groundwater supplies require the development of increased capacity for potable

water generation.[1] Reverse osmosis (RO) is more cost-effective than thermal methods of desalination, and its market growth has outpaced that of its competitors.[2] The current predominant material used in RO production facilities is a crosslinked aromatic polyamide.[3] While offering excellent salt rejection and water flux, this material has two significant drawbacks. The interfacial synthesis of the polyamide produces a rough surface, which affords both a greater surface area for the adhesion of biofouling microbes as well as areas that are shielded from the shear force of the feedstream. Together, these provide an environment conducive to biofouling.[4-6] Secondly, the amide bond of the crosslinked aromatic polyamide dense membrane is susceptible to attack by chlorinated disinfectants, resulting in chain scission.[7] To avoid membrane degradation, a pretreatment process is required wherein the feedstream is first chlorinated to reduce microbial levels, then dechlorinated with sodium bisulfite before being passed through the membrane to avoid membrane degradation, and re-chlorinated after membrane desalination. A membrane that is stable in the presence of these chlorinated disinfectants would reduce the time and expense necessary for the separation, and it potentially could also reduce biofouling due to the introduction of disinfectants at the membrane surface.[8-11]

Research is underway to develop an alternative membrane which lacks chlorine susceptibility, while offering a smoother membrane surface and comparable water transport properties. A number of studies have been performed on sulfonated poly(arylene ether sulfone)s, demonstrating good chlorine resistance and smooth surfaces, with good transport properties.[11-13] These materials have been synthesized from a combination of nonsulfonated and disulfonated monomers. Some investigations have indicated that the partially disulfonated polymers feature compromised sodium chloride rejection when calcium salts are present in the feedstream. It has

been proposed that the compromising effect of calcium is due to the small distance between the sulfonic acid groups on the disulfonated poly(arylene ether sulfone)s.

A potential alternative is to prepare a monosulfonated poly(arylene ether sulfone) where the sulfonation is conducted post-polymerization. Post-polymerization as an approach for sulfonating poly(arylene ether)s was evaluated in the 1980s, and then abandoned due to poor control over the extent of sulfonation, inability to control the microstructure of the sulfonated units, decrease in molecular weight due to chain scission, and unstable sulfonic acid groups.[14] While most of the current synthetic investigations use the direct copolymerization of a disulfonated monomer to produce novel hydrophilic materials, select cases in which post-sulfonation is a viable and potentially advantageous method may still exist.

This work describes the copolymerization and post-sulfonation of polymers derived from dichlorodiphenylsulfone with a systematic series of mixtures of hydroquinone and bisphenol S. Post-sulfonation takes place almost exclusively on the hydroquinone rings since all of the other rings are substituted with electron-withdrawing sulfone groups that are deactivated toward electrophilic aromatic sulfonation. This avoids the issues associated with the microstructure of the sulfonate ions since these copolymers should have the hydroquinone distributed randomly along the chains. A series of investigations on this class of materials have been published confirming the selectivity of this reaction, but consistent, detailed descriptions of the reaction kinetics and rates of molecular weight degradation were not provided.[15-17] In this current research, the reaction kinetics and measurements of molecular weight degradation were studied to optimize the sulfonation process with a minimal level of chain scission. This information is to be used as a model study for developing a series of post-sulfonated polymers with varying structures in order to determine their resistance to the compromising effects of calcium on sodium rejection.

3.2 Experimental

3.2.1 Materials

Radel-A™ was kindly provided by Solvay and used as received. The structure of Radel-A is illustrated in Figure 3-1 below. It is a poly(arylene ether sulfone) with approximately 29% of the repeat units containing hydroquinone (rather than bisphenol S). The precise composition of hydroquinone was obtained from calculations using integrations of ^{1}H NMR spectra. Concentrated sulfuric acid (H_2SO_4) was obtained from VWR and used as received. *N*,*N*-dimethylacetamide was used as received from Aldrich.

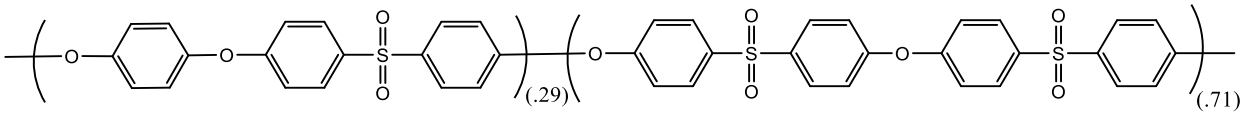

Figure 3-1. Structure of Radel-A.

3.2.2 Sulfonation of Radel A

Prior to the sulfonation reaction, a solution of 30% (w/v) Radel-A in dimethylacetamide was made and precipitated in deionized water in a blender to provide a high surface area powder. This facilitated rapid dissolution during the sulfonation reaction. The precipitated polymer was filtered, washed with deionized water, dried without vacuum at 100 ^{o}C for 12 h and then under vacuum at 110 ^{o}C for 12 h to remove the solvent.

For the sulfonation reaction, a four-necked flask equipped with an overhead stirrer, nitrogen inlet, condenser and a thermometer adapter was assembled. An oil bath with a thermocouple was used to control the reaction temperature. Radel A powder (15 g) and sulfuric acid (150 mL) were added into the flask. Reactions were performed at 40, 50, and 60 ^{o}C. Time zero was designated when the temperature reached the desired point for the kinetics experiment

(~2 min). Aliquots of 5-10 mL were removed at 5, 10, 15, 30, 60, and 120 min. The aliquots were quenched by precipitation in deionized water, followed by washing with copious amounts of deionized water until the pH reached at least 5.

3.2.3. ^{1}H NMR

Samples were dried overnight at 110 °C in a vacuum oven. In a scintillation vial with molecular sieves, approximately 10 mg of the polymer was dissolved in 700 µL of d_6-DMSO. Spectra were collected on a Varian Unity Plus spectrometer operating at 400 MHz. COSY experiments were performed with 16 increments per second and 200 scans.

3.2.4. Water Uptake

Water uptake was measured gravimetrically. Polymer films (100 mg) were cast from a 10% (w/v) solution in DMAc onto a clean glass plate and placed under an IR lamp for 6-12 h. Films were removed via immersion in deionized water, and heated in water at 80 °C for 3 h to remove any residual solvent. The samples were dried overnight at 110 °C under vacuum. Films were then equilibrated in deionized water overnight, converted from the acid to their salt form by heating in 1.0 M NaCl at 80 °C for two h, then they were kept at room temperature in the water overnight. They were blotted and weighed to obtain the wet weight (W_{wet}). Films were dried under vacuum at 110 °C for 12 h to obtain dry weights (W_{dry}). The water uptake in the sodium salt form was determined as follows:

$$Water\ Uptake = \frac{W_{wet} - W_{dry}}{W_{dry}} * 100\%$$

3.2.5 Size Exclusion Chromatography

Size exclusion chromatography (SEC) was conducted on the polymers to measure molecular weights and molecular weight distributions. The solvent was DMAc that was distilled from CaH_2 and that contained dry LiCl (0.10 M). The column set consisted of 3 Agilent PLgel 10-μm Mixed B-LS columns 300x7.5 mm (polystyrene/divinylbenzene) connected in series with a guard column having the same stationary phase. The column set was maintained at 50 °C. An isocratic pump (Agilent 1260 infinity, Agilent Technologies) with an online degasser (Agilent 1260), autosampler and column oven was used for mobile phase delivery and sample injection. A system of multiple detectors connected in series was used for the analyses. A multi-angle laser light scattering (MALLS) detector (DAWN-HELEOS II, Wyatt Technology Corp.), operating at a wavelength of 658 nm, a viscometer detector (Viscostar, Wyatt Technology Corp.), and a refractive index detector operating at a wavelength of 658 nm (Optilab T-rEX, Wyatt Technology Corp.) provided online results. The system was corrected for interdetector delay and band broadening. Data acquisition and analysis were conducted using Astra 6 software from Wyatt Technology Corp. Validation of the system was performed by monitoring the molar mass of a known molecular weight polystyrene sample by light scattering. The accepted variance of the 21,000 g/mole polystyrene standard was defined as 2 standard deviations (11.5% for M_n and 9% for M_w) derived from a set of 34 runs.

3.3 Results and Discussion

3.3.1. Post-sulfonation of Radel A

Radel-A is a poly(arylene ether sulfone) with approximately 29% hydroquinone-containing comonomer, as shown in Figure 3-1. It is chemically resistant with good mechanical properties, and was selected as a material for post-sulfonation kinetics in order to develop a

baseline for sulfonation parameters to be tested on materials with varying hydroquinone compositions in later studies.

It was expected that sulfonation would predominantly occur on the hydroquinone rings of the poly(arylene ether sulfone) because all of the other rings were deactivated toward electrophilic aromatic substitution by the presence of the electron withdrawing sulfone linkages. The compositions of the non-sulfonated starting material and the post-sulfonated samples were investigated with ^{1}H NMR. Figures 3-2 and 3-3 compare the chemical structures of the non-sulfonated and post-sulfonated Radel-A after 2 hours of sulfonation at 60 ^{o}C. In the non-sulfonated Radel-A, the A and A1 peaks resonate at 7.95 and 7.93 ppm and overlap somewhat. The B and B1 peaks resonate at 7.23 and 7.11 ppm and are better separated so that the relative number of units adjacent to the hydroquinone can be distinguished. The C peak that corresponds to the hydroquinone protons resonates as a singlet at 7.17 ppm. The amount of hydroquinone-containing repeat units was calculated to be 29% (Figure 3-2) based on the integrals of the B1 and C peaks.

Protons on the post-sulfonated Radel-A structure in the ^{1}H NMR spectrum are distinguished from their non-sulfonated predecessors by the presence of a prime after the peak labels (Figure 3-3). In the post-sulfonated Radel spectrum, the A' and A1' peaks resonate at 7.96 and 7.83 ppm, with the A1' peaks somewhat shifted due to the proximity of the sulfonated hydroquinone. The B' and B1' peaks resonated at 7.24 and 6.97 ppm, with the shift of the B1' peak again reflecting the adjacent sulfonated hydroquinone rings. The small peak at 7.18 ppm is attributed to residual non-sulfonated hydroquinone. The ratio of the B1' to B' integrals could not be precisely determined during the course of the kinetics study due to overlap of the unreacted B, B', and D' peaks. The sulfonated hydroquinone peaks C', D', and E' resonate at 7.4, 7.15, and

7.05 ppm. The peak corresponding to the D' proton also overlaps with neighboring peaks and unreacted B and B1 proton peaks.

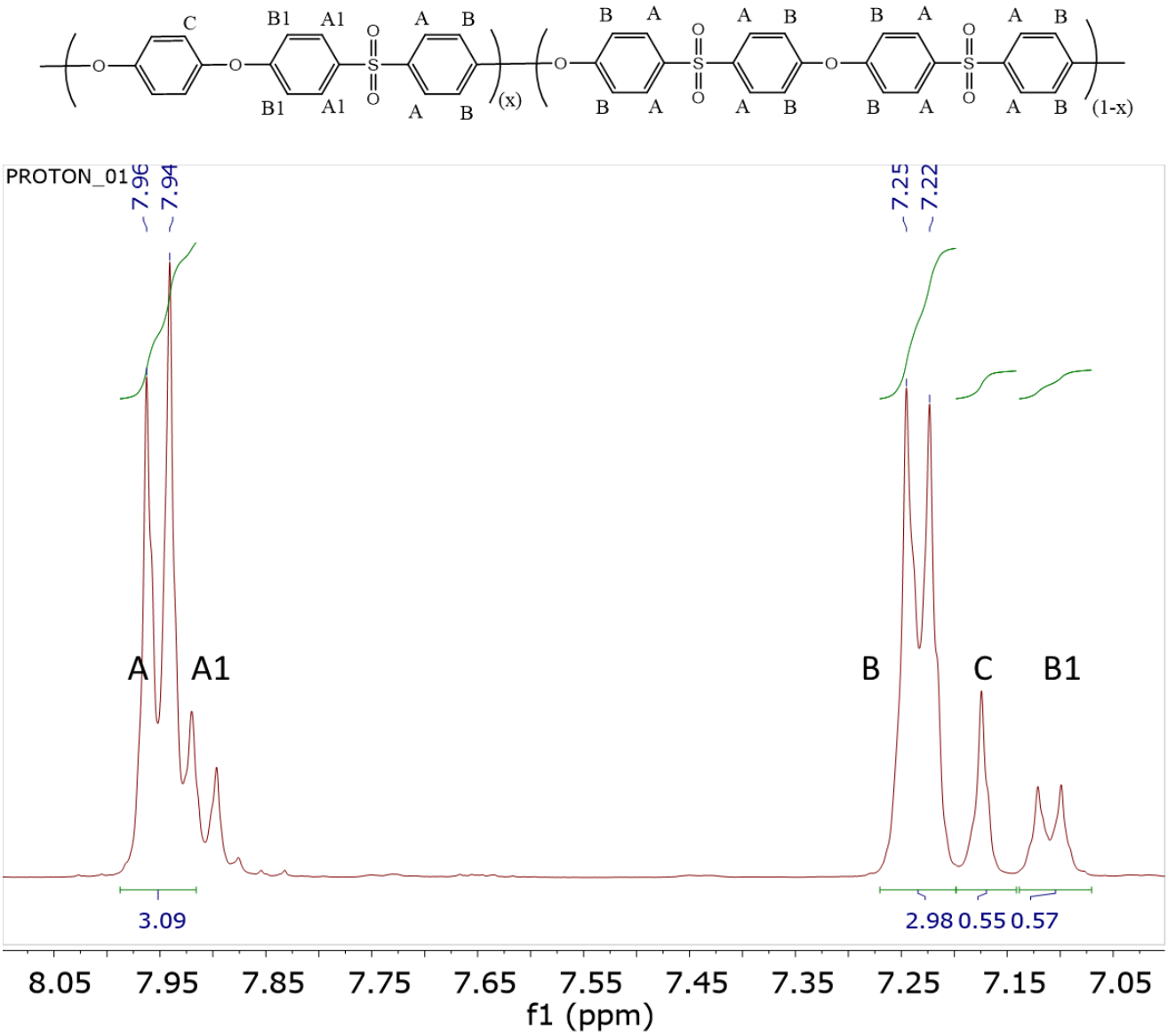

Figure 3-2. Structure and ^{1}H NMR of the non-sulfonated Radel-A.

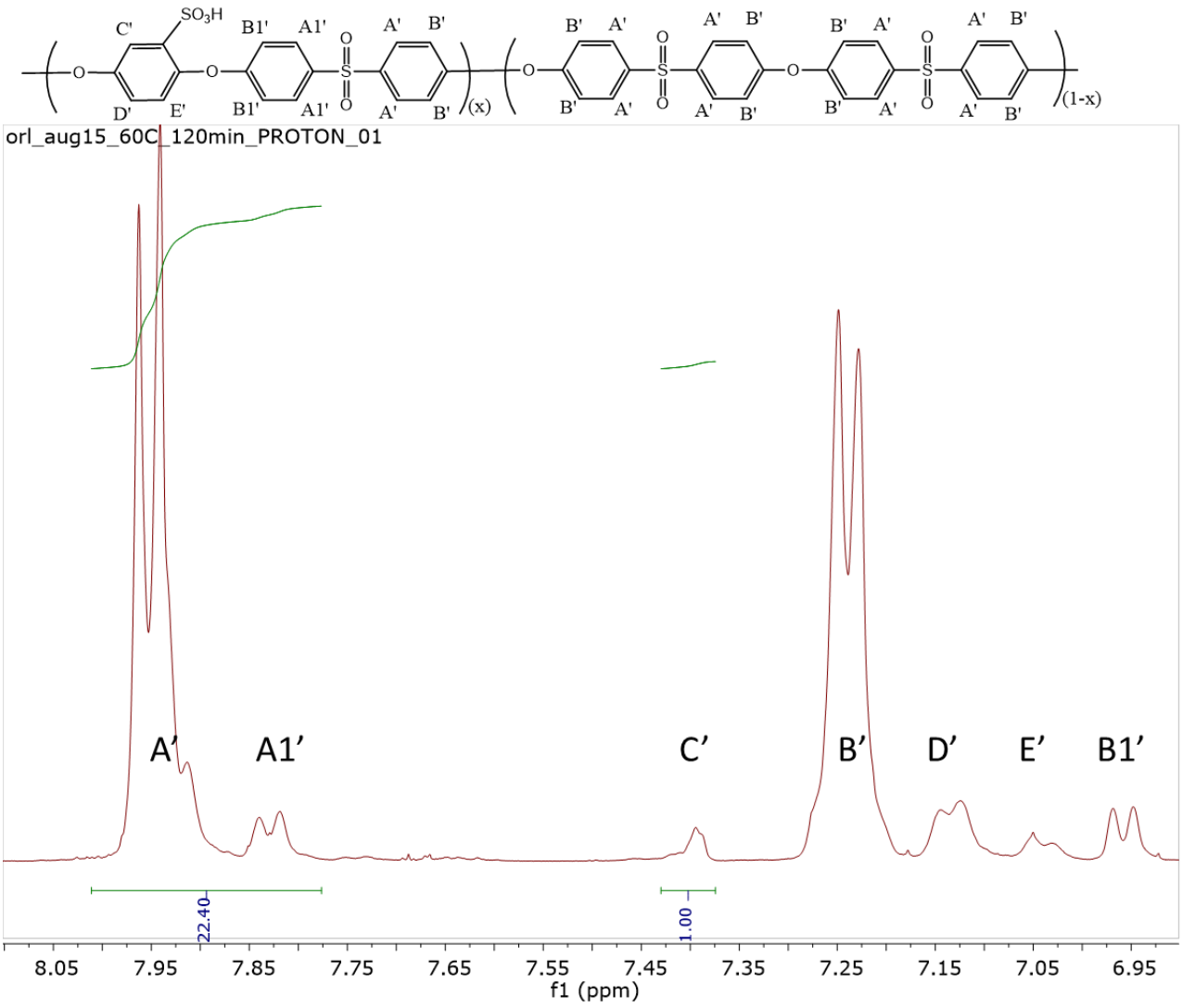

Figure 3-3. Structure of ^{1}H NMR of sulfonated Radel-A with peak assignments.

In order to confirm the sulfonated copolymer structure, 2-D homonuclear correlational spectroscopy experiments were performed to investigate correlations between neighboring protons. In the COSY NMR (^{1}H-^{1}H) spectrum (Figure 3-4), the C' proton (7.45 ppm) has a weak interaction with the D' proton, as indicated by the light blue lines identifying those protons and their correlating peak on the COSY spectrum. This weak interaction is due to coupling across 4 bonds of the aromatic ring and protons, rather than the 3 bonds that are otherwise observed in this

spectrum. The D’ and E’ protons correlate strongly with each other, as highlighted by the black lines in Figure 3-3. A’ and B’, as well as A1’ and B1’ protons, show a stronger correlation due to a smaller number of bonds of separation, but there are no correlations or peaks suggesting a secondary sulfonation site anywhere other than the hydroquinone repeat unit.

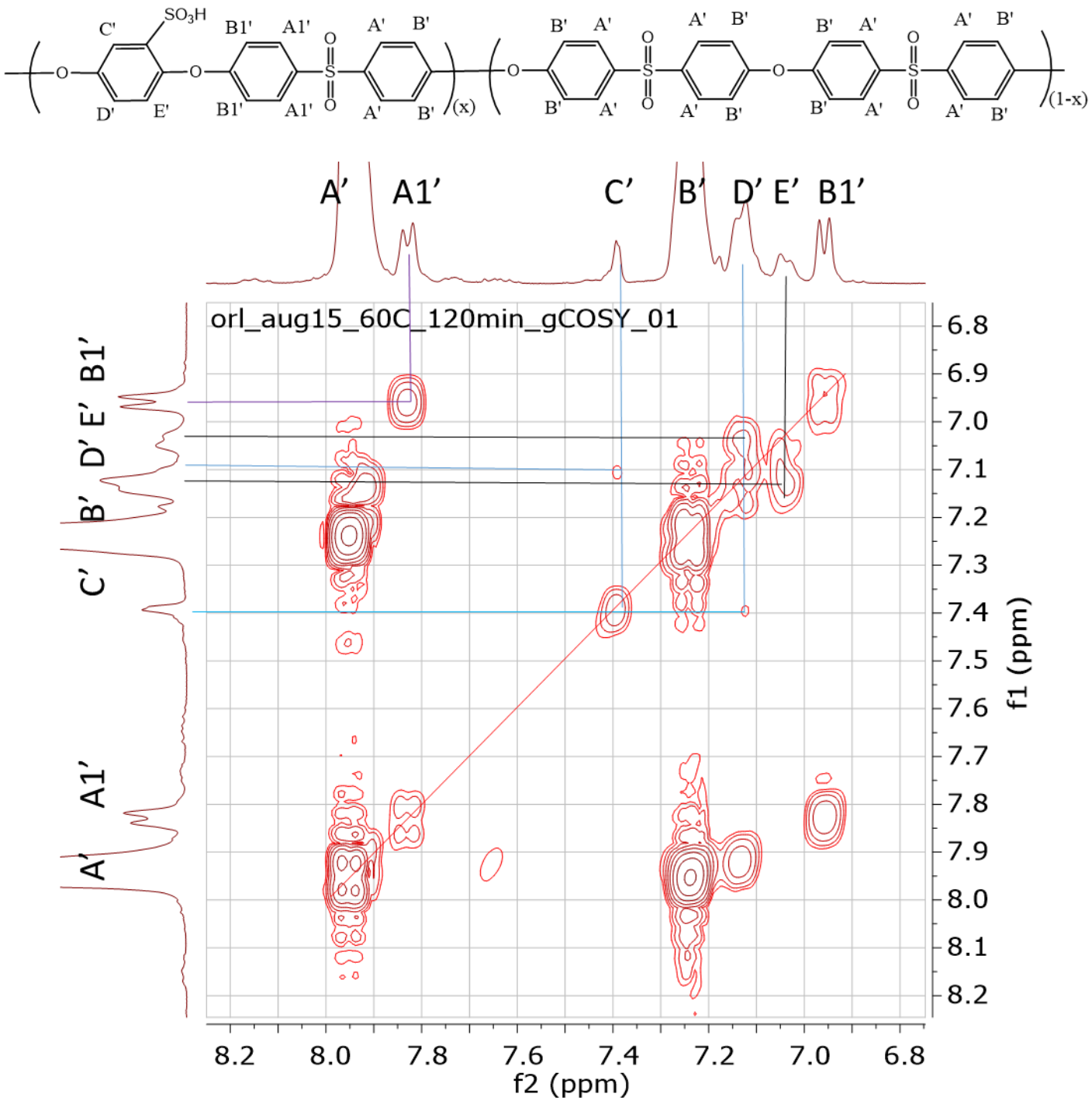

Figure 3-4. The COSY (^{1}H-^{1}H) spectrum of Radel-A after 2 hours of sulfonation at 60 °C. Black lines indicate the proximity of the C and D protons, with no other correlations for the C proton.

3.3.2 Kinetics

After confirming the structure of the sulfonated Radel-A and the absence of significant side reactions, the level of sulfonation at varying sulfonation temperatures and times was determined.

The spectrum of the polymer that was sulfonated for 2 hours at 60 °C was used to confirm the degree of sulfonation of a fully sulfonated Radel-A polysulfone (Figure 3-3). The reaction was considered complete since the peak corresponding to residual unsulfonated hydroquinone was negligible. The ratio of the A' and A1' integrals to the C' integral was used to determine the ratio of hydroquinone-containing repeat units to bisphenol sulfone repeat units. The integrations were normalized such that the C' integral was set to 1. The integral of the A' + A1' peaks (21.8) was divided by 2 to determine the number of rings proximate to sulfone groups (10.9). Two of the sulfone rings were assigned to the hydroquinone-containing repeat unit, while the remainder of 8.9 were assigned to the bisphenol sulfone repeat unit. The number of rings next to a sulfone on the hydroquinone-containing repeat unit was divided by two rings per repeat unit, giving one repeat unit. The number of rings on the bisphenol sulfone repeat unit (8.9) were divided by 4 rings per repeat unit, giving a relative number of 2.25 repeat units per each hydroquinone-containing repeat unit. The percentage of hydroquinone-containing repeat units was determined as the number of hydroquinone units divided by the sum of the hydroquinone-containing repeat units and bisphenol sulfone repeat units (1/(1+2.25)). The percentage of bisphenol sulfone-containing repeat units was determined as the number of bisphenol sulfone units divided by the sum of the hydroquinone-containing repeat units and bisphenol sulfone repeat units (2.25/(1+2.25). The ratio was calculated to be 30.8% sulfonated hydroquinone-containing repeat units, which is within the margin of error of the 29% non-sulfonated hydroquinone determined from the ^{1}H NMR spectrum of the original Radel-A.

For partially sulfonated polymers collected during the course of sulfonation, the following is a representative calculation for the percentage of sulfonation of the hydroquinone-containing units. In the sample removed at 60 ^{o}C after 15 min of sulfonation, the integral of the A'+ A1' peaks

was 36.85 and the integral of the C' peak was normalized to 1. The A'+A1' peak integral was divided by 2 to provide the number of sulfone-proximate rings (18.4). The ratio of sulfone-proximate rings in the hydroquinone-containing units relative to the bisphenol sulfone-containing units is 0.43. From the number of calculated rings, 14.75 rings and 3.69 repeat units were attributed the bisphenol sulfone-containing units and 3.25 rings and 1.63 repeat units were attributed to the hydroquinone-containing comonomers. Therefore, 1/1.63 repeat units provided a sulfonation level of 61%.

In Figure 3-5, the percentage of hydroquinone that was sulfonated as determined by ^{1}H NMR is shown as a function of sulfonation time and reaction temperature. It indicates that the reaction is effectively complete after 2 hours at 50 ^{o}C. The rate of sulfonation is likely very dependent on the rate of dissolution of the polymer powder. The reaction appears to change from a cloudy mixture of suspended particles upon initial mixing, and becomes a clear dark amber by the 120 minute mark.

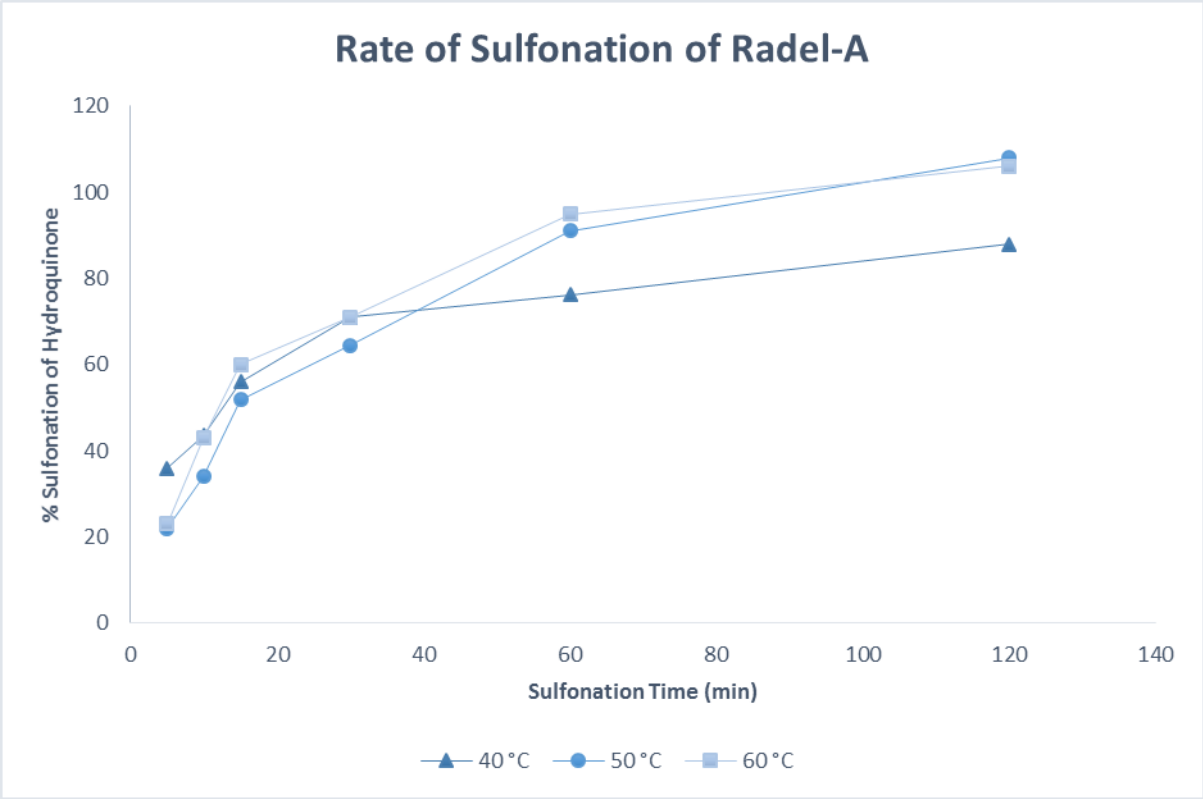

Figure 3-3. Sulfonation of hydroquinone (%) as a function of reaction time and temperature.

3.3.2. Molecular weights

SEC results indicate that the sulfonation process does not produce significant degradation within the sulfonation conditions studied (Table 3-1). It should be noted that according to NMR calculations, the polymer collected after 120 minutes of sulfonation at 40 ^{o}C is not yet fully sulfonated and thus, it was not evaluated further. The molecular weight results provide good evidence that the reaction conditions utilized herein can avoid the molecular weight degradation that has previously caused concern in other post-sulfonated polysulfones, where the sulfonation took place on the biphenol group. The more rapid reaction of the hydroquinone allows for sulfonation to proceed before chain degradation can take place. This provides a useful reference for reaction conditions for the post-sulfonation of a polymer series with a variable hydroquinone content, which may be of use in membrane separations applications.

Table 3-1. M_w of Radel A (g/mole) before and after post-sulfonation at 50 and 60 °C. M_w obtained by SEC in DMAc with 0.10 M LiCl.

Time (min)	50 °C	60 °C
0	35,000	35,000
60	42,600	36,800
120	56,600	32,300

3.4 Conclusions

The hydroquinone unit of the Radel-A™ polymer investigated in this study was rapidly post-sulfonated in a sulfuric acid solution. This is a rapid, facile and quantitative method for mild sulfonation of only the activated rings. Using these mild conditions, SEC results showed that the sulfonation procedure did not degrade the polymers. Due to the structure of the polymer, this ensures that the sulfonate ions cannot be on adjacent rings. Importantly, this spaces the ions sufficiently far apart that chelation or binding to multivalent cations will not be likely due to adjacent sulfonates.

1. Elimelech, M.; Phillip, W. A., The Future of Seawater Desalination: Energy, Technology, and the Environment. *Science* **2011,** *333* (6043), 712-717.
2. Greenlee, L. F.; Lawler, D. F.; Freeman, B. D.; Marrot, B.; Moulin, P., Reverse osmosis desalination: Water sources, technology, and today's challenges. *Water Res.* **2009,** *43* (9), 2317-2348.

3. Amjad, Z., *Reverse osmosis : membrane technology, water chemistry & industrial applications*. Van Nostrand Reinhold: New York, 1993.
4. Elimelech, M.; Zhu, X.; Childress, A. E.; Hong, S., Role of membrane surface morphology in colloidal fouling of cellulose acetate and composite aromatic polyamide reverse osmosis membranes. *J. Membr. Sci.* **1997,** *127* (1), 101-109.
5. Zhu, X. Colloidal fouling of thin film composite and cellulose acetate reverse osmosis membranes. 1996.
6. Zhu, X.; Hong, S.; Childress, A. E.; Elimelech, M. In *Colloidal fouling of reverse osmosis membranes: Experimental results, fouling mechanisms, and implications for water treatment*, American Water Works Association: 1995; pp 251-263.
7. Nielsen, W., *Membrane Filtration and Related Molecular Separation Technologies*. APV Systems: 2000.
8. McGrath, J. E. In *Chlorine resistant membranes for reverse osmosis and nanofiltration*, American Chemical Society: 2009; pp POLY-224.
9. McGrath, J. E.; Park, H. B.; Freeman, B. D. Chlorine resistant desalination membranes based on directly sulfonated poly(arylene ether sulfone) copolymers. US20070163951A1, 2007.
10. Park, H. B.; Xie, W.; Freeman, B. D.; Paul, M.; Roy, A.; Sankir, M.; Lee, H.-S.; Riffle, J. S.; McGrath, J. E. In *Chlorine-tolerant desalination membranes*, American Chemical Society: 2008; pp POLY-312.
11. Paul, M.; Park, H. B.; Freeman, B. D.; Roy, A.; McGrath, J. E.; Riffle, J. S., Synthesis and crosslinking of partially disulfonated poly(arylene ether sulfone) random copolymers as candidates for chlorine resistant reverse osmosis membranes. *Polymer* **2008,** *49* (9), 2243-2252.
12. Geise, G. M.; Park, H. B.; Sagle, A. C.; Freeman, B. D.; McGrath, J. E., Water permeability and water/salt selectivity tradeoff in polymers for desalination. *J. Membr. Sci.* **2011,** *369* (1-2), 130-138.
13. Park, H. B.; Freeman, B. D.; Zhang, Z.-B.; Fan, G.-Y.; Sankir, M.; McGrath, J. E. In *Water and salt transport behavior through hydrophilic-hydrophobic copolymer membranes and their relations to reverse osmosis membrane performance*, American Chemical Society: 2006; pp PMSE-495.
14. McGrath, J. E.; Wightman, J. P.; Lloyd, D. R. *Novel poly(aryl ether) membranes for desalination by reverse osmosis*; Virginia Polytech. Inst. and State Univ.: 1984; p 139 pp.
15. Rose, J. B. Sulfonated polyarylethersulphone copolymers. EP8894A1, 1980.
16. Rose, J. B. Sulfonated polyaryletherketones. EP8895A1, 1980.
17. Rose, J. B. Sulfonated poly(aryl ether ketones). EP41780A1, 1981.

4.0 Synthesis, Characterization and Post-sulfonation of a Polysulfone Series Incorporating Hydroquinone for Reverse Osmosis Membranes

Ozma Lane, E. S. Jang, S. R. Choudhury, S. J. Mecham, B. D. Freeman, J. S. Riffle, J. E. McGrath

4.1 Introduction

In recent decades, there has been a growing demand for production of potable drinking water around the world. This growth is due to the combination of growing populations, as well as contamination of freshwater sources and increasing energy costs for production of potable water. This has have created a demand for more reverse osmosis plants and improved materials and procedures.[1] Of the methods available for the desalination of seawater, reverse osmosis has a clear cost advantage over thermal processes that were developed decades earlier. Membrane separations avoid the high cost of phase transitions.[1] The predominant current material used in most reverse osmosis applications is a crosslinked aromatic polyamide, produced by the Dow Chemical Company under the trade name "FilmTec 30". While this material has good transport properties, it is susceptible to biofouling due to the rough surface produced during the interfacial crosslinking reaction, as well as degradation of the polyamide in the presence of chlorine.[2-4]

Research has been underway to find novel materials or material modifications with improved chlorine tolerance or resistance to biofouling.[5-9] Disulfonated poly(arylene ether sulfone)s are promising candidates, with excellent chlorine tolerance and a smooth material surface that offers no rough topology for the adhesion of microbes.[10, 11] Those polymers are prepared directly from a disulfonated monomer that has two sulfonate groups on adjacent rings. However,

the sodium rejection in some of these materials is compromised in the presence of calcium.[12] It was hypothesized that this compromise may be a result of the close spacing between sulfonic acid groups on adjacent rings on the polymer backbone.

In this research, we have investigated the development of a post-sulfonated material with a monosulfonated hydroquinone unit as a potential candidate for reverse osmosis. Most previous work on post-sulfonation of polysulfones required rather harsh conditions because the rings to be sulfonated included both activated and deactivated rings toward the electrophilic aromatic sulfonation reaction. Those studies on post-sulfonation of polysulfones found difficulties with the control of molecular weight, targeting of sulfonation levels, and in the relative placement of sulfonates along the chain (i.e., the microstructure).[13] Alternatively, the hydroquinone-based copolymers studied in this research can avoid these disadvantages by utilizing mild reaction conditions.[14, 15] The sulfonation proceeds only on the hydroquinone unit, while the other comonomers feature electron-withdrawing groups that discourage side reactions. These materials offer the advantage of being synthesized from commercially available reagents, allowing for economical scale-up in addition to synthetic precision.

4.2 Experimental

4.2.1 Materials

Dichlorodiphenyl sulfone (DCDPS) was kindly provided by Solvay, and was recrystallized in toluene and dried for 12 h under vacuum at 110 ^{o}C prior to use. Bisphenol sulfone (BisS), was kindly provided by Solvay, and was recrystallized in methanol and dried for 12 h under vacuum at 110 ^{o}C prior to use. Hydroquinone (HQ) was provided by Eastman Chemical Company and was recrystallized in methanol and dried for 12 h under vacuum at 110 ^{o}C prior to use. *m*-Xylene,

sulfuric acid, and dimethylacetamide (DMAc) were obtained from Sigma Aldrich and used as received. Sulfolane was obtained from Sigma Aldrich and heated with a 30% (v/v) portion of toluene at 160 °C for 12 h to azeotropically remove any water. Potassium carbonate was obtained from Sigma Aldrich and was dried for 12 h under vacuum at 180 °C prior to use.

4.2.2. Synthesis and Sulfonation

The hydroquinone sulfone (HQS) series was synthesized using a nucleophilic aromatic substitution reaction as shown in Figure 4-1. A sample reaction follows: 4.955 g (45 mmol) of HQ, 25.844 g (90 mmol) of DCDPS, 11.262 g (45 mmol) of BisS, and 100 mL of sulfolane were added to a 3-necked round bottom flask equipped with nitrogen inlet, overhead stirrer, and condenser with a Dean Stark trap. The reaction temperature was controlled with a thermocouple in a salt bath. The reaction temperature was initially raised to 160 °C, 50 mL of m-xylene and 14.5 g (105 mmol) K_2CO_3 were added, and the reaction refluxed for 4 h to azeotropically remove any water. The reaction temperature was then raised to 200-210 °C, and the *m*-xylene was removed from the Dean Stark trap. After 36 h of reaction, the mixture was allowed to cool and diluted with 40 mL of DMAc. The solution was hot filtered to remove salts and precipitated in water. The polymer was boiled with three changes of water to remove trace amounts of sulfolane, then dried at 50 °C for 4 h, followed by 12 h under vacuum at 110 °C.

To sulfonate the polymer, the dried polymer powder was dissolved in a 10% solution of sulfuric acid in a 3-necked round bottom flask equipped with nitrogen inlet and thermometer, overhead stirrer, and condenser with a Dean Stark trap. An oil bath was used to maintain a reaction temperature of approximately 50 °C. The reaction was stirred vigorously to promote rapid dissolution and to break up any clumps of acid-swollen polymer. After 1 h of reaction, the solution

was precipitated into ice cold water, and rinsed thoroughly to remove all acid. Samples to be analyzed were converted to their salt form by heating in 1.0 M NaCl for 2 h, then dried at 50 °C for 4 h at atmospheric pressure, followed by 12 h under vacuum at 110 °C.

4.2.3. Characterization

4.2.3.1 NMR

Samples were dried overnight at 110 °C in a vacuum oven. In a scintillation vial with molecular sieves, approximately 10 mg of the polymer was dissolved in 700 µL of d_6-DMSO. Spectra were collected on a Varian Unity Plus spectrometer operating at 400 MHz.

4.2.3.2. Water Uptake

Water uptake was measured gravimetrically. Polymer films (100 mg) were cast from a 10% (w/v) solution of DMAc onto a clean glass plate and placed under an IR lamp for 6-12 h. Films were removed via immersion in deionized water, and heated in water at 80 °C for 3 h to remove any residual solvent. The samples were dried overnight at 110 °C under vacuum. Films were then equilibrated in deionized water overnight, converted from the acid to their salt form by heating in 1.0 M NaCl at 80 °C for two h, then they were kept at room temperature in the water overnight. They were blotted and weighed to obtain the wet weight (W_{wet}). Films were dried under vacuum at 110 °C for 12 h in order to obtain dry weights (W_{dry}). The water uptake in the salt form was determined as follows:

$$Water\ Uptake = \frac{W_{wet} - W_{dry}}{W_{dry}} * 100\%$$

4.2.3.3. Molecular Weight Characterization

Size exclusion chromatography (SEC) was conducted on the polymers to measure molecular weight distributions. The solvent was DMAc that was distilled from CaH_2 and that contained dry LiCl (0.10 M). The column set consisted of 3 Agilent PLgel 10-µm Mixed B-LS

columns 300x7.5 mm (polystyrene/divinylbenzene) connected in series with a guard column having the same stationary phase. The column set was maintained at 50 °C. An isocratic pump (Agilent 1260 infinity, Agilent Technologies) with an online degasser (Agilent 1260), autosampler and column oven was used for mobile phase delivery and sample injection. A system of multiple detectors connected in series was used for the analyses. A multi-angle laser light scattering (MALLS) detector (DAWN-HELEOS II, Wyatt Technology Corp.), operating at a wavelength of 658 nm, a viscometer detector (Viscostar, Wyatt Technology Corp.), and a refractive index detector operating at a wavelength of 658 nm (Optilab T-rEX, Wyatt Technology Corp.) provided online results. The system was corrected for interdetector delay and band broadening. Data acquisition and analysis were conducted using Astra 6 software from Wyatt Technology Corp. Validation of the system was performed by monitoring the molar mass of a known molecular weight polystyrene sample by light scattering. The accepted variance of the 21,000 g/mole polystyrene standard was defined as 2 standard deviations (11.5% for Mn and 9% for M_w) derived from a set of 34 runs.

4.2.3.4 Transport Property Measurement

The water permeability (L μm m^{-2} h^{-1} bar^{-1} or cm^2 s^{-1}), salt permeability (cm^2 s^{-1}), salt rejection (%) and water/NaCl selectivity were determined at 25°C using stainless steel crossflow cells. The pressure difference across the membrane (15.1 cm^2) was 400 psi. The aqueous feed contained 2000 ppm NaCl, and the feed solution was circulated past the samples at a continuous flow rate of 3.8 (L min^{-1}). The feed pH was adjusted to a range between 6.5 and 7.5 using a 10 g/L sodium bicarbonate solution. NaCl concentrations in the feed water and permeate were

measured with an Oakton 100 digital conductivity meter.

4.3 Results and Discussion

4.3.1 Synthesis

In the sulfonation reaction, the hydroquinone was selectively sulfonated while the electron-withdrawing sulfone groups on all of the other rings did not react under the mild conditions utilized (Figure 4-1).

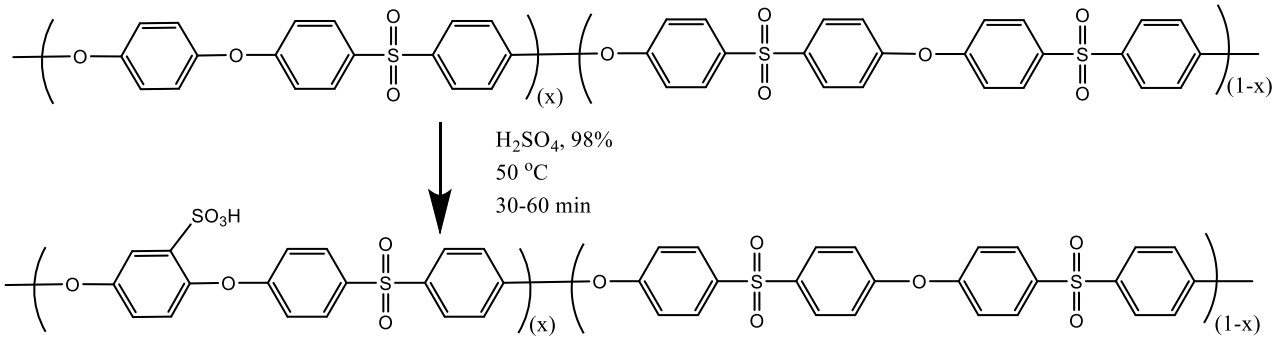

Figure 4-1. Sulfonation of random poly(arylene ether sulfone) copolymers containing varied levels of hydroquinone.

The chemical compositions of the post-sulfonated polymers were investigated using ^1H NMR. In the representative spectrum shown below, the A and A1 peaks resonated at 7.95 and 7.83 ppm, the B and B1 peaks resonated at 7.24 and 6.97 ppm, and the hydroquinone peaks C, D, and E resonated at 7.4, 7.15, and 7.05 ppm, respectively. The peak at 7.18 ppm corresponds to unreacted hydroquinone, indicating an incomplete sulfonation reaction. The NMR procedure described in Chapter 3 was used to determine the degree of sulfonation, and the IEC was calculated from the NMR data.

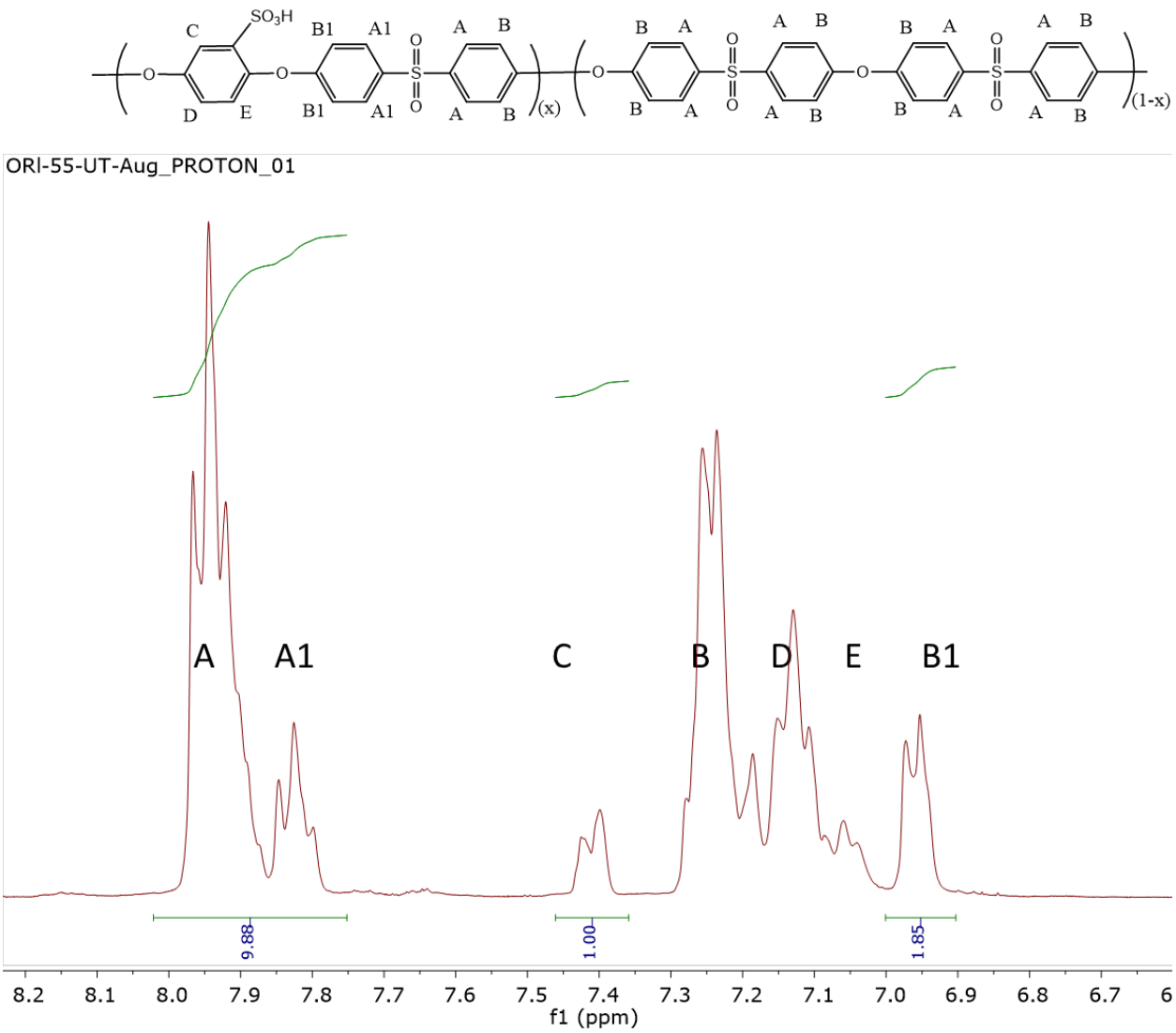

Figure 4-2. Chemical structure and ^{1}H NMR spectrum of SHQS-55 copolymer.

4.3.2 Membrane Properties

A series of three copolymers were synthesized with monomer ratios calculated to provide a hydroquinone-containing repeat unit content of 45, 50, 55, and 60%. These values were targeted to provide IECs of 0.99, 1.11, 1.21, and 1.33, respectively. The copolymer physical properties are summarized in Table 4-1. Measured IECs and sulfonation levels were slightly lower than targeted

values, which is due to incomplete sulfonation as determined by the peak corresponding to unreacted hydroquinone in Figure 4-2. This was due to an insufficient sulfonation reaction of 50°C for one hour. The polymers had good molecular weights and produced clear, tough films. The increase in molecular weight from SHQS-45 and -50 to the higher weights in SHQS-55 and -60 occurred with a new lot of sulfolane solvent, which may have contained fewer impurities than the solvent used for previous synthetic reactions even after heating with toluene to azeotropically remove any water. The solvent used initially also may have absorbed a large amount of water from the atmosphere, and the toluene may have been insufficient to remove it entirely. Sulfolane and water are highly miscible, and therefore even small amounts may be able to remain in the solvent and interfere with achieving a high degree of polymerization.

Sample	**Target IEC**	**IEC [a]**	**Sulfonation [b]**	**Water Uptake (%)**	**M_w[c] (g/mole)**
SHQS-45	0.99	0.92	42%	24	32,300
SHQS-50	1.11	1.06	48%	28	40,200
SHQS-55	1.21	1.14	51%	31	101,000
SHQS-60	1.33	1.21	54%	33	99,000

Table 4-1. Membrane Physical Properties

a) determined from ^{1}H NMR
b) determined from ^{1}H NMR
c) determined from SEC

4.3.3 Transport Data

The SHQS-50 membrane was evaluated for transport properties, and showed promising sodium rejection and water permeability values (Table 4-2). The BPS-20 and BPS-30 materials are a disulfonated poly(arylene ether sulfone) series that has been evaluated previously. The

number 20 in BPS 20 indicates that 20% of the repeat units had disulfonated comonomers, which is similar in terms of IEC to a SHQS copolymer that contains 45-50% of the sulfonated hydroquinone. Despite having a measured IEC only slightly higher than BPS20, the water permeability was significantly higher, with only a small drop in sodium rejection. This may be due to the monosulfonated repeat units forming fewer aggregates, allowing more homogenous distribution of ionic domains throughout the membrane.

The mixed-feed data showed a constant salt rejection in the presence of up to 400 ppm of calcium in the feed stream (Figure 4-2), with no screening by calcium of the Donnan exclusion effect that is requisite to achieve high salt rejection. The compromised salt rejection of a 32% disulfonated poly(arylene ether sulfone (BPS-32) is shown as a comparison. This confirms the viability of post-sulfonated hydroquinone-containing copolymers as alternative candidates for reverse osmosis membranes.

Table 4-2. Transport Properties of Selected Membranes

	IEC[a] (meq/g)	IEC[b] (meq/g)	Water permeability ($L \cdot \mu m/m^2 \cdot h \cdot bar$)	NaCl rejection (%)*
SHQS-50	1.11	1.06	0.27	98.3
SHQS-60	1.21	1.14	0.45	98.3
BPS-20	0.93	1.01	0.05	99.2
BPS-30	1.34	1.32	0.96	91.3

[a]Theoretical calculation

[b]Based on ^{1}H NMR

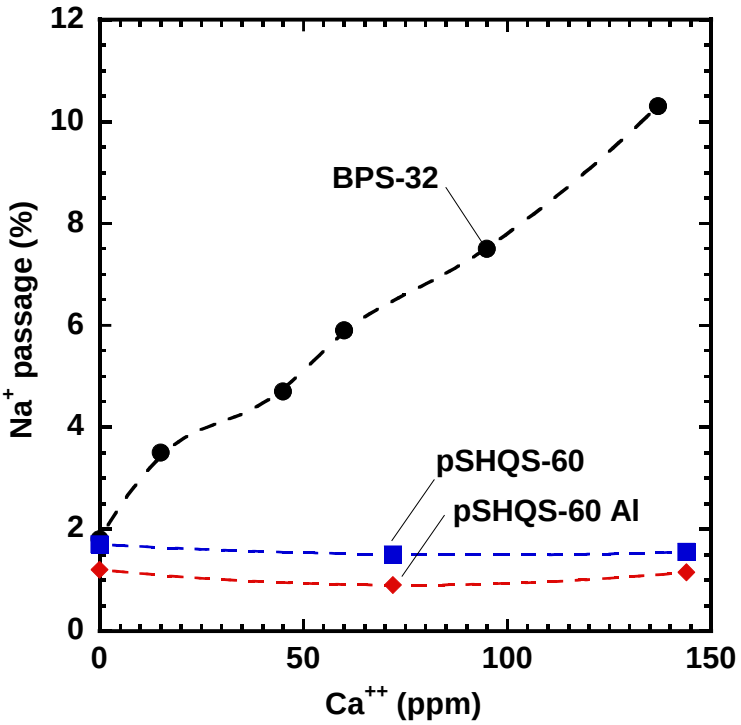

Figure 4-3. Sodium rejection in post-sulfonated hydroquinone-containing copolymers remains constant in the presence of calcium.

4.4 Conclusions

A series of poly(arylene ether sulfone)s with varying hydroquinone content were synthesized and post-sulfonated. The IEC and sulfonation levels were slightly below the targeted values, indicating incomplete sulfonation. This was confirmed by the small residual peak of unreacted hydroquinone in the ^{1}H NMR spectra. The post-sulfonated polymers produced tough, ductile membranes with good molecular weights. Initial transport data shows promising performance for the SHQS copolymer series, with transport properties comparable to those of the disulfonated poly(arylene ether sulfone) systems. Mixed-feed testing confirms resistance to

calcium-induced compromise of sodium rejection. Future work will include further optimization of polymer composition in order to approach transport properties of state-of-the-art commercial RO membranes.

References

1. Greenlee, L. F.; Lawler, D. F.; Freeman, B. D.; Marrot, B.; Moulin, P., Reverse osmosis desalination: Water sources, technology, and today's challenges. *Water Res.* **2009,** *43* (9), 2317-2348.
2. Amjad, Z., *Reverse osmosis : membrane technology, water chemistry & industrial applications*. Van Nostrand Reinhold: New York, 1993.
3. Kucera, J. In *Reverse osmosis membrane fouling control*, CRC Press: 2010; pp 247-270.
4. Elimelech, M.; Zhu, X.; Childress, A. E.; Hong, S., Role of membrane surface morphology in colloidal fouling of cellulose acetate and composite aromatic polyamide reverse osmosis membranes. *J. Membr. Sci.* **1997,** *127* (1), 101-109.
5. Freeman, B.; McGrath, J. E. In *Advances in polymer membranes for water purification*, American Chemical Society: 2010; pp MATNANO-191.
6. Guiver, M. D.; Robertson, G. P.; Tam, C. M., Functionalized polysulfones: methods for chemical modification and membrane applications. *Polym. Mater. Sci. Eng.* **1997,** *77*, 347-348.
7. Lee, Y. T.; Kim, N. W.; Shin, D. H. Polyamide composite membrane having fouling resistance and chlorine resistance and composite membrane fabrication. WO2010062016A2, 2010.
8. Meng, J.; Ni, L.; Li, X.; Zhang, Y. Antifouling chlorine-resistant polyamide RO composite membrane and preparation method thereof. CN103331110A, 2013.
9. Xu, J.; Wang, Z.; Yu, L.; Wang, J.; Wang, S., Reverse osmosis membrane with regenerable anti-biofouling and chlorine resistant properties. *J. Membr. Sci.* **2013,** *435*, 80-91.
10. Lee, C. H.; McCloskey, B. D.; Cook, J.; Lane, O.; Xie, W.; Freeman, B. D.; Lee, Y. M.; McGrath, J. E., Disulfonated poly(arylene ether sulfone) random copolymer thin film composite membrane fabricated using a benign solvent for reverse osmosis applications. *Journal of Membrane Science* **2012,** *389* (0), 363-371.
11. Geise, G. M.; Park, H. B.; Sagle, A. C.; Freeman, B. D.; McGrath, J. E., Water permeability and water/salt selectivity tradeoff in polymers for desalination. *J. Membr. Sci.* **2011,** *369* (1-2), 130-138.
12. Stevens, D. M.; Mickols, B.; Funk, C. V., Asymmetric reverse osmosis sulfonated poly(arylene ether sulfone) copolymer membranes. *J. Membr. Sci.* **2014,** *452*, 193-202.
13. McGrath, J. E.; Wightman, J. P.; Lloyd, D. R. *Novel poly(aryl ether) membranes for desalination by reverse osmosis*; Virginia Polytech. Inst. and State Univ.: 1984; p 139 pp.
14. Lloyd, D. R.; Gerlowski, L. E.; Sunderland, C. D.; Wightman, J. P.; McGrath, J. E.; Igbal, M.; Kang, Y., Poly(aryl ether) membranes for reverse osmosis. *ACS Symp. Ser.* **1981,** *153* (Synth. Membr., Vol. 1), 327-50.
15. Bunn, A.; Rose, J. B., Sulfonation of poly(phenylene ether sulfones) containing hydroquinone residues. *Polymer* **1993,** *34* (5), 1114-16.

5.0 Synthesis and Characterization of a Hydrophilic-Hydrophobic Multiblock Copolymer for Membrane Electrolysis Applications

Ozma Lane[a], Jarrett Rowlett[a], Cortney Mittlesteadt[b], Jason Willey[b], Amin Daryaei[a], James McGrath[a], Sue J. Mecham[a] and J. S. Riffle[a]*

[a]Macromolecular Science and Engineering, Macromolecular and Interfaces Institute
Virginia Tech, Blacksburg, VA 24061

[b]Giner, Inc.
89 Rumford Avenue, Newton, MA 02466

*judyriffle@aol.com

Abstract

Membrane electrolysis of water is a method of producing ultra high-purity hydrogen. Novel materials are under investigation to design a membrane with high proton conductivity and minimal hydrogen crossover. A multiblock hydrophilic-hydrophobic poly(arylene ether sulfone) copolymer was synthesized and investigated. The focus was on the impact of film casting conditions on membrane morphology and performance. Solvent selection and solution concentration had a significant impact on long-range order and surface morphology of films. A multiblock membrane with optimized casting conditions outperformed the conductivity/hydrogen permeability ratio of Nafion™ by a factor of ~6. The hydrogen permeability of the partially disulfonated poly(arylene ether sulfone) copolymer was much lower than for Nafion.

5.1 Introduction

The increasing energy demands created by a growing population and limited fossil fuel reserves is driving research into alternative methods of energy production. Part of the diverse array of energy sources includes renewable energy sources such as solar, hydroelectric and wind energy. Renewable energy offers several advantages over fossil fuel-based resources that dominate the current energy economy, a critical one being a reduction in the carbon dioxide output per unit of energy. One of the criticisms of renewable energy is that it has unpredictable availability, frequently generating power when not needed and being unavailable during hours of high demand.

A potential answer to both criticisms is the development of proton exchange membrane (PEM) electrolysis systems, which can produce hydrogen via the electrolysis of water using energy generated during off-peak hours.[1] The hydrogen can be stored for use in vehicles which rely on PEM fuel cells, or used in stationary power applications to supplement the electrical grid during peak demand hours. PEM electrolysis has the advantage of producing very high purity hydrogen gas, which is essential for use in PEM fuel cells.[2] A good PEM for electrolysis should:

- Have excellent mechanical properties to withstand the pressurized environment of the electrolysis process
- Have good proton conductivity
- Have low hydrogen gas permeability
- Be easily fabricated into a membrane
- Resistant to chemical and oxidative degradation
- Stable under a constant applied voltage
- Have a high glass transition temperature

- Be affordable[3]

Of these, two critical issues for efficiency and safety are high proton conductivity with low hydrogen permeability. The latter is important to obtain high product purity and because the crossover of hydrogen through the membrane to the oxygen-producing side becomes a safety hazard.[1, 4]

The predominant commercial membrane used for PEM electrolysis is Nafion, a poly(perfluorosulfonic acid) ionomer. While it provides good proton conductivity, its high hydrogen permeability requires a thicker membrane to reduce crossover. Furthermore, its low hydrated glass transition temperature hinders performance at temperatures above about 80 ^{o}C, with reduced electrolysis performance and mechanical properties.[5, 6] As a result, new approaches that permit a higher operating temperature and pressure would significantly improve the performance of PEM electrolysis operations.[4]

A number of multiblock copolymers have been explored as alternatives to Nafion for PEM fuel cell applications.[7-11] In this research, a hydrophilic-hydrophobic multiblock copolymer based on partially disulfonated poly(arylene ether sulfone)s was synthesized and evaluated under different casting conditions. Its conductivity and hydrogen permeability were evaluated as a function of two different casting solvents. Bulk morphologies were investigated as a function of casting solvent, solution concentration, and annealing conditions to develop morphology-processing relationships for the membrane films.

5.2 Experimental

5.2.1 Materials

4,4'-biphenol (BP) was obtained from ChrisKev Company, Inc. and dried at 60 °C for 24 h under vacuum before use. Hydroquinone was kindly provided by Eastman Chemical, and was recrystallized from ethanol and dried at 110 °C under vacuum prior to use. 4,4'-Dichlorodiphenylsulfone (DCDPS) was kindly provided by Solvay Advanced Polymers and was recrystallized from toluene and dried at 110 °C prior to use. 3,3'-Disulfonated-4,4'-dichlorodiphenylsulfone (SDCDPS) was obtained from Akron Polymer Systems and was dried under vacuum at 160 °C for 72 h before use. Hexafluoroisopropylidine diphenol (6FBPA) was obtained from (Riedel-deHäen) and sublimed, then recrystallized from toluene, and dried under vacuum at 110 °C for 12 h prior to use. *N,N*-Dimethylacetamide (DMAc) and *N*-methyl-2-pyrrolidone (NMP) were obtained from Aldrich, and were vacuum-distilled from calcium hydride onto molecular sieves and stored under nitrogen immediately before use. Potassium carbonate (K_2CO_3, Aldrich) was dried under vacuum at 120 °C overnight before use. Toluene, cyclohexane, methanol, acetone, and isopropyl alcohol (IPA) were obtained from Aldrich and used as received. Concentrated sulfuric acid (H_2SO_4) was obtained from VWR and used to make a 0.5 M aqueous solution. Difluorodiphenyl sulfone (DFBPS) was obtained from Aldrich and dried under vacuum at 110 °C for 12 h prior to use.

Lead acetate was obtained from VWR and diluted to a 0.1% solution in deionized water prior to use. Epo-fix™ epoxy was obtained from Electron Microscopy Services.

5.2.3 Synthesis

5.2.3.1 Synthesis of a HQSH100 Hydrophilic Block

The hydrophilic block synthesis was adapted from a previously reported procedure.[8] A representative procedure follows: 8.41 g (15.75 mmol) of 98% SDCDPS, 1.93 g (17.53 mmol) of HQ, and 35 mL of DMSO were added to a three neck flask equipped with an overhead stirrer, a

condenser with a Dean Stark trap, and nitrogen inlet. An oil bath equipped with a thermocouple was used to heat the reaction to 135 °C, at which point toluene (55 mL) and potassium carbonate (2.78 g, 20.1 mmol) were added and the mixture was refluxed for 4 h to azeotropically remove any water. The reaction was then heated to 150 °C, and the toluene was removed via the Dean Stark trap. After 96 h of reaction, the solution was diluted with 30 mL of DMF and hot filtered to remove salts, then precipitated in isopropanol. A second hydrophilic block was produced with a 4,000 g/mol number average molecular weight.

5.2.3.2. Synthesis and Endcapping of Hydrophobic Blocks

DCDPS (9.54 g, 33.22 mmol), 6FBPA (12.04 g, 35.81 mmol) and DMAc (100 mL) were added to a three neck flask equipped with an overhead stirrer, a condenser with Dean Stark trap, and a nitrogen inlet. An oil bath equipped with a thermocouple was used to heat the reaction to 140 °C, at which point toluene (55 mL) and potassium carbonate (5.70 g, 41.2 mmol) were added and the mixture was refluxed for 4 h to azeotropically remove any water. The reaction was then heated to 160 °C, and the toluene was removed via the Dean Stark trap. The reaction proceeded for 24 h, then the temperature was lowered to 120 °C and decafluorobiphenyl (34.61 g, 103.6 mmol) was added (20-fold molar excess). The endcapping reaction proceeded for 8 h. The solution was hot filtered to remove salt, and precipitated in isopropanol. The yield was 81%.

5.2.3.3 Coupling Reaction of the Hydrophilic and Hydrophobic Blocks

HQS100 (4.62 g) and DMF (45 mL) were added to a three-neck, 100-mL round bottom flask equipped with a mechanical stirrer, condenser, nitrogen inlet and Dean-Stark trap. The solution was heated to 130 °C, then cyclohexane (15 mL) and K_2CO_3 (0.2 g, 1.45 mmol) were added and the mixture was refluxed for 4 h to remove water from the system. The cyclohexane was drained from the Dean Stark trap and then the mixture was cooled to 90°C. After cooling, the 6FBPS0 hydrophobic oligomer (4.25 g) was added. The bath temperature was raised to 120°C and

maintained for 24 h. The reaction mixture was diluted with DMF (35 mL) and allowed to cool to room temperature. The multiblock copolymer was precipitated into isopropanol (1000 mL) and stirred for 12 h. The product was filtered, then washed in deionized (DI) water at 90°C for 12 h, filtered again, and then dried *in vacuo* at 150°C for 24 h.

5.2.4.1 Synthesis of the Fluorine-Terminated Hydrophobic Block

An additional hydrophobic block was synthesized with DFBPS (12.18 g, 47.9 mmol), 6FBPA (15.24 g, 45.4 mmol) and NMP (135 mL) were added to a three neck flask equipped with an overhead stirrer, a condenser with Dean Stark trap, and a nitrogen inlet. An oil bath equipped with a thermocouple was used to heat the reaction to 148 °C, at which point cyclohexane (70 mL) and potassium carbonate (7.3 g, 52.8 mmol) were added and the mixture was refluxed for 4 h to azeotropically remove any water. The reaction was then heated to 165 °C, and the cyclohexane was removed via the Dean Stark trap. The reaction proceeded for 12 h. The solution was diluted with NMP (50 mL), hot filtered to remove salt, and precipitated in isopropanol.

5.2.4.2 Coupling of the Hydrophilic and Fluorine-Terminated Hydrophobic Blocks

HQS100 (16.4 g, 2.83 mmol) and DMF (190 mL) were added to a three-neck, 100-mL round bottom flask equipped with a mechanical stirrer, condenser, nitrogen inlet and Dean-Stark trap. The solution was heated to 130 °C, then cyclohexane (60 mL) and K_2CO_3 (1.0 g, 7.25 mmol) were added and the mixture was refluxed for 4 h to remove water from the system. The cyclohexane was drained from the reaction and then the mixture was cooled to 90°C. After cooling, the 6FBPS0 hydrophobic oligomer (21.5 g, 2.15 mmol) (~ 10,000 g/mol) was added. Excess hydrophilic monomer was used in this case due to the large difference in molecular weight between the two oligomers. The bath temperature was raised to 145°C and kept at this temperature for 48 h. The reaction mixture was diluted with DMF and allowed to cool to room temperature. The multiblock copolymer was precipitated into isopropanol (2000 mL) and stirred

for 12 h. The product was filtered then washed in deionized (DI) water at 90°C for 12 h, filtered again, and then dried *in vacuo* at 150°C for 24 h.

5.2.5 Characterization

5.2.5.1 NMR spectroscopy

^{1}H and ^{19}F NMR spectroscopy analyses were performed on a Varian INOVA 400 spectrometer operating at 400 and 376 MHz respectively. Spectra were obtained from a 10% solution (w/v) solution in *d*-$CDCl_3$ at ambient temperature.

5.2.5.2 Film Casting, Annealing, and Acidification

Films were cast by dissolving the copolymer to afford either 5% or 10% (w/v) solutions in DMAc or NMP. The solutions were filtered through a 0.1 μm PTFE Acrodisc filter onto a clean glass plate. The films were heated under an IR lamp for 12 h at 60 °C, and then under vacuum at 110°C for 24 h. Annealed films were produced by additionally heating under vacuum at 220 °C for 12 h. Films were acidified by boiling in 0.05 M H_2SO_4 for 2 h, and then in deionized water for 2 h. Note that for cases where the polymer was annealed, it was acidified after the annealing step.

5.2.3.3 Water Uptake

Water uptake was measured gravimetrically. Polymer films (100 mg) in acid form were equilibrated in deionized water overnight, then kept at room temperature for 12 h. They were blotted with a Kimwipe to remove surface water and weighed to obtain the wet weight (W_{wet}). Films were dried under vacuum at 110 °C for 12 h in order to obtain dry weights (W_{dry}). The water uptake in the salt form was determined as follows:

$$Water\ Uptake = \frac{W_{wet} - W_{dry}}{W_{dry}} * 100\%$$

5.2.3.3 Transmission Electron Microscopy

For transmission electron microscopy imaging, acidified membranes were stained with a 0.1% lead acetate aqueous solution to enhance the electron density of the hydrophilic block and provide contrast within the sample. Samples were sputter coated with a Au/Pd alloy to improve adhesion, then embedded in epoxy Epo-fix™ (electron microscopy services) and microtomed into approximately 70-nm thick sections with a diamond knife. Samples were then imaged on a JEOL 2100 Transmission Electron Microscope using an accelerating voltage of 120 kV.

5.3 Results

5.3.1 Synthesis

5.3.1.1 Hydrophilic Oligomer Synthesis

The synthesis of the hydrophilic HQS100 block via nucleophilic aromatic substitution is illustrated in Figure 5-1. The long reaction time was necessary due to the relatively low reactivity of both monomers. DMSO was used as a reaction solvent due to limited solubility of both monomers in other polar aprotic solvents.

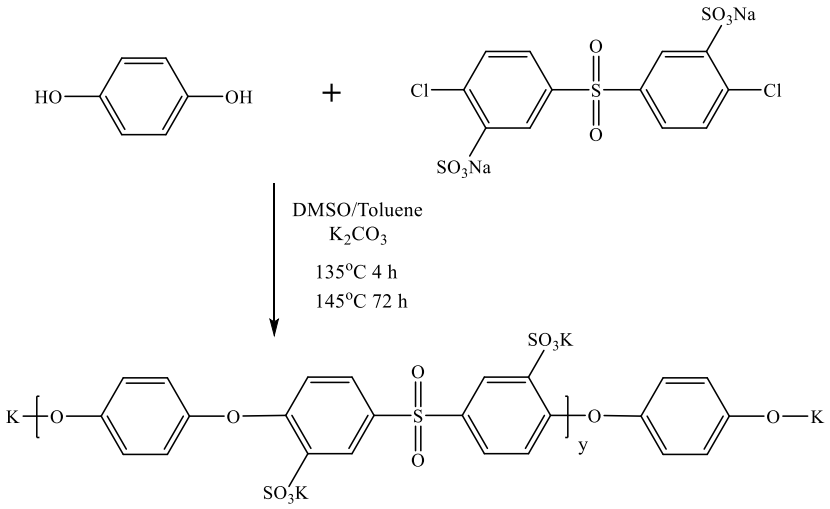

Figure 5-1. Schematic of hydrophilic oligomer synthesis.

^{1}H NMR was utilized to analyze the structure of the resulting oligomer (Figure 5-2). The protons on the sulfonated aromatic rings are attributed to the indicated A, B, and C protons located at 8.25, 7.83, and 6.93 ppm, respectively. The main chain hydroquinone protons (D) resonate at 7.08 ppm. The phenoxide endgroups resonate at 6.75 and 6.85 ppm (E and F). The singlet peak at 7.9 ppm is attributed to a small amount of dimethylformamide contamination. The peaks at 8.32, 7.7 and 7.65 ppm are attributed to SDCDPS endgroups (A', B' and C'). While Figure 5-2 illustrates both types of endgroups, it should be noted that they are not present in a 1:1 ratio.

Integrations of the endgroup peaks show a ratio of approximately 60% SDCDPS and 40% HQ endgroups. The molecular weight calculated from the ratio of endgroup peaks to the (A) proton on the SDCDPS repeat unit was approximately 3000 g/mol. The initial monomer ratios were calculated to produce an oligomer with phenoxy endgroups. However, due to the slow reactivities of both monomers, both types of endgroups were present after reaction.

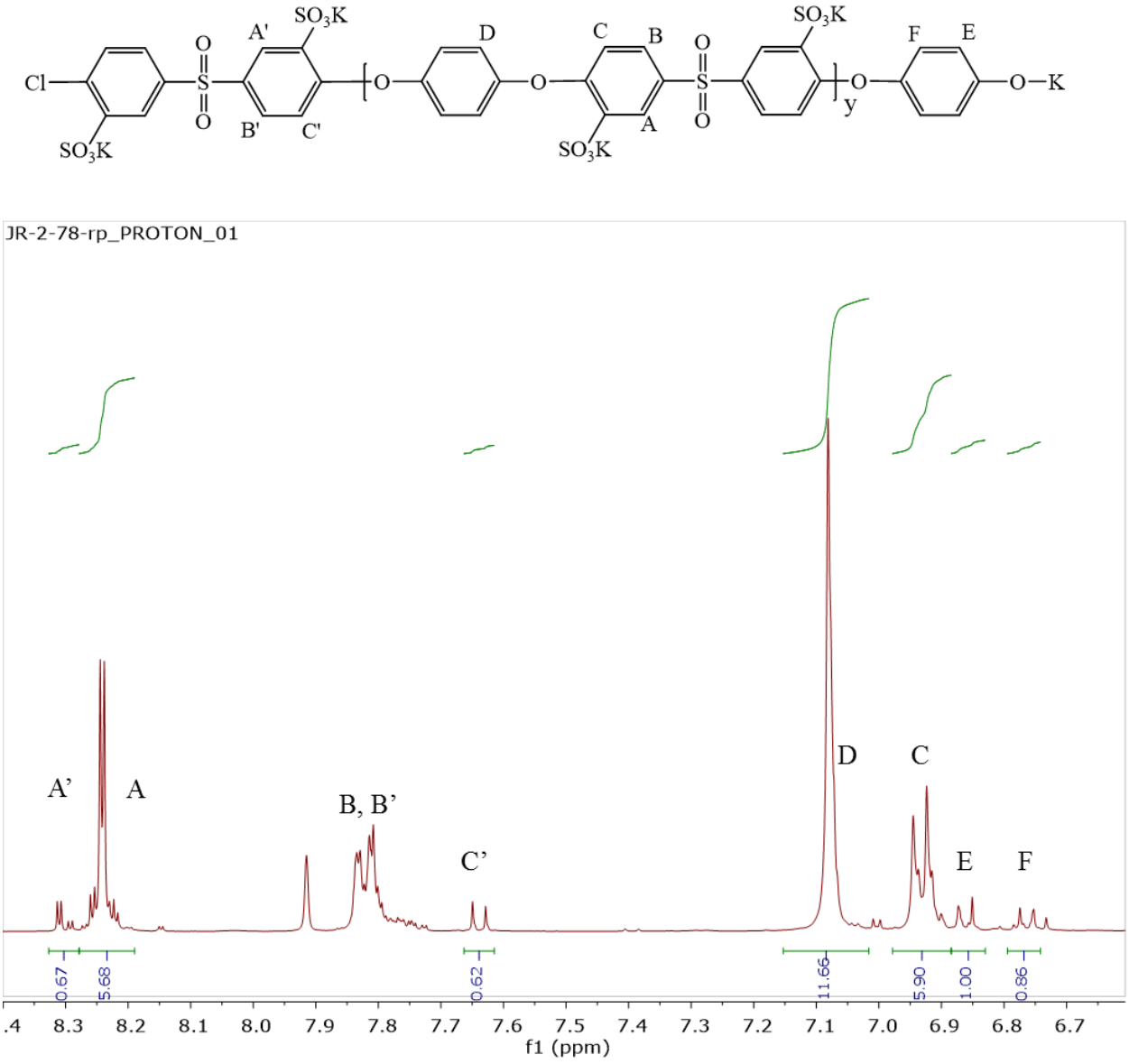

Figure 5-2. ^{1}H NMR of a 3K hydrophilic block

5.3.1.2 Synthesis of the Hydrophobic Oligomer

The hydrophobic oligomer was synthesized from the reaction of 6FBPA with DCDPS, and then it was endcapped with a large excess of decafluorobiphenyl (Figure 5-3). Decafluorobiphenyl was used as an endcapping reagent in order to increase reactivity, so that the block copolymer coupling reaction could be carried out at a sufficiently low temperature to avoid transetherification.

Transetherification is a major concern in the synthesis of poly(arylene ether sulfone) multiblocks as the interchange of ether groups would disrupt the block structure.

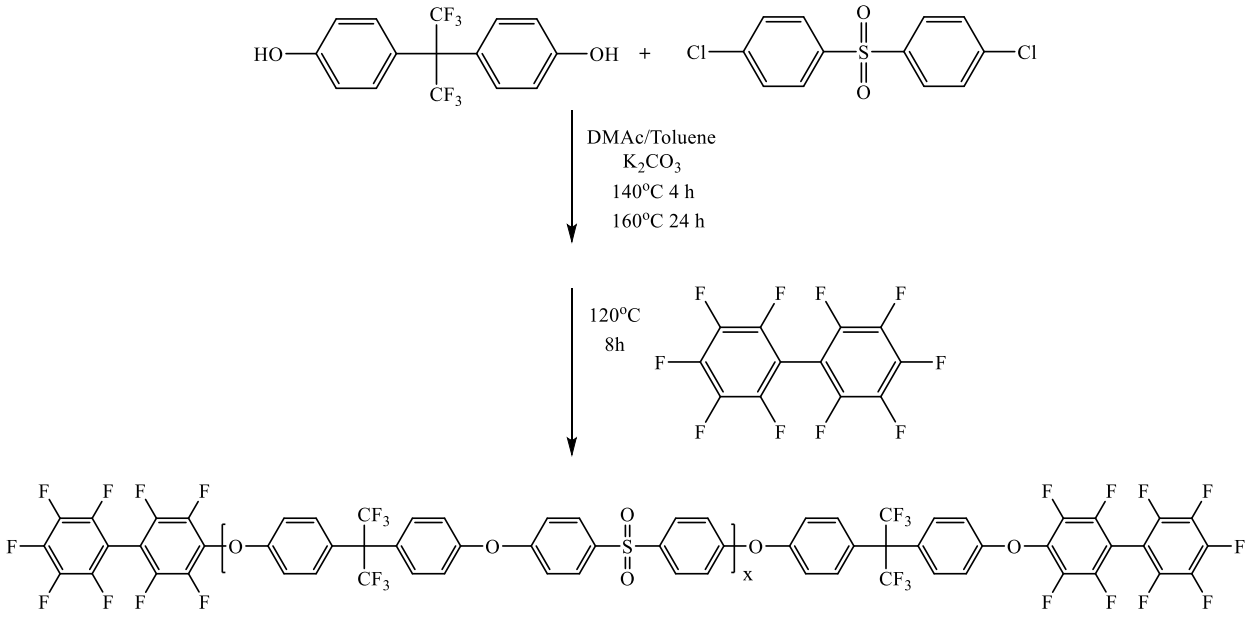

Figure 5-3. Synthesis and endcapping of 6FS hydrophobic block.

^{1}H and ^{19}F NMR were used to confirm the expected structure of the resulting oligomer (Figures 5-4 and 5-5). The aromatic protons from the 6FBPA unit resonated at 7.35 (B) and 7. 15 (A) ppm, while the aromatic protons from the sulfone unit resonated at 7.15 (C) and 7.92 ppm (D). In the ^{19}F NMR, the peak at -64 resonates with the CF_3 groups on the oligomer backbone. The -141, -150, -152, and -160 resonate with the C, A, D, B fluorines indicated in Figure 5-5. The ratio of the integrals of the 6F fluorines and the C fluorines on the endgroups was used to determine a number average molecular weight of 10,000 g/mol.

For the fluorine-terminated hydrophobic block, the molecular weight was determined by ^{19}F NMR to be 6100 g/mol.

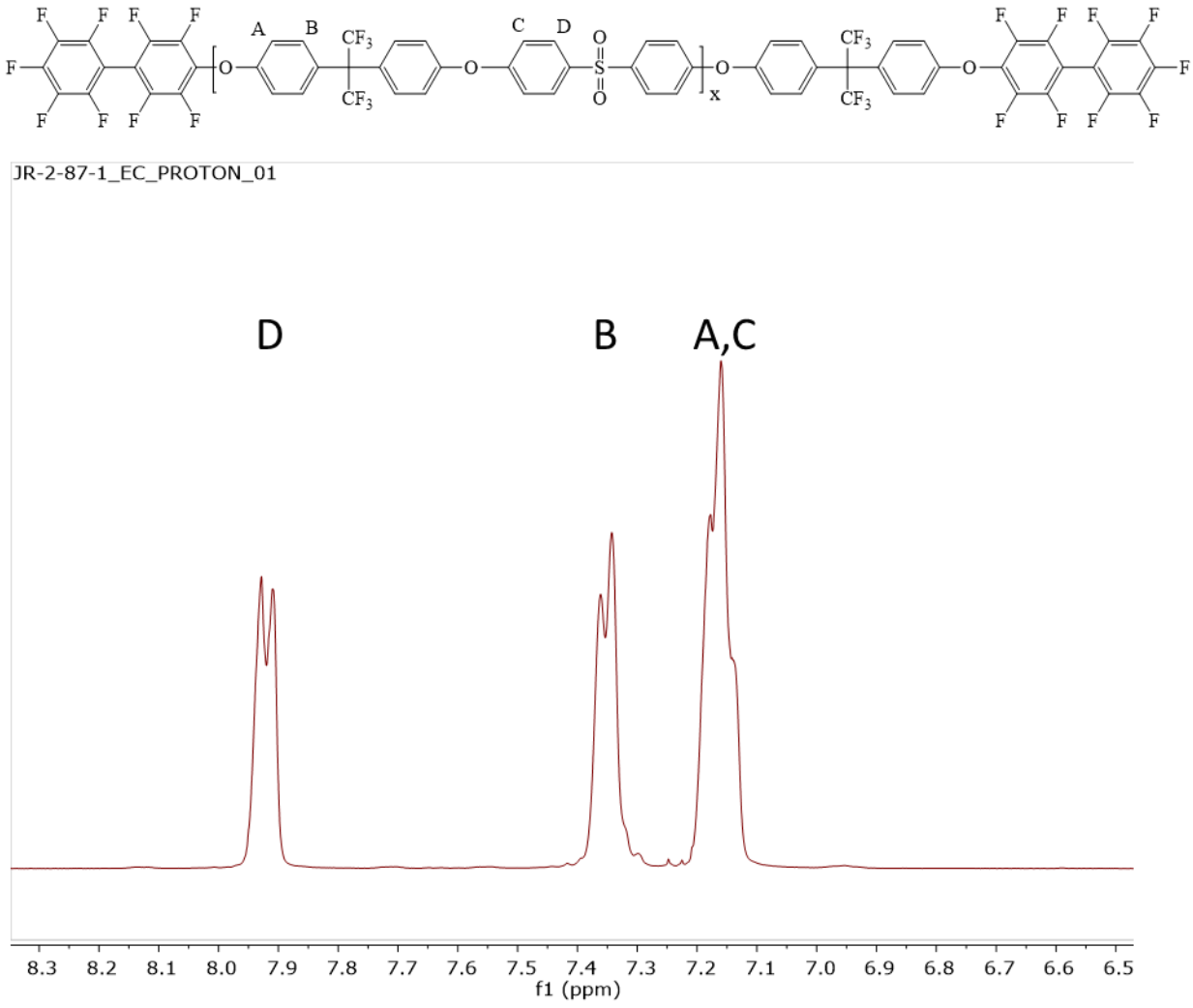

Figure 5-4. Structure and ^{1}H NMR spectrum of DFBP-endcapped 6FS hydrophobic oligomer.

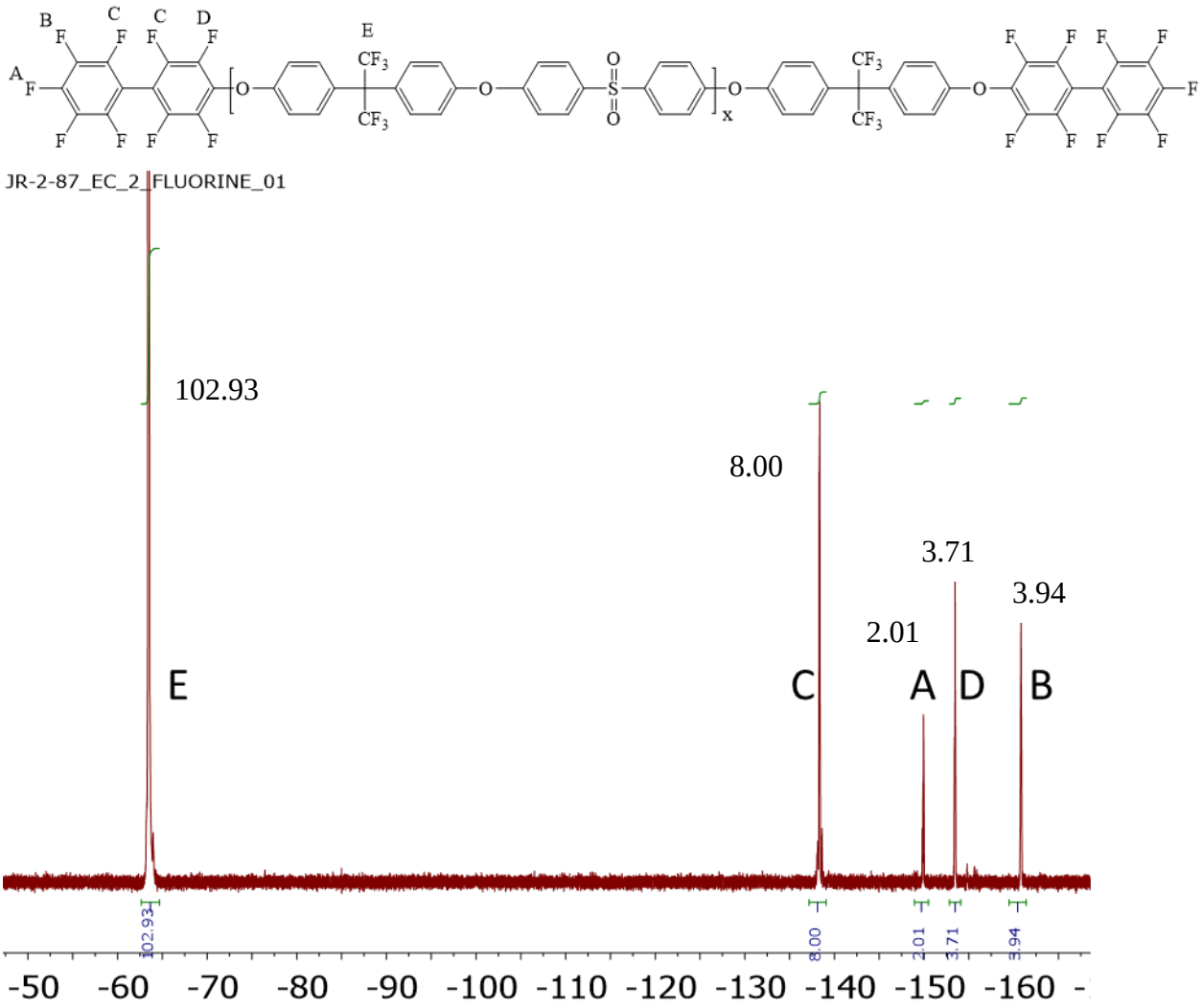

Figure 5-5. ^{19}F NMR of DFBP-endcapped hydrophobic 6FS oligomer.

5.3.1.3 Coupling of Hydrophilic and Hydrophobic Oligomers

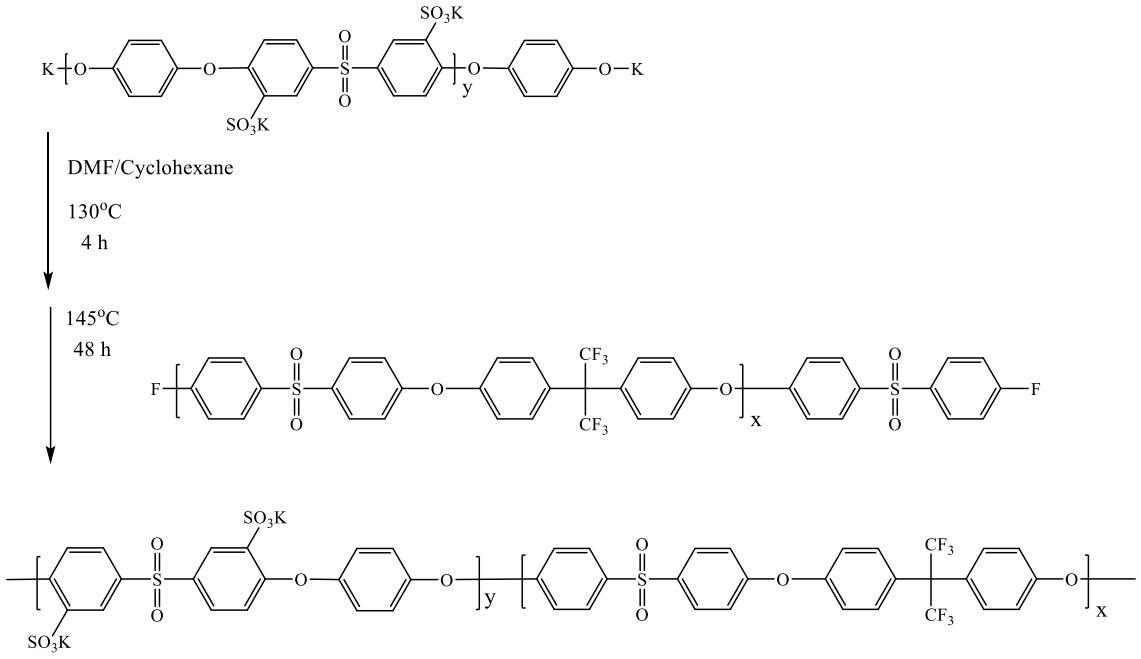

Figure 5-6. Coupling reaction to form the multiblock copolymer.

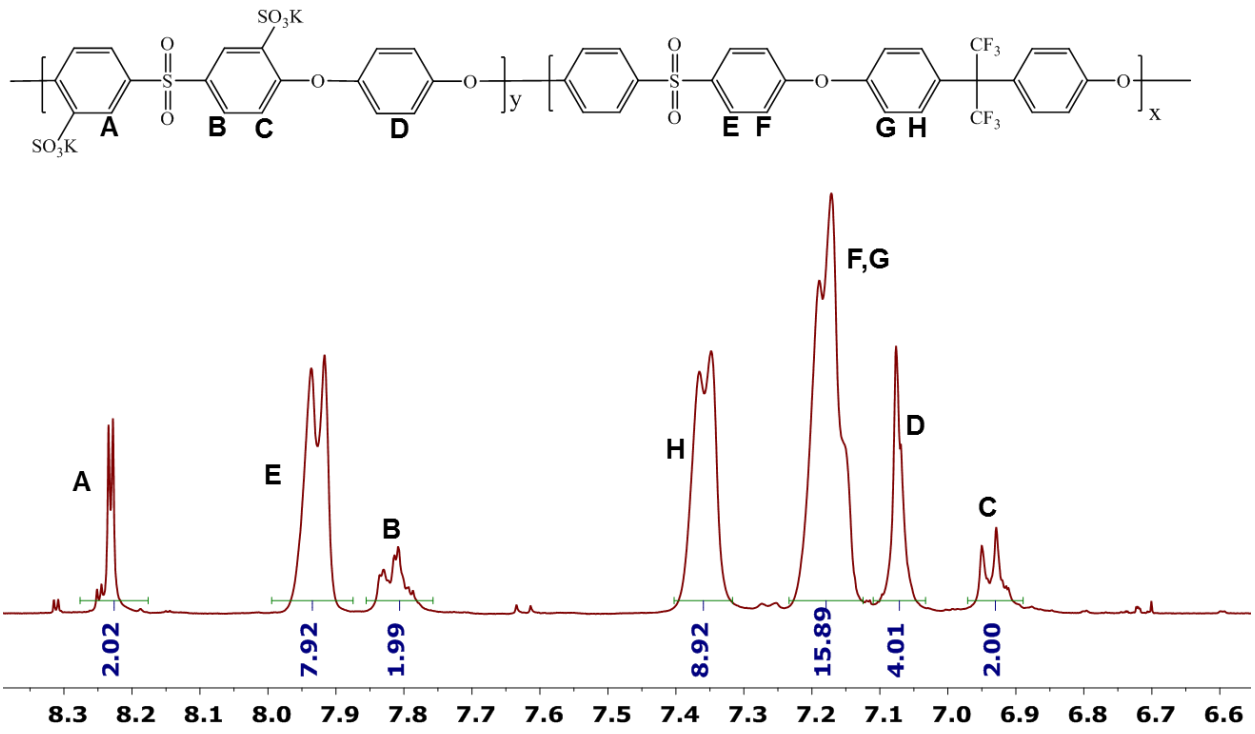

Figure 5-7. ^{1}H NMR of the multiblock copolymer.

The block copolymers were prepared by the coupling reaction of the fluorine terminated hydrophobic oligomer and the phenoxide endgroups of the hydrophilic oligomer (Figure 5-6). Oligomers terminating in chlorine endgroups at either end were unreactive under the reaction conditions, and oligomers with both a phenoxide and chlorine endgroup likely formed a terminal block of the multiblock copolymer.

The A, B, and C protons of the disulfonated unit in Figure 5-7 resonate at 8.22, 7.81, and 6.94 ppm, respectively. The A' peak corresponding to the SDCDPS endgroup resonates at 8.32. The ratio of A and A' integrals indicates that about 40% of the SDCDPS endgroups were lost in the coupling reaction or during isolation of the block copolymer. The D peak corresponding to the hydroquinone protons resonates at 7.07 ppm, and the E peak corresponding to the inner protons

on the DCDPS unit resonates at 7.94 ppm. The F and G peaks of the ether-proximate protons on both the 6FBPA and DCDPS units overlap, resonating at approximately 7.17 ppm. The H peak corresponding to the inner protons on the 6FBPA unit resonates at 7.36 ppm.

Integrations of the A, A' and H peaks were used to calculate the ion exchange capacity (meq of ions/g), listed with other membrane properties in Table 5-1. The IEC of the 10K-3K hydrophobic-hydrophilic multiblock copolymer was determined to be 1.10 meq/g. ^{1}H NMR analysis indicated a hydrophilic weight fraction of 35%, and a hydrophobic weight fraction of 65%. This is slightly higher than that of the Nafion 1100 films (0.91 meq/g) which were also evaluated for proton conductivity and hydrogen permeability. The second multiblock, coupled from a fluorine-terminated hydrophobic block without a decafluorobiphenyl linkage group, the hydrophobic oligomer was 6100 g/mol and the hydrophilic was 4000 g/mole. The overall composition was determined to be 60% hydrophobic and 40% hydrophilic. Despite having very different IECs, the samples showed very similar water uptake behavior. This may be due to differing morphologies as a result of the distinct oligomer block compositions.

Hydrophobic-Hydrophilic block length	Ion Exchange Capacity (NMR)	Water Uptake (%)
10K-3K	1.10	47
6K-4K	1.41	48

Table 5-1. Membrane Properties of Multiblock Copolymers

5.3.1.4 Bulk Morphology

5.3.1.5 Effect of Annealing and Molecular Weight

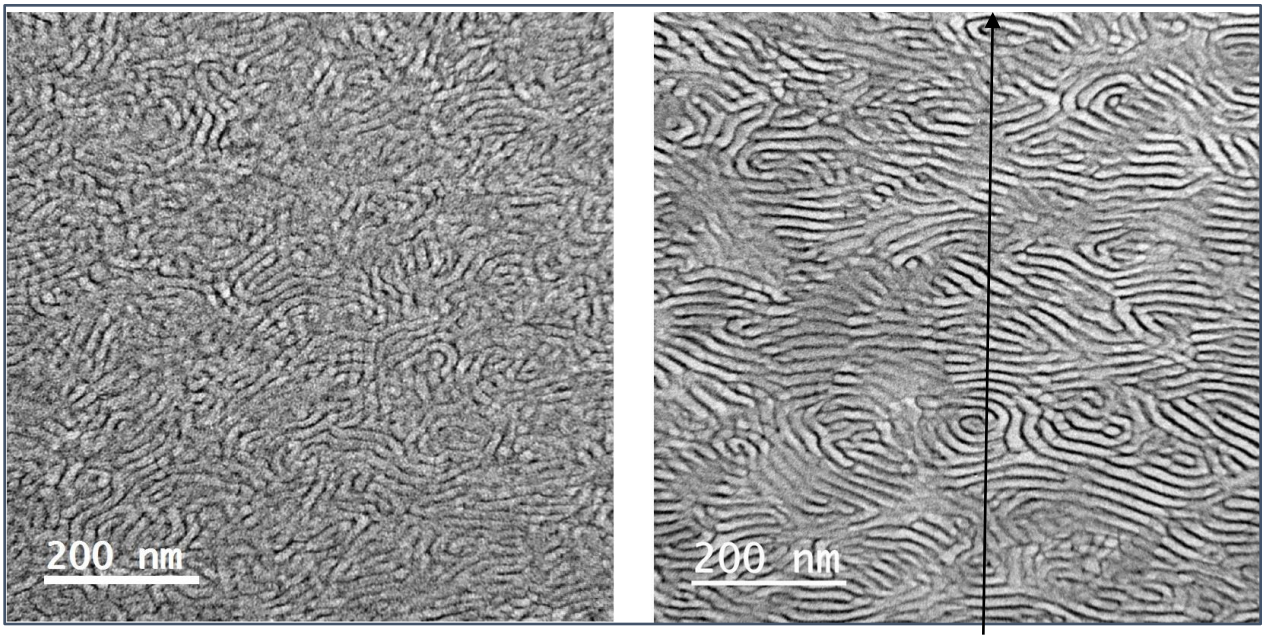

Figure 5-4. TEM image of a cross-section of the 11K-3K 6FBPS0-HQSH100 copolymer, (left) before and (right) after annealing. All films were cast from 5% DMAc. Arrow points across the film thickness (glass side to air side of film).

Figure 5-8 shows the TEM images of through-plane cross-sections of thin films of multiblock copolymers. Dark areas indicate hydrophilic regions of the copolymer films that have been stained with lead acetate, while light areas indicate hydrophobic regions. The annealed samples were heated for 12 hours at 220 ^{o}C under vacuum, which is just above the Tg of the hydrophobic block. The impact of annealing on long-range order and lamellar orientation is shown in the 11K-3K 6FBPS0-HQSH100 copolymers cast from 5% DMAc. The images were obtained under ultra high vacuum, and so during PEM electrolysis, the dark hydrophilic regions would be much larger. For the 8K-5K 6FBPS0-HQSH100 copolymer, the upper left-hand image illustrates the non-annealed sample, which shows little long-range assembly, and no apparent orientation of morphology with respect to any direction. However, after annealing between the two T_gs of the hydrophilic and hydrophobic phases, the same material shows both long range ordered lamellae, persisting in some cases for over 100 nm, and with significant orientation of the lamellae with

respect to the membrane surfaces. This orientation is likely due to preferential affinity of the hydrophobic block for the membrane surfaces, due to lower surface energy. During the annealing process, the hydrophobic block forms lamellae parallel to the surface, which propagates a degree of orientation throughout the membrane thickness as the hydrophobic domains re-assemble. The higher block length copolymer shows more long range order before annealing (lower left and lower right images), but also shows orientation parallel to the surfaces post-annealing. In both cases, the morphological comparisons were made from sections of the same film, one stained after casting and acidification and one stained after casting, annealing and acidification, to avoid any variations between different films.

5.3.1.6 Impact of Casting Solution on Film Morphology

A comparison was also made between films cast from 5% solutions in NMP (left) and DMAc (right) from the 8K-5K 6FBPS0-HQSH100 copolymer (Figure 5-9). The films were cast, annealed, and acidified together to ensure identical casting conditions. Even though the solvent should be almost entirely removed prior to annealing, it appears there was still a solvent effect in terms of the capacity for the morphology to become re-ordered after annealing. The NMP-cast film had a less ordered lamellar morphology, with no apparent orientation, while the DMAc-cast film again showed an ordered, oriented lamellar structure.

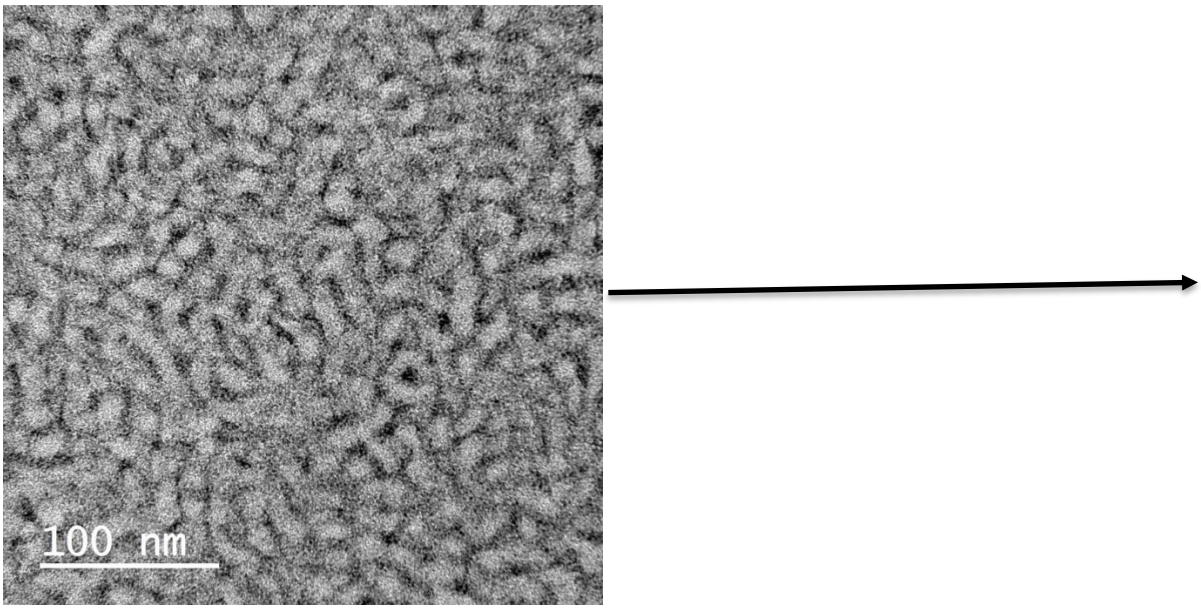

Figure 5-5. TEM images of the 10K-4K 6FS-HQSH100 copolymer cast from (left) a 5% NMP solution and (right) a 5% DMAc solution. Arrow again indicates thickness of film, going from glass side of film to air side.

5.3.1.7. Conductivity and Permeability

The conductivity data for the copolymers compares two different casting methods: the 10K-3K copolymer cast from 10% polymer in NMP, and the copolymer cast from 5% polymer in DMAc. In these results, the film cast from DMAc shows a significant increase in proton conductivity over the NMP-cast film, but also a decrease in hydrogen (H_2) permeability. These two improvements combine to provide a sharp increase in the conductivity/permeability ratio for the NMP-cast film relative to the DMAc-cast film. The improvement in proton conductivity is likely due to the improvements in long-range order of the hydrophilic block providing longer proton-conducting channels. However, the increase in orientation of the lamellae parallel with the plane of the film likely drives the drop in hydrogen permeability. The orientation increases the number of layers that the hydrogen must cross in order to permeate the thickness of the membrane, and each lamella represents an additional step of adsorption, diffusion and desorption into the next layer. Thus it is

hypothesized that the lamellae effectively form hurdles that slow the hydrogen transport through the thickness of the film.

Table 5-1. Proton Conductivity and hydrogen gas permeability, all numbers relative to Nafion 100.

	Conductivity	Permeability	C/P Ratio
Giner HQSH100-6FBP0	0.6	0.5	1.1
VT HQSH100-6FBPS0	1.1	0.18	6.1
Nafion 1100	1.0	1.0	1.0

5.4 Conclusions

A hydrophobic-hydrophilic 10K-3K multiblock poly(arylene ether) sulfone copolymer was synthesized with terminal hydrophilic blocks. Thin films cast from 5% polymer in DMAc and then annealed at 220 ^{o}C (above Tg of hydrophobic block) had highly aligned lamellar morphology parallel to the plane of the film. Proton conductivity in liquid water at 95 ^{o}C exceeded that of Nafion 1100, with significantly lower hydrogen (H_2) permeability. This is important for efficiency of membrane electrolysis of water, because high conductivities with low hydrogen cross-over are a priority for alternative materials development.

Morphology was characterized as a function of casting solution, concentration, and acidification treatment. Annealing was shown to not only increase long-range order as expected, but also induced orientation parallel to the film surfaces which propagated throughout the bulk of

the film. The high weight fraction of the hydrophobic oligomer together with highly mobile, hydrophilic endgroups in water led to materials with ordered surfaces and orientation of the lamellae in the plane of the film as illustrated in the TEM micrographs. The small weight fraction of the hydrophilic phase combined with the greater mobility of the hydrophilic end blocks likely contributed to the high proton conductivity combined with the low hydrogen permeability.

1. Carmo, M.; Fritz, D. L.; Mergel, J.; Stolten, D., A comprehensive review on PEM water electrolysis. *Int. J. Hydrogen Energy* **2013,** *38* (12), 4901-4934.
2. Smolinka, T.; Rau, S.; Hebling, C. In *Polymer electrolyte membrane (PEM) water electrolysis*, Wiley-VCH Verlag GmbH & Co. KGaA: 2010; pp 271-289.
3. Arico, A. S.; Siracusano, S.; Briguglio, N.; Baglio, V.; Blasi, A.; Antonucci, V., Polymer electrolyte membrane water electrolysis: status of technologies and potential applications in combination with renewable power sources. *J. Appl. Electrochem.* **2013,** *43* (2), 107-118.
4. Gandia, L. M., Arzamendi, G., Diéguez, P.M., *Renewable hydrogen technologies: production, purification, storage, applications and safety*. Elsevier

2013.
5. Mauritz, K. A.; Moore, R. B., State of understanding of Nafion. *Chem. Rev. (Washington, DC, U. S.)* **2004,** *104* (10), 4535-4585.
6. Phillips, A. K.; Moore, R. B., Mechanical and transport property modifications of perfluorosulfonate ionomer membranes prepared with mixed organic and inorganic counterions. *J. Polym. Sci., Part B: Polym. Phys.* **2006,** *44* (16), 2267-2277.
7. Chen, Y.; Rowlett, J. R.; Lee, C. H.; Lane, O. R.; Van, H. D. J.; Zhang, M.; Moore, R. B.; McGrath, J. E., Synthesis and characterization of multiblock partially fluorinated hydrophobic poly(arylene ether sulfone)-hydrophilic disulfonated poly(arylene ether sulfone) copolymers for proton exchange membranes. *J. Polym. Sci., Part A: Polym. Chem.* **2013,** *51* (10), 2301-2310.
8. Lee, H.-S.; Lane, O.; McGrath, J. E., Development of multiblock copolymers with novel hydroquinone-based hydrophilic blocks for proton exchange membrane (PEM) applications. *J. Power Sources* **2010,** *195* (7), 1772-1778.
9. Lee, H.-S.; Roy, A.; Lane, O.; Dunn, S.; McGrath, J. E., Hydrophilic-hydrophobic multiblock copolymers based on poly(arylene ether sulfone) via low-temperature coupling reactions for proton exchange membrane fuel cells. *Polymer* **2008,** *49* (3), 715-723.
10. Rowlett, J. R.; Chen, Y.; Shaver, A. T.; Lane, O.; Mittelsteadt, C.; Xu, H.; Zhang, M.; Moore, R. B.; Mecham, S.; McGrath, J. E., Multiblock poly(arylene ether nitrile) disulfonated poly(arylene ether sulfone) copolymers for proton exchange membranes: Part 1 synthesis and characterization. *Polymer* **2013,** *54* (23), 6305-6313.
11. Rowlett, J. R.; Shaver, A. T.; Lane, O.; Mittelsteadt, C.; Xu, H.; Zhang, M.; Moore, R. B.; Mecham, S.; McGrath, J. E. In *Properties and performance of multiblock copolymers based upon a varying hydrophilicity backbone*, American Chemical Society: 2014; pp ENFL-76.

6.0 Synthesis and Characterization of Hydrophobic-Hydrophilic Block Copolymers for Proton Exchange Membranes

*Ozma R. Lane, Rachael A. VanHouten, Desmond J. VanHouten, James E. McGrath, J. S. Riffle**

Macromolecular Science and Engineering, Macromolecular and Interfaces Institute

Virginia Tech, Blacksburg, VA 24061

*judyriffle@aol.com

Submitted to the Journal of Membrane Science, August 2015

Abstract

A series of hydrophobic-hydrophilic multiblock poly(arylene ether sulfone) copolymers based on highly fluorinated and sulfonated monomers were synthesized and characterized for use as proton exchange membranes in fuel cell applications. A preformed hydrophilic oligomer was reacted with the monomers for the hydrophobic component to form segmented copolymers containing highly fluorinated hydrophobic segments and 100% disulfonated hydrophilic blocks via a nucleophilic aromatic substitution step polymerization reaction. This approach afforded high molecular weight, transparent, and ductile copolymers with good mechanical properties. At comparable ion exchange capacities, water uptake increased with block length, suggesting that the extent of nanophase separation was a function of block length. This was confirmed by TEM and AFM images. These copolymers showed improved proton conductivity under partially-humidified conditions with increasing block length. A series of multiblock hydrophobic-

hydrophilic copolymers using the same co-monomers and oligomer molecular weights was also synthesized and evaluated for comparison.

6.1 Introduction

With the growing economic and environmental costs associated with fossil fuel extraction, there is an increasing need for viable alternatives to current combustion engine technology. Hydrogen-powered proton exchange membrane fuel cells (PEMFCs) are viewed as a promising candidate for powering 21st century vehicles.[1, 2] Fuel cells using other fuels—for example, methanol or ethanol—may also be adapted for portable power applications such as personal electronic devices (e.g., laptop computers and cell phones). PEMFCs have a number of advantages compared to other types of fuel cells.[1] For example, they are able to generate more power for a given volume or weight of the fuel cell. This high power density enables their use in applications such as personal vehicles. In addition, their low operating temperature (below 100ºC) allows rapid start-up. Most importantly, PEMFCs have a negligible environmental impact with only water and heat produced during operation. These traits make them superior candidates for automotive power applications.[3]

There are, however, a number of technical hurdles to overcome before the large-scale commercial production of PEMFC vehicles can be realized. In addition to the difficulty of hydrogen storage, hydrogen distribution and delivery will require the construction of a costly infrastructure combining transport and storage of hydrogen and the development of a dense network of refueling stations.[4-6] But as those problems are addressed, research must also resolve the challenges associated with materials development. Specifically, the predominant commercial membrane in use today is Nafion®, which is a poly(perfluorosulfonic

acid) ionomer. While it displays good proton conductivity, it has several drawbacks which at present limit practical commercial application. These include high permeability to both hydrogen and methanol, excessive materials cost, the difficulty in processing the copolymer, and a low operating temperature of about 80°C under hydrated conditions.[7, 8] A number of alternate proton exchange membrane candidates, membrane treatment procedures, and membrane additives are under development to overcome these challenges.[9-16]

Our group has investigated partially disulfonated statistical and multiblock poly(arylene ether sulfone) copolymers as alternative PEM candidates. These materials offer improvement both in raw materials cost and ceiling operating temperature, but the statistical copolymers have reduced conductivities as humidity is decreased.[17, 18] The later development of nanophase-separated multiblock copolymers has shown improved proton conductivity under partially humidified conditions.[19-21] The formation of hydrophilic channels that retain water improves conductivity, while the highly hydrophobic channels provide mechanical strength and reduce water loss. The multiblock copolymers allow for higher ion exchange capacities (IEC) without loss of mechanical properties relative to the statistical copolymers. The nanophase separation additionally results in anisotropic water uptake behavior which could reduce membrane stresses due to reduced in-plane swelling. [19-21] During fuel cell operation, stresses are caused by in-plane swelling and deswelling due to hydration and dehydration of the membrane electrode assembly (MEA). This can cause failure between the electrode and polymer electrolyte layers. The swelling behavior becomes more anisotropic with higher oligomer block lengths. Thus, there is interest in developing nanophase-separated multiblock copolymers to optimize PEMFC performance both in terms of proton conductivity and fuel cell durability.[16, 22]

Previously in our group, highly sulfonated, highly fluorinated multiblock copolymers were synthesized from a hydrophobic block comprised of decafluorobiphenyl and bis(4-hydroxyphenyl) sulfone coupled with a hydrophilic block of 4,4'-biphenol and SDCDPS.[23] Those copolymers showed good proton conductivity and mechanical properties. A highly fluorinated monomer was chosen to be incorporated into the hydrophobic oligomer to achieve phase separation. The highly activated decafluorobiphenyl endgroups were also an advantage so that the oligomer coupling reaction could be conducted at relatively low temperatures to avoid any transetherification. A series of multiblock copolymers with these structures having approximately equal block lengths of the oligomers, but with varied block lengths were investigated. These multiblock copolymers with the longer block lengths featured improved conductivities under partially humidified conditions, comparable or competitive with that of Nafion® 212.

The focus of this research has been to simplify the method for making the multiblock copolymers. We compared the properties of a nanophase-separated series of copolymers with analogous structures that were prepared in a one-pot synthetic process versus the more traditional "two preformed" oligomer approach. In this technique, the hydrophilic block was preformed with phenol endgroups and then this was copolymerized with the monomers for the hydrophobic block in-situ. While this general technique is not new, it was not known whether this simplified approach would yield materials with the excellent transport properties that are ideal for the fuel cell application. This method is an attractive synthetic technique for several reasons. Using this one-pot technique, multiblock copolymers can be synthesized more easily in a shorter amount of time because there is no need to synthesize both oligomers separately and then couple them together. The one-pot "segmented" technique can also sometimes allow for more choice of solvents compared to coupling two preformed oligomers that may differ greatly in chemical polarity. This

avoids the often observed polymer-polymer incompatibilities between two oligomers that can complicate block copolymer synthesis.

In this paper, we discuss the synthesis and properties of multiblock copolymers comprised of decafluorobiphenyl, bis(4-hydroxyphenyl)sulfone, biphenol and SDCDPS using two synthetic routes. In the oligomer-oligomer method, each oligomer was separately preformed, then they were coupled. This was compared with a segmented, streamlined approach wherein only the hydrophilic oligomer was preformed, then that oligomer was copolymerized with the monomers to form the hydrophobic block in-situ. The effect of block length on copolymer properties including proton conductivity, water uptake, and dimensional swelling are discussed.

6.2 Experimental Section

6.2.1 Materials

Decafluorobiphenyl (DFBP) was obtained from Matrix Scientific and dried under vacuum at ambient temperature for 12 h. Bis(4-hydroxyphenyl)sulfone (Bis-S) was kindly supplied by Solvay Advanced Polymers and dried under vacuum at 60 ^{o}C for 24 h before use. Monomer grade 4,4'-biphenol (BP) was obtained from ChrisKev Company, Inc. and dried at 60 ^{o}C for 24 h under vacuum before use. 4,4'-Dichlorodiphenylsulfone (DCDPS) was kindly provided by Solvay Advanced Polymers and used as received to synthesize 3,3'-disulfonated-4,4'-dichlorodiphenylsulfone (SDCDPS) according to a previously reported procedure.[24] SDCDPS was dried under vacuum at 160 ^{o}C for 48 h before use. *N*,*N*-Dimethylacetamide (DMAc, Aldrich) and *N*-methyl-2-pyrrolidone (NMP, Aldrich) were vacuum-distilled from calcium hydride onto

molecular sieves and stored under nitrogen immediately before use. Potassium carbonate (K_2CO_3, Aldrich) was dried under vacuum at 120 °C overnight before use. Toluene, cyclohexane, acetone, and isopropyl alcohol (IPA) were obtained from Aldrich and used as received. Concentrated sulfuric acid (H_2SO_4) was obtained from VWR and used to make a 0.5 M aqueous solution.

6.2.2. Synthesis of Phenoxide-Terminated Hydrophilic Blocks (BPS-100).

Phenoxide-terminated hydrophilic blocks were synthesized using a previously published procedure. The targeted molecular weights of the blocks ranged from 3000 to 9000 g/mol. In a typical procedure to achieve a M_n of 3000 g/mol, the following conditions were utilized. BP (4.7322 g, 25.41 mmol), SDCDPS (10.2764 g, 20.92 mmol), and DMAc (75 mL) were charged to a three-neck, round-bottom flask, equipped with a mechanical stirrer, a Dean-Stark trap and condenser, and N_2 inlet. The reaction temperature was maintained at 85 °C utilizing a thermocouple-controlled oil bath and the monomers were dissolved. K_2CO_3 (4.039 g, 29.23 mmol) and toluene (38 mL) were added. The temperature of the oil bath was increased to 155 °C, and the reaction was refluxed for 4 h to azeotropically remove water. Toluene was removed from the system by increasing the bath temperature to 175 °C. The reaction was allowed to proceed for 96 h. After cooling to ambient temperature, the solution was filtered using an aspirator to remove salts and precipitated into acetone. The resulting oligomer was dried at 110 °C for at least 24 h under vacuum and had an M_n of 3300 g/mol determined by end group analysis using ^{1}H NMR.

6.2.3. Synthesis of Segmented Copolymers.

This copolymer series is referred to BisSF-BPSH100, where BisSF describes to the hydrophobic block synthesized from bis(4-hydroxyphenyl) sulfone and decafluorobiphenyl, and BPSH100 refers to the hydrophilic block synthesized from SDCDPS and 4,4'-biphenol. A sample

copolymerization procedure was as follows. A three-neck, round-bottom flask, equipped with a mechanical stirrer, a Dean-Stark trap, and a condenser, and N_2 inlet was loaded with BPS-100 (M_n=3300 g/mol, 4.0418 g, 1.225 mmol), Bis-S (1.6700 g, 6.673 mmol), and NMP (29 mL). After dissolution of the reactants, K_2CO_3 (1.255 g, 9.081 mmol) and cyclohexane (5 mL) were added to the reaction solution. The oil bath was heated to 110 ^oC, and the reaction was azeotroped to remove water for 4 h. The cyclohexane was drained, and the oil bath temperature was lowered to 90 ^oC. DFBP (2.6391 g, 7.899 mmol) and NMP (13 mL) were added to the reaction flask and the temperature was maintained at 90 ^oC for 36 h. The viscous solution was cooled, filtered with an aspirator, and precipitated into IPA (1 L). The product was filtered and washed in deionized water at 60 ^oC for 12 h and acetone for 12 h. It was dried under vacuum at 110 ^oC for 24 h before casting into films.

6.2.4. Synthesis of BisSF-BPSH100 Multiblock Copolymer Controls.

Multiblock copolymer controls were synthesized according to a previously published method.[23] Some modifications were made to the procedure and are reflected below.

6.2.4.1. Synthesis of Fluorine-Terminated Hydrophobic Blocks (BisSF) (2).

Fluorine-terminated hydrophobic blocks were synthesized with targeted molecular weights ranging from 3000 to 9000 g/mol. For a M_n of 3000 g/mol, the following synthetic procedure was utilized. Bis-S (2.5045 g, 10.01 mmol), DFBP (4.0263 g, 12.05 mmol), and DMAc (38 mL) were added to a three-neck, round-bottom flask, equipped with mechanical stirrer, Dean-Stark trap with condenser, and N_2 inlet. The oil bath was heated to 50 ^oC. After dissolving the monomers, K_2CO_3 (1.798 g, 13.01 mmol) and cyclohexane (7 mL) were added. The bath temperature was gradually raised to 110 ^oC over 30 min. The reaction was allowed to proceed for 5 h at 110 ^oC. After cooling to ambient temperature, the reaction was filtered to remove salts and precipitated into a solution

of methanol:water (1:1 v:v, 1 L). The oligomer was washed for 12 h in DI water and dried at 90 ^{o}C for 24 h under vacuum before further use. It had a M_n of 3200 g/mol determined by endgroup analysis using ^{19}F NMR.

6.2.4.2. Synthesis of Phenoxide-Terminated Hydrophilic Blocks (BPS-100) (1).

Phenoxide-terminated hydrophilic blocks were synthesized with targeted molecular weights ranging from 3000 to 9000 g/mol. To obtain a targeted molecular weight of 3000 g/mol, the following reaction procedure was utilized. BP (0.7939 g, 4.263 mmol), SDCDPS (1.7466 g, 3.555 mmol), and NMP (20 mL) were added to a three-neck, round-bottom flask, equipped with a mechanical stirrer, Dean-Stark trap with condenser, and N_2 inlet. The oil bath was heated to 85 ^{o}C. Upon dissolution of the monomers, K_2CO_3 (0.766 g, 5.543 mmol) and toluene (10 mL) were added to the flask. The bath temperature was increased to 155 ^{o}C, and the reaction was refluxed for 4 h. Toluene and water was removed azeotropically, then the reaction bath temperature was increased to 190 ^{o}C for 36 h. The bath temperature was lowered to 85 ^{o}C. The resulting oligomer had a M_n of 3300 g/mol determined by end group analysis using ^{1}H NMR. This product was not isolated and was used directly in the synthesis of a BisSF-BPS100 multiblock copolymer as described below.

6.2.4.3. Synthesis of BisSF-BPS100 Multiblock Copolymers.

Oligomer **(2)** (M_n=3200 g/mol, 2.0244 g, 0.6135 mmol) was added to the solution containing **(1)** and NMP (16 mL) was used to obtain a 14% w/v reaction solution. The bath temperature was increased to 90 ^{o}C, and the reaction proceeded for 36 h. The resulting viscous solution was precipitated into IPA (500 mL) to form fibrous strands. The product was filtered and washed in deionized water at 60 ^{o}C for 12 h and acetone for 12 h. It was dried under vacuum at 110 ^{o}C for 24 h before casting into films.

6.2.5. Characterization of Copolymers.

^{1}H and ^{19}F NMR spectroscopy analyses were performed on a Varian INOVA 400 spectrometer operating at 400 and 376 MHz respectively. ^{13}C NMR analyses were performed on a Varian Unity 400 MHz spectrometer operating at 100 MHz. Spectra were obtained from a 10% solution (w/v) solution in d_6-DMSO at ambient temperature. Intrinsic viscosities of the copolymers were determined using size exclusion chromatography (SEC). The experiments were performed on a liquid chromatograph equipped with a Waters 1515 isocratic HPLC pump, Waters Autosampler, Waters 2414 refractive index detector and Viscotek 270 dual detector. NMP containing 0.05 M LiBr was used as the mobile phase. The column temperature was maintained at 60 ^{o}C because of the viscous nature of NMP. Both the mobile phase and sample solution were filtered before injection into the SEC system.

6.2.6. Membrane Preparation.

Membranes were cast from a 7% w/v solution of polymer in DMAc onto a clean glass plate. Solvent was removed using an IR lamp. The film was held at 30-35 ^{o}C for 24 h and then raised to 60 ^{o}C for an additional 24 h. It was dried under vacuum at 110 ^{o}C for 24 h. The film was removed from the glass plate by submersion in water and acidified in boiling 0.5 M H_2SO_4 for 2 h, followed by 2 h in boiling deionized water.

6.2.7. Determination of Water Uptake and Dimensional Swelling.

The membrane water uptake was determined gravimetrically, using films with 100-150 mg dry weight. Acidified membranes were equilibrated in water at room temperature for 24 h. Wet membranes were removed from the water, blotted dry to remove excess water, and quickly weighed. They were then dried at 110 ^{o}C under vacuum for 24 h and reweighed. Water uptake

was calculated according to Equation 1 where $mass_{dry}$ and $mass_{wet}$ refer to the mass of the dry and wet membranes, respectively. An average of three samples was used for each measurement.

$$(1)\ Water\ Uptake = 100 * \frac{Mass_{Wet} - Mass_{Dry}}{Mass_{Dry}}$$

Percent swelling of the membranes was determined in the in-plane (x and y) and through-plane (z) directions. Wet measurements were performed after equilibrating membranes in deionized water for 24 h at room temperature. Membranes were then dried in a convection oven at 80 °C for 2 h and measured again. Percent swelling was reported for three directions and calculated according to Equation 2 where $length_{wet,i}$ and $length_{dry,i}$ refer to the length (where *i* represents the x, y, or z direction) of the wet and dry membrane, respectively.

$$(2)\ Dimentional\ Swelling = 100 * \frac{Length_{Wet,i} - Length_{Dry,i}}{Length_{Dry,i}}$$

6.2.8. Measurement of Proton Conductivity.

Proton conductivity at 30 °C in liquid water was determined in a window cell geometry using a Solartron 1252 + 1287 Impedance/Gain-Phase Analyzer over the frequency range of 10 Hz to 1 MHz. In determining proton conductivity in liquid water, membranes were equilibrated at 30 °C in DI water for 24 h prior to testing.

Proton conductivity under partially hydrated conditions was measured at 80 °C. Membranes were equilibrated at 80% RH for 8 h in a humidity-temperature oven (ESPEC, SH-240). The conductivity measurements were made at varying RH beginning from high RH to low RH. Membranes were allowed to equilibrate for 4 h prior to measuring conductivity at each RH. Measurements were done at 95, 80, 70, 60, 50, 40 and 30%. Due to the changing membrane thickness at different RH, film thickness was measured at 95, 80 and 30% RH using a micrometer.

The conductivity values at 70 and 60% RH were determined using the thickness measured at 80% RH. The conductivity values at 50, 40 and 30% RH were determined using the thickness measurement at 30% RH.

6.2.9. Tensile Testing.

Uniaxial load tests were performed using an Instron 5500R universal testing machine equipped with a 200-lb load cell at room temperature and 44-54% RH. Crosshead displacement speed was 5 mm/min and gauge length were set to 25 mm. The films were ~30 μm thick. A dogbone die was used to punch specimens 50 mm long with a minimum width of 4 mm. Prior to testing, specimens were dried under vacuum at 110 ^{o}C for at least 24 h and then equilibrated at 44% RH and 30 ^{o}C. All specimens were mounted in manually tightened grips. Approximate tensile moduli for each specimen were calculated based on the stress and elongation values for the specimen at 2% elongation.

6.2.10. Surface Morphology.

Tapping mode AFM was performed using a Digital Instruments MultiMode Scanning Probe microscope with a NanoScope IVa controller. A Veeco silicon probe with an tip radius <10 nm and a force constant K of 42 N/m was used to image samples. Samples were in their acid form and equilibrated at 40% RH and 30 ^{o}C for at least 12 h prior to imaging.

6.2.11. Bulk Morphology.

For transmission electron microscopy imaging, acidified membranes were stained with a lead acetate aqueous solution to enhance the electron density of the hydrophilic block and provide contrast within the sample. Samples were embedded in epoxy Epo-fix (electron microscopy

services) and microtomed into approximately 70-nm thick sections with a diamond knife. Samples were then imaged on a Philips EM 420 Transmission Electron Microscope using an accelerating voltage of 100 kV.

6.3. Results and Discussion

6.3.1. Synthesis of Hydrophilic Oligomers.

Phenoxide-terminated, fully disulfonated poly(arylene ether sulfone) hydrophilic oligomers (BPS100) were synthesized via nucleophilic aromatic substitution (Figure 6-1). A small molar excess of BP relative to SDCDPS was used to control the molecular weight of the oligomers, targeting number average molecular weights (M_n) of 3, 5, or 9 kg/mol. Proton NMR was used to analyze the structures of the oligomers including both the biphenol endgroups and internal units. M_n's of the oligomers were calculated by ratioing the integrals of the endgroup peaks relative to the internal units by assuming that all of the endgroups were phenolic (Figure 6-2). Protons from the terminal BP groups were assigned to the peaks at 6.8, 7.05, 7.4, and 7.55 ppm, whereas protons from the BP in the middle of the backbone resulted in peaks at 7.1 and 7.65 ppm. Theoretical and experimental M_n values are summarized in Table 1, along with intrinsic viscosity (I.V.) measured by SEC. An increase in I.V. was observed as M_n of the oligomers increased. A log-log plot of M_n derived from the NMR spectra versus intrinsic viscosity (Figure 6-3) had a linear relationship, suggesting successful control of molecular weight.

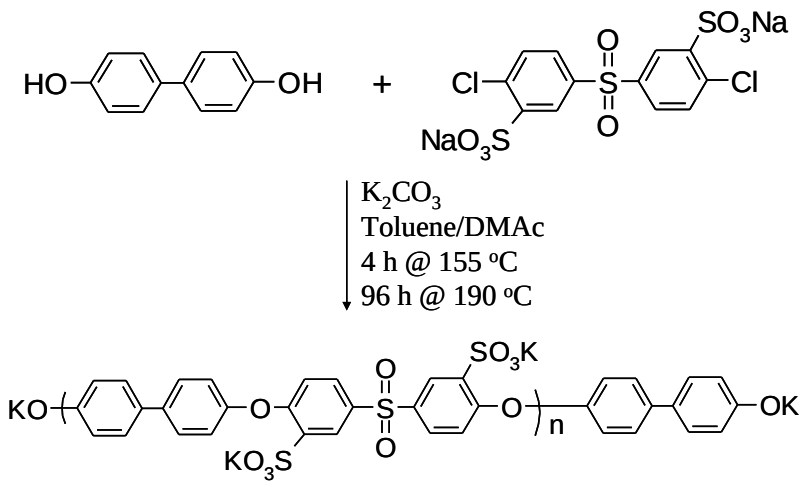

Figure 6-1. Phenoxide-Terminated BPS-100 with Controlled Molecular Weight

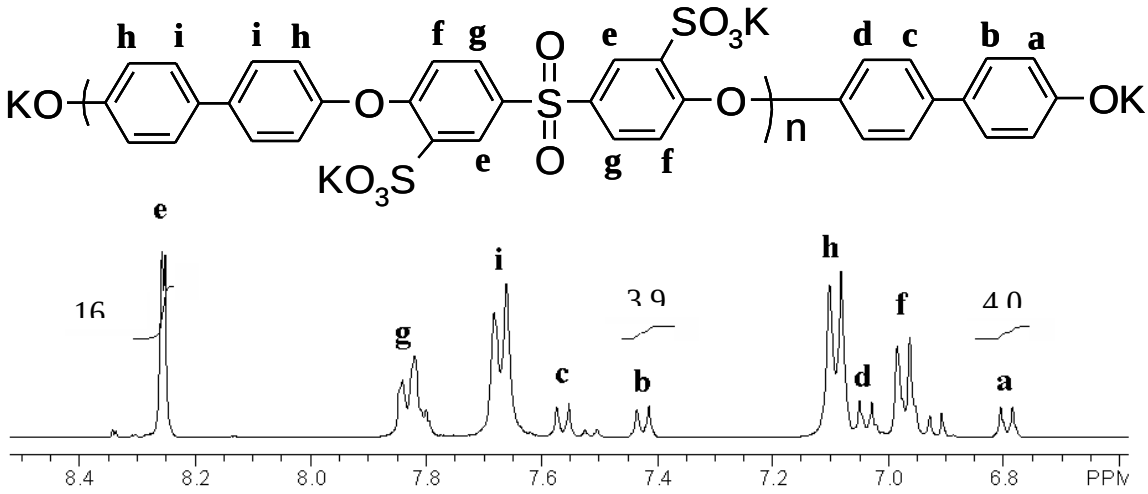

Figure 6-2. ^{1}H NMR Spectrum of BPS-100 Oligomer

Table 6-1. Characterization of Hydrophilic Telechelic Oligomers

Molecular Weight		
Target[1]	Experimental[a]	I.V.[b] (dL/g)
3000	2900	0.14
5000	4900	0.20
9000	9200	0.29

a) Calculated using ^{1}H NMR
b) SEC of the oligomer in its salt form performed in NMP with 0.05 LiBr

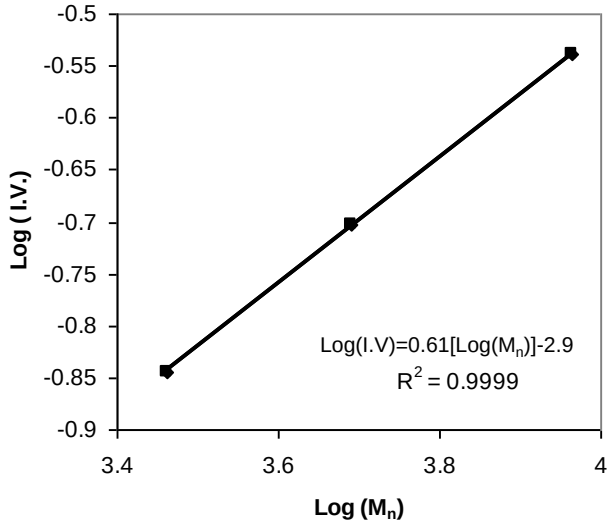

Figure 6-3. Log (M_n) vs log (I.V.) for the hydrophilic oligomers

6.3.2. Synthesis of BisSF-BPSH100 Segmented Copolymers.

The segmented copolymers were formed by reacting phenoxide-terminated hydrophilic oligomers with DFBP and Bis-S monomers in a step growth polymerization as illustrated in Figure 6-4. Simultaneous formation of the hydrophobic segments and the block copolymer eliminated the need to synthesize and isolate a separate hydrophobic block before coupling it to the hydrophilic block. The stoichiometry was controlled such that the DFBP and Bis-S monomers formed the hydrophobic segments of the copolymer, while also reacting with the phenoxide-terminated hydrophilic oligomer. The molecular weights of the hydrophobic segments were targeted to be 3, 5, or 9 kg/mol and copolymers with approximately equal hydrophobic and hydrophilic block lengths were obtained. To achieve high molecular weight, it was important to ensure that the overall ratio of phenoxide to *para*–fluorine endgroups was 1:1. An excess of phenoxide groups was disadvantageous because once the *para*-fluorines were consumed, the *ortho*-fluorines on the DFBP could react with the excess phenoxide groups, resulting in a crosslinked network. However, if insufficient phenoxide groups were present, high molecular weight copolymer was not achieved.

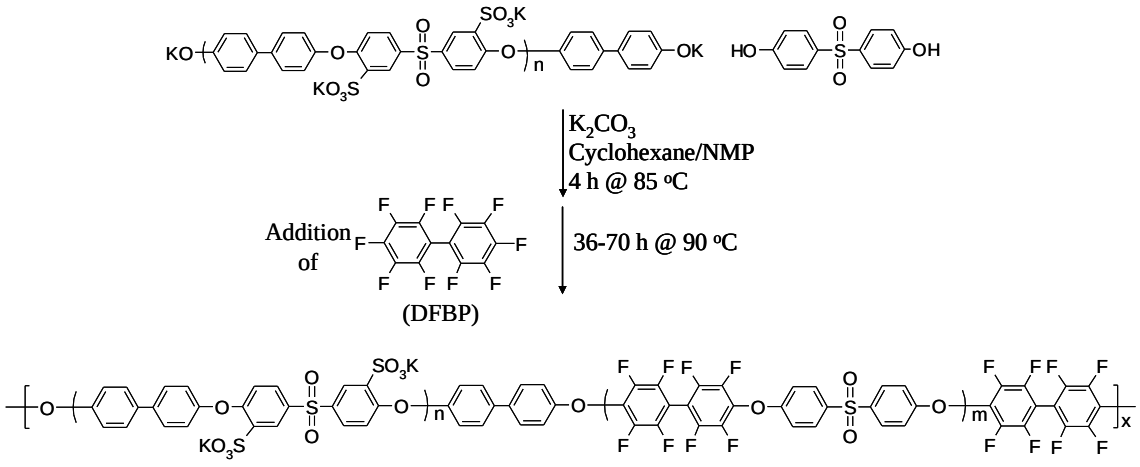

Figure 6-4. BisSF-BPSH100 segmented copolymer

Representative ^{1}H and ^{19}F NMR spectra of a segmented copolymer are shown in Figure 6-5. There were no peaks due to endgroups in either spectrum, which signifies successful segmented copolymer formation. The peak at 7.3 ppm has been assigned to the protons of the BP in the linking unit.

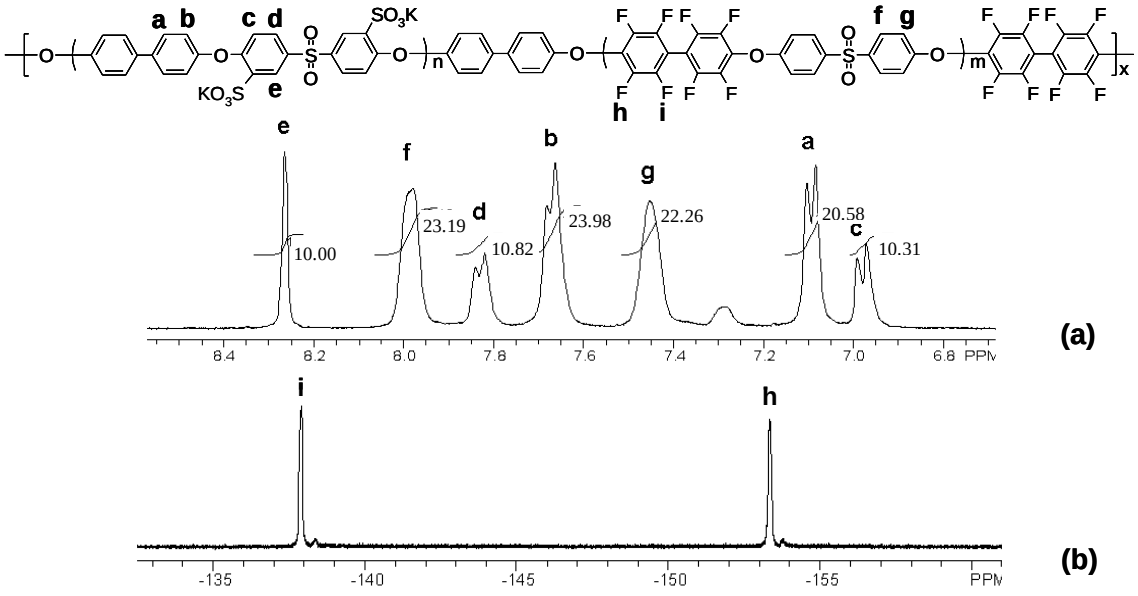

Figure 6-5. (a) ^{1}H and (b) ^{19}F NMR Spectra of a BisSF-BPS100 Segmented Copolymer

The highly reactive DFBP monomer allowed for mild reaction temperatures (90-110 ^{o}C) to be used during synthesis, which eliminated randomization by ether-ether interchange. Monomer sequencing is highly ordered in block copolymers. Therefore, most of the carbons have only one possible chemical environment. Random copolymers develop a larger number of short

sequences during the copolymerization. This causes different chemical environments for similar carbons, which results in splitting of the ^{13}C NMR peaks. If substantial ether-ether interchange occurred during a segmented copolymerization, a scrambling in the backbone would occur. This would be evidenced by peak splitting similar to a random copolymer. The singlets in the ^{13}C NMR spectrum of a segmented copolymer were the same as for a multiblock copolymer with a similar composition, both shown in Figure 6-6, which strongly supports the avoidance of ether-ether interchange.

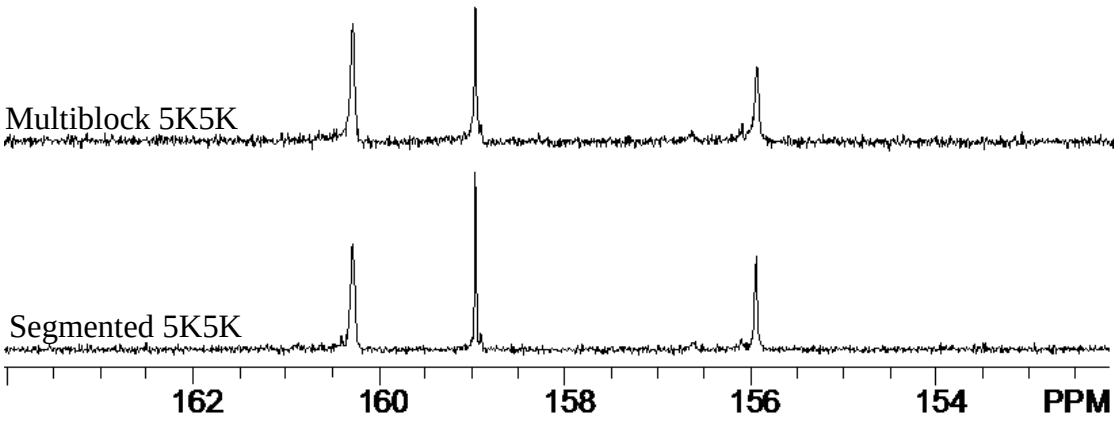

Figure 6-6. ^{13}C NMR Spectra of BisSF-BPS100 Multiblock and Segmented Copolymers

6.3.3. Synthesis of BisSF-BPSH100 Multiblock Copolymer Controls.

BisSF-BPSH100 multiblock copolymer controls were synthesized as described in the literature. Phenoxide-terminated, BPS100 oligomers were prepared using a slight molar excess of BP to SDCDPS to control M_n. Hydrophobic oligomers (BisSF) were synthesized using a slight molar excess of DFBP relative to Bis-S to achieve fluorine-terminated oligomers with controlled

M_n. Both hydrophilic and hydrophobic block lengths were targeted at 3, 5, or 9 kg/mol. Experimental M_n's were determined by endgroup analysis from ^1H and ^{19}F NMR for BPS100 and BisSF oligomers, respectively, and agreed well with the target values (Table 6-2). BPS100 and BisSF oligomers were coupled using a 1:1 molar ratio of the oligomers to form multiblock copolymers with approximately equal hydrophilic and hydrophobic block lengths. The overall synthetic procedure is depicted in Figure 6-7.

Table 6-2. Characterization of Hydrophilic and Hydrophobic Telechelic Oligomers for BisSF-BPSH100 Multiblock Copolymers

Molecular Weight (M_n) (g/mol)		
	BPSH100	BisSF
Target	Experimental[a]	Experimental[b]
3000	3300	3200
5000	5000	6100
9000	9200	9300

a) Calculated from ^{1}H NMR

b) Calculated from ^{19}F NMR

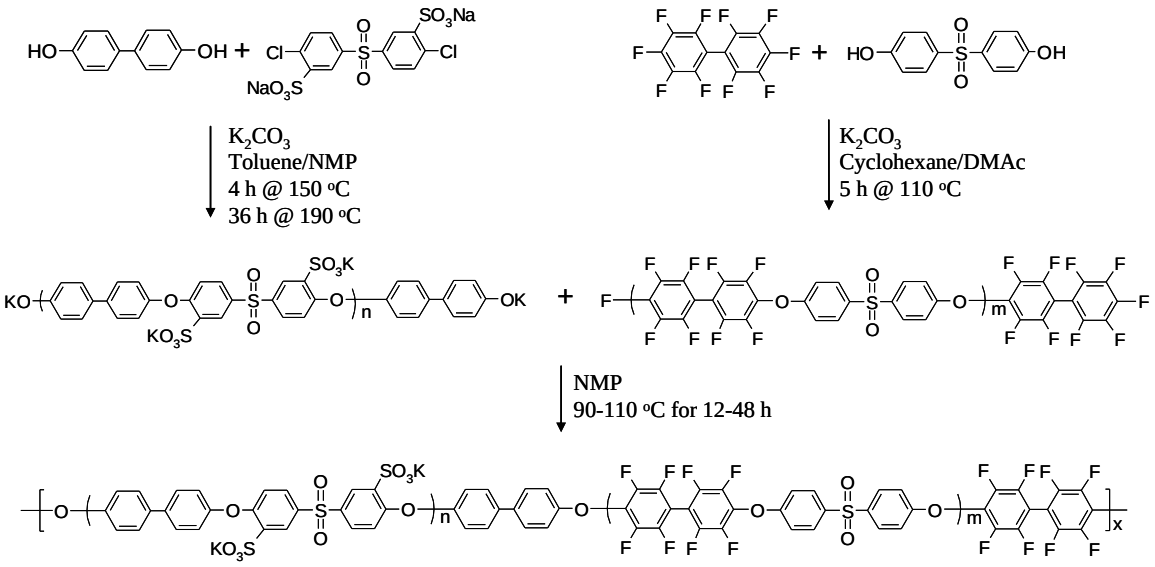

Figure 6-7. Overview of Synthesis of BisSF-BPSH100 Multiblock Copolymer

6.3.4. Comparison of BisSF-BPSH100 Segmented and Multiblock Copolymer Properties.

The main objective of this research was to compare the properties of polymers produced via a simplified synthetic technique relative to the traditional two-oligomer method. Select properties of both systems are summarized in Table 6-3. Experimental IEC values were calculated from ^{1}H NMR by determining the weight ratios of the hydrophobic versus hydrophilic oligomers. They were in good agreement with theoretical values, confirming that the hydrophobic segments were systematically incorporated into the copolymer backbones. The I.V. data confirmed that high

molecular weight polymers were achieved using both synthetic methods. When comparing polymers with similar IEC values, water uptake increased with longer block lengths. Tensile properties were also comparable for polymeric membranes prepared from both synthetic techniques, as shown in Table 6-4.

Table 6-3. Characterization of Segmented and Multiblock BisSF-BPSH100 Copolymers

Polymer		IEC (meq/g)		I.V. (dL/g)	Conductivity[c] (S/cm)	Water Uptake (%)
		Theoretical[a]	Experimental[b]			
Segmented	3K-3K	1.6	1.8	0.63	0.10	62
	5K-5K	1.6	1.5	0.50	0.11	51
	9K-9K	1.7	1.5	0.82	0.15	74
Multiblock	3K-3K	1.8	1.8	1.07	0.13	73
	5K-5K	1.6	1.6	0.89	0.13	78
	9K-9K	1.7	1.6	0.84	0.13	101

a) Determined from reactant weights

b) Determined from ^{1}H NMR

c) Determined in liquid water

Table 6-4. Comparison of Tensile Properties for Segmented and Multiblock Copolymers

Copolymer		Modulus (Mpa)	Tensile Strength (Mpa)	Elongation (%)	Max Elongation (%)
Segmented	3K-3K	1500±160	42±5	43±27	74
	5K-5K	1470±120	39±2	16±5	21
	9K-9K	1510±80	46±4	24±16	47
Multiblock	3K-3K	1380±200	42±3	43±15	55
	5K-5K	1450±150	41±4	47±21	71
	9K-9K	1390±200	43±3	22±4	26

Dimensional swelling was measured on both series of copolymers. The results for the segmented and multiblock copolymers were also compared to a random copolymer (BPSH35) (Figure 6-8). The segmented and multiblock copolymers exhibited anisotropic swelling in contrast to the isotropic swelling of the random copolymer. Overall, swelling through the plane (z-

direction) increased with block length, while in-plane swelling (x- and y-directions) stayed the same or decreased. This is likely indicative of the well-ordered morphology that develops as block length increases. Membrane electrode failure, due to changes in humidity levels (swelling and deswelling cycling), may be minimized with a reduction of in-plane swelling.

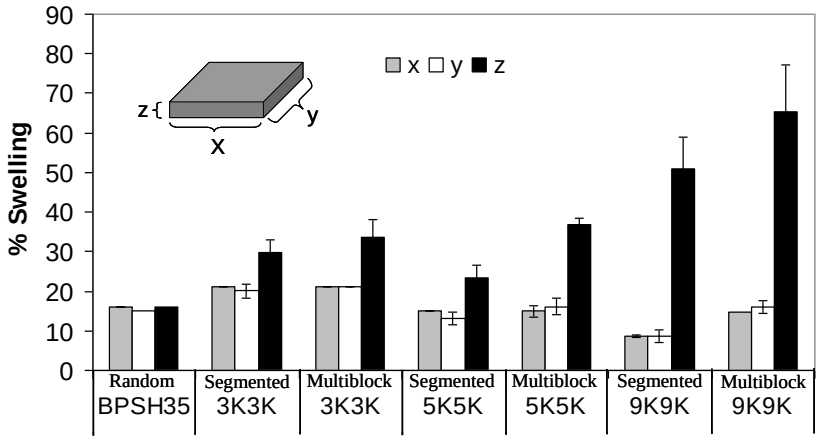

Figure 6-8. Comparison of Dimensional Swelling for Segmented, Multiblock, and Random Copolymers

The effect of block length on proton conductivity under partially hydrated conditions was assessed for both systems. A plot of proton conductivity versus relative humidity is shown in Figure 6-9. The segmented and multiblock copolymers had similar proton conductivities across the entire RH range when comparing copolymers with equivalent block lengths. Conductivity also increased over the entire RH range at greater block lengths. This indicates that increasing the block length of the hydrophilic and hydrophobic segments improves the connectivity in the hydrophilic channels, regardless of synthetic approach.

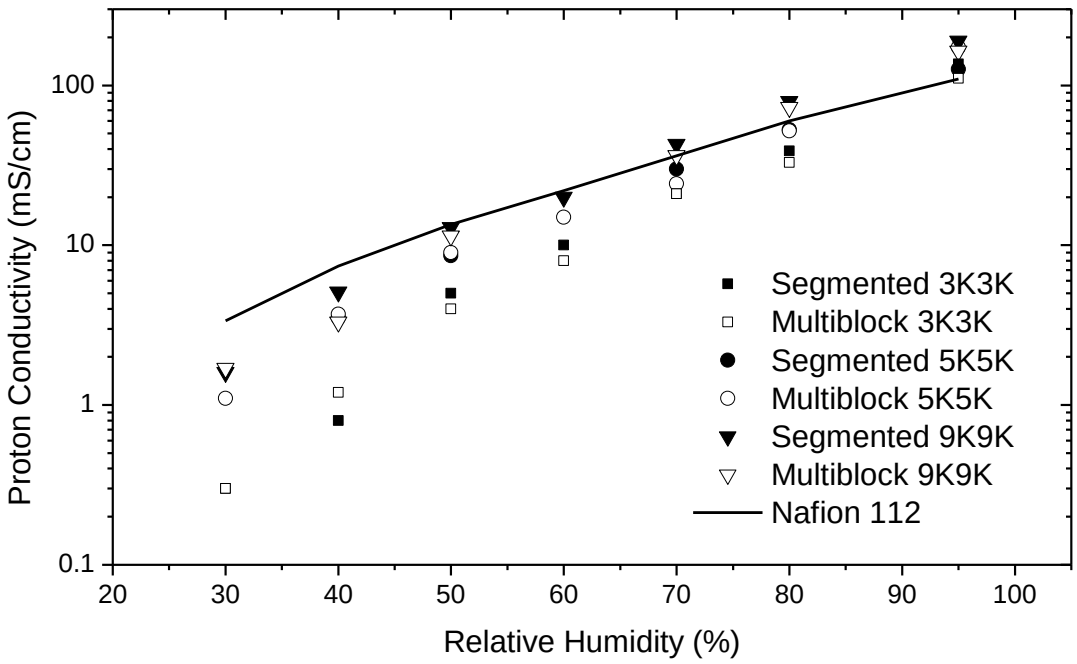

Figure 6-9. Comparison of Proton Conductivity Under Partially Hydrated Conditions for Segmented and Multiblock Copolymers

TEM images shown in Figure 6-10 reflect both the development of long-range domain order with an increase in block length from 5K-5K to 9K-9K, and also show similar trends for the segmented and multiblock series. This is consistent with our observations of other multiblock copolymer systems.[25-30] The AFM images in Figure 6-11 similarly show the development of long-range order with an increase in block length. This phase separated morphology correlates well with the anisotropy of the dimensional water uptake data. Longer block lengths using either synthetic method promote the formation of a lamellar morphology. As has been shown in other multiblock systems, longer-range order correlates with reduced swelling in the X-Y directions (in-plane), and increased Z-direction (through-plane) swelling. The hydrophobic lamellae may restrict in-plane swelling in going from a dry to a fully humidified state. The hydrophobic domains may also reduce water loss at reduced humidities, thus improving proton conductivity at low RH.

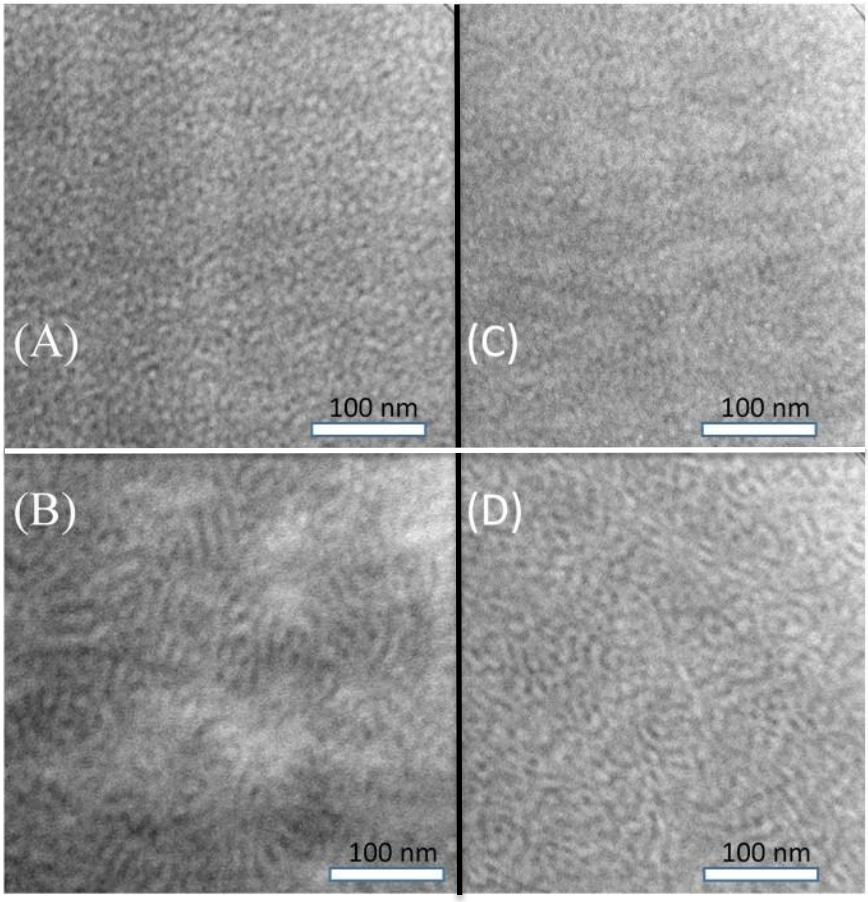

Figure 6-10. TEM images of (A) 5K-5K Multiblock, (B) 9K-9K Multiblock, (C) 5K-5K Segmented, and (D) 9K-9K Segmented BisSF-BPSH100 copolymers. All images are taken at 96000 magnification.

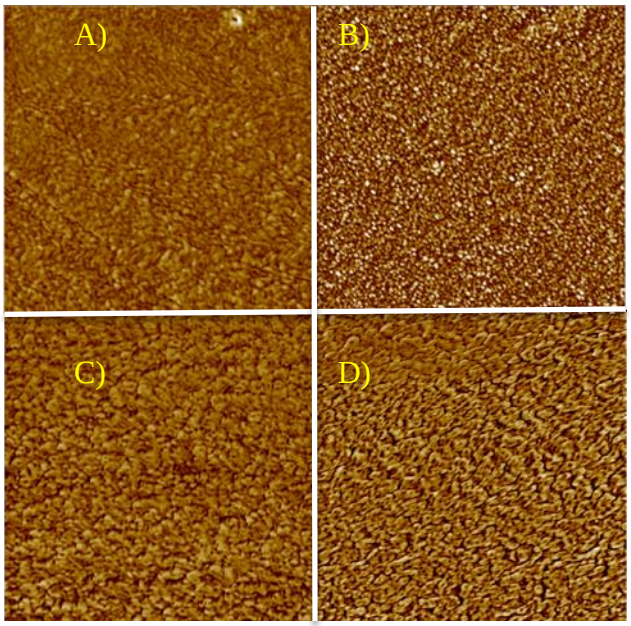

Figure 6-11. AFM images of (A) 5K-5K Multiblock, (B) 9K-9K Multiblock, (C) 5K-5K Segmented, and (D) 9K-9K Segmented BisSF-BPSH100 copolymers. All images are 1 micron by 1 micron.

6.4. Conclusions

Multiblock copolymers containing highly fluorinated hydrophobic blocks and 100% disulfonated hydrophilic blocks have been synthesized using a simplified segmented approach. The performance of these copolymers, particularly with respect to fuel cell operation, were in good agreement with the properties of those synthesized using a more cumbersome oligomer-oligomer approach. Increased conductivity over the entire RH range was evidence that a connected phase morphology developed with longer block length. This morphology was confirmed by surface and bulk investigations. The segmented method by all measures herein can be regarded as a potential alternative for the production of phase-separated multiblock copolymers.

Acknowledgement. The authors would like to acknowledge the Department of Energy (DE-FG36-06G016038) and NSF IGERT (DGE-0114346) for funding.

Reference:

1. Hickner, M. A.; Ghassemi, H.; Kim, Y. S.; Einsla, B. R.; McGrath, J. E., Alternative Polymer Systems for Proton Exchange Membranes (PEMs). *Chem. Rev. (Washington, DC, U. S.)* **2004,** *104* (10), 4587-4611.
2. Hamrock, S. J.; Herring, A. M.; Zawodzinski, T. A., Fuel cell chemistry and operation. *J. Power Sources* **2007,** *172* (1), 1.
3. Borup, R.; Meyers, J.; Pivovar, B.; Kim, Y. S.; Mukundan, R.; Garland, N.; Myers, D.; Wilson, M.; Garzon, F.; Wood, D.; Zelenay, P.; More, K.; Stroh, K.; Zawodzinski, T.; Boncella, J.; McGrath, J. E.; Inaba, M.; Miyatake, K.; Hori, M.; Ota, K.; Ogumi, Z.; Miyata, S.; Nishikata, A.; Siroma, Z.; Uchimoto, Y.; Yasuda, K.; Kimijima, K.-i.; Iwashita, N., Scientific Aspects of Polymer Electrolyte Fuel Cell Durability and Degradation. *Chem. Rev. (Washington, DC, U. S.)* **2007,** *107* (10), 3904-3951.
4. Lefebvre-Joud, F.; Mougin, J.; Antoni, L.; Bouyer, E.; Gebel, G.; Nony, F., Materials pertaining to hydrogen production and conversion. *Tech. Ing., Mater. Fonct.* **2010,** *8* (N 12), N1205/1-N1205/21,Doc.N1205/1-Doc.N1205/4.
5. McVeigh, C., The hydrogen economy revisited: Solar Hydrogen: Moving Beyond Fossil Fuels Joan M. Ogden and Robert H. Williams World Resources Institute, Washington, DC, USA, 1989, US$10.00, 124 pp. *Energy Policy* **1990,** *18* (2), 208-209.
6. White, R.; Yeh, S.; Goldstein, N. In *Future water challenges of a hydrogen economy*, American Chemical Society: 2008; pp ENVR-189.
7. Mauritz, K. A.; Moore, R. B., State of understanding of Nafion. *Chem. Rev. (Washington, DC, U. S.)* **2004,** *104* (10), 4535-4585.
8. Hickner, M. A.; Pivovar, B. S., The chemical and structural nature of proton exchange membrane fuel cell properties. *Fuel Cells (Weinheim, Ger.)* **2005,** *5* (2), 213-229.
9. Iulianelli, A.; Basile, A., Sulfonated PEEK-based polymers in PEMFC and DMFC applications: A review. *International Journal of Hydrogen Energy* **2012,** *37* (20), 15241-15255.
10. Bae, B.; Miyatake, K.; Watanabe, M., Poly(arylene ether) block copolymer membranes: synthesis, properties and durability. *ECS Trans.* **2009,** *25* (1, Proton Exchange Membrane Fuel Cells 9), 415-422.
11. Im, S. J.; Patel, R.; Shin, S. J.; Kim, J. H.; Min, B. R., Sulfonated poly(arylene ether sulfone) membranes based on biphenol for direct methanol fuel cells. *Korean J. Chem. Eng.* **2008,** *25* (4), 732-737.
12. Jung, M. S.; Kim, T.-H.; Yoon, Y. J.; Kang, C. G.; Yu, D. M.; Lee, J. Y.; Kim, H.-J.; Hong, Y. T., Sulfonated poly(arylene sulfone) multiblock copolymers for proton exchange membrane fuel cells. *Journal of Membrane Science* **2014,** *459* (0), 72-85.
13. Matsumoto, K.; Ando, S.; Ueda, M., Synthesis of sulfonated poly(1,4-diphenoxybenzene) for proton exchange membrane. *Polym. J. (Tokyo, Jpn.)* **2007,** *39* (8), 882-887.
14. McGrath, J. E.; Roy, A.; Lee, H.-S.; Yu, X.; Badami, A.; Li, Y.; Wang, H., Multiblock hydrophilic-hydrophobic proton exchange membranes for direct methanol based fuel cell. *ECS Trans.* **2007,** *2* (24, Direct Methanol Fuel Cells), 55-62.
15. Miyatake, K.; Chikashige, Y.; Watanabe, M., Novel Sulfonated Poly(arylene ether): A Proton Conductive Polymer Electrolyte Designed for Fuel Cells. *Macromolecules* **2003,** *36* (26), 9691-9693.
16. Nakabayashi, K.; Matsumoto, K.; Ueda, M., Synthesis and properties of sulfonated multiblock copoly(ether sulfone)s by a chain extender. *J. Polym. Sci., Part A: Polym. Chem.* **2008,** *46* (12), 3947-3957.

17. Einsla, B. R.; Harris, L. A.; Hill, M. L.; McGrath, J. E., Direct copolymerization of wholly aromatic and partially fluorinated disulfonated poly(arylene ether sulfone)s. *Prepr. Symp. - Am. Chem. Soc., Div. Fuel Chem.* **2005,** *50* (2), 571-572.
18. Roy, A.; Einsla, B. R.; Harrison, W. L.; McGrath, J. E., Synthesis and characterization of hydroquinone based disulfonated poly (arylene ether sulfone)s via direct copolymerization. *Prepr. Symp. - Am. Chem. Soc., Div. Fuel Chem.* **2004,** *49* (2), 614-615.
19. Badami, A. S.; Roy, A.; Lee, H.-S.; Li, Y.; McGrath, J. E., Morphological investigations of disulfonated poly(arylene ether sulfone)-b-naphthalene dianhydride-based polyimide multiblock copolymers as potential high temperature proton exchange membranes. *J. Membr. Sci.* **2009,** *328* (1+2), 156-164.
20. Lee, H.-S.; Roy, A.; Lane, O.; Lee, M.; McGrath, J. E., Synthesis and characterization of multiblock copolymers based on hydrophilic disulfonated poly(arylene ether sulfone) and hydrophobic partially fluorinated poly(arylene ether ketone) for fuel cell applications. *J. Polym. Sci., Part A: Polym. Chem.* **2010,** *48* (1), 214-222.
21. Roy, A.; Lee, H.-S.; McGrath, J. E., Hydrophilic-hydrophobic multiblock copolymers based on poly(arylene ether sulfone)s as novel proton exchange membranes - Part B. *Polymer* **2008,** *49* (23), 5037-5044.
22. Shin, D. W.; Lee, S. Y.; Lee, C. H.; Lee, K.-S.; Park, C. H.; McGrath, J. E.; Zhang, M.; Moore, R. B.; Lingwood, M. D.; Madsen, L. A.; Kim, Y. T.; Hwang, I.; Lee, Y. M., Sulfonated Poly(arylene sulfide sulfone nitrile) Multiblock Copolymers with Ordered Morphology for Proton Exchange Membranes. *Macromolecules (Washington, DC, U. S.)* **2013,** *46* (19), 7797-7804.
23. Yu, X.; Roy, A.; Dunn, S.; Badami, A. S.; Yang, J.; Good, A. S.; McGrath, J. E., Synthesis and characterization of sulfonated-fluorinated, hydrophilic-hydrophobic multiblock copolymers for proton exchange membranes. *J. Polym. Sci., Part A: Polym. Chem.* **2009,** *47* (4), 1038-1051.
24. Sankir, M.; Bhanu, V. A.; Harrison, W. L.; Ghassemi, H.; Wiles, K. B.; Glass, T. E.; Brink, A. E.; Brink, M. H.; McGrath, J. E., Synthesis and characterization of 3,3'-disulfonated-4,4'-dichlorodiphenyl sulfone (SDCDPS) monomer for proton exchange membranes (PEM) in fuel cell applications. *J. Appl. Polym. Sci.* **2006,** *100* (6), 4595-4602.
25. Badami, A. S.; Lane, O.; Lee, H.-S.; Roy, A.; McGrath, J. E., Fundamental investigations of the effect of the linkage group on the behavior of hydrophilic-hydrophobic poly(arylene ether sulfone) multiblock copolymers for proton exchange membrane fuel cells. *J. Membr. Sci.* **2009,** *333* (1+2), 1-11.
26. Badami, A. S.; Lee, H.-S.; Li, Y.; Roy, A.; Wang, H.; McGrath, J. E., Molecular weight effects on poly(arylene ether sulfone)-based random and multiblock copolymers characteristics for fuel cells. *ACS Symp. Ser.* **2010,** *1040* (Fuel Cell Chemistry and Operation), 65-81.
27. Ghassemi, H.; Harrison, W.; Zawodzinski, T.; McGrath, J. E. In *New multiblock copolymers containing hydrophilic-hydrophobic segments for proton exchange membranes*, American Chemical Society: 2004; pp POLY-420.
28. Lee, H.-S.; Lane, O. R.; McGrath, J. E. In *Synthesis and characterization of multiblock copolymers with hydrophilic-hydrophobic sequences for proton exchange membranes*, American Chemical Society: 2008; pp FUEL-098.
29. Lee, H.-S.; Roy, A.; Lane, O.; Dunn, S.; McGrath, J. E., Hydrophilic-hydrophobic multiblock copolymers based on poly(arylene ether sulfone) via low-temperature coupling reactions for proton exchange membrane fuel cells. *Polymer* **2008,** *49* (3), 715-723.
30. Lee, M.; Park, J. K.; Lee, H.-S.; Lane, O.; Moore, R. B.; McGrath, J. E.; Baird, D. G., Effects of block length and solution-casting conditions on the final morphology and properties of disulfonated poly(arylene ether sulfone) multiblock copolymer films for proton exchange membranes. *Polymer* **2009,** *50* (25), 6129-6138.

7.0 Future Work

7.1 Post-sulfonated hydroquinone-containing poly(arylene ether sulfone)s

The development of precisely tailored post-sulfonated hydroquinone-containing copolymers has several interesting avenues for further investigation. The most obvious is the fundamental work of synthesizing and sulfonating series with varying comonomer structures and investigating the impact of the chemical composition on transport properties. The IECs investigated in this research were fairly limited, and it would be informative to evaluate post-sulfonated SHQS materials with a higher degree of hydrophilicity. This would be interesting at a fundamental level to confirm if the calcium effect returns at higher sulfonate group concentrations. Once a broad spectrum of IECs have been investigated for transport properties, it might be informative to replace the bisphenyl sulfone with a more hydrophobic monomer. The synthesis of a highly hydrophilic (60-80% hydroquinone-containing comonomers) oligomer, which is then crosslinked in order to optimize both water flux and salt rejection, would be an intuitive approach in the search for an improved membrane. It may also be informative in future mixed-feed evaluations to compare a directly copolymerized (BPS) material that has been exchanged with aluminum (Al^{3+}), to gain a fundamental understanding of the impact of counterion charge density and valence to limit or negate the screening effect of calcium.

However, the post-sulfonated poly(arylene ether sulfone) system may also provide a novel approach for the synthesis of multiblock copolymers. The resistance to calcium compromise of salt transport is an advantage unique to the application of reverse osmosis, but the synthetic approach may afford an additional advantage for fuel cell or polymer membrane electrolysis applications. While multiblock hydrophilic-hydrophobic poly(arylene ether sulfone)s

have been developed at Virginia Tech for a decade, the synthetic process remains lengthy and delicate. Oligomer molecular weight, particularly of the hydrophilic block, is difficult to control due to the poorly reactive sulfonated monomer and practical control over synthesis is very limited.

In contrast, the synthesis of two nonsulfonated oligomers would be more rapid, particularly if conducted at the high reaction temperatures of sulfolane, and the greater reactivity should facilitate oligomer molecular weight control. A multiblock analogue of the series described in Chapter 4, with a 'pre-hydrophilic' block composed of DCDPS and hydroquinone, and a hydrophobic block of DCDPS and bisphenyl sulfone, would be comprised entirely of commercially available monomer and very inexpensive to produce. After sulfonation and recovery, the hydrophobic and hydrophilic oligomers could be coupled to produce a much more feasible and affordable multiblock. This would allow for more rapid development and optimization of multiblock architectures.

Alternately, it may also be possible to synthesize and couple the oligomers prior to sulfonation of the final multiblock. While the hydrophobic component should not be soluble in sulfuric acid by itself, the solubility of the reacting hydrophilic groups may be sufficient to keep the multiblock dissolved.

One of the apparent hurdles to the development of post-sulfonated hydrophilic-hydrophobic multiblock copolymers is the limited hydrophilicity of the monosulfonated unit. Substituting the bisphenyl sulfone comonomer with for a deactivated dihalide with a single ring would provide a final product with a similar ionic density. The spacing between the sulfonate

groups would not be a concern, and could possibly be advantageous in boosting connectivity between hydrophilic domains of the resulting multiblock.

7.2 Structure-property-processing relationships in multiblock copolymers

The results published here on the impact of various casting conditions were remarkable in how widely the final polymer performance varied as a consequence of casting solvent and polymer concentration. Previously, few systematic studies were done on our hydrophilic-hydrophobic blocks and their casting conditions. Future work in characterizing multiblock materials should include a systematic evaluation of casting conditions and morphological characterization. It may be desirable to revisit previously described systems that showed competitive performance to commercial state-of-the-art membranes such as Nafion, in the event that optimized casting conditions may provide superior performance. Due to its relative simplicity and affordability, the potential post-sulfonated block copolymer described above would be an ideal candidate.